Catalysis at the Interface-

Elucidation of the Activation Process and Coupling of Catalysis and Compartmentalization of the Peripheral Membrane Protein Pyruvate Oxidase from *Escherichia coli*

Dissertation

for the award of the degree

"Doctor rerum naturalium"

of the Georg-August-Universität Göttingen

within the doctoral program *Biomolecules: Structure-Function-Dynamics*

of the Georg-August University School of Science (GAUSS)

submitted by

Astrid Sitte

born in Lutherstadt Wittenberg

Göttingen 2013

Everything is made for the best purpose.

Our noses were made to carry spectacles,

so we have spectacles.

Legs were clearly intended for breeches,

and we wear them.

after Dr. Pangloss in Voltaire's *Candide*

Members of the Thesis Committee:

Prof. Dr. Kai Tittmann (Reviewer)

Abteilung Bioanalytik

Albrecht-von-Haller-Institut für Pflanzenwissenschaften

Georg-August-Universität Göttingen

Prof. Dr. Ulf Diederichsen (Reviewer)

Institut für Organische und Biomolekulare Chemie

Georg-August-Universität Göttingen

Dr. Lars T. Kuhn

Abteilung Biomolekulare NMR Spektroskopie

European Neuroscience Institute

Göttingen

Herewith I declare that I prepared this thesis "Catalysis at the Interface - Elucidation of the Activation Process and Coupling of Catalysis and Compartmentalization of the Peripheral Membrane Protein Pyruvate Oxidase from *Escherichia coli*" independently and with no other sources and aids than quoted.

Göttingen, 14.03.2013

Astrid Sitte

I. Table of Content

II. List of figures

III. List of tables

IV. Abbreviations

CMC	critical micelle concentration
DPC	n-dodecyl phosphocholine
Ec	*Escherichia coli*
FAD	flavin adenine dinucleotide
$FADH_2$	reduced form of FAD
FMN	flavin mononucleotide
IPTG	isopropyl β-D-thiogalactopyranoside
ITC	isothermal titration calorimetry
Lp	*Lactobacillus plantarum*
MAP	methyl acetyl phosphate
MPD	hexylene glycol
NMR	nuclear magnetic resonance
PAGE	polyacrylamide gel electrophoresis
PEG	polyethylene glycol
POX	pyruvate oxidase
$Q_{(0\text{-}8)}$	ubiquinone-(0-8)
RP-HPLC	reversed-phase high performance liquid chromatography
R-state	resting state
SB-state	substrate-bound state
SDS	sodium dodecyl sulfate
SR-state	substrate-reduced state
SUMO	small ubiquitin-like modifier
TEMED	tetramethylethylenediamine
TFA	trifluoroacetic acid
ThDP	thiamine diphosphate

Within this thesis the three-letter code was used for specific amino acid residues and the one-letter code for variants thereof.

1. Introduction

1.1 Regulation of enzymatic activity

Organisms need to preserve metabolic homeostasis although manifold biotic and abiotic environmental factors affect them to a different extent. Therefore, regulation of certain biochemical processes within the organism is mandatory. Key players in this regard are enzymes since they govern all biological reactions in the cell. Tight control is necessary to provide that enzymes are active at the right time and the right place. Two major modes of enzyme regulation are typically described in text books:

The *amount of an enzyme* can be controlled on different levels through its synthesis or degradation. On the gene level synthesis of the enzyme is either regulated by transcription of the gene [1] or by translation of the corresponding messenger RNA [2]. Degradation of proteins is typically initiated by ubiquitination [3]. This response to a stimulus is less immediate but with longer a duration.

The *activity of an enzyme* can be regulated and typically allows fast answer of the organism to the particular stimulus. Regulation includes numerous principles whereat binding of inhibitors and covalent modifications are the most common ones. Although a great number of posttranslational modifications are described in the literature, nearly all principles constitute reversible alterations of a pre-existing enzyme (also called pre-enzyme). Here, the pre-enzyme represents the non-active enzyme which becomes activated after modification. Noteworthy, inverted cases are also known where the existing enzyme resembles the active form which is turned off due to the modification. Activation is often initiated by a conformational transition which finally leads to a change of enzymatic activity. Due to the multitude of principles only a selected number of activity modulations are discussed here in more detail (figure 1):

A: *Allosteric control*. An effector of an enzyme can bind to an allosteric site which is different in shape and position compared to the active site. A prominent kind of allosteric control is the feedback mechanism where the end product of a multistep pathway inhibits an enzyme that catalyzes the first reaction of this pathway [4].

B: *Covalent modifications*. Covalent modifications cover phosphorylation, acetylation, glycosylation, myristoylation, palmitoylation and can be reversible or irreversible. Only two examples are described in more detail.

Myristoylation of a pre-enzyme is performed by N-myristoyltransferase which covalently attaches a myristoyl moiety to an N-terminal Gly of the protein. The process is irreversible and mediates membrane binding of the enzyme or interaction with other proteins [5].

Proteases can activate pre-enzymes (here also termed zymogens) via *proteolytic cleavage* of a polypeptide part [6]. To turn off the irreversibly activated enzyme further enzymes are mandatory.

C: *Protein-protein interactions*. Many enzymes need other proteins like regulatory subunits for functional activity [7]. Also the formation of catalytically active homooligomers for example dimerization of membrane-bound receptors is known [8].

D: *Localization in a different environment*. Enzymes need defined milieus like an optimal pH or oxidative environment for their functionality. The optimal milieu can either contribute to a functional active site or to the global structure [9].

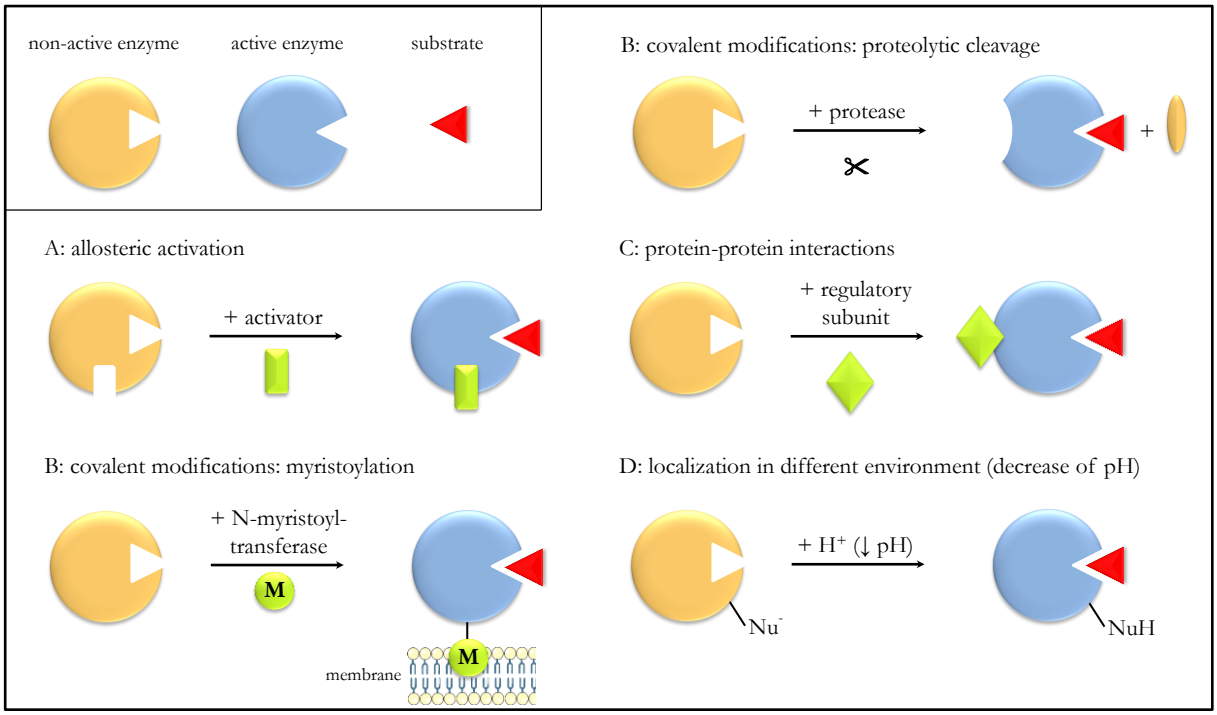

figure 1: Regulation modes of enzymes. The non-active enzyme (orange) is converted to the active form (blue), which is able to react with the substrate (red). Different activation modes are A: allosteric activation, B: covalent modifications, C: protein-protein interactions, D: localization in a different environment.

Often enzymes are regulated by multiple modes to adapt perfectly on different metabolic conditions. For instance enzymes which become covalently modified with a myristoyl anchor subsequently change their localization to the hydrophobic environment of a lipid bilayer [10] [11].

In this thesis the regulation of the peripheral membrane protein pyruvate oxidase from *E. coli* (*Ec*POX) is analyzed in detail. *Ec*POX is a metabolic enzyme which is localized in the cytosol and only recruited to the membrane in response to a certain stimulus [12]. Association of *Ec*POX to the lipid bilayer converts this enzyme from a fairly unreactive to a powerful catalyst by enhancing the catalytic efficiency by several orders of magnitude [13]. Aim of this thesis is to elucidate the molecular mechanism which controls *Ec*POX activation and membrane binding.

1.2 Pyruvate oxidase from *E.coli*

Pyruvate oxidase from *E. coli* (EC 1.2.2.2, *Ec*POX) is a peripheral membrane protein which was first found in the soluble fraction of *E. coli* lysate by Hager in 1957 [14]. The enzyme is a homotetramer with a subunit size of 62 kDa and requires one thiamine diphosphate (ThDP) and one flavin adenine dinucleotide (FAD) as cofactors per monomer for catalysis [15] [16]. *Ec*POX catalyzes the oxidative decarboxylation of pyruvate yielding acetate and carbon dioxide. During this reaction two electrons arise which are initially stored at the flavin cofactor. Subsequently, both electrons are used to reduce ubiquinone-8 (Q_8), a membrane-bound electron carrier of the respiratory chain [17]. According to the localization the overall reaction catalyzed by pyruvate oxidase can be divided into two parts:

cytosol: $Ec\text{POX-ThDP-FAD} + \text{pyruvate} + H_2O \rightarrow Ec\text{POX-ThDP-FADH}_2 + CO_2 + \text{acetate}$

membrane: $Ec\text{POX-ThDP-FADH}_2 + Q_8 \rightarrow Ec\text{POX-ThDP-FAD} + Q_8H_2$

Pyruvate binding and conversion can take place in the cytoplasm. However, the reduced enzyme must be attached to the membrane in order to transfer electrons to Q_8. Therefore, *Ec*POX was described as peripheral membrane protein which is mainly found in the cytosol [18] [17].

1.2.1 The catalytic cycle of *Ec*POX

The detailed reaction mechanism of *Ec*POX is similar to other thiamine enzymes and follows the descriptions of Breslow and Schellenberger (figure 2) [19] [20]. The thiamine cofactor is bound in its typical V-conformation [21] which ensures deprotonation of the C2-atom of the thiazolium ring as prerequisite for catalysis [22]. Therefore, a co-catalytic function of the N1'- and N4'-atom of the aminopyrimidine ring in combination with a conserved Glu (Glu50 in *Ec*POX), which acts as acid/base catalyst for proton abstraction, can be supposed. The resulting ylide moiety at the C2-atom can attack the substrate pyruvate in a nucleophilic forming lactyl-ThDP (L-ThDP), which is decarboxylated yielding the resonance-stabilized hydroxyethyl-ThDP (HE-ThDP) intermediate. Starting from HE-ThDP the catalytic pathway is subdivided: two electrons are transferred from HE-ThDP to the flavin cofactor and acetyl-ThDP (Ac-ThDP) is formed. This is further hydrolyzed resulting in the product acetate and regenerated ThDP. For complete regeneration of the enzyme the reduced flavin cofactor needs to be oxidized. Therefore, *Ec*POX, which was hitherto localized in the cytoplasm, is recruited to the membrane where it transfers both electrons to the final acceptor Q_8.

*Ec*POX catalysis can be described as ping-pong mechanism with pyruvate and water as substrates and carbon dioxide and acetate as corresponding products [23]. According to the redox state of the flavin cofactor the catalytic cycle can be divided into two half-reactions [24]. The reductive half-reaction includes all processes yielding the reduced flavin and refer to formation of L-ThDP, decarboxylation, and formation of Ac-ThDP with concomitant flavin reduction (yellow half-cycle in figure 2). Contrary, the part of the catalytic cycle which leads to reoxidation of the flavin cofactor by Q_8 constitutes the oxidative half-reaction (white half-cycle in figure 2).

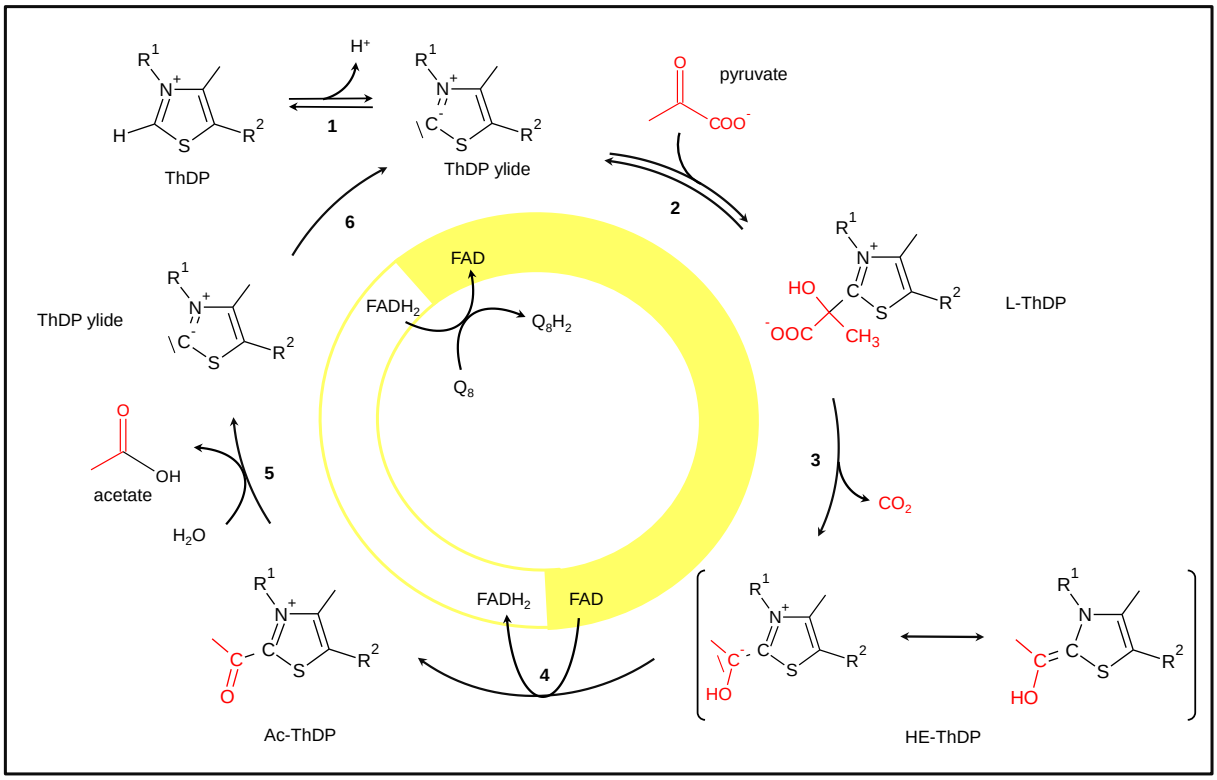

figure 2: Catalytic cycle of *Ec*POX. 1: activation of ThDP, 2: covalent binding of pyruvate, 3: decarboxylation of lactyl-ThDP, 4: electron transfer to FAD, 5: hydrolysis of acetyl-ThDP, 6: FAD reoxidation by membrane-bound Q_8. Further explanations are given in the text. (R^1 = aminopyrimidine moiety, R^2 = diphosphate anchor)

1.2.2 The physiological function of *Ec*POX

Typically, *E. coli* cells gain energy via the pivotal pyruvate dehydrogenase (PDH) complex which utilizes pyruvate to produce acetyl-CoA and NADH [25]. Acetyl-CoA can be feed in the citric acid cycle or used to generate fatty acids or steroids. The product NADH, which resembles reducing equivalents, serves as electron donor for the respiratory chain. In this regard, the reaction catalyzed by *Ec*POX seems to be non-essential and wasteful, because *Ec*POX converts pyruvate only to low-energy acetate and reducing equivalents. Other enzymes like acetokinase, phosphotransacetylase or acetyle-CoA synthetase are required to produce acetyl-CoA in ATP-dependent reactions [26]. Thus, the physiological role of *Ec*POX remained enigmatic for a long time.

In 1994 Chang *et al.* demonstrated that *Ec*POX is expressed in the early stationary phase and during anaerobic growth [27]. Since in both cases the PDH complex functions poorly they speculated that *Ec*POX serves as a backup system to provide acetyl-CoA. This assumption was further supported by Abdel-Hamid and coworkers [28] who showed that in PDH-deficient *E. coli* strains *Ec*POX takes over the function of the PDH complex and supports acetate-independent growth. Additionally, expression of the *poxB* gene (encoding for *Ec*POX) and activity of the corresponding acetyl-CoA producing enzymes was increased in these *E.coli* strains. Moreover, in an *Ec*POX-deficient *E. coli* strain less carbon units were utilized to produce biomass and an increased carbon amount was used for energy metabolism. This led to

the conclusion that *Ec*POX contributes to aerobic growth [28], but the question remained open how this is achieved.

1.2.3 Activation of *Ec*POX

When Hager first described the thiamine-dependent enzyme pyruvate oxidase from *E.coli* in 1957 he also reported that a manifold increase in activity was observed if the protein is incubated with trypsin [14]. Similar results were observed by Williams *et al.*, who added surfactants like SDS and lipid extracts to the enzyme [15]. Both effects were later termed *activation* and remained a subject of interest during the last 50 years.

Proteolytic and amphiphile-mediated activation are attributed to the C-terminal part of *Ec*POX

Recny *et al.* showed that the proteolytic digestion of *Ec*POX leading to activation is related to removal of the last 23 amino acids of the C-terminus, which "locks" the enzyme irreversibly in the activated state [29]. Interestingly, the resulting *Ec*POX Δ23 deletion variant shows a severely reduced affinity for lipids and detergents [18]. Therefore, it was proposed that the 23 C-terminal amino acids act as membrane anchor and promote the attachment of *Ec*POX to the lipid bilayer. The anchor was later called alpha-peptide due to the truncation by alpha-chymotrypsin [29]. Additionally, it was deciphered that two C-termini are mandatory for functional membrane binding of an *Ec*POX tetramer [30] [31].

Since detergent-stimulated *Ec*POX shows similar catalytic parameters like Δ23 it was suggested that also in amphiphile-mediated activation the C-terminus is involved [13]. Proteolytic digestion of *Ec*POX in the presence of detergents reveals no proposed truncation to Δ23 [13] which gives evidence that a direct interaction of the detergent with the Δ23 cleavage site and thus with the membrane anchor can be observed [13]. Further, while the full-length enzyme is activated by 80 different amphiphiles, activity of *Ec*POX Δ23 is not further enhanced in the presence of any detergent [27]. These findings foster the idea that proteolytic and amphiphile-mediated activation are attributed to interactions with the C-terminal membrane anchor of *Ec*POX. The crucial role of the C-terminal part for the physiological function of *Ec*POX was also demonstrated *in vivo*. *E.coli* strains expressing the truncated pyruvate oxidase show no oxidase activity [32] and cannot restore acetate-independent growth contrary to the full-length protein [28].

Both, proteolytic and amphiphile-mediated activation were equally applied in the past as substitute for the native membrane binding process [33] [32]. However, it turned out that the presence of pyruvate is mandatory for *Ec*POX activation. Proteolysis of *Ec*POX in the absence of pyruvate leads to inactivation of the enzyme [18] and a similar effect is observed for amphiphilic stimulations [34]. Therefore, it was assumed that pyruvate-triggered reduction of the flavin cofactor induces a conformational change which leads to exposition of the membrane anchor [35].

Model of *Ec*POX activation

A model of *Ec*POX activation and concomitant structural changes was proposed by Neumann and Weidner *et al.* [35] (figure 3). Resting state *Ec*POX is localized in the cytosol and shows poor basal activity (K_m = 90 mM, k_{cat} = 7 s^{-1}). The C-terminal membrane anchor is attached to the protein surface which prevents membrane binding. Elevated concentrations of the substrate pyruvate lead to reduction of the flavin cofactor and trigger a conformational change which comprises exposure of the membrane anchor. After association to the membrane *in vivo* the enzyme is activated characterized by a 30fold increased k_{cat} and a 8fold decreased K_m (K_m = 12 mM, k_{cat} = 200 s^{-1}).

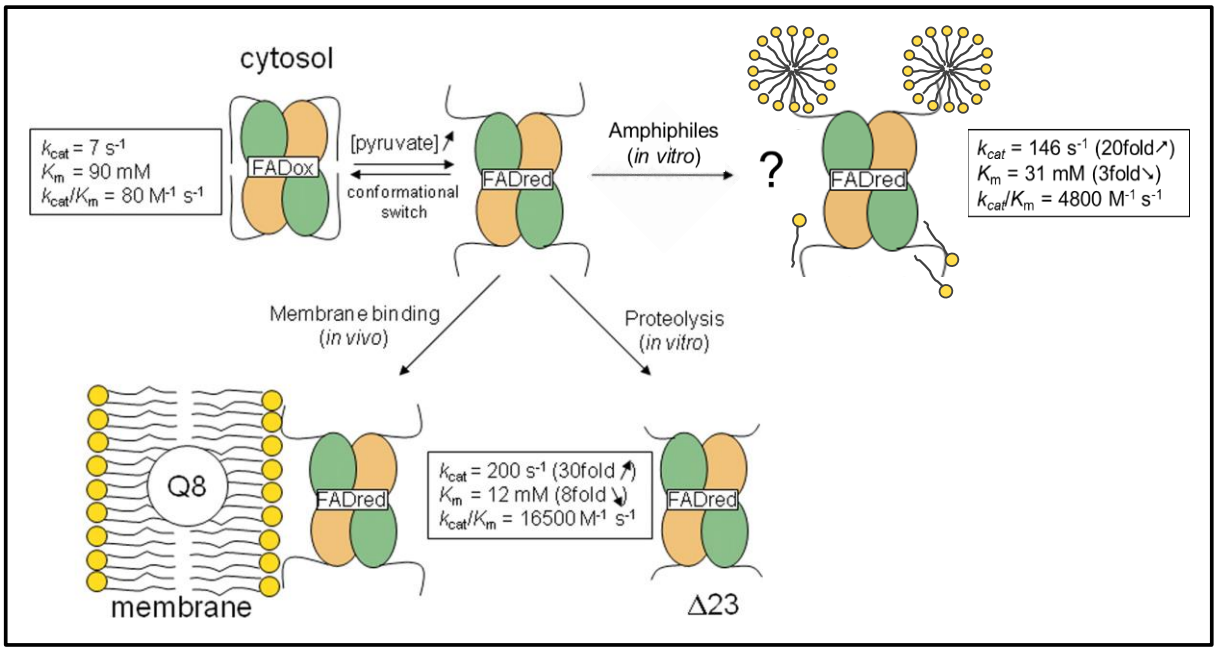

figure 3: Activation model of *Ec*POX. *Ec*POX is localized in the cytosol with a protein-bound membrane anchor. Elevated concentrations of pyruvate trigger membrane anchor exposure. Subsequently, *Ec*POX is either activated in vivo by membrane association or in vitro by limited proteolysis or amphiphiles. In all cases catalytic efficiency is manifold enhanced. Since the interaction mode with amphiphiles is unclear so far contacts of monomers or amphiphilic micelles with the membrane anchor are indicated. Catalytic constants for amphiphile-mediated activation were determined in the presence of 100 µM SDS. Figure was taken from Neumann and Weidner *et al.* [35] and modified.

Similar effects are observed *in vitro* if reduced *Ec*POX is subjected to limited proteolysis which causes C-terminal truncation of the enzyme leading to irreversibly activated *Ec*POX Δ23. Also amphiphiles like detergents and lipids are able to increase the activity to a similar activation level as observed *in vivo*. Although the detailed interaction mechanism of amphiphilic molecules with *Ec*POX is still unclear [34] [13] [36], these substances are apparently applied to mimic the native membrane.

One of the central conclusions that can be drawn from the model of Neumann and Weidner *et al.* is that the membrane anchor undergoes a conformational transition due to pyruvate conversion, which promotes release of the membrane anchor. Additionally, in all three activation modes the exposed membrane anchor is either stabilized by the membrane and mimics thereof or removed due to proteolytic digestion. Which step of *Ec*POX catalysis constitutes the initial signal for displacement of the membrane anchor was further investigated by limited proteolysis [29] [18] [35].

1.2.4 Limited proteolysis of *Ec*POX

Limited proteolysis of *Ec*POX is an artificial process exclusively observed *in vitro* and has no relevance for *Ec*POX functionality *in vivo* [32]. However, it is often used to investigate the activation of *Ec*POX since proteolytically truncated enzyme and lipid-activated *Ec*POX show similar catalytic enhancements [18]. With the help of substrate surrogates, cofactor analogs and artificial reduction by sodium dithionite the step of the catalytic mechanism, which controls fundamental membrane anchor release, was identified.

Flavin reduction is the initial signal for membrane anchor exposure

Proteolytic digestion of *Ec*POX was detailed investigated in the past [29] [18] [35] [37]. All findings are summarized in a figure from Neumann and Weidner *et al.* who analyzed *Ec*POX fragments derived from proteolytic cleavage by gel electrophoresis (figure 4 A) [35].

It was demonstrated that in the absence of pyruvate *Ec*POX is cleaved at its C-terminal end into a non-active Δ101 variant and the beta-peptide (101 amino acids). Contrary, incubation with pyruvate prior to protease addition leads to the formation of catalytically activated *Ec*POX Δ23 and the C-terminal alpha-peptide (23 amino acids).

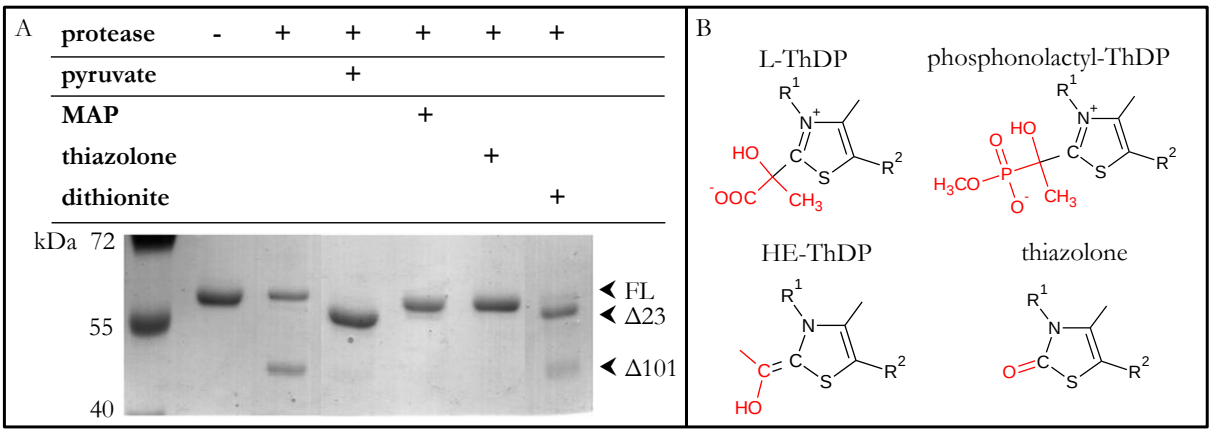

figure 4: A: SDS-PAGE analysis of proteolytic digestion of *Ec*POX. 3 mg/mL (51 µM active sites) *Ec*POX wt were subjected to proteolytic digestion (+) with alpha-chymotrypsin (20 µg/ml): in the absence of substrate (resting state), in the presence of pyruvate (200 mM), after reaction with 20 mM MAP, reconstituted with 100 µM thiamin thiazolone diphosphate, after artificial reduction with 290 µM sodium dithionite under anaerobic conditions. **B: Structures of ThDP intermediates of the catalytic cycle of *Ec*POX and mimics thereof.** L-ThDP and its related substrate surrogate-ThDP complex phosphonolactyl-ThDP. HE-ThDP and the corresponding ThDP analog thiamine thiazolone. R^1 and R^2 represent the aminopyrimidine ring and diphsophate anchor, respectively. Figure A was taken from Neumann and Weidner *et al.* [35] and modified.

The first step of the catalytic cycle can de simulated by incubation of *Ec*POX with the pyruvate analogue methyl acetyl-phosphonate (MAP) (figure 4 B). Similar to pyruvate MAP covalently binds to ThDP yielding a phosphonolactyl-ThDP adduct which mimics the pre-decarboxylation intermediate L-ThDP. Since the phosphonate moiety of MAP cannot be cleaved off in contrast to the carboxylic function of pyruvate MAP is a potent, covalent and competitive inhibitor. After addition of MAP and alpha-chymotrypsin *Ec*POX remains in the uncleaved form indicating that both cleavage sites leading to *Ec*POX Δ101 or Δ23 are protease-protected. Further, thiamine thiazolone (a structural mimic of the HE-ThDP

intermediate) was used instead of thiamine to simulate the post-decarboxylation intermediate (figure 4 B). In this case, both cleavage sites are also inaccessible.

Remarkably, artificial reduction of the flavin by sodium dithionite is sufficient to induce a conformational change which leads to exposure of the activating Δ23 cleavage site even in the absence of reactions at the thiamine cofactor. However, also slight amounts of *Ec*POX Δ101 can be detected which implies that protection of the inactivating restriction site is not complete in the artificially reduced enzyme.

A minimal model comprises three conformations of *Ec*POX

Combining the obtained results, a minimal model of three different *Ec*POX conformations can be created (figure 5).

- In the resting state (R) the alpha-peptide is bound to the protein which results in protection of the Δ23 cleavage site (*Ec*POX Y549-M550). Contrary, the Δ101 restriction site (*Ec*POX K471-A472) is accessible and the beta-peptide can be truncated by the protease.
- The substrate-bound state (SB) resembles the formation of covalent ThDP intermediates, while the flavin cofactor is still in the oxidized state. These intermediates induce a first structural change leading to protection of both cleavage sites and thus to attachment of both alpha- and beta-peptide segments.
- The substrate-reduced state (SR) is induced by electron transfer to FAD which initiates a second conformational switch. In this state the beta-peptide part is protein-bound resulting in an inaccessible Δ101 cleavage site, whereas the exposed alpha-peptide part leads to accessibility of the Δ23 cleavage site.

Although these three conformations of *Ec*POX can be fairly characterized by proteolysis studies, the underlying molecular mechanism which controls the conformational changes is still unknown. Especially amino acid residues which sense the different structural states or which are involved in their interconversion were unknown. New insights into the activation mechanism gave the crystal structures of full-length and proteolytically activated *Ec*POX Δ23, which were solved recently [35].

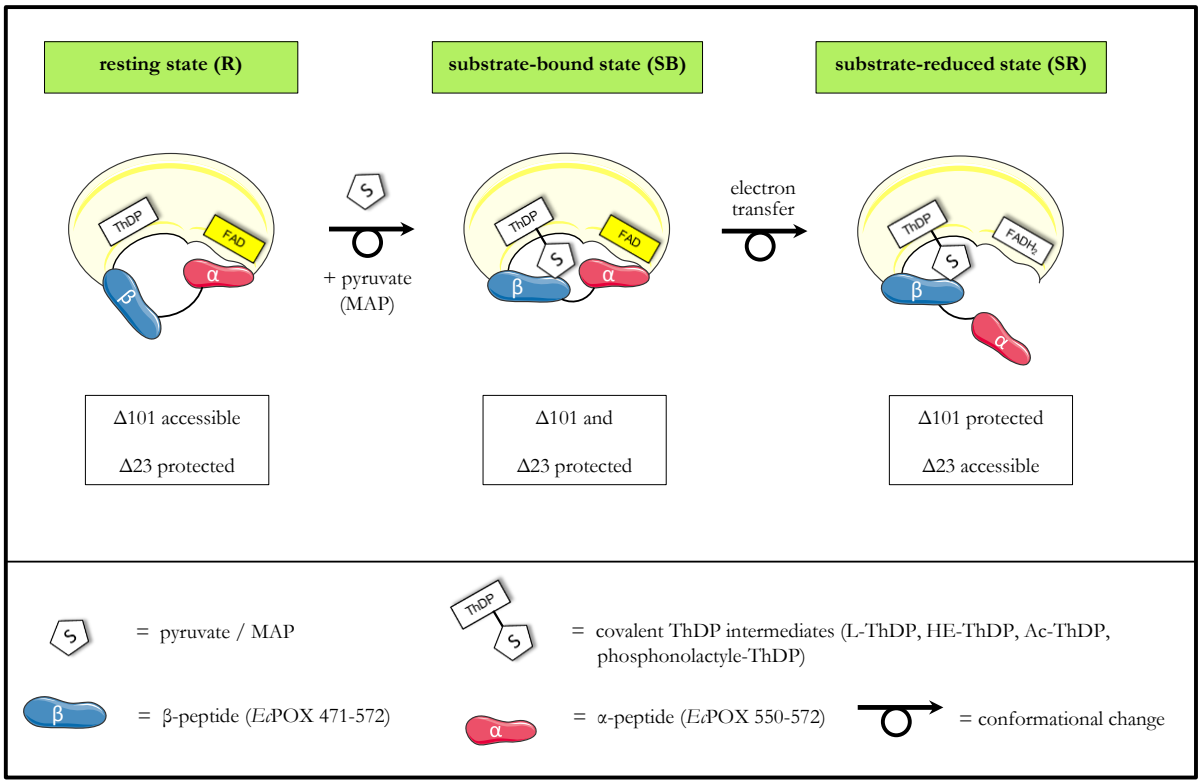

figure 5: Minimal model of *Ec*POX conformations. In the **resting state (R)** the Δ101 cleavage site is accessible whereas the Δ23 restriction site is protected. The **substrate-bound state (SB)** is induced by formation of covalent ThDP-intermediates, while FAD remains unaffected. Both protease cleavage sites are protected. The **substrate-reduced state (SR)** is formed due to reduction of FAD. While the Δ101 cleavage site remains inaccessible, the Δ23 restriction site is exposed. The functional tetramer of *Ec*POX is simplified illustrated as monomer for better visualization. Note that the alpha-peptide is displayed separately from the beta-peptide, although the alpha-peptide resembles the C-terminal part of the beta-peptide.

1.2.5 X-ray structures of *Ec*POX

In 2008 Neumann and Weidner *et al.* succeeded in solving the crystal structure of pyruvate oxidase from *E. coli* [35]. Since it is a peripheral membrane protein it was remarkable that full-length enzyme could be crystallized with the complete membrane anchor in absence of any hydrophobic or amphiphilic additives. Additionally, the structure of the proteolytically activated form *Ec*POX Δ23, which typically mimics the membrane-bound state of *Ec*POX, was determined. This allowed a direct comparison and gave new insights into the mechanism of *Ec*POX activation.

The global structure of *Ec*POX consists of 4 domains

The resting-state enzyme crystallized in tetragonal space group $P4_32_12$ with half of the tetramer per asymmetric unit (figure 6 A). The cofactors thiamine diphosphate and FAD are located at the subunit interface of a catalytically active dimer implying that the resulting active sites are composed of amino acid residues originating also from two subunits. All residues are resolved and only a loop of 12 amino acids (residues 466-478) shows poor density indicating higher flexibility of this part.

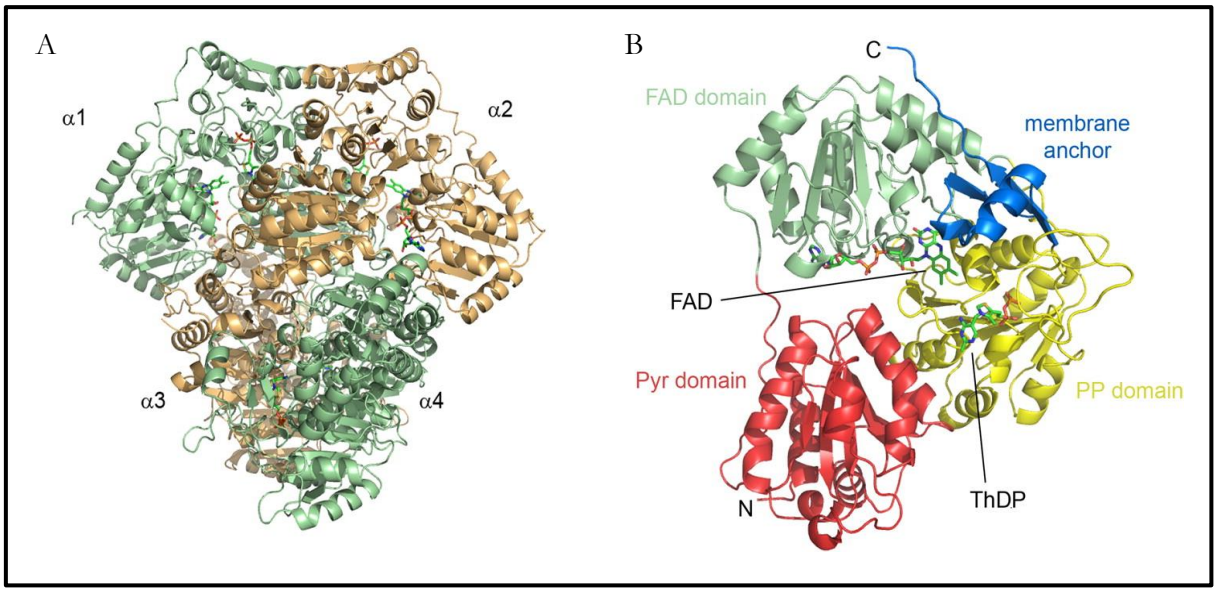

figure 6: Structure of full-length *Ec*POX. A: Structure of the tetramer. Cofactors are shown in stick representation and highlight the position of the active sites at the subunit interface. The catalytic active dimers (α1-α2 and α3-α4) are colored in orange and green. B: Domain structure of an *Ec*POX monomer. The four domains are displayed in different colors. Cofactors ThDP and FAD are presented in stick format. Figures were taken from Neumann and Weidner *et al.* [35].

A monomeric structure consists of 3 domains (figure 6 B) also found on other thiamine enzymes [38] [21]. The Pyr domain (residues 2-172) harbors the pyrimidine moiety of the ThDP cofactor, whereas the PP-binding domain (residues 358-530) is responsible for binding of the diphosphate anchor of thiamine with the help of a bivalent magnesium ion. The FAD domain (residues 188-323) mediates binding of the flavin cofactor. Interestingly, a fourth domain (531-572) is exclusively found in *Ec*POX which was termed the C-terminal membrane binding region.

The proteolytically activated enzyme crystallizes in orthorhombic space group $P2_12_12_1$ containing three functional tetramers in the asymmetric unit. However, the structure is very similar compared to the enzyme in the resting state. Only slight positional deviations are detected within the active site. The dominant difference is found in the C-terminal membrane binding region. This part is only defined up to Lys539 in *Ec*POX Δ23, although the protease truncates the C-terminus only at Tyr549 implying a less stabilized terminus. Additionally, several residues starting from Glu531 that were previously organized in a beta-sheet in full-length *Ec*POX are now rearranged resulting in an undefined structure (figure 7). Similar to the full-length enzyme the loop from residue 466-477 is found to be highly flexible.

<u>The active site of *Ec*POX favors decarboxylation and electron transfer to FAD</u>

The identical active site of the full-length *Ec*POX is constructed similar to other enzymes of the thiamine family. The cofactor ThDP is bound in its typical V-conformation ensuring spatial orientation of the reactive C2-atom of the thiazolium ring to the pyrimidine 4'-amino function acting as acid/base catalyst [22] [21]. The flavin cofactor is located in close proximity (approximately 12 Å) to the carbon-2 atom of ThDP. The isoalloxazine ring of FAD is bent by 15°, which is suggested to favor the electron transfer reaction since the distortion destabilizes the oxidized form of the flavin [39]. A similar

observation can be made for other flavoenzymes like pyruvate oxidase from *Lactobacillus plantarum* (*Lp*POX) [39] or glucose oxidase from *aspergillus niger* [40]. Additionally, mainly hydrophobic residues are located in the active site which facilitates decarboxylation [41].

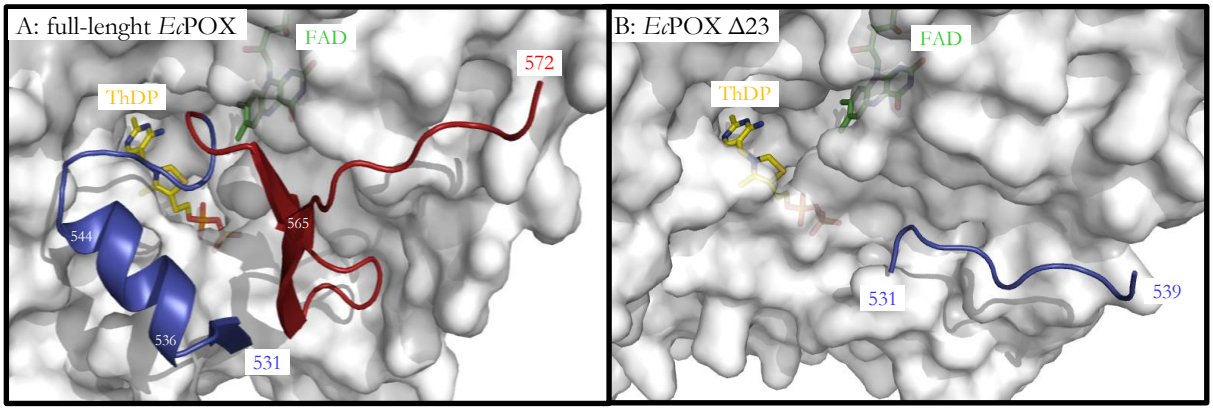

figure 7: Active site accessibility of full-length *Ec*POX and *Ec*POX Δ23. The position of the active site is highlighted by the cofactors ThDP (yellow) and FAD (green) in stick representation. A: full-length *Ec*POX (pdb: 3EY9). The linker region (residues 531-549) of the lipid binding domain is depicted in blue and the alpha-peptide (residues 550-572) is presented in red cartoon format. B: *Ec*POX Δ23. The residual linker domain (residues 531-539) after proteolytic processing is shown in blue.

*Ec*POX Δ23 shows improved accessibility to the active site and can accelerate electron transfer

The main difference between the structure of the full-length protein and the activated form Δ23 is the accessibility of the catalytic center (figure 7). In the resting state, the active site is blocked by a helix (residues 536-544), which is part of the lipid binding domain. Due to truncation this helix is disordered in *Ec*POX Δ23 which provides improved access to the thiamine and flavin cofactor. This observation explains the 8fold decreased K_m for pyruvate due to proteolytic activation (full-length *Ec*POX: K_m = 90 mM, Δ23 = 12 mM) [35] which clearly indicates an increased affinity for the substrate of the proteolytically activated form. Thus, the membrane binding region is proposed to act as autoinhibitory domain in the resting state of the enzyme [35].

Comparison of active site residues of both enzyme species reveals no significant positional differences of central amino acid residues or both cofactors. The only prominent discrepancy is that Phe465, which is located in close proximity to both cofactors in the resting state (approximately 11 Å to C2-atom of ThDP), undergoes a conformational transition upon activation (figure 8). It swings between ThDP and FAD (approximately 6 Å to C2-atom of ThDP) and is suggested to facilitate electron transfer from thiamine to the flavin, which is drastically increased in the proteolytically activated variant (full-length *Ec*POX: $3s^{-1}$, *Ec*POX Δ23: approximately 400 s^{-1}) [42]. This assumption is further supported by structural analysis of related thiamine-dependent flavoenzymes. In constitutively activated pyruvate oxidase from *Lactobacillus plantarum* side chain Phe479 occupies the same position like activated Phe465 in *Ec*POX. Remarkably, acetohydroxyacid synthase from *yeast* contains no corresponding residue at this location and utilizes the redox feature of the flavin only in a minor side reaction [43] [44]. The reorganization of

Phe465 concomitant with an improved electron transfer could also explain the increased catalytic activity upon activation (full-length *Ec*POX: k_{cat} = 7 s^{-1}, *Ec*POX Δ23: k_{cat} = 200 s^{-1}) [35].

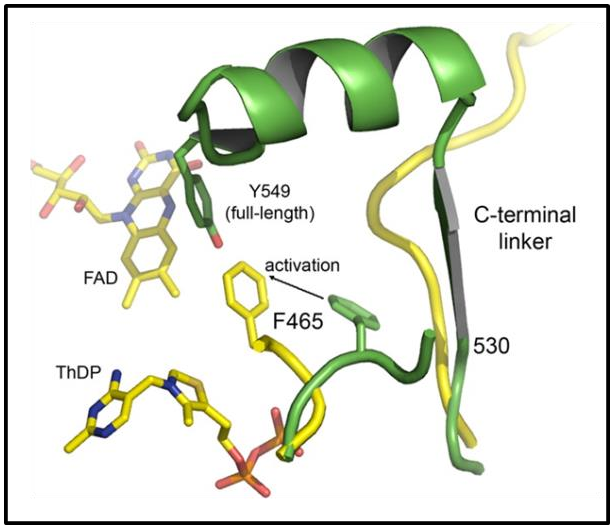

figure 8: Structural transition of *Ec*POX upon proteolytic activation. The resting state of *Ec*POX is depicted in green whereas the structure of *Ec*POX Δ23 is illustrated in yellow. The cofactors ThDP and FAD are highlighted as yellow sticks. Upon proteolytic activation the linker region of the lipid binding domain is rearranged leading to unfolding of the helix (green) and beta-strand motif (gray). Further, F465 is repositioned and swings between both cofactors to facilitate electron transfer from ThDP to FAD. Figure was taken from Neumann and Weidner *et al.* [35].

The full-length enzyme stabilizes the membrane anchor via numerous interactions

As stated earlier, the C-terminal lipid binding domain of *Ec*POX is a unique structural element within thiamine enzymes. It can be divided into a linker region (residues 531-549), which mainly covers the active site, and the alpha-peptide (residues 550-572), which was identified to be the membrane anchor [18] [13, 35]. In the crystal structure of the resting-state enzyme the membrane binding domain is completely traced. Remarkably, the entire domain is attached to the protein surface. At the protein surface of full-length *Ec*POX a four-stranded half barrel structure is formed by beta-strands derived from the PP- and membrane binding domain (residues 531-534, 552-555, 560-565, and 467-469) (figure 9). Additionally, an alpha-helix composed of residues 536-544 can be observed, which is responsible for inaccessibility of the active center. The last 8 amino acids of the C-terminus do not show a defined secondary structure.

Besides the stabilization by the half-barrel motif several interactions support the attachment of the lipid binding domain to the protein surface (figure 9). Gln537 of the N-terminal helix forms a hydrogen bond with Glu564. Further, a kink in the middle of the alpha-peptide is stabilized by an intramolecular hydrogen bond between Asp560 and Ser556. Additionally, the protein core interacts by two prominent salt bridges with the center of the membrane anchor (Asp348-Arg558) and the C-terminal edge (Asp328-Arg572).

All interactions are evenly distributed over the entire membrane binding domain, which ensures comprehensive stabilization in the resting state. However, due to the release of the membrane anchor in response to flavin reduction it is assumed that the anchor undergoes a structural reorganization to facilitate subsequent membrane binding. The conformation of the alpha-peptide competent to bind the membrane was recently investigated by Neumann and Weidner [35] [45].

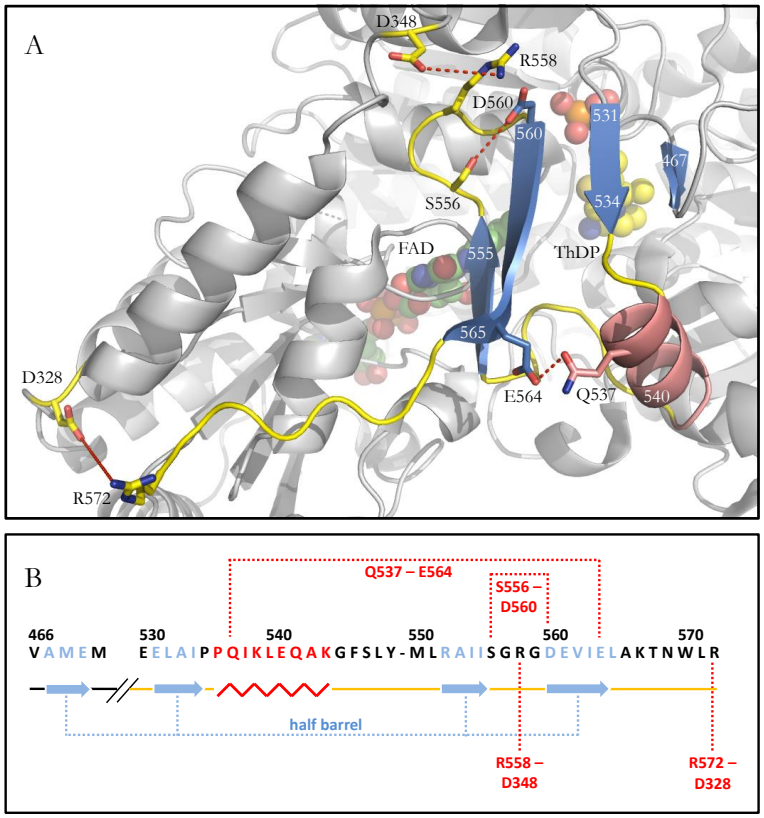

figure 9: Structure of the C-terminal lipid binding domain of full-length *Ec*POX. A: The lipid binding domain is attached to the protein surface of *Ec*POX (gray) and is displayed in cartoon format. The 4-stranded half-barrel motif is highlighted in blue and the alpha-helix of the linker is depicted in pink. The cofactors ThDP and FAD are shown as yellow and green spheres. Three prominent electrostatic interactions and one hydrogen bond, which stabilize the membrane anchor to the protein surface, are indicated as red dashed lines. B: Primary sequence and secondary structure assignments of the lipid binding domain. Beta-strands are presented as blue arrows whereas the alpha-helix is highlighted as red zigzag. Hydrogen bonds and salt bridges of selected residues are indicated by red dashed lines.

1.2.6 Structural analysis of the membrane anchor of *Ec*POX

The crystal structure of the resting-state enzyme reveals that the protein-bound form of the membrane anchor (residues 550-572) shows two beta-strand elements and loop structures (figure 9) [35]. However, it remains to be analyzed how the single peptide can mediate membrane binding of *Ec*POX. Since analysis of the primary amino acid sequence predicts an amphipathic helix conformation for the alpha-peptide part it was suggested that the helical structure resembles the membrane-associated form of the alpha-peptide [29].

This assumption was further proved by Neumann and Weidner who demonstrated that the isolated alpha-peptide adopts a random-like structure if dissolved in buffer (helix content 0 %), but forms an alpha-helix in the presence of SDS micelles (helix content 33 %) [35] [45]. Further studies of the isolated alpha-peptide by liquid-state nuclear magnetic resonance (NMR) spectroscopy supported the previous findings [45]. Here, the structure of the peptide was solved on a molecular level in the presence of deuterated SDS micelles, which can be used to mimic a membrane [46].

The alpha-peptide shows a characteristic asymmetric structure typical for amphipathic helices (figure 10). Polar and negatively charged residues are located at one half of the helical axis whereas hydrophobic amino acids and positively charged side chains contribute to the opposite site. Since the surface of SDS micelles consists of negatively charged sulfate groups it was supposed that the peptide binds to the micelles with the hydrophobic and positively charged face [45]. Noteworthy, the helix is marginally extended and the helical axis is slightly bended. These effects can be related to the high surface curvature and small diameter of 4 nm of SDS micelles [47] [48].

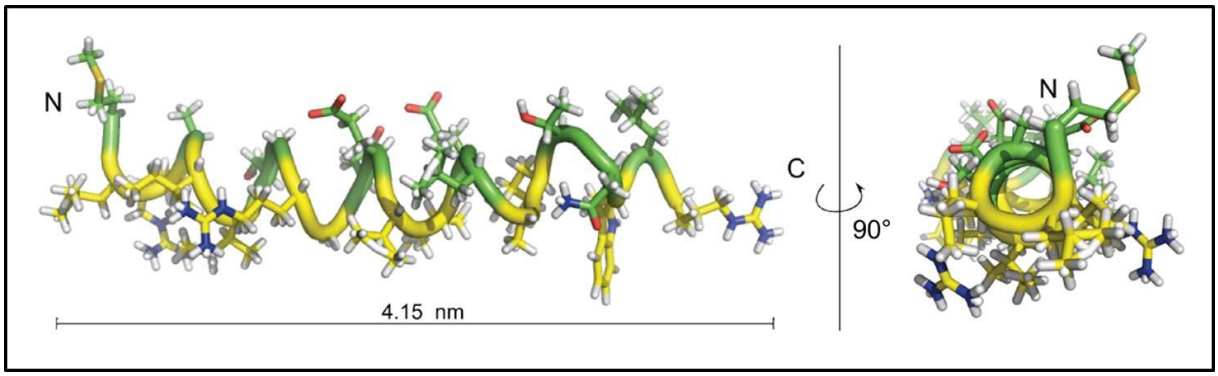

figure 10: Structure of the isolated alpha-peptide in the presence of deuterated SDS micelles. 1 mM of the alpha-peptide was incubated with 150 mM deuterated SDS and analyzed by liquid-state NMR. Yellow color highlights positively charged and hydrophobic residues of one helix site; green color represent negatively charged and hydrophobic amino acids of the opposite face. Figure was taken from Weidner [45].

In summary, the membrane anchor of *Ec*POX can adopt at least two different conformations. The protein-bound form is characterized by beta-strands and loop structures, whereas the membrane-bound peptide (in the presence of SDS micelles) can form an amphipathic helix.

Reversible membrane binding via amphipathic helices is not only observed for *Ec*POX, but it is a common principle of peripheral membrane proteins.

1.2.7 Membrane binding via amphipathic helices

Amphitropic membrane proteins can localize in two compartments

In 1988 Burn described amphitropic proteins to be a new class of membrane proteins [49]. In contrast to traditional integral membrane proteins, localization of amphitropic or peripheral membrane proteins is not restricted to the lipid bilayer since these proteins are also found in the aqueous compartment. Their ability to associate to the membrane is reversible and a subject of regulation [50]. Several peripheral membrane proteins are localized in the aqueous compartment and undergo a conformational transition, which promotes membrane binding [51] [52]. Once attached to the lipid bilayer their catalytic function is often accelerated [53], they assemble with other proteins [54] or have access to lipophilic substrates [55].

Amphipathic helices as membrane binding mediators

A common feature of peripheral proteins to associate to the membrane is via *amphipathic helices*. These helices are characterized by a structural asymmetry with one lipophilic face containing mostly hydrophobic residues and an opposite face harboring polar amino acids [56]. The resulting electrostatic asymmetry allows parallel partition into the bilayer where the hydrophobic part of the helix penetrates the membrane and the polar surface of the helix can interact with lipid head groups and the aqueous compartment [56] [57].

Membrane binding of amphipathic helices requires electrostatic and hydrophobic interactions with the lipids and can be described as a two-step process [50]. First, electrostatic interactions are mandatory to

attract the protein from the bulk solvent and bring it in spatial vicinity to the bilayer surface. Positively charged amino acids contribute to this process [58] [59] which explains the preference of amphipathic helices to bind to anionic phospholipids [56]. The second step includes the integration of the helix into the membrane by hydrophobic contacts [60]. For most peripheral membrane proteins the hydrophobic part is dominant over the electrostatic and thus the driving force for membrane insertion [56].

Interestingly, some amphipathic helices also contain negatively charged amino acids which would lead to unfavored electrostatic repulsion with the negatively charged lipid head groups if the helix is inserted deep enough into the membrane. The detailed function of these residues is questionable so far, but it was reported that they might serve as charge sensor to mediate selectivity [58] [61]. Additionally one can speculate that they are involved in the dissociation process of the helix to ensure reversibility.

Often lipid molecules do not only provide a hydrophobic surface, but they are actively involved in the pivotal structural change of amphipathic helices. Many of these helices are unstructured in an aqueous compartment and undergo a disorder-order transition due to contact with membranes. Therefore, lipids are supposed to either stabilize the amphipathic structure [57] [62] or can actively catalyze the folding process [63].

1.2.8 The electron transfer to Q_8 – a challenging task

The catalytic cycle of *Ec*POX is completed by a final two-electron transfer from the reduced flavin cofactor to Q_8 [17]. However, this redox reaction includes not only simple shuffling of reducing equivalents between donor ($FADH_2$) and acceptor (Q_8), but also translocation of the hitherto cytosolic enzyme to the cell membrane to provide access to Q_8. This is ensured by the alpha-peptide which forms an amphipathic helix in the presence of lipids [35] [45] (chapter 1.2.6). Embedding of this helix into the lipid bilayer shortens the distance between active site-flavin and Q_8. However, detailed insights how the electron transfer reaction proceeds after membrane binding are still missing. According to Forneris and Mattevi two strategies of substrate-binding modes can be discussed for *Ec*POX [64].

Enigma of enzymatic reactions combining hydrophobic and hydrophilic substrates

Forneris and Mattevi described the challenge to enzymes to convert substrates originating from opposite compartments [64]. They mainly focused on different concepts of enzymes which combine catalysis of hydrophilic water with lipophilic substrates dissolved in the cellular membrane. Two interaction modes described by Forneris and Mattevi can also be supposed for *Ec*POX (figure 11):

A: *Desorb-and-modify*. The active site of the protein is located in the aqueous compartment and the lipophilic substrate is extracted from the bilayer by hydrophobic tunnels or cavities. The mechanism of substrate desorption is poorly understood but often the membrane binding mediator of the enzyme is involved.

B: *Working at the interface*. The catalytic center is precisely located at the membrane surface allowing both hydrophobic and hydrophilic substrates to stay in their original environment during catalysis.

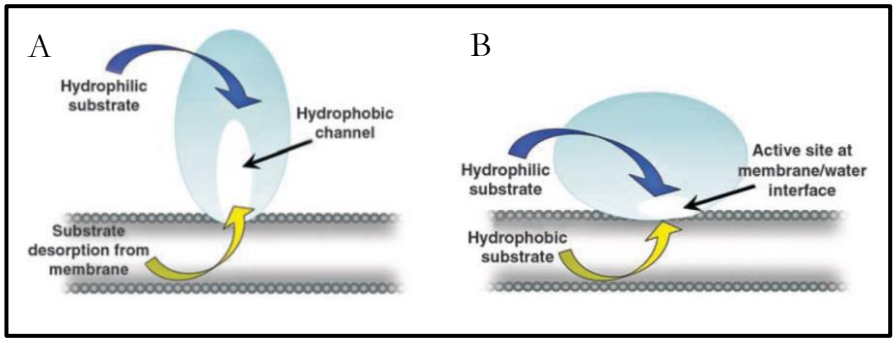

figure 11: Catalytic strategies used by enzymes to convert hydrophobic and hydrophilic substrates. A: Desorb-and-modify. B: Working at the interface. Detailed descriptions are given in the text. Figure was taken from Forneris and Mattevi [64].

Influence of the substrate-interaction mode on the electron transfer of *Ec*POX

Based on the two possible concepts for the interaction of cytosolic *Ec*POX with lipophilic ubiquinone, the mechanism of electron transfer to Q_8 could also be determined. According to *desorb-and-modify*, the benzoquinone moiety of Q_8 could stick partially out of the membrane to enter the active site, whereas the isoprenoid tail is still in contact with the lipid bilayer. Interaction of $FADH_2$ with Q_8 could support a direct electron transfer via tunneling which can be roughly described as a single transfer step (figure 12) [65]. Since electron tunneling rates decrease exponentially with the distance of both redox centers, this mechanism becomes unlikely if an edge-to-edge distance of 14 Å between flavin and the ubiquinone head group is exceeded [66] [67]. The second opportunity, *working at the interface*, would require ubiquinone to stay in the membrane. Here, hopping of electrons from $FADH_2$ to Q_8 has to take place since the active site is not directly located at the membrane-cytosol interface. Hopping can be simplified illustrated as multiple electron transfer steps (or hops) between donors and acceptors (figure 12) [65]. One or more intermediates are involved that transiently stabilize electrons. Therefore, the protein matrix could provide temporary electron storage places. Given that both electrons transfer mechanism from the reduced flavin to Q_8 can occur in *Ec*POX further analysis is required to understand this puzzling process.

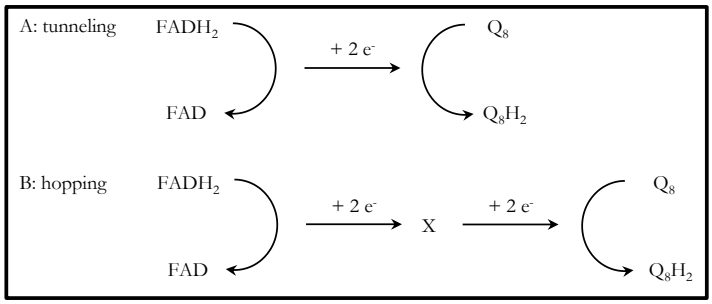

figure 12: Scheme of possible electron transfer mechanisms for *Ec*POX. A: Electron tunneling. Electrons are directly transferred from $FADH_2$ to Q_8. B: Electron hopping. Electrons are transferred by multiple steps from $FADH_2$ to Q_8. X resembles one or more transient intermediates of the process.

1.2.9 *Ec*POX and its reactivity towards oxygen

Since the final catalytic step in *Ec*POX is the electron transfer from reduced flavin to Q_8 and not to oxygen the name "pyruvate oxidase" is misleading. Oxygen can replace the electron acceptor Q_8 just in a minor side reaction in *Ec*POX [45]. Thus, *Ec*POX shares characteristic features of dehydrogensases [68].

Classification of flavoenzymes

Flavoenzymes are ubiquitously distributed and involved in versatile processes like electron transfers [69], dehydrogenations [70], halogenations [71], and even protein folding [72]. According to their reactivity towards oxygen or electron acceptors three groups of flavoenzymes can be distinguished [68] (figure 13):

A: *Dehydrogenases* react slowly or not at all with oxygen and typically regenerate the reduced flavin cofactor by electron transfer to small molecules like ubiquinones.

B: *Oxidases* catalyze rapid electron transfer to oxygen yielding hydrogen peroxide as product.

C: *Monooxygenases* also show fast reaction with oxygen and formation of a stable C4a-peroxyflavin-intermediate. Subsequently, monooxygenases incorporate one oxygen atom into the substrate.

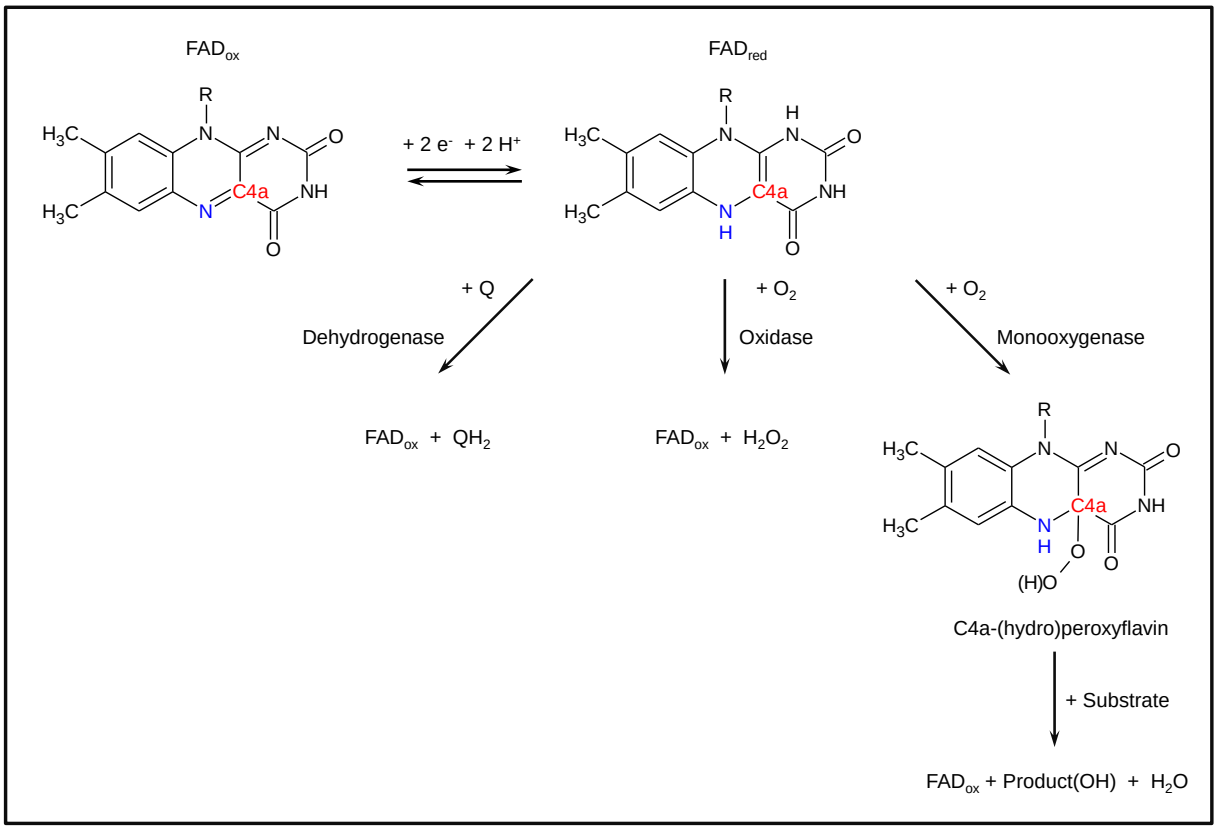

figure 13: Classification of flavoenzymes according to their reactivity towards oxygen. Prior to oxygen reaction the flavin cofactor is reduced during catalysis. Subsequently, dehydrogenases do not react with oxygen but rather reoxidize their flavin using small electron acceptors like ubiquinones (Q). Oxidases utilize oxygen for flavin regeneration yielding hydrogen peroxide. Monooxygenases form a (hydro)peroxyflavin-intermediate with oxygen and subsequently insert one oxygen atom into the substrate leading to water as second product. The N5- and C4a-atom involved in flavin redox reactions are colored red and blue.

Does Tyr278 regulate oxygen reactivity in *Ec*POX?

According to the previously discussed flavoenzyme groups *Ec*POX can be classified as dehydrogenase which utilizes small electron acceptors like quinones for flavin regeneration. Interestingly, pyruvate oxidase from *Lactobacillus plantarum* (*Lp*POX), which is closely related to *Ec*POX, is a functional oxidase [73]. *Lp*POX is also a thiamine-dependent flavoenzyme and utilizes pyruvate as substrate in a similar reaction to *Ec*POX (figure 14 A and figure 41) [74]. However, the energy-conserving step in *Lp*POX is the formation of high-energy acetyl phosphate. The two arising reducing equivalents are only transferred to oxygen yielding hydrogen peroxide as waste product [75]. The product acetyl phosphate is further utilized by substrate-level phosphorylation to generate ATP since *Lactobilli* contain no respiratory chain in contrast to *Enterobacteria* [76].

Since both enzymes have similar catalytic sites the question arises how each enzyme promotes its individual catalytic reaction in a similar constructed environment. Comparison of the catalytic centers reveals that a central difference is observed near the reactive N5- and C4a-atom of the flavin cofactor. While *Ec*POX contains Tyr278 at this position, Phe289 is found in *Lp*POX (figure 14 B). One can speculate that Tyr278 suppresses oxidase activity in *Ec*POX since it is positioned to effectively shield the N5-position of the flavin cofactor against oxygen attack. This idea is supported by other reports about flavoenzymes which showed that particularly the local environment and access to the reactive N5-locus controls reactivity with oxygen [77] [78].

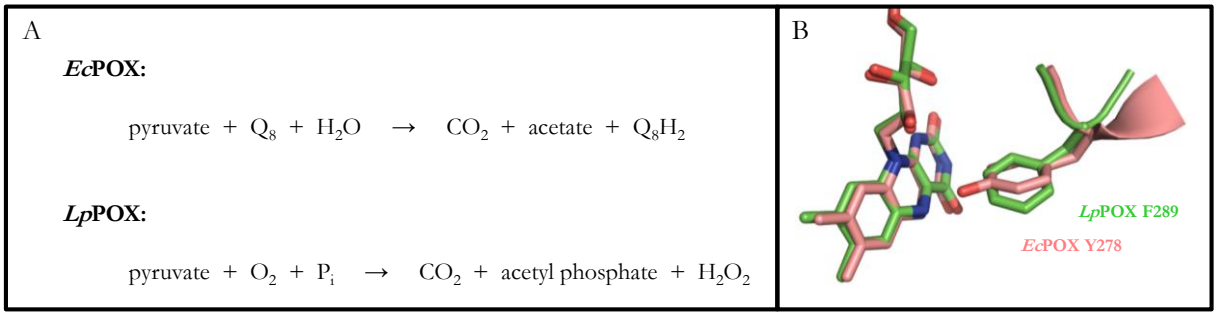

figure 14: Comparison of *Ec*POX and *Lp*POX. A: Net reactions of *Ec*POX and *Lp*POX. Both enzymes catalyze the oxidative decarboxylation of pyruvate. However, they differ in the energy-conserving step which is the reduction of Q_8 for *Ec*POX and the formation of acetyl phosphate for *Lp*POX. B: Selected amino acids near flavin N5- and C4a-atom of *Lp*POX and *Ec*POX. Structures of *Ec*POX wt (pdb: 3EY9) and *Lp*POX wt (unpublished high-resolution structure at 1.09 Å, friendly provided by Dr. Danilo Meyer, Department of Bioanalytics, Göttingen) were aligned at the N5- and C4a-atom.

2. Motivation

Aim of this thesis is to elucidate the molecular mechanism which controls activation and membrane binding of the peripheral membrane protein pyruvate oxidase from *E. coli* (*Ec*POX). Activation of *Ec*POX is initiated by reduction of the flavin cofactor at elevated concentrations of pyruvate. This induces cytosolic exposure of the hitherto protein-associated membrane anchor and triggers membrane binding. Association to the lipid bilayer promotes accessibility to Q_8 and accelerates the catalytic activity of *Ec*POX by several orders of magnitude. To analyze the activation and subsequent membrane binding process of *Ec*POX four main topics are addressed in this thesis:

1. How is the initial signal for membrane anchor release perceived and how is this information transferred from the reduced flavin cofactor at the active site to the membrane anchor at the protein surface?

This question should be answered by a detailed structural and mechanistic analysis of the protein variants Y278F, F465A, Y549A and F260A (figure 15 A). Tyr278 could sense the redox state via a hydrogen bond to the redox-active N5-atom of the flavin. Phe465 swings between both cofactors due to proteolytic activation and facilitates electron transfer to FAD. In cooperation with Tyr549 Phe465 is suggested to initiate membrane anchor exposure since the activated conformation of Phe465 would clash with Tyr549. This might lead to repulsion of Tyr549 out of the active site and subsequent destabilization of the entire membrane anchor. A similar function can be supposed for Phe260 which shows an alternative conformation after proteolytic digestion. Interconversion between both orientations would collide with Ile554 and Leu565 of the membrane anchor which might promote membrane anchor release (figure 15 A).

2. How is the membrane anchor stabilized at the protein surface and in the membrane-bound form?

To study this topic the following variants should be generated: 3x (D328A, D348A, Q537A), F260A, I554A/G, L565A/G, W570A/G and the double mutant 2G (I554G, L565G). While the triple mutant 3x lacks electrostatic interactions and hydrogen bonds to the membrane anchor (figure 15 B), the other variants show decreased hydrophobic contacts (figure 15 C and D). Note that amino acid exchanges of *Ec*POX 3x and F260A change the protein part, while I554A/G, L565A/G, 2G and W570G alter the primary sequence of the membrane anchor itself.

Additionally, the structural determination of the isolated membrane anchor (alpha-peptide) in the presence of different membrane mimics and compositions should be examined by far-UV CD spectroscopy and NMR spectroscopy.

3. How are the electrons transferred from the reduced flavin cofactor to membrane-dissolved Q_8?

A direct interaction of Q_8 with the active site of *Ec*POX should be elucidated by X-ray crystallography of an *Ec*POX Δ23:ubiquinone complex.

4. How can the protein matrix of *Ec*POX suppress unfavored electron transfer to oxygen?

Tyr278 is predicted to prevent oxygen reactivity of *Ec*POX by its interaction with the reactive N5- and C4a-locus of FAD. Reciprocal mutations of *Ec*POX (Y278F) and *Lp*POX (F289Y), an enzyme which utilizes oxygen as substrate, should prove this hypothesis (figure 14).

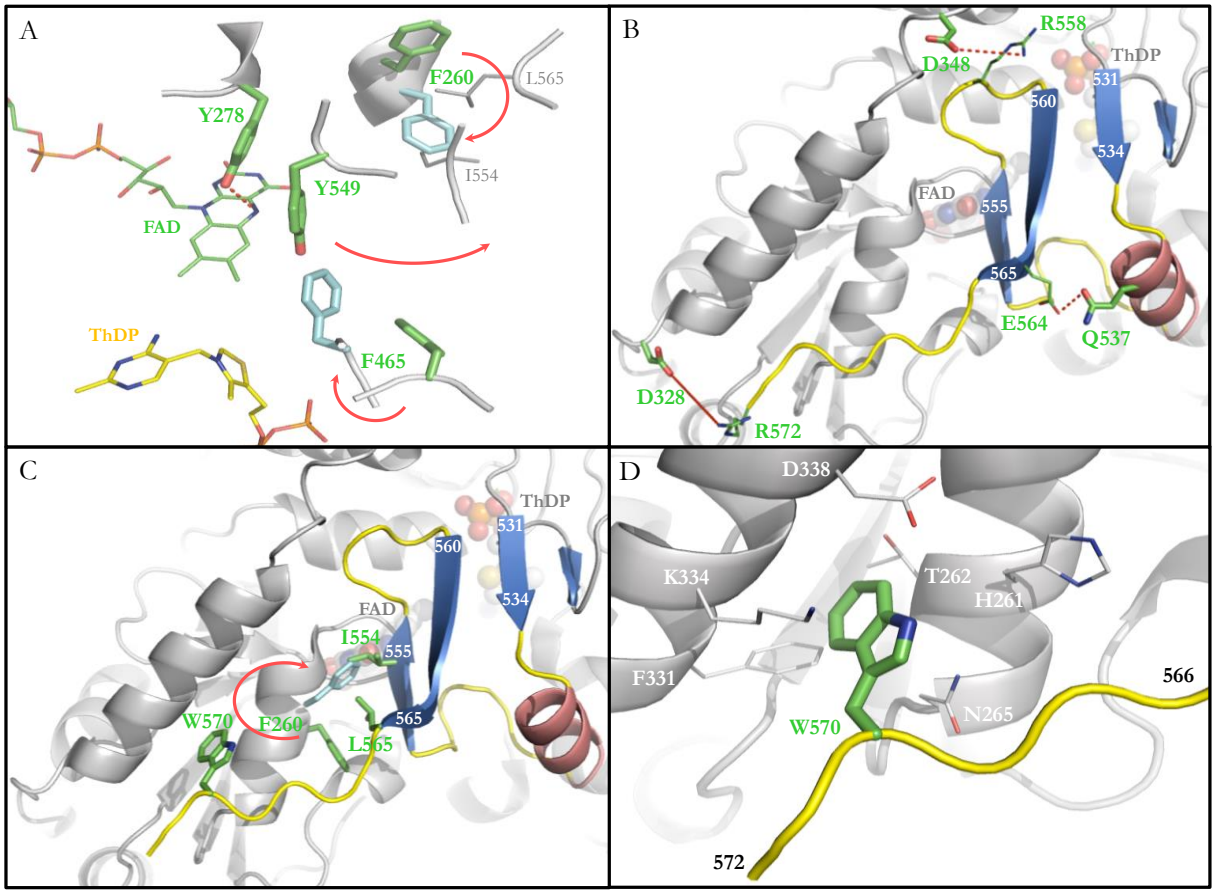

figure 15: Active site rearrangements during proteolysis and potential interactions of the membrane anchor with the protein surface of *Ec*POX. The entire membrane binding domain is represented as colored cartoon where beta-strands are shown in blue and the alpha-helix is depicted in red. The cofactors ThDP and FAD are either presented as yellow and green lines (A) or shown as gray spheres (B-D) and highlight the active site. Conformational changes due to proteolytic activation are indicated by red arrows.
A: Active site rearrangements due to proteolytic activation. Amino acids potentially involved in the signal transfer process are shown as green (resting-state *Ec*POX) and blue (Δ23) sticks. A hydrogen bond between Y278 and N5-flavin is indicated as red dashed line. B: Membrane anchor stabilization at the protein. The alpha-peptide is stabilized at the protein by two salt bridges (D328-R572 and D348-R558) and one hydrogen bond (E564-Q537) indicated as red dashed lines. Central amino acids of the protein surface are shown as green sticks whereas interaction partners of the membrane anchor are presented as green lines. C: Potential hydrophobic interactions of the membrane anchor with the protein surface. Central amino acids are shown as green (resting-state *Ec*POX) and blue (Δ23) sticks. D: The pocket which stabilizes W570 (green sticks) at the protein surface is composed of charged, polar and hydrophobic residues (gray lines).

3. Materials and Methods

Media, buffers, and solutions were prepared with double-deionized water. All chemicals used in this thesis were assigned to be of highest purity.

3.1 Chemicals

acetic acid	Carl Roth GmbH & Co. KG, Karlsruhe
acetonitrile (HPLC gradient grade)	Fischer Scientific UK Ltd., Loughborough
acrylamide (30 %) 37.5:1	Carl Roth GmbH & Co. KG, Karlsruhe
agar-agar	AppliChem GmbH, Darmstadt
albumin fraction V	AppliChem GmbH, Darmstadt
ammonium chloride	Carl Roth GmbH & Co. KG, Karlsruhe
^{15}N-ammonium chloride (99 %)	Euriso-Top, Saint-Aubin Cedex
ammonium peroxodisulfate	Carl Roth GmbH & Co. KG, Karlsruhe
ammonium sulfate	Carl Roth GmbH & Co. KG, Karlsruhe
ampicillin	AppliChem GmbH, Darmstadt
aprotinin	AppliChem GmbH, Darmstadt
beta-mercaptoethanol	Carl Roth GmbH & Co. KG, Karlsruhe
BME vitamins 100x solution	Sigma-Aldrich Chemie GmbH, Munich
bromophenol blue	AppliChem GmbH, Darmstadt
BugBuster master mix	Merck KGaA, Darmstadt
calcium chloride dihydrate	Carl Roth GmbH & Co. KG, Karlsruhe
coomassie brilliant blue G250	AppliChem GmbH, Darmstadt
2,6-dichlorphenolindophenol	Merck KGaA, Darmstadt
dithiothreitol	AppliChem GmbH, Darmstadt
n-dodecyl phosphocholine (DPC)	Avanti Polar Lipids, USA
ethylene glycol	Sigma-Aldrich Chemie GmbH, Munich
flavin adenine dinucleotide (FAD)	Sigma-Aldrich Chemie GmbH, Munich
flavin mononucleotide (FMN)	Sigma-Aldrich Chemie GmbH, Munich
D(+)-glucose	AppliChem GmbH, Darmstadt

^{13}C- D(+)-glucose (99 %)	Euriso-Top, Saint-Aubin Cedex
glycerole	AppliChem GmbH, Darmstadt
hexylene glycol (MPD)	Sigma-Aldrich Chemie GmbH, Munich
imidazole	AppliChem GmbH, Darmstadt
isopropyl β-D-thiogalactopyranoside (IPTG)	AppliChem GmbH, Darmstadt
kanamycine sulfate	Carl Roth GmbH & Co. KG, Karlsruhe
D(+)-lactose	AppliChem GmbH, Darmstadt
magnesium sulfate (heptahydrate)	Carl Roth GmbH & Co. KG, Karlsruhe
methanol	Sigma-Aldrich Chemie GmbH, Munich
polyethylene glycole 2000 (PEG 2000)	Merck KGaA, Darmstadt
potassium dihydrogen phosphate	Carl Roth GmbH & Co. KG, Karlsruhe
potassium hexacyanoferrate (III)	Riedel de Haën, Seelze
potassium pyruvate	Sigma-Aldrich Chemie GmbH, Munich
protamine sulfate	Sigma-Aldrich Chemie GmbH, Munich
sodium chloride	Carl Roth GmbH & Co. KG, Karlsruhe
sodium dihydrogen phosphate dihydrate	Carl Roth GmbH & Co. KG, Karlsruhe
sodium dodecyl sulfate (SDS)	AppliChem GmbH, Darmstadt
sodium hydroxide	AppliChem GmbH, Darmstadt
streptomycin sulfate	AppliChem GmbH, Darmstadt
tetramethylethylenediamine (TEMED)	Carl Roth GmbH & Co. KG, Karlsruhe
thiamine diphosphate	Sigma-Aldrich Chemie GmbH, Munich
thiamine hydrochloride	AppliChem GmbH, Darmstadt
trifluoroacetic acid (HPLC grade) (TFA)	AppliChem GmbH, Darmstadt
2,2,2-trifluoroethanol	Carl Roth GmbH & Co. KG, Karlsruhe
tryptone	AppliChem GmbH, Darmstadt
ubiquinone-0, ubiquinone-1, ubiquinone-2	Sigma-Aldrich Chemie GmbH, Munich
yeast extracts	AppliChem GmbH, Darmstadt

3.2 Proteins and Enzymes

alpha-chymotrypsin (from bovine pancreas, 1600 U/mg)	AppliChem GmbH, Darmstadt
DNase I (5811 U/mg)	AppliChem GmbH, Darmstadt
Dpn I (10 U/µL)	Fermentas, St. Leon-Rot
glucose oxidase (from *Aspergillus niger*, 17300 U/g)	Sigma-Aldrich Chemie GmbH, Munich
lysozyme (25000 U/mg)	AppliChem GmbH, Darmstadt
Phusion F-530S (2 U/µL)	Thermo Scientific GmbH, Schwerte
SUMO-protease (16.1 µM)	friendly provided by Dr. Stefan Lüdtke

3.3 Devices

Centrifuges:	Universal 320R	Hettich AG, Bach, Switzerland
	AvantiJ-30I	Beckmann Coulter GmbH, Krefeld
	AvantiJ-20XPI	Beckmann Coulter GmbH, Krefeld
	Biofuge Pico	UniEquip GmbH, Martinsried
Chirascan	CD spectrometer	Applied Photophysics Ltd., UK
Electrophorese device, EV 231		Consort nv, Belgium
Electroporator, MicroPulser electroporator		Bio-Rad Laboratories GmbH, Munich
FPLC-Systems: ÄKTA*prime* plus, ÄKTA*purifier*		GE Healthcare
HPLC-System:	DG-2080-54 4-line degasser, LC-Net II/ADC, PU-2086 Plus intelligent prep. Pump, UV-2077 4-λ Plus intelligent UV-Vis detector	Jasco, Gross-Umstadt
	Rheodyne 7725(i) manuel sample injector	IDEX Health & Science, USA

Incubation shaker, Unitron	Infors AG, Bottmingen, Switzerland
ITC-System, ITC200	GE Healthcare
Lyophilizer Lyovac GT3	Lyotech, Griesheim
Microfluidizer, M-110S Small Volume Pneumatic	Microfluidics (Division of MFIC Corp.), USA
Nanodrop 2000	Thermo scientific
pH electrode	Mettler Toledo, Gießen
SX.20 Stopped-flow spectrometer	Applied Photophysics Ltd., UK
Thermoblock, Digital Dry Bath 3721D	Fisher Bioblock Scientific, UK
Thermocycler, TProfessional Standard 96 well Gradient	Whatman BiometraR, Göttingen
X-ray: MM-007 rotating-anode generator, Micromax 007- HF X-stream 2000, R-AXIS IV++ imaging-plate system	Rikagu Corp., USA
UV-Vis Spectrometer, V-650	Jasco GmbH, Groß-Umstadt

3.4 Commodities and Columns

Columns: HiLoad Superdex 200 (16/60, 120 mL), HiLoad Q-Sepharose (26/10, 50 mL), HisTrap FF (5 mL), HiTrap Desalting (5 mL)	GE Healthcare, Solingen
Nucleosil C_{18} 120-5, 250 x 2 mm, Nucleosil C_{18} 120-5, 250 x 4 mm	Macherey & Nagel, Düren
Crystallization cover plates, 18 mm	VWR International GmbH, Darmstadt
Crystallization plates (24 well), costar	Corning, Inc., USA
Vivaspin 20 MWCO 50 and 10	Sartorius, Göttingen
Vivaspin 20 diafiltration cups	Sartorius, Göttingen

3.5 *E. coli* strains

The following *E. coli* strains were used for plasmid amplification or protein expression (table 1). *E. coli* strain C600 contained an additional plasmid pFDX500Δdra, which encodes for the lac-repressor with an additional kanamycin resistance [79].

table 1: *E. coli* strains used in this thesis.

***E. coli* strains**	**genotype**	**source**
***E. coli* ZK126**	F- *W3110 tna2 ββa ⊿lac U169*	Prof. Dr. R. Kolter, USA
***E. coli* BL 21 (DE3)**	F- *ompT gal dcm lon hsdS$_B$ (r_B^- m_B^-) λ(DE3 [lacI lacUV5-T7 gene 1 ind1 sam7 nin5])*	Novagen, USA
***E. coli* XL-1 blue**	F'*endA1 gyrA96(nal^R) thi-1 recA1 lac glnV44 [::Tn10 pro AB$^+$ lacI^q ⊿(lacZ)M15] hsd*R17(r_K^- m_K^+)	Stratagene, USA
***E. coli* C600**	F- *glp*R200(*glp^c*) *thiE1 thr-1 leuB6*(Am) *lacY1 glnV44*(AS) *rfbC1 fhuA21 λ-*	Stratagene, USA

3.6 Plasmids

The following plasmids were used for protein expression as well as templates for site-directed mutagenesis (table 2). The *poxB* gene encoding for *Ec*POX wt was located on the pYYC102 plasmid. *Lp*POX was expressed or mutated using the vector pBP 200. Expression of the isolated alpha-peptide was performed as SUMO (small ubiquitin-like modifier) fusion construct using the pET SUMO-alpha plasmid.

table 2: Vectors used in this thesis.

plasmid	**characteristics**	**resistance**	**source**
pYYC102	*poxB* gene encodes for *Ec*POX expression	ampicillin^R	friendly provided by Prof. Dr. John E. Cronan, USA
pET SUMO-alpha	expression of SUMO-alpha fusion construct	kanamycin^R	friendly provided by Dr. Annett Weidner, Martin-Luther-University Halle-Wittenberg [45]
pBP 200	Expression of *Lp*POX	ampicillin^R	friendly provided by Dr. Danilo Meyer, Georg-August-University Göttingen [80]

3.7 Site-directed mutagenesis

To introduce specific amino acid exchanges within the sequence of *Ec*POX and *Lp*POX, site-directed mutagenesis was used. Variants were generated according to the QuikChange-Kit (Stratagene, USA) with oligonucleotides containing the mutated nucleotides (table 3, synthesized at Sigma Aldrich). Based on the native sequence mutations were introduced using polymerase chain reaction following the protocol of the Phusion F-530S polymerase (Thermo Scientific, Schwerte). Double and triple variants were generated starting with a single or double mutated plasmid as template. Plasmid pYYC102 F465A encoding for the variant *Ec*POX F465A was friendly provided by Dr. Annett Weidner (Martin-Luther-University Halle-Wittenberg [45]).

table 3: Oligonucleotides used in this thesis. Underlined codons resemble the substituted amino acids.

oligonucleotide	sequence 5' → 3'
***Ec*POX D328A forward**	GGAAGAAAAAGCCGCTCGCAAGTTTCTG
***Ec*POX D328A reverse**	CAGAAACTTGCGAGCGGCTTTTTCTTCC
***Ec*POX D348A forward**	CGCAAAGGGCTGGACGCTTTAGCTAAACC
***Ec*POX D348A reverse**	GGTTTAGCTAAAGCGTCCAGCCCTTTGCG
***Ec*POX Q537A forward**	GTTAGCCATTCCACCGGCGATCAAACTCG
***Ec*POX Q537A reverse**	CGAGTTTGATCGCCGGTGGAATGGCTAAC
***Ec*POX F260A forward**	CGGCTTCTCGTCAGGTGCCCATACCATGATG
***Ec*POX F260A reverse**	CATCATGGTATGGGCACCTGACGAGAAGCCG
***Ec*POX L565A forward**	GGTGATGAAGTGATCGAAGCGGCGAAAACAAAC
***Ec*POX L565A reverse**	GTTTGTTTTCGCCGCTTCGATCACTTCATCACC
***Ec*POX L565G forward**	GGTGATGAAGTGATCGAAGGGGCGAAAACAAAC
***Ec*POX L565G reverse**	GTTTGTTTTCGCCCCTTCGATCACTTCATCACC
***Ec*POX I554A forward**	ATGCTGCGCGCAGCCATCAGCGGACG
***Ec*POX I554A reverse**	CGTCCGCTGATGGCTGCGCGCAGCAT
***Ec*POX I554G forward**	ATGCTGCGCGCAGGCATCAGCGGACG
***Ec*POX I554G reverse**	CGTCCGCTGATGCCTGCGCGCAGCAT
***Ec*POX Y549A forward**	GGCCAAAGGTTTCAGCCTGGCGATGCTGC
***Ec*POX Y549A reverse**	GCAGCATCGCCAGGCTGAAACCTTTGGCC
***Ec*POX W570G forward**	CGAAAACAAACGGGCTAAGGTAGAGC
***Ec*POX W570G reverse**	GCTCTACCTTAGCCCGTTTGTTTTCG
***Ec*POX Y278F forward**	CACGCAATTTCCCTTCCGCGCCTTC
***Ec*POX Y278F reverse**	GAAGGCGCGGAAGGGAAATTGCGTG
***Lp*POX F289Y forward**	GGTAATAATTATCCGTATGCAGAAGTTTCCAAAGC
***Lp*POX F289Y reverse**	GCTTTGGAAACTTCTGCATACGGATAATTATTACC
***Ec*POX sequencing 1 reverse**	GCCGTTGATTAAGTGCAGGT
***Ec*POX sequencing 2 forward**	GTCTTAATCGCATGGGCACCAT
***Ec*POX sequencing 3 forward**	TGCGCGGTAAAGAACATGTC
***Ec*POX sequencing 4 forward**	TCTCAGTAGTGCAGATGAAA
***Lp*POX seq 1369-1389 forward**	TTGGCGACGCAAGTTCAATAC
***Lp*POX seq 866-885 forward**	TTGCAGAAGTTTCCAAAGCG
***Lp*POX seq 567-589 forward**	TCAAACGCCGTTATTACCAGAAC
***Lp*POX seq 251-273 forward**	GACCTGGTGGCACTCATCTTATG
***Lp*POX seq 505-522 reverse**	CCATGGTAAATCGACTGG
SUMO-alpha sequence reverse	AGCTAGTTATTGCTCAGCGG

After the mutagenesis reaction the template plasmid was digested using Dpn I (10 U/µl, overnight at room temperature). The PCR product was transformed into competent *E. coli* XL-1 blue cells via electroporation [81]. Clones containing the mutated plasmid were selected on LB-agar plates

supplemented with the corresponding antibiotics. Plasmid DNA was isolated from an overnight culture of transfected *E. coli* XL-1 blue cells using the Qiaprep Spin Miniprep Kit (Qiagen, Hilden). Successful introduction of mutations was verified by DNA sequencing at SEQLAB (SEQLAB Sequence-Laboratories GmbH, Göttingen). Plasmids with the correct mutations were finally transformed into electrocompetent *E. coli* cells (*E. coli* ZK126 cells for *Ec*POX, *E.coli* C600 cells for *Lp*POX).

3.8 Expression of *Ec*POX

*Ec*POX wt and variants were expressed in *E. coli* ZK126 cells with the plasmid pYYC102 as already described [82]. Using this plasmid protein expression was auto-induced by rpoS gene encoded σ^S-factor, a growth factor which is expressed in the early stationary phase. Therefore, an overnight pre-culture was used to inoculate 6 x 1 L LB-media (10 g/L tryptone, 5 g/L yeast extract, 5 g/L NaCl, 100 mg/L ampicillin) to an OD_{600} of 0.1. Cells were grown at 37 °C and 200 rpm and harvested by centrifugation (4000 x g, 4 °C, 30 min) after 16-20 hours. The cells were flash-frozen with liquid nitrogen and stored at - 20 °C. 20-30 g cells were obtained from 6 L media.

3.9 Purification of *Ec*POX

*Ec*POX wt and variants were purified according to an already established protocol [82] with slight modification. Usually, 10 g cells were resuspended in 30 mL low salt buffer (20 mM KH_2PO_4 pH 6.5) supplemented with 100 µM FAD and disrupted by three passages through a microfluidizer. Cell debris was removed by centrifugation (70000 x g, 8 °C, 30 min). 0.5 % (w/v) streptomycin sulfate was added to the supernatant and incubated for 30 min at 4 °C to precipitate nucleic acids. After a second centrifugation step (70000 x g, 8 °C, 30 min) the supernatant was subjected to a heat precipitation step (3 min at 65 °C). Afterwards, the solution was cooled immediately and centrifuged (70000 x g, 8 °C, 30 min). The supernatant was loaded onto a Q-Sepharose anion exchange column, which was equilibrated with low salt buffer before. Unbound proteins were removed by a washing step of 30 % high salt buffer (300 mM KH_2PO_4 pH 6.5). *Ec*POX was eluted from the Q-Sepharose by a linear gradient of 30-100 % high salt buffer over six column volumes. Fractions containing *Ec*POX were analyzed by SDS-PAGE and combined. Homogenous protein fractions were concentrated up to 30-50 mg/mL with a Vivaspin concentrator (molecular weight cut off 50 kDa) and stored at -20 °C. Fractions containing impure *Ec*POX were also concentrated and afterwards loaded onto a HiTrap Superdex-200 gel filtration column pre-equilibrated with high salt buffer. The protein was eluted with high salt buffer and analyzed by SDS-PAGE. Fractions containing pure *Ec*POX were concentrated like described before and stored at -20 °C. The overall amount of pure *Ec*POX wt and variants was typically 30-50 mg/L media.

3.10 Expression of *Lp*POX

*Lp*POX wt and variants were expressed in *E.coli* C600 cells relying on an already established protocol [83]. Briefly, an overnight culture was used to inoculate 6 x 0.7 L TBY-media (10 g/L tryptone, 5 g/L yeast extract, 100 mM KH_2PO_4, 100 µM $MgSO_4$, 100 mg/L ampicillin, 50 mg/L kanamycin sulfate)

supplemented with the cofactor precursors thiamine hydrochloride (37 mg/L) and flavin mononucleotide (30 mg/L), which should increase the expression of *Lp*POX. Cells were cultivated at 28 °C and 200 rpm. Expression was induced by the addition of 15 g/L lactose and cells were harvested by centrifugation (4000 x g, 4 °C, 30 min) after 16-20 hours. Typically, 6 g cells were obtained per L media.

3.11 Purification of *Lp*POX

According to Wille *et al.* [83] 25 g of cells were resuspended in 40 mL low salt buffer (20 mM KH_2PO_4 pH 6.0, 1 mM $MgSO_4$, 100 µM ThDP) supplemented with 20 µM FAD and disrupted by 3 passages through a microfliudizer. Cell debris was removed by centrifugation (70000 x g, 8 °C, 30 min). Streptomycin sulfate (0.8 % (w/v)) was added to the supernatant, which was subsequently incubated for 30 min at 4 °C with constant stirring. Precipitated nucleic acids were removed by centrifugation (70000 x g, 8 °C, 30 min). The supernatant was subjected to a fractionated ammonium sulfate precipitation between 23-33 % (w/v). The resulting pellet was dissolved in low salt buffer and dialyzed over night at 4 °C against low salt buffer. The obtained protein solution was then loaded onto a Q-Sepharose anion exchange column, which was previously equilibrated with low salt buffer. Unbound proteins were removed from the column with low salt buffer. *Lp*POX was eluted with a linear gradient from 0-100 % high salt buffer (150 mM KH_2PO_4 pH 6.0, 1 mM $MgSO_4$, 100 µM ThDP) with 3 column volumes. Fractions containing *Lp*POX were analyzed by SDS-PAGE and combined. The protein was concentrated by a Vivaspin concentrator (molecular weight cut off 30 kDa) up to a volume of 2 mL. The obtained protein concentrate was subsequently loaded onto a HiTrap Superdex-200 gel filtration column, pre-equilibrated with buffer containing 200 mM KH_2PO_4 pH 6.0, 1 mM $MgSO_4$, 100 µm ThDP. *Lp*POX was eluted with the same buffer and fractions were analyzed by SDS-PAGE. Fractions containing *Lp*POX were combined and concentrated up to 10-30 mg/mL. The final concentrate of *Lp*POX was flash-frozen with liquid nitrogen and stored at -20 °C. 25 g cells led finally to 36 mg of *Lp*POX.

3.12 Expression of non-labeled SUMO-alpha fusion construct

The SUMO-alpha fusion construct was expressed in *E. coli* BL21 (DE3) cells containing the plasmid pET SUMO-alpha. A pre-culture was used to inoculate 6 x 1 L LB-media (10 g/L tryptone, 5 g/L yeast extract, 5 g/L NaCl, 50 mg/L kanamycin sulfate) to an OD_{600} of 0.1. Cells were grown at 37 °C and 200 rpm until an OD_{600} of 1 was reached. Expression of the SUMO-fusion protein was induced by the addition of 1 mM IPTG. After 4 hours cells were harvested (4000 x g, 4 °C, 30 min), flash-frozen with liquid nitrogen and stored at -20 °C. Typically, 20 g cells were obtained out of 6 L media.

3.13 Purification of non-labeled SUMO-alpha fusion construct

20 g of cells containing SUMO-alpha fusion protein were resuspended in 60 mL low imidazole buffer (50 mM KH_2PO_4 pH 7.2, 300 mM NaCl, 20 mM imidazole) supplemented with 10 mg lysozyme, 5 µg/mL DNase I and 10 mM $MgSO_4$. Cells were disrupted by 3 passages through a microfluidizer and cell debris was removed by centrifugation (70000 x g, 8 °C, 30 min). Afterwards, the supernatant was loaded onto a

His-Trap column (5 mL), which was pre-equilibrated with low imidazole buffer. Unbound protein was removed from the column with 50 mL low imidazole buffer. SUMO-alpha was eluted from the column by a linear gradient of 0-100 % high imidazole buffer (50 mM KH_2PO_4 pH 7.2, 300 mM NaCl, 250 mM imidazole) over 10 column volumes. Elution fractions were analyzed by SDS-PAGE and fractions containing SUMO-alpha were combined. For further digestion of the SUMO-alpha fusion construct with the SUMO-protease imidazole needed to be removed. Therefore, SUMO-alpha was concentrated to a volume of 1 mL with a Vivaspin concentrator (molecular weight cut off 10 kDa). Buffer was exchanged to desalting buffer (50 mM KH_2PO_4 pH 7.2, 300 mM NaCl) directly in the concentrators using Vivaspin diafiltration cups. The obtained concentrate of SUMO-alpha was either directly digested or flash-frozen and stored at -20 °C. Typically, 50 mg of the SUMO-alpha fusion construct were obtained out of 6 L media.

3.14 Expression of ^{13}C- and ^{15}N-labeled SUMO-alpha fusion construct

Heavy-atom labeled SUMO-alpha was expressed according to the protocol of Marley *et al.* [84]. Due to multiple steps performed during expression particular attention was paid to sterile conditions. A pre-culture was prepared to inoculate 10 x 0.5 L LB-media (10 g/L tryptone, 5 g/L yeast extract, 5 g/L NaCl, 50 mg/L kanamycine sulfate) to an OD_{600} of 0.1. Cells were grown at 37 °C and 200 rpm in baffled flasks up to an OD of 0.7-1. Cells were harvested by centrifugation (4000 x g, 4 °C, 20 min) and gently resuspended in 250 mL of M9 salts (15 g/L KH_2PO_4, 37.3 g/L NaH_2PO_4 * 2 H_2O, 2.5 g/L NaCl) to wash the cells. Washing solution was removed by centrifugation (2000 x g, 4 °C, 20 min) and the pelletized cells were gently resuspended in 1.25 L M9 minimal media (supplemented with 50 mg/L kanamycin sulfate) containing the labeled nutrients ^{15}N-ammonium chloride and ^{13}C-glucose. Complete composition of the M9 minimal media is listed in table 4. The resuspended cells were then split into 5 x 1 L baffled flasks (5 x 250 mL cultivation volume) and further grown at 37 °C and 200 rpm. After one hour, which allowed clearance of unlabeled nutrients and recovery of the cells, SUMO-alpha expression was induced by the addition of 0.8 mM IPTG. After 4 hours cells were harvested (4000 x g, 4 °C, 30 min), flash-frozen with liquid nitrogen and stored at -20 °C. Approximately 2.5 g cells were obtain per 250 mL M9 minimal media.

table 4: Final composition of M9 minimal media containing labeled nutrients.

substance		concentration in M9 minimal media
^{15}N-ammonium chloride		0.25 g/250 mL
^{13}C-glucose		1 g/250 mL
M9 salts:	**KH_2PO_4**	0.75 g/250 mL
	NaH_2PO_4 * 2 H_2O	1.9 g /250 mL
	NaCl	0.125 g/250 mL
BME vitamins 100 x		1 x
$MgSO_4$ * 7 H_2O		0.124 g/250 mL
$CaCl_2$ * 2 H_2O		3.7 mg/250 mL

3.15 Purification of labeled SUMO-alpha fusion construct

Due to the low yield of SUMO-alpha and the amount needed for further experiments the purification procedure was slightly modified compared with unlabeled protein. 2.5 g cells were resuspended in 13 mL BugBuster master mix and gently stirred for 20 min at room temperature. BugBuster master mix is a detergent mix supplemented with lysozyme which offers gentle lysis of the cells. Additionally, benzonase nuclease is included to digest DNA simultaneously during resuspension. After incubation with the mix 20 mL low imidazole buffer (50 mM KH_2PO_4 pH 7.2, 300 mM NaCl, 20 mM imidazole) was added and cell debris was removed by centrifugation (70000 x g, 8 °C, 30 min). The supernatant was loaded onto a His-Trap column (5 mL) which was previously equilibrated with low imidazole buffer. Unbound proteins as well as the BugBuster master mix were removed by washing the column with 50 mL low imidazole buffer. The labeled SUMO-alpha construct was eluted by a linear gradient from 0-100 % high imidazole buffer (50 mM KH_2PO_4 pH 7.2, 300 mM NaCl, 250 mM imidazole) over 10 column volumes. Eluted fractions were analyzed by SDS-PAGE and fractions containing the SUMO-alpha fusion construct were combined. For the following digestion with the SUMO-protease SUMO-alpha was concentrated to a volume of 1 mL using Vivaspin concentrator (molecular weight cut off 10 kDa) and buffer was exchanged to desalting buffer (50 mM KH_2PO_4 pH 7.2, 300 mM NaCl) containing no imidazole. Therefore, Vivaspin diafiltration cups were used which allowed direct buffer exchange in the concentrator. The obtained concentrate contained ~30 mg SUMO-alpha from 250 mL M9 minimal media. It was then subjected to the digestion reaction with SUMO-protease like described for the non-labeled SUMO-alpha fusion construct.

3.16 SUMO-alpha digestion

The protein concentration of the SUMO-alpha fusion construct (non-labeled and labeled) was determined by Bradford assay [85] prior to digestion. For the digestion approach the concentration of SUMO-alpha was set to 10-15 mg/mL by dilution with digestion buffer (50 mM KH_2PO_4 pH 7.2). SUMO-protease (16.1 μM in 50 % (v/v) glycerol, 25 mM Tris-HCl pH 8.0, 250 mM NaCl, 0.5 mM dithiothreitol, 0.1 % (v/v) IGEPAL, friendly provided by Dr. Stefan Lüdtke) was added in a 1:2000 molar ratio to SUMO-alpha and the approach was incubated at 4 °C overnight. To separate the SUMO-protein from the alpha-peptide the digestion approach was applied to a 1 mL His-Trap column, which was pre-equilibrated with desalting buffer (50 mM KH_2PO_4 pH 7.2, 300 mM NaCl). The alpha-peptide, which could not bind to the column any longer, was in the flow-through or further eluted from the column with desalting buffer. However, the SUMO-protein as well as the SUMO-protease attached to the column due to a polyhistidine-tag and are washed from the His-Trap column with high imidazole buffer (50 mM KH_2PO_4 pH 7.2, 300 mM NaCl, 250 mM imidazole). The flow-through and fractions containing the alpha-peptide were combined, stored on ice or flash-frozen with liquid nitrogen and stored at -20 °C.

3.17 Alpha-peptide purification

After crude extraction of the alpha-peptide by a His-Trap column (chapter 3.16), which followed the digestion reaction, further purification was performed by reversed-phase HPLC (RP-HPLC). Initially, an

analytical C18 column (Nucleosil 120-5, 250 x 2 mm) was used with a solvent system A and B (table 5). 100 µL of the combined alpha-peptide fractions was loaded on the column pre-equilibrated with 5 % solvent B and a flow rate of 0.4 mL/min. The alpha-peptide was eluted with a stepwise gradient from 5-100 % solvent B (table 6) with 0.4 mL/min and monitored at 220 and 280 nm. Peaks with different retention times were identified by mass spectrometry (chapter 3.19).

table 5: Composition of solvents used for reversed phase HPLC.

solvent	composition
A	99.9 % H_2O, 0.1 % TFA
B	10 % H_2O, 89.9 % acetonitrile, 0.1 % TFA

For preparative purification of the alpha-peptide an optimized procedure was used. 1.5 mL of the crude alpha-peptide was loaded on a semi-preparative C18 column (Nucleosil 120-5, 250 x 4 mm, friendly provided by Professor Ivo Feußner) using a 2 mL loop. The column was previously equilibrated with 5 % solvent B with a flow rate of 1 mL/min. The alpha-peptide or shorter fragments were eluted from the column with an optimized gradient (table 6) from 5-100 % solvent B and a flow rate of 1 mL/min. Elution was monitored at 220 and 280 nm and fractionized. The alpha-peptide content of the fractions was analyzed by analytical RP-HPLC using the previously assigned retention times. Fractions containing the pure alpha-peptide were combined and acetonitrile was removed by evaporation using a stream of nitrogen. The aqueous solution was than flash-frozen with liquid nitrogen and water was removed by lyophilization to dryness. The peptides were stored as solid powders at -20 °C. Approximately 1 mg of non-labeled peptide was obtained from 1 L LB-media and 1.3 mg of labeled alpha-peptide from 250 mL M9 minimal media.

table 6: HPLC gradients used for analytical and preparative purification of the alpha-peptide.

analytical gradient		preparative gradient	
time (min)	**solvent B (%)**	**time (min)**	**solvent B (%)**
0	5	0	5
10	30	5	35
30	41	20	41
40	100	21	100
50	100	31	100

3.18 Determination of protein concentration

3.18.1 *Ec*POX

Concentration of *Ec*POX was determined spectroscopically at 438 nm with the NanoDrop 2000 since at this wavelength the protein-bound flavin cofactor has its absorbance maximum. An extinction coefficient of 13721 $M^{-1}cm^{-1}$ was used for *Ec*POX wt, Δ23 and all variants, which was determined by Dr. Annett Weidner specifically for *Ec*POX [45]. A molecular weight of 62 kDa and 59.4 kDa was used for full-length *Ec*POX and *Ec*POX Δ23, respectively.

3.18.2 *Lp*POX

At 280 nm the concentration of *Lp*POX was determined by a NanoDrop 2000. At this wavelength the extinction coefficient of the holo-enzyme (including enzyme-bound ThDP- and FAD-cofactor) was calculated to be 108900 $M^{-1}cm^{-1}$ [74]. A molecular weight of 66 kDa was used for *Lp*POX wt and variants.

3.18.3 SUMO-alpha

To determine the concentration of the SUMO-alpha fusion construct Bradford assay was used [85]. Prior to this a calibration line with albumin fraction V was recorded. The molecular weight of 16.0 kDa included 2.6 kDa of the isolated alpha-peptide and 13.4 kDa of the SUMO-protein.

3.18.4 Alpha-peptide

Concentration of the isolated alpha-peptide was determined spectroscopically at 280 nm using the NanoDrop 2000. Due to the fact that the alpha-peptide contained only one optically active Trp residue (sequence is displayed bellowed), the extinction coefficient for Trp was used ($\varepsilon_{280\ nm}$ = 5500 $M^{-1}cm^{-1}$) [86]. The molecular weight of the isolated alpha-peptide was calculated with 4 molecules of TFA as counter ions additionally to the alpha-peptide mass, which are residual artifacts from RP-HPLC purification.

Amino acid sequence of the alpha-peptide (corresponds to *Ec*POX 550-572):

H-Met-Leu-Arg-Ala-Ile-Ile-Ser-Gly-Arg-Gly-Asp-Glu-Val-Ile-Glu-Leu-Ala-Lys-Thr-Asn-Trp-Leu-Arg-OH

3.19 Mass spectrometry of the isolated alpha-peptide

Mass spectrometry analysis of the alpha-peptide and variants was performed, by Dr. Holm Frauendorf (at the Institute of Organic and Biomolecular Chemistry in the Department Zentrale Analytik und Massenspektrometrie, Göttingen). Typically, peaks with the appropriate retention time were collected from an analytical HPLC run. Peptide samples contained 30-40 % acetonitrile in water supplemented with 0.1 % TFA. Peptide masses were determined by electro spray ionization and an APEX IV (FTICR-MS) instrument (Bruker). Measured masses were deconvoluted prior to analysis.

To analyze the amount of incorporated 15N- and 13C-atoms into the labeled alpha-peptide the calculated molecular weights of non-labeled ($C_{116}H_{197}N_{35}O_{33}S$: 2639 g/mol) and completely labeled alpha-peptide

($^{13}C_{116}H_{197}{}^{15}N_{35}O_{33}S$: 2790 g/mol) were compared. The difference of both masses (151 g/mol) corresponded to heavy-atom enrichment of 100 %.

3.20 Q_0 steady-state assay

Enzymatic activity of *Ec*POX was monitored at 20 °C on a Jasco spectrometer by the loss of absorbance of coenzyme Q_0 at 408 nm. A 10 mM stock solution of Q_0 was prepared with water and stored at room temperature. The molar extinction coefficient of oxidized Q_0 was determined by UV-Vis spectroscopy to be ε_{408} = 722.5 $M^{-1}cm^{-1}$. Sodium dithionite-reduced Q_0 showed no absorbance in this range (figure 16).

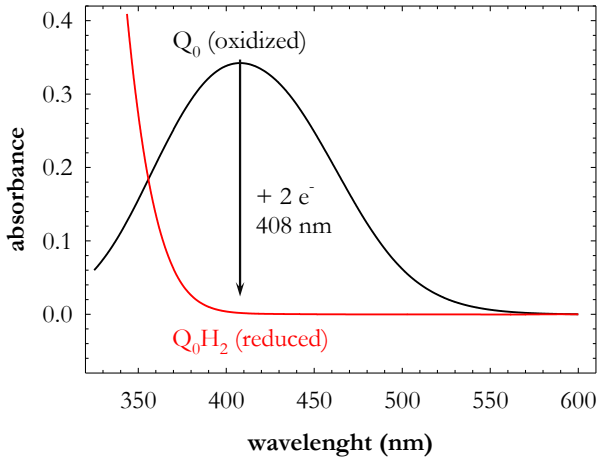

figure 16: UV-Vis spectra of oxidized and reduced ubiquinone-0. 500 µm oxidized Q_0 were reduced with 1 mM sodium dithionite leading to completely reduced Q_0H_2.

For the Q_0 steady-state assay *Ec*POX (0,81 µM full-length *Ec*POX, 32 nM *Ec*POX Δ23) was pre-incubated for 2 min at 20 °C in buffer containing 100 mM KH_2PO_4 pH 6.0, 10 mM $MgSO_4$ and 200 µM ThDP supplemented with 200 mM pyruvate in a 1 mL cuvette. Subsequently, the reaction was started by the addition of 500 µM Q_0 and Q_0 reduction was monitored. Equation 1 was used to determine the specific activity:

equation 1

$$A_s = \frac{\Delta E/\text{min} * V}{\varepsilon_{Q_0} * d * V_E * c}$$

A_s = specific activity (U/mg)

ΔE/min = change in Q_0-absorbance per minute

V = volume of the cuvette (µL)

ε_{Q_0} = extinction coefficient of Q_0 (ε_{408} = 722.5 $M^{-1}cm^{-1}$)

d = path length of the cuvette (cm)

V_E = volume of *Ec*POX solution added to the cuvette (µL)

c = *Ec*POX concentration of the stock solution

3.21 Flavin reduction of *Ec*POX and *Lp*POX

Pyruvate-triggered reduction of the flavin cofactor was carried out with a SX.20 stopped-flow spectrophotometer relying on Tittmann *et al.* [73]. Change in flavin absorbance of *Ec*POX was observed at

438 nm with a path length of 1 cm and at 20 °C with a photomultiplier or photodiode array. For aerobic reactions 2 mg/mL *Ec*POX were pre-incubated for 2 min in reaction buffer (100 mM KH2PO4 pH 6.0, 10 mM MgSO4 and 200 µM ThDP) in one stopped-flow syringe. The second syringe contained 200 mM pyruvate dissolved in reaction buffer. FAD reduction was initiated by rapid mixing of *Ec*POX and pyruvate in 1+1 ratio. Anaerobic measurements in the absence of oxygen were performed under the same conditions, but β-D-glucose (4 mg/mL) and glucose oxidase (GOX, 2.6 µg/mL) were added to both the substrate and enzyme solution, respectively. Both solutions were incubated for 2 min at 20 °C in the stopped-flow device prior to the experiments. The oxygen-consuming reaction of GOX consists of two steps:

$$\beta\text{-D-glucose} + \text{GOX-FAD} \rightarrow \gamma\text{-D-gluconolactone} + \text{GOX-FADH}_2$$

$$\text{GOX-FADH}_2 + \text{O}_2 \rightarrow \text{GOX-FAD} + \text{H}_2\text{O}_2$$

To compare *Ec*POX and *Lp*POX variants the same experiment was performed for *Lp*POX using similar conditions. 2 mg/mL *Lp*POX were incubated for 2 min at 25 °C in 200 mM KH2PO4 pH 6.0, 1 mM MgSO4, 100 µm ThDP and subsequently mixed with 100 mM pyruvate in the same buffer. Absorbance of protein-bound flavin of *Lp*POX was monitored at 457 nm. For anaerobic measurements β-D-glucose and GOX were added to enzyme and substrate solution as already described.

All progress curves were normalized by correlating the overall amplitude to 100 % oxidized FAD. For aerobic measurements the position of the FAD:$FADH_2$ steady state was determined. To analyze anaerobic curves a single exponential equation was used for *Ec*POX (equation 2) and a double-exponential equation was applied to decipher the rate constant of FAD reduction for *Lp*POX (equation 3).

equation 2 $$y = a * e^{-k_{red} * t} + c$$

y = FAD signal at 438 nm
a = amplitude of FAD reduction
k_{red} = rate constant of FAD reduction (s^{-1})
t = time (s)
c = offset (corresponds to $FADH_2$ absorbance)

equation 3 $$y = a_1 * e^{-k_{red} * t} + a_2 * e^{-k_{lag} * t} + c$$

y = FAD signal at 457 nm
a_1 = amplitude of FAD reduction
k_{red} = rate constant of FAD reduction (s^{-1})
a_2 = amplitude of lag phase
k_{lag} = rate constant of lag phase (s^{-1})
t = time (s)
c = offset (corresponds to $FADH_2$ absorbance)

3.22 Proteolytic activation of *Ec*POX

3.22.1 Analytical proteolysis of *Ec*POX

The protease alpha-chymotrypsin was used to irreversibly activate *Ec*POX wt and variants by mild limited proteolysis according to an already established protocol [35]. A 1 mg/mL stock solution of lyophilized alpha-chymotrypsin (1500 U/mg) was prepared in 1 mM hydrochloric acid. Aliquots were flash-frozen, stored at -20 °C and only used once. In a typical experiment, 3 mg/mL of *Ec*POX were pre-incubated for 10 min at room temperature in 100 mM KH_2PO_4 pH 6.0, 1 mM $MgSO_4$ and 200 µM ThDP supplemented with 200 mM pyruvate, which led to the reduction of enzyme-bound FAD and Δ23 cleavage site exposure. To investigate the effect of substrate analogs, 20 mM MAP were added instead of pyruvate. Subsequently, 10 µg/mL alpha-chymotrypsin were added to initiate limited proteolysis. The digestion reaction was either monitored by SDS-PAGE or by activity assay. For analyses by SDS-PAGE 10 µL of the digestion reaction were mixed after defined time points with 200 µL gel sample buffer (0.1 M Tris pH 6.8, 25 % (v/v) glycerol, 2 % (w/v) SDS, 0.02% (v/v) bromophenol blue, 2.5 % (v/v) β-mercaptoethanol) and immediately heated to 95 °C for 5 min. 0.5 µg *Ec*POX were loaded on a 10 % SDS gel. Simultaneously, the activation process was monitored using the Q_0 steady-state assay. 10 µL of the proteolysis mixture were rapidly diluted into 140 µL reaction buffer including 200 mM pyruvate. 10 µL of this dilution were transferred to a 1 mL reaction assay containing 200 mM pyruvate. Activity measurements were immediately initiated by the addition of 500 µM Q_0.

The half-life of the digestion reactions was determined to be the time when 50 % of the full-length enzyme is cleaved to Δ23. Based on a single-exponential approximation the obtained half-life was used to calculate the rate constant k_{act} according to equation 4. Data of the activity assay were analyzed using a single-exponential equation 5 yielding the rate constant k_{act} of activation.

equation 4

$$k_{act} = \frac{\ln 2}{t_{1/2}}$$

k_{cat} = rate constant of proteolytic activation (min^{-1})

$t_{1/2}$ = half-life of the proteolytic activation

equation 5

$$y = a * e^{-k_{act} * t} + c$$

y = specific activity (U/mg)

a = amplitude of the specific activity

t = alpha-chymotrypsin incubation time

c = offset (corresponds to resting-state activity of *Ec*POX)

k_{act} = rate constant of activation process (min^{-1})

A critical point was the construction of the assay. It was assumed that the rate constant k_{act} exclusively dependents on the equilibrium of protein-bound and cytosol-exposed membrane anchor. This would

mean that chymotrypsin digestion is rather fast and transition from closed to the open form is the rate limiting step. Thus, the rate constant should be independent of the chymotrypsin concentration. However, if higher amounts of chymotrypsin were added, the half-life was decreased for the wt enzyme. Therefore, the measured rate constant k_{act} needed to be related to the applied protease concentration used in the assay. To avoid an influence of the protease concentration *Ec*POX wt and all variants were examined under standard conditions to compare the individual rate constants and the effect of the introduced mutations on the activation process.

3.22.2 Preparative proteolysis of *Ec*POX

To generate higher amounts of proteolytic activated *Ec*POX a modified digestion assay was used. 3 mg/mL of *Ec*POX were pre-incubated for 10 min at room temperature in 100 mM KH_2PO_4 pH 6.0, 1 mM $MgSO_4$ and 200 µM ThDP with 200 mM sodium pyruvate. The proteolysis reaction was started by the addition of 15 µg/mL alpha-chymotrypsin and incubated for 40 min at room temperature. The digestion reaction was stopped by the addition of 150 µg/mL aprotinin (40fold molar excess to alpha-chymotrypsin). The protease and smaller peptide fragments as well as pyruvate were removed by a HiTrap Superdex-200 gel filtration column. The digestion reaction was applied to the column, which was previously equilibrated with 100 mM KH_2PO_4 pH 6.0, 10 mM $MgSO_4$ and 1 mM ThDP, and eluted with the same buffer. Fractions containing *Ec*POX Δ23 were analyzed by SDS-PAGE and further concentrated to 20-50 mg/mL. Due to decreased stability *Ec*POX Δ23 was only stored on ice and not flash-frozen.

3.22.3 Limited proteolysis under turnover conditions

Limited proteolysis under steady-state conditions was performed slightly different than the analytical approaches. In prior studies appropriate concentrations of *Ec*POX and Q_0 were identified which ensured a sufficient amount of *Ec*POX to be loaded on the gel as well as an adequate period of time to monitor Q_0 consumption. In the digestion reaction 0.186 mg/mL of *Ec*POX were pre-incubated for 10 min at room temperature in 100 mM KH_2PO_4 pH 6.0, 1 mM $MgSO_4$ and 200 µM ThDP supplemented with 200 mM pyruvate. The steady-state reaction was started by the addition of 10.4 mM Q_0. Within 30 s the steady state phase was reached and 20 µg/mL alpha-chymotrypsin were added to initiate the proteolytic cleavage. Q_0 consumption was monitored at 500 nm (ε_{500} = 123 $M^{-1}cm^{-1}$). Simultaneously, gel samples were prepared after defined time points to document the digestion pattern of *Ec*POX. 40 µL of the reaction were mixed with 10 µL gel sample buffer (0.1 M Tris pH 6.8, 25 % (v/v) glycerol, 2 % (w/v) SDS, 0.02 % 8v/v) bromophenol blue, 2.5 % (v/v) β-mercaptoethanol) and immediately heated to 95 °C for 5 min. 0.5 µg *Ec*POX were loaded on a 10 % SDS-PAGE. As reference experiments the same reactions were performed either in the absence of pyruvate or Q_0.

3.23 SDS-mediated activation of *Ec*POX

As previously described *Ec*POX can be activated by amphiphiles like SDS similar to mild limited proteolysis [34]. To study the SDS-mediated activation a modified Q_0 steady-state assay was used. Measurements were performed using a SX.20 stopped-flow spectrophotometer at 20 °C and a path length

of 1 cm. 10 µg/mL *Ec*POX were pre-incubated in buffer (containing 100 mM KH_2PO_4 pH 6.0, 10 mM $MgSO_4$ and 200 µM ThDP) supplemented with 200 mM pyruvate for 2 minutes at room temperature. Afterwards, a given SDS amount was added and the mixture was rapidly loaded into one syringe of the stopped-flow device. The second syringe contained 1 mM Q_0 dissolved in the same buffer including 200 mM pyruvate and SDS. Four shots were performed as quickly as possible to equilibrate the system. After distinct delay times Q_0 and *Ec*POX were mixed in 1+1 ratio and Q_0 reduction was monitored at 408 nm. Typically, 1 minute passed between SDS addition and the first measurement. The start activity was determined using a linear fit of the first 5 seconds and equation 1. To compare the different variants the final activity obtained at saturating concentrations of SDS was adjusted to 100 %.

3.24 Thermic stability determined by CD spectroscopy

Thermic stability of different *Ec*POX variants was determined by far-UV CD spectroscopy using a Chirascan CD spectrometer. The secondary structure of active *Ec*POX variants at 20 °C was determined from 190-260 nm and compared with the unfolded structure at 95 °C. Due to the fact that the highest difference occurred at 208 nm, this wavelength was chosen to record the temperature dependent unfolding of the protein. For the reaction 0.1 mg/mL *Ec*POX was incubated in 100 mM KH_2PO_4 pH 6.0, 10 mM $MgSO_4$ and 200 µM ThDP in a 1 mm cuvette. A linear gradient from 20-95 °C was used with the following settings: step 0.5 °C, heating rate 2 °C/min, tolerance 0.2 °C, record time 12 s/point.

The transition of the melting curve, which corresponds to the apparent melting temperature (T_m), was determined using equation 6 according to Pace [87]. This equation describes the reversible unfolding of proteins, which is inaccurate for such irreversible denatured proteins like *Ec*POX, due to the fact that T_m is influenced by different parameters like the heating rate. However, the equation of Pace was used as approximation to determine an apparent melting temperature, since all variants were examined under the same conditions. Therefore, a qualitative comparison of the different *Ec*POX variants was feasible.

equation 6

$$y = \frac{(y_f + m_f * T) + (y_u + m_u * T) * \exp\left[\left(\frac{\Delta H_m}{R * T}\right) * \left(\frac{T - T_m}{T_m}\right)\right]}{1 + \exp\left[\left(\frac{\Delta H_m}{R * T}\right) * \left(\frac{T - T_m}{T_m}\right)\right]}$$

y = CD signal at 208 nm (mdeg)

T = temperature (K)

T_m = melting temperature (here the apparent melting temperature in K)

R = universal gas constant (8.315 $JK^{-1}mol^{-1}$)

ΔH_m = change of the enthalpy at T_m

y_f, m_f = parameters of the baseline of the folded protein

y_u, m_u = parameters of the baseline of the unfolded protein

3.25 Crystallization of *Ec*POX

*Ec*POX wt and different variants were crystallized relying on an already established protocol [82]. Briefly, prior to crystallization all *Ec*POX variants were rebuffered into crystallization buffer (20 mM KH_2PO_4 pH 6.0, 10 mM $MgSO_4$, 10 mM ThDP) using a HiTrap Desalting column. Yellow fractions containing *Ec*POX were enriched using a Vivaspin concentrator (molecular weight cut off 30 kDa) up to a concentration of 20 mg/mL. Crystallization experiments were set up using 24-well hanging drop plates with varying concentrations of *Ec*POX in the droplets after mixing.

Crystals of full-length *Ec*POX were set up at room temperature by mixing 2 µL of protein (5-20 mg/mL) with 2 µL of the reservoir solution. The reservoir contained 0.2-0.8 % (w/v) PEG 2000 and 0.05 % (w/v) protamine sulfate (always freshly prepared) dissolved in 80 mM KH_2PO_4 pH 6.0. The protein droplets were incubated over 500 µL of the reservoir and yellow crystals appeared within 2-5 days at 6 °C in darkness. Prior to flash-cooling the crystals were cryo-protected by subsequent incubation in three cryo-solutions with increasing amounts of ethylene glycol (5, 15 and 30 % (v/v) mixed with the reservoir solution. The crystal was incubated for 10 s in 5 % ethylene glycol, followed by 3 min in 15 % ethylene glycol and finally a short soaking step for a few seconds in 30 % ethylene glycol before flash-cooling.

*Ec*POX Δ23 was crystallized in the dark at 20 °C. The reservoir mixture contained 20-28 % (v/v) MPD and 100 mM MES-NaOH pH 6.2. 2 µL of this reservoir were mixed with 2 µL of *Ec*POX (5-20 mg/mL) and crystallization was initiated by streak seeding. Therefore, an old *Ec*POX Δ23 crystal was crashed and diluted with crystallization buffer prior to seeding. The protein droplets were equilibrated against 500 µL of the reservoir solution and crystals were observed after a few weeks. Due to large amounts of MPD no further cryo-protection was necessary and crystals could be directly flash-cooled in a liquid-nitrogen.

Crystal structures of *Ec*POX Δ23 in complex with Q_0 were obtained by co-crystallization. Therefore, the protein was transferred into crystallization buffer and subsequently incubated with Q_0 (2-50 molar equivalents) for one hour at 4 °C. Crystals were set up by streak seeding and flash-cooled as described above. Q_0-soaking trials were performed with *Ec*POX Δ23 crystals obtained as already described which were incubated in soaking solutions containing 5-20 mM Q_0 in 40 mM MES-NaOH pH 6.2 supplemented with 20-30 % (v/v) MPD. Soaking was performed in the dark at 20 °C for 1-24 hours. Prior to data collection crystals were flash-cooled in a liquid nitrogen without further cryo-protection.

3.26 Crystallization of *Lp*POX

*Lp*POX variants were crystallized like wt according to a procedure described previously [88]. Crystals were set up at room temperature by mixing 2 µL of the reservoir with 2 µL *Lp*POX (12-15 mg/mL in 200 mM KH_2PO_4 pH 6.0, 1 mM $MgSO_4$, 100 µm ThDP). The reservoir solution contained 1.5-1.7 M ammonium sulfate in 200 mM KH_2PO_4 pH 6.0, 1 mM $MgSO_4$ and 100 µm ThDP. Crystals were grown within 1 month at 6 °C in the dark. The obtained crystals were cryo-soaked in 115 mM KH_2PO_4 pH 5.8, 1.3 M ammonium sulfate and 25 % (v/v) glycerol for a few seconds before flash-cooling in a liquid nitrogen.

3.27 Data collection and processing of *Ec*POX and *Lp*POX crystals

X-ray diffraction data sets were collected at different synchrotron sources (Swiss Light Source (SLS) in Villingen, Helmholtz-Zentrum Berlin für Materialien und Energie (HZB) and Deutsches Elektronen Synchrotron Hamburg Petra III (DESY)) or with an in-house source at the Department for Molecular Structural Biology, Göttingen at cryogenic temperatures (table 7). Data were mainly collected by Dr. Piotr Neumann (Deparment for Molecular Structural Biology, Göttingen) and Dr. Stefan Lüdtke (former Deparment of Bioanalytics, Göttingen).

Data were processed and scaled with XDS [89] performed by Dr. Piotr Neumann (Department for Molecular Structural Biology, Göttingen) or Dr. Stefan Lüdtke (former Department of Bioanalytics, Göttingen). To solve the structures of different variants initial rigid body refinements were performed using the corresponding wt structures as primary models (*Ec*POX: pdb 3EY9 [35], *Lp*POX: pdb 4FEG [90]). Subsequently, alternating cycles of model building and refinement were performed using COOT, Refmac and PHENIX [91] [92] [93]. Simulated annealing omit maps calculated using CNS [94] were generated for variant *Ec*POX I554G by Dr. Piotr Neumann (Department for Molecular Structural Biology, Göttingen).

table 7: Beamlines and resolution of data sets collected at different synchrotrons.

X-ray structure	beamline	resolution (Å)
***Ec*POX Y278F**	HZB 14.1	2.96
***Ec*POX D328A, D348A, Q537A**	SLS PX II	3.20
***Ec*POX F260A**	HZB 14.1	3.08
***Ec*POX Y549A**	HZB 14.1	2.79
***Ec*POX I554A**	DESY P14	3.02
***Ec*POX I554G**	DESY P14	2.90
***Ec*POX L565A**	HZB 14.1	3.24
***Ec*POX Δ23:Q_0**	in-house	3.20
***Lp*POX F289Y**	HZB 14.1	1.43

3.28 Secondary structure of the alpha-peptide determined by CD spectroscopy

The secondary structure of the alpha-peptide was determined by far-UV CD spectroscopy with a Chirascan CD spectrometer. 0.1 mg/mL of the peptide was incubated in 50 mM NaH_2PO_4 pH 6.0 at 20 °C in a 1 mm cuvette. The effect of detergent micelles was studied by addition of 50 mM SDS (CMC = 1.9 mM) or 50 mM DPC (CMC = 1.3 mM). As positive control the peptide solution was supplemented with 50 % (v/v) trifluoroethanol, which is known to induce helical structures [95]. The following settings were used for all measurements: 190 – 250 nm, step: 0.5 nm, record time 1 s/point, 3 repeats. To

determine the percentage of secondary structure elements spectra were corrected for baseline and buffer and deconvoluted with the program CDNN [96].

3.29 Structure determination of the alpha-peptide by NMR spectroscopy

The molecular structure of micelles-bound alpha-peptide was determined by solution-state NMR spectroscopy by Dr. Piotr Wysoczanski and Prof. Dr. Markus Zweckstetter (Department of Structure determinations of Proteins using NMR, Max-Plack-Institute for biophysical chemistry, Göttingen). Therefore, ^{13}C- and ^{15}N-labelled peptide was investigated in the presence of deuterated DPC micelles. 1mM of the labeled peptide was incubated with 50 mM D-DPC in 50 mM potassium phosphate pH 6.0 (supplemented with 10 % D_2O) for several hours on ice.

The NMR spectra of the free peptide and peptide bound to DPC micelles were measured on 700 MHz NMR spectrometer equipped with room temperature 5 mm HCN, Z-gradient probe. The sample was placed in 3 mm tube and all measurements were taken at 298 K. Following experiments were run in order to assign the chemical shifts of backbone atoms and CB: ^{1}H, ^{15}N HSQC, HNCO, HNCA, HNCACB, HNHA. HNHA was also used to extract 3J HN-HA values. Also, ^{1}H, ^{15}N HSQC was measured for the free peptide.

Spectra were processed using NMRpipe [97] and assigned using ccpn analysis 2.2.1 [98]. Secondary chemical shifts were calculated according to [99] and 3J HN-HA values were fitted to Karplus equations to extract the phi dihedral angle values [100].

Protein backbone atoms chemical shifts are sensitive to the secondary structure of a protein and thus provide a reliable method to detect the conformational preferences. By calculating secondary chemical shifts (difference between the measured chemical shift and the value expected from a random coil) one can extract relative likelihood of a given residue to occupy ramachandran space corresponding to an alpha-helix, a random coil or a beta-sheet. Additionally, 3J HN-HA values are modulated by the dihedral angle formed by H-N-Ca-Ha atoms thus providing an even more direct measure of a protein secondary structure. TALOS [101] and SSP were used [102] to get a global likelihood of the secondary structure and TALOS to predict the S2 order parameter [103].

3.30 Determination of critical micelle concentration of SDS and DPC

The critical micelle concentration (CMC) of the surfactants SDS and n-Dodecyl phosphocholine (DPC) was determined under different conditions by isothermal titration calorimetry (ITC) relying on already published procedures [104] [105].

The CMC of the surfactants was determined in water and in phosphate buffer containing 50 mM NaH_2PO_4 pH 6.0. SDS stock solutions (50 – 100 mM) were prepared by weighing a specific SDS amount and dissolving it in water or in the appropriate buffer. DPC was used as powder and also weighed and dissolved in either water (75 mM DPC) or 50 mM NaH_2PO_4 pH 6.0 (50 mM DPC).

Measurements were performed with an ITC_{200} at 20 °C. All experiments were repeated 3 times and the average of the CMC value was calculated. The reference cell of the ITC device contained water, whereas the measuring cell was either filled with water or the corresponding buffer. The ITC syringe was loaded with the detergent stock solution, which was stepwise titrated into the measuring cell. The following settings were used for all experiments:

cell temperature:	20 °C	injections:	
stirring speed:	1000 rpm	1:	0.2 µL, spacing 90 s
reference power:	5-7	2-50:	0.5 µM, spacing 120 s
response:	high	filter period:	5 s

Data were baseline-corrected and analyzed according to [106]. The results are shown in the appendix (chapter 8.1).

4. Results

4.1 Analysis of the information transfer from the active site to the membrane anchor and stabilization of the protein-bound membrane anchor at the protein surface

4.1.1 Q_0 steady-state assay

Q_0 acts as water-soluble substitute for the native substrate Q_8

To analyze the activity of *Ec*POX wt and variants a new steady-state assay was established. In former activity assays cofactor-reconstituted enzyme transferred pyruvate-derived electrons to artificial electron acceptors like ferricyanide or 2,6-dichlorophenolindophenol [15]. Reduction of these acceptors was followed by UV-Vis spectroscopy. However, these electron acceptors show severe structural differences compared with the native substrate Q_8 (figure 17). Further, properties of electron acceptance vary significantly. While in the native reaction two electrons are completely transferred to one Q_8 molecule, only one electron can be accepted by ferricyanide. Additionally, it is possible that artificial electron acceptors, once passed the active site, can uptake reducing equivalents not only from the reduced flavin cofactor, but already from HE-ThDP intermediate [107].

In the new approach Q_0 was used as final electron acceptor. Q_0 is a water-soluble analogue of the native substrate Q_8, which lacks the 8 isoprenoid units necessary for membrane anchoring. Since the benzoquinone head groups of Q_8 and Q_0, which are considered to facilitate substrate binding to the active site, are identical one can assume that electron transfer proceed in a similar way for both ubiquinones. Comparison of the catalytic constants using ferricyanide and Q_0 as electron acceptors revealed no significant differences (data not shown). Therefore, the Q_0 steady-state assay was used for further applications instead of ferricyanide or 2,6-dichlorophenolindophenol. Prior to activity measurements of different *Ec*POX variants the Q_0 amount required for saturation was determined. For *Ec*POX wt and all mutants a final concentration of 500 µM Q_0 was sufficient in the assay (full-length *Ec*POX and Δ23: K_m = ~30 µM, data not shown).

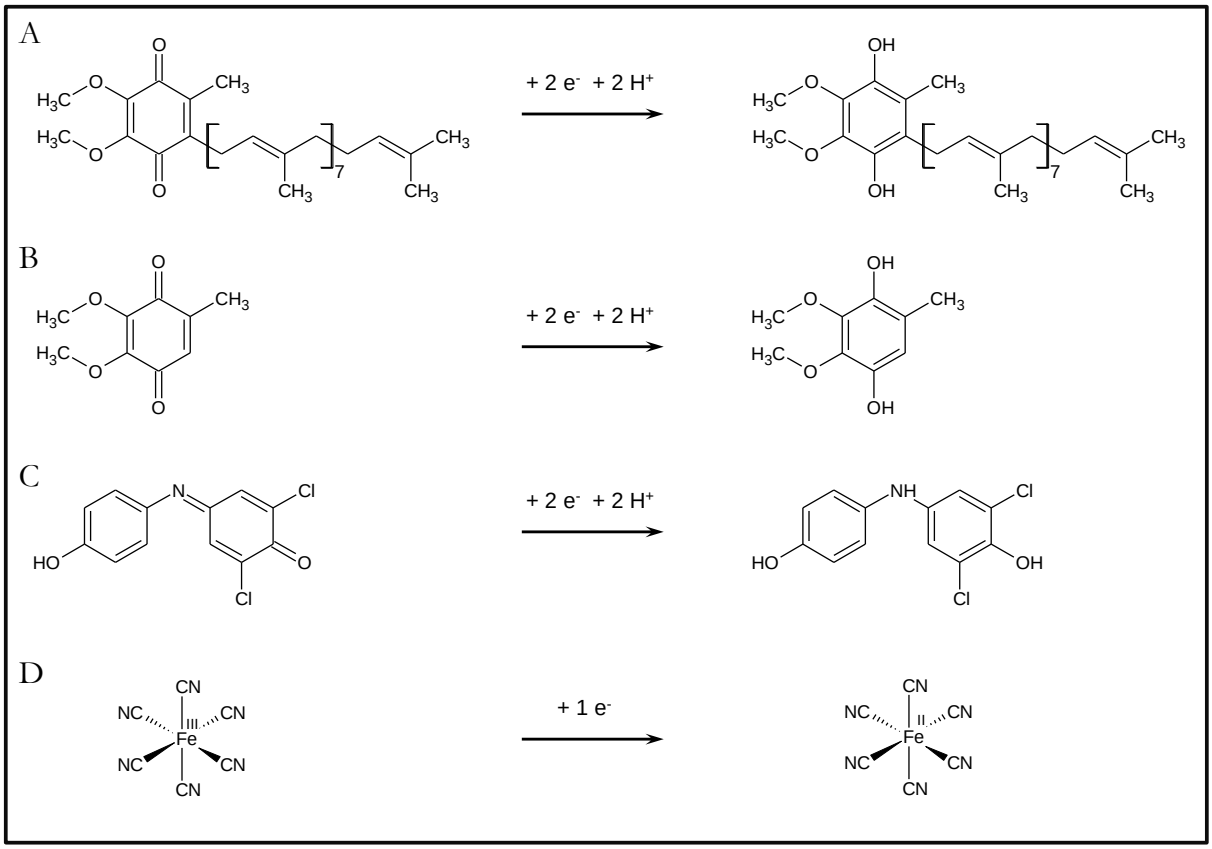

figure 17: Overview of different terminal electron acceptors converted by *Ec*POX. The following electron acceptors are used by *Ec*POX *in vivo* or *in vitro*. A: Q_8. B: Q_0. C: 2,6-dichlorophenolindophenol. D: ferricyanide. Redox reactions are indicated by addition of electrons and protons.

Pyruvate dependence of the steady-state activity follows Michaelis-Menten kinetics

The steady-state activity of *Ec*POX wt and variants was studied by Q_0 steady-state assay. The catalytic parameters were calculated using the Michaelis-Menten equation 7, which is based on the following reaction scheme:

$$E + S \underset{k_{-1}}{\overset{k_1}{\rightleftharpoons}} ES \xrightarrow{k_2} E + P$$

E = enzyme, S = substrate (pyruvate)

ES= enzyme-substrate complex, P = product

equation 7

$$v = \frac{V_{max} * [S]}{K_m + [S]}$$

v = specific activity (U/mg)

V_{max} = maximum activity (U/mg)

[S] = pyruvate concentration (mM)

K_m = Michaelis constant (mM)

According to this scheme, the enzyme reacts with substrate to an ES-complex which either can be irreversibly converted to form the product, or can degrade to the free enzyme and substrate. The

Michaelis constant K_m is derived from the rate constants of several processes (equation 8). It consists of the dissociation constant of the ES-complex (k_{-1}/k_1) and the overall rate constant k_2, which reflects all steps following ES formation.

equation 8

$$K_m = \frac{k_{-1} + k_2}{k_1}$$

K_m = Michaelis constant

k_{-1} = rate constant of ES-complex degradation

k_1 = rate constant of ES-complex formation

k_2 = rate constant of product formation

However, the catalyzed reaction of *Ec*POX includes more steps than formation of an ES-complex and product generation. Thus, the determined values can only been seen as approximation of the overall reaction and cannot be assigned to specific rate constants or single catalytic steps. In this regard a decreased K_m value of a variant should not automatically be interpreted as increased affinity for the substrate pyruvate, since the smaller Michaelis constant could only reflect a decelerated rate constant k_2, while association of the ES-complex is not affected.

steady-state activity of *Ec*POX variants

EcPOX wt and activated enzyme forms:

As previously described in the literature *Ec*POX wt exhibits a k_{cat} of 6.6 ± 0.2 s^{-1}, whereas the proteolytically activated Δ23 variant or the addition of 100 µM SDS to the wt enzyme lead to 25-30fold increase in catalytic activity and simultaneously to a 3-6fold decreased K_m [18] [108] (figure 18 and table 8).

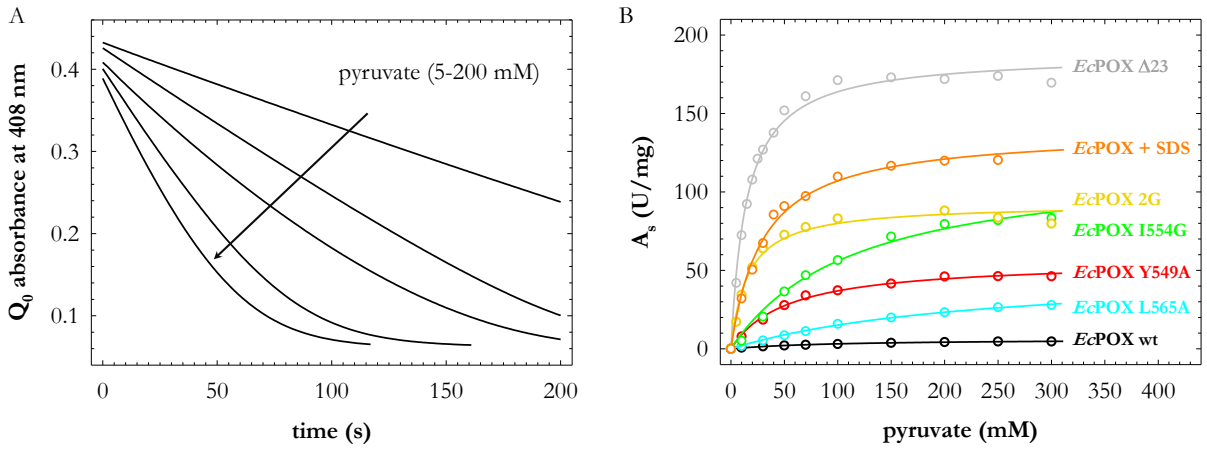

figure 18: Steady-state activity of *Ec*POX wt and selected variants in dependence of pyruvate concentration. A: Progress curves of Q_0 conversion by *Ec*POX wt at different pyruvate concentrations (5-200 mM). B: Pyruvate dependence of selected *Ec*POX variants. Data (dots) were fitted according to Michaelis-Menten equation (lines). Obtained catalytic parameters for all variants are listed in table 8.

Putative signal transfer variants F465A, Y278F, Y549A and F260A:

Wt-like activities were observed for variants F260A and Y278F (figure 18 and table 8). Surprisingly, mutant *Ec*POX Y549A showed a 10fold increased k_{cat} which implies a partially activated enzyme already in the resting state. F465A is the only variant with significantly reduced activity (k_{cat} = 0.1 ± 0.01 s^{-1}) indicating a vital role of this residue for the catalytic mechanism.

Potential alpha-peptide binding variants 3x, I554A/G, L565A/G, 2G, W570G:

Variants supposed to be involved in hydrophobic membrane anchor binding (L565A/G, I554A/G, W570G) show an increased k_{cat} similar to fully activated enzyme already in the resting state (figure 18 and table 8). These results implicate that semi-activated variants are generated due to removal of hydrophobic methyl units in the variants. Remarkably, the double mutant *Ec*POX 2G is completely activated showing a catalytic efficiency similar to activated Δ23. Contrary, variant *Ec*POX 3x (lacking electrostatic contacts and hydrogen bonds for alpha-peptide attachment) exhibits wt-like activity.

table 8: Steady-state constants of *Ec*POX variants. Parameters were calculated from data of the Q_0 steady-state assay using Michaelis-Menten equation 7. Plots of pyruvate dependence for individual *Ec*POX variants are displayed in the appendix (chapter 8.2).

***Ec*POX variant**	**K_m (pyruvate) (mM)**	**V_{max} (U/mg)**	**k_{cat} (s-1)**	**k_{cat}/K_m ($M^{-1} * s^{-1}$)**
wt	99.1 (± 6.8)	6.4 (± 0.2)	6.6 (± 0.2)	67
wt + 100 µM SDS	30.7 (± 2.4)	141.0 (± 3.3)	145.7 (± 3.4)	4746
wt Δ23	14.6 (± 0.9)	187.7 (± 2.8)	185.8 (± 2.7)	12726
F465A	48.3 (± 6.0)	0.1 (± 0.01)	0.1 (± 0.01)	2
Y278F	69.9 (± 9.5)	2.9 (± 0.1)	3.0 (± 0.1)	43
Y549A	52.5 (± 4.6)	56.3 (± 1.5)	58.2 (± 1.6)	1109
F260A	68.8 (± 3.5)	11.4 (± 0.2)	11.8 (± 0.2)	172
D328A, D348A, Q537A (*Ec*POX 3x)	114.0 (± 7.0)	5.7 (± 0.1)	5.9 (± 0.2)	52
L565A	188.0 (± 20.4)	41.4 (± 2.3)	42.8 (± 2.4)	228
L565G	94.6 (± 9.7)	78.7 (± 3.2)	81.3 (± 3.3)	860
I554A	232.7 (± 16.6)	50.5 (± 2.0)	52.2 (± 2.1)	224
I554G	115.6 (± 14.9)	120.8 (± 6.6)	124.8 (± 6.8)	1080
L565G, I554G (*Ec*POX 2G)	15.6 (± 1.9)	92.4 (± 2.5)	95.5 (± 2.6)	6122
W570G	117.5 (± 8.1)	23.7 (± 0.7)	24.5 (± 0.7)	209

In conclusion, results obtained from the activity assay indicate that variants with decreased hydrophobic contacts between the alpha-peptide and the protein surface (L565A/G, I554A/G, 2G, W570G) show Δ23-like behavior. It can be speculated that these variants mimic the proteolytically activated enzyme with improved active site accessibility and at least with a partially released membrane anchor.

4.1.2 Flavin reduction at anaerobic conditions

The reductive half-reaction of *Ec*POX

In the absence of any terminal electron acceptor the catalytic cycle of *Ec*POX is incomplete (figure 19). Pyruvate can undergo just one cycle yielding acetate, but the flavin cofactor cannot be regenerated and remains in the reduced form $FADH_2$. Subsequently, a second pyruvate molecule can only be converted to HE-ThDP since no oxidized flavin cofactor is available to accept further electrons which is a prerequisite for HE-ThDP depletion. Hence, two equivalents of pyruvate are utilized, whereas only single-turnover of FAD can be observed. This simplified catalytic cycle is called reductive half-reaction [24] and resembles pre-steady-state conditions of *Ec*POX. In contrast to the Q_0 steady-state assay, where overall rate constants are determined, the catalytic constants derived from this approach can be attributed only to steps yielding the reduced flavin cofactor.

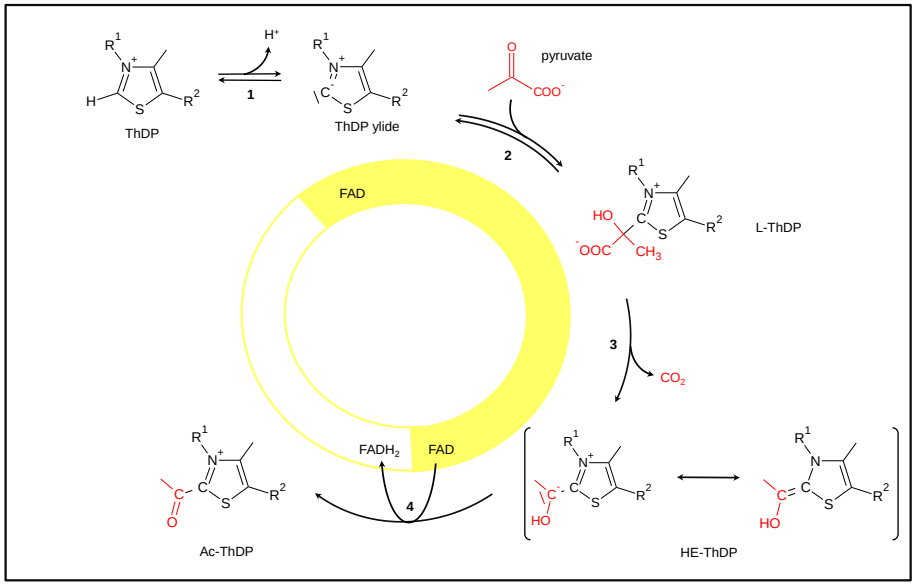

figure 19: Reductive half-reaction of *Ec*POX. Activation of ThDP yields the reactive ylide form (1). Covalent pyruvate binding leads to L-ThDP (2) followed by decarboxylation (3). The resulting HE-ThDP intermediate can transfer two electrons to the flavin cofactor (4). In the absence of any electron acceptor flavin regeneration does not occur and the catalytic cycle stops at this stage. Acetate hydrolysis and subsequent binding of a second pyruvate molecule are neglected for clarity. (R^1 = aminopyrimidine moiety, R^2 = diphosphate anchor)

Pre-steady-state conditions allow determination of the flavin reduction rate

In the pre-steady-state assay, *Ec*POX was rapidly mixed with pyruvate using a stopped-flow device and flavin reduction was detected at 438 nm. Anaerobic conditions were applied since molecular oxygen can reoxidize the previously reduced flavin cofactor [45] [109]. The loss of absorbance at 438 nm corresponds to formation of completely reduced $FADH_2$ from FAD induced by pyruvate. The resulting progress curves of selected *Ec*POX variants at standard conditions are displayed in figure 20 and were compared to the wt enzyme.

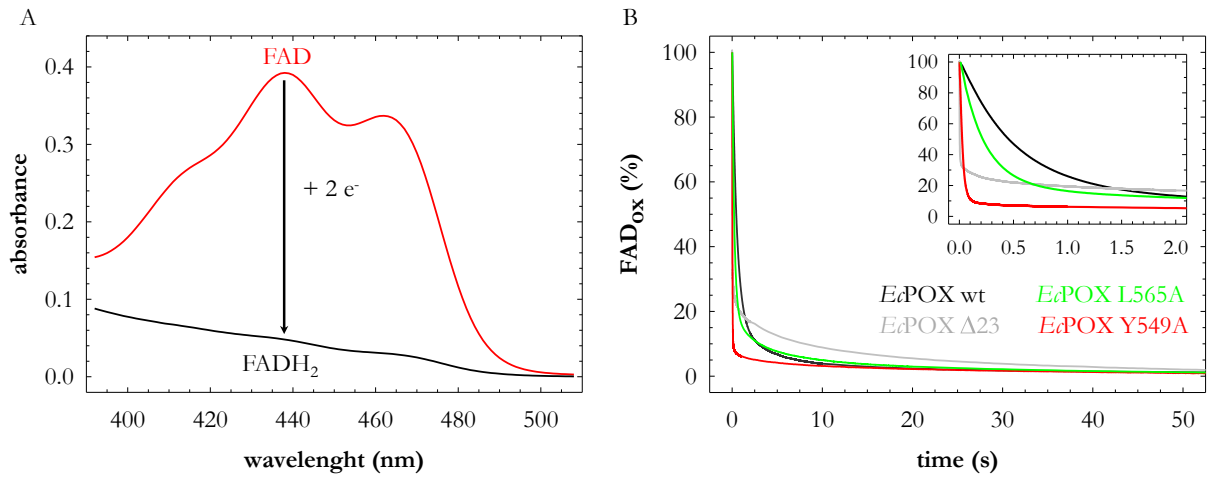

figure 20: Pyruvate-induced flavin reduction of *Ec*POX wt and variants. A: Spectra of oxidized and pyruvate-reduced *Ec*POX wt. 2 mg/mL *Ec*POX wt (red) were reduced (black) with 100 mM pyruvate. B: Kinetics of *Ec*POX flavin reduction at anaerobic conditions. 2 mg/mL of *Ec*POX were rapidly mixed with 200 mM pyruvate in the absence of oxygen or other electron acceptors. Flavin reduction was monitored at 438 nm and 20 °C with a stopped-flow device. Progress curves were converted to relative amount of oxidized flavin. The rate constant of the first phase k_{red} was determined by a single-exponential equation (fit not shown). Rate constants of all *Ec*POX variants are listed in table 9. Inset: FAD reduction within the first 2 seconds.

The pre-steady-state curve of *Ec*POX wt shows two different phases. The first phase corresponds to nearly 90 % of the overall amplitude and is finished after approximately 5 seconds. This phase is interpreted as pyruvate-triggered flavin reduction and can be analyzed by a single-exponential equation yielding the rate constant k_{red} which includes the microscopic rate constants of pyruvate binding, L-ThDP decarboxylation and flavin reduction. The second phase is rather slow and even not finished after 1000 s when the measurement was stopped (data not shown). Amplitude and rate constant of this phase are independent of the pyruvate concentration. The molecular origin of this phase is unclear but it seems possible that a less-active enzyme species exists in solution, which could be reduced rather slowly.

Flavin reduction rate of *Ec*POX variants

EcPOX wt and proteolytically activated ⊿23:

In contrast to *Ec*POX wt proteolytically activated enzyme exhibits a 400fold increased k_{red} (*Ec*POX wt: k_{red} = 1.9 ± 0.001 s^{-1}, Δ23: k_{red} = 848 ± 78 s^{-1}) which is already indicated in the steady-state assay.

Putative signal transfer variants F465A, Y278F, Y549A and F260A:

Similar flavin reduction rate like for *Ec*POX wt is detected for variant Y278F. In this regard it can be concluded that all steps leading to reduced FAD are not influenced and catalytic processes starting from $FADH_2$ are mainly affected in this variant.

Remarkably, F465A is the only variant that shows an impaired flavin reduction with a 100fold decreased k_{red}. This implies that pyruvate binding, decarboxylation or electron shuffling to FAD are disturbed in F465A. The low k_{red} value is also reflected in poor catalytic activity monitored in the steady-state assay.

table 9: Flavin reduction rate of *Ec*POX variants. k_{red} was determined from progress curves shown in figure 20 by a single-exponential equation (equation 2) under saturating concentrations of pyruvate (100 mM). Progress curves of flavin reduction for individual *Ec*POX variants are displayed in the appendix (chapter 8.5). (n. d. = not determined)

***Ec*POX variant**	k_{red} **(s^{-1})**
wt	1.9 (± 0.001)
wt Δ23	848 (± 78)
F465A	0.02 (± 0.00002)
Y278F	2.1 (± 0.002)
Y549A	37.9 (± 0.13)
F260A	4.6 (±0.003)
D328A, D348A, Q537A (*Ec*POX 3x)	n. d.
L565A	5.2 (± 0.007)
L565G	16.3 (± 0.043)
I554A	4.4 (± 0.017)
I554G	4.6 (± 0.007)
L565G, I554G (*Ec*POX 2G)	n. d.
W570G	2.2 (± 0.003)

A 2.5fold increased k_{red} relative to the wt enzyme is detected for variant *Ec*POX F260A. Due to the position of Phe260 on the protein surface a catalytic function during flavin reduction can be excluded. It seems more likely that a partially released membrane anchor improves active site accessibility leading to enhanced substrate binding. Since covalent binding of pyruvate yielding L-ThDP was reported to be the rate-limiting step in *Ec*POX [45], acceleration of this process would consequently lead to an increased k_{red}.

Noteworthy, *Ec*POX Y549A shows a 20fold increased k_{red} of 37.9 ± 0.13 s^{-1}. Although Tyr549 is located in close proximity to the flavin and thiamine cofactors it seems unlikely that the substituted Ala can improve electron transfer compared to Tyr549. One could speculate that Phe465 already switch to the activated position in variant Y549A and facilitates electron shuffling like observed in *Ec*POX Δ23. However, the flavin reduction rate is still 20fold slower with respect to the proteolytically activated enzyme. On the other hand, the increased k_{red} could be explained by improved active site accessibility already suggested for variant F260A which is provided by partial release of the membrane anchor from the protein surface.

Potential alpha-peptide binding variants I554A/G, L565A/G, W570G:

Variants supposed to be involved in hydrophobic membrane anchor binding (L565A/G, I554A/G, W570G) show accelerated flavin reduction. However, the obtained rate constants are still 50fold slower

compared to the proteolytically activated enzyme (variants: k_{red} = 2.2 – 16.3 s^{-1}). Thus, it is questionable that these minor changes are caused by a reorganized active site with Phe465 already occupying its activated position to promote electron transfer to FAD. A reasonable explanation for the slightly increased reduction rates in these variants could be again improved substrate binding caused by increased accessibility of the active site.

Analyses of anaerobic flavin reduction was not only mandatory to decipher the electron transfer within the active site of *Ec*POX but also necessary for further membrane binding studies. Proper flavin reduction is a prerequisite for membrane anchor exposition. The latter step can be monitored for instance by limited proteolysis experiments (chapter 4.1.4) or SDS-mediated activation of *Ec*POX (chapter 4.1.5).

4.1.3 Flavin reduction under steady-state conditions

Flavin reoxidation by molecular oxygen is an artificial side reaction

*Ec*POX is an enzyme involved in energy metabolism of the bacterial cell. It converts energy-rich pyruvate to low energetic products acetate and carbon dioxide. Additionally, during this reaction arise two electrons which are initially stored at the flavin cofactor. The final energy conserving steps are the transfer of the two reducing equivalents into the membrane to Q_8, which subsequently feeds energy rich electrons into the respiratory chain. Most important for energy conservation within *Ec*POX is the absence of electron acceptors since reduction of unpreferred low energetic products would lead to a waste of energy.

In vitro, an artificial energy-wasting reaction can be observed for *Ec*POX: the reoxidation of the reduced flavin cofactor by molecular oxygen yielding the final product hydrogen peroxide. This process is described as artificial oxidative half-reaction in thesis, since the native oxidative half-reaction corresponds to flavin reoxidation by Q_8. In contrast to electron transfer from HE-ThDP to ferricyanide, the artificial oxidative half-reaction was reported to be rather slow [42] [45]. Poor oxygen reactivity of *Ec*POX is not astonishing since the enzyme is a dehydrogenase rather than a functional oxidase (see chapter 1.2.9). This implicates, that the active site is constructed in a way to prevent such an artificial reaction.

Steady-state conditions allow determination of the flavin reoxidation rate

The rate constant of the artificial oxidative half-reaction k_{reoxi} was indirectly determined using a modified assay of the reductive half-reaction (chapter 4.1.2). In this steady-state assay *Ec*POX was mixed with pyruvate dissolved in air-saturated buffer solution. Again the flavin cofactor was used as intrinsic probe and decrease in absorbance was monitored at 438 nm, which corresponds to FAD reduction.

Initial loss of absorbance is caused by pyruvate-triggered reduction of FAD in the pre-steady-state phase (figure 21) as observed in the reductive half-reaction (chapter 4.1.2). Subsequently, in a counteracting process the previously reduced $FADH_2$ is reoxidized by molecular oxygen observed as increase in absorbance due to formation of oxidized flavin. A steady state of FAD and $FADH_2$ is established after 10 seconds for *Ec*POX wt (figure 21). However, this phase only takes a few seconds and ends due to oxygen

depletion, which also causes the slow loss of absorbance until the measurement finishes. Once oxygen is completely converted, *Ec*POX catalysis stops at HE-ThDP intermediate.

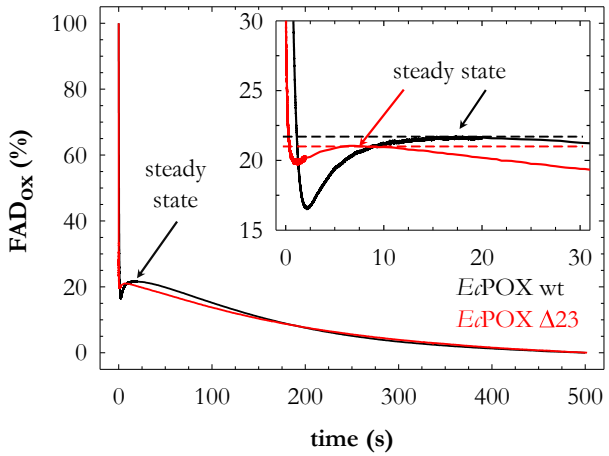

figure 21: Pyruvate-induced flavin reduction of *Ec*POX wt and Δ23 at aerobic conditions. 2 mg/mL of *Ec*POX were rapidly mixed with 200 mM pyruvate in the presence of oxygen. Flavin reduction was monitored at 438 nm and 20°C. Progress curves were converted to relative amount of oxidized flavin. The position of the steady state is indicated with an arrow. Inset: FAD reduction of the first 30 seconds. Dashed lines highlight the amount of oxidized FAD in the steady state (*Ec*POX wt: 22 % FAD_{ox}, Δ23: 21 % FAD_{ox}).

Since net rates of reduction (k_{red}) and reoxidation (k_{reoxi}) are equal during steady state, equilibrium of oxidized and reduced flavin is established. The position of this equilibrium in combination with the previously determined k_{red} of the reductive half-reaction (chapter 4.1.2 table 9) can be used to calculate the reoxidation rate according to equation 9 and equation 10. As described for the rate constant k_{red}, k_{reoxi} is also a mixed constant which reflects not only the electron transfer from $FADH_2$ but also oxygen binding and product release.

equation 9 $$\frac{FAD}{FADH_2} = \frac{k_{reoxi}}{k_{red}}$$

FAD = amount of oxidized FAD in equilibrium (%)

$FADH_2$ = amount of reduced FAD in equilibrium (%)

k_{red} = rate constant of reductive half reaction (s^{-1})

k_{reoxi} = rate constant of $FADH_2$ reoxidation (s^{-1}) by oxygen

equation 10 $$k_{reoxi} = \frac{FAD}{FADH_2} * k_{red}$$

Flavin reoxidation rate of *Ec*POX variants

EcPOX wt and proteolytically activated ⊿23:

The different resting-state activities of full-length *Ec*POX and *Ec*POX Δ23 are also reflected in the rate constants of flavin reduction and reoxidation. While the wt enzyme shows slow reduction of the flavin cofactor in the pre-steady state (k_{red} = 1.9 ± 0.001 s^{-1}) and poor reoxidation by molecular oxygen (k_{reoxi} = 0.54 ± 0.0003 s^{-1}), the proteolytic activated Δ23 variant can accelerate both processes approximately 400fold (k_{red} = 848 ± 78 s^{-1}, k_{reoxi} = 225 ± 21 s^{-1}) (figure 21 and table 10).

The observed enhancements due to proteolytic truncation are presumably caused by both a more accessible active site, which improves substrate binding (this was reported to be the rate-limiting step in *Ec*POX catalysis [45]), and repositioning of the residue Phe465 that can accelerate the electron transfer between both cofactors in *Ec*POX Δ23. A similar effect of significantly increased flavin reoxidation upon proteolytic processing was described for xanthine oxidoreductase [110]. This enzyme is expressed as dehydrogenase showing poor reoxidation, but is activated to a functional oxidase due to proteolytic digestion. Here, the increased reoxidation rate is attributed to rearrangement of loop Gln423-Lys433 closing the active site after proteolysis, which suppresses access of other electron acceptors than oxygen. Consequently, ubiquitous oxygen is utilized for cofactor regeneration yielding enzymatic oxidase activity.

In connection with the physiological function the different reoxidation rates of full-length *Ec*POX and Δ23 seem to be astonishing on the first view since one would expect poor artificial flavin reoxidation also in activated *Ec*POX. One interpretation could be that inhibition of artificial reoxidation plays only a minor role in catalysis of *Ec*POX Δ23. The pyruvate-reduced full-length enzyme needs to inhibit unfavored reoxidation in the cytosol until it is recruited to the membrane and interacts with the electron acceptor Q_8. Otherwise, energy is not conserved by *Ec*POX. Once attached to the membrane, fast electron transfer to Q_8 seems to be beneficial. This membrane-bound state is resembled by the activated variant Δ23, which favors an accessible active site concomitant with accelerated electron transfer. Suppression of reoxidation by oxygen in this state seems to be less importance.

Although the physiological relevance of different reoxidation rates of full-length *Ec*POX and activated Δ23 is still unclear, the reoxidation rate can be used as parameter to classify the examined variants.

Putative signal transfer variants F465A, Y278F, Y549A and F260A:

As stated earlier, *Ec*POX has to prevent electron transfer to oxygen while localized in the cytosol to conserve energy. Since shuffling of the electrons starts from $FADH_2$, it seems reasonable that the enzyme matrix suppresses oxygen reactivity already near the flavin cofactor. One predestined candidate for shielding the flavin against oxygen could be Tyr278. The crystal structure of the resting-state enzyme implies that this residue is positioned in 3.2 Å vicinity to the redox active N5- and C4a-atom of the flavin and forms a hydrogen bond to flavin-N5 (figure 22 and figure 14). However, the relevance of this hydrogen bond needs to be examined.

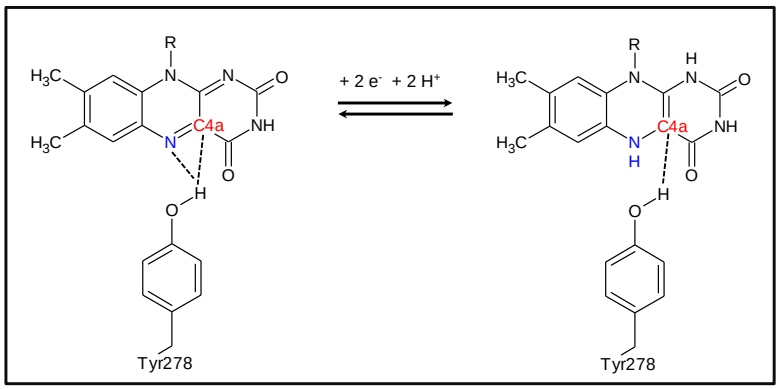

figure 22: Redox reaction of the flavin cofactor and interactions of the isoalloxazine ring with Tyr278. The redox active centers N5 and C4a are highlighted in blue and red color, respectively. The potential hydrogen bond between Tyr278 and N5-atom as well as the interaction with C4a-atom are indicated by dashed lines.

The amount of oxidized FAD in equilibrium is shifted for *Ec*POX Y278F by 12 % towards the oxidized species with respect to the wt enzyme (*Ec*POX wt: 23 % FAD, Y278F: 35 % FAD) leading to k_{reoxi} of 0.54 ± 0.0003 s^{-1} and 1.11 ± 0.001 s^{-1} for *Ec*POX wt and Y278F, respectively (figure 23 and table 10). Since flavin reduction is not affected in Y278F (chapter 4.1.2), the 2fold increased reoxidation rate can be directly related to events starting from the reduced flavin cofactor. Due to the fact that no structural changes are observed for the variant compared to *Ec*POX wt (chapter 4.1.7), it is reasonable to assume that oxygen migration to the active site or product release are identical for wt enzyme and Y278F. Thus, the increased k_{reoxi} can be attributed to a participation of Tyr278 in the reoxidation process. One can propose that the hydroxyl function of Tyr278 is involved in suppression of unfavored electron transfer to molecular oxygen. This hypothesis was further investigated with pyruvate oxidase from *Lactobacillus plantarum*, an enzyme which can be classified as real oxidase (chapter 4.4).

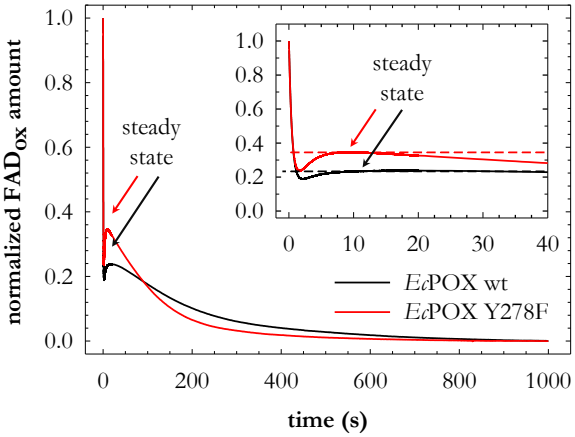

figure 23: Pyruvate-induced flavin reduction of *Ec*POX wt and Y278F at aerobic conditions. 2 mg/mL of *Ec*POX were rapidly mixed with 200 mM pyruvate in the presence of oxygen. Flavin reduction was monitored at 438 nm and 20°C. Progress curves were converted to relative amount of oxidized flavin. The position of the steady state is indicated by an arrow. Inset: FAD reduction of the first 40 seconds. Dashed lines highlight the amount of oxidized FAD in the steady state (*Ec*POX wt: 22 % FAD_{ox}, Y278F: 35 % FAD_{ox}).

As already observed for flavin reduction, variant F260A shows slightly accelerated flavin reoxidation. However, a 1.5fold increased k_{reoxi} is most likely caused by a more accessible active site which improves oxygen migration within the enzyme.

Surprisingly, a 10fold increased k_{reoxi} can be detected for variant *Ec*POX Y549A with respect to the wt enzyme. This increase of the flavin reoxidation rate in combination with a 20fold accelerated flavin reduction rate is most likely related to increased accessibility of the catalytic center. Improved accessibility could be provided by release of the membrane anchor from the protein surface.

Reoxidation of the flavin cofactor in variant F465A was demanding to investigate since analysis of the reductive half-reaction already revealed disturbed electron transfer to FAD (chapter 4.1.2). Although the progress curve of the steady-state assay showed a decrease of oxidized FAD, no steady state was established after subsequent reoxidation within the measuring time of 1000 seconds (chapter 8.5). Therefore, it was not possible to calculate k_{reoxi}. It can be suggested that in variant F465A flavin reduction and reoxidation are severely impaired which underlines the pivotal role of Phe465 in *Ec*POX catalysis.

Potential alpha-peptide binding variants I554A/G, L565A/G, W570G:

The reoxidation rates of semi-activated variants, which are potentially involved in hydrophobic membrane anchor binding, are analyzed from another point of view. Here the difference between the full-length variants and *Ec*POX wt Δ23 are of great importance. Nearly all variants showed accelerated flavin reduction in combination with an at least 2fold increased reoxidation rate. However, these results indicate that the variants are still wt-like enzymes and are less similar to *Ec*POX Δ23. As already discussed for flavin reduction (chapter 4.1.2), the slight changes observed are most likely caused by increased accessibility of the active site due to a partly released membrane anchor which enhances oxygen migration into the active site.

table 10: Overview of rate constants for the reductive and oxidative half-reaction for *Ec*POX variants. k_{red} was determined by a single-exponential equation from progress curves of the reductive half-reaction (table 9). k_{reoxi} was calculated from progress curves of flavin reduction at steady-state conditions using equation 10. Individual progress curves for all examined *Ec*POX variants are displayed in the appendix (chapter 8.5). (n. d. = not determined, [a] = no steady state was established)

***Ec*POX variant**	k_{red} **(s^{-1})**	k_{reoxi} **(s^{-1})**	**FAD : $FADH_2$ (%)**
wt	1.9 (± 0.001)	0.54 (± 0.0003)	22 : 78
wt Δ23	848 (± 78)	225 (± 21)	21 : 79
F465A	0.02 (± 0.00002)	- [a]	- [a]
Y278F	2.1 (± 0.002)	1.11 (± 0.001)	35 : 65
Y549A	37.9 (± 0.13)	7.22 (± 0.025)	16 : 84
F260A	4.6 (± 0.003)	0.88 (± 0.0006)	16 : 84
D328A, D348A, Q537A (*Ec*POX 3x)	n. d.	n. d.	n. d.
L565A	5.2 (± 0.007)	1.30 (± 0.002)	20 : 80
L565G	16.3 (± 0.043)	3.34 (± 0.009)	17 : 83
I554A	4.4 (± 0.017)	1.31 (± 0.005)	23 : 77
I554G	4.6 (± 0.007)	1.01 (± 0.002)	18 : 82
L565G, I554G (*Ec*POX 2G)	n. d.	n. d.	n. d.
W570G	2.2 (± 0.003)	0.42 (± 0.0006)	16 : 84

4.1.4 *Ec*POX activation by limited proteolysis

Limited proteolysis of *Ec*POX is an artificial process exclusively observed *in vitro* which has no relevance for *Ec*POX functionality *in vivo* [32]. However, it was often used in the past as substitute for membrane binding studies of *Ec*POX since proteolytically activated enzyme and membrane-bound *Ec*POX show similar catalytic parameters [18]. In both cases the increased catalytic activity is attributed to removal of

the membrane anchor from the protein surface. This anchor is either truncated, as observed during proteolysis reaction, or stabilized by lipids of the membrane.

Extension of the minimal model of three different *Ec*POX conformations

As detailed described in the introduction (chapter 1.2.4) proteolysis studies of *Ec*POX allow creation of a minimal model comprising three different enzyme conformations (figure 5). In the resting-state enzyme (R-state) the activating Δ23 cleavage site is protected, while a non-activating restriction locus leading to *Ec*POX Δ101 is exposed. Pyruvate binding, resembled by the substrate-bound state (SB-state), induces a first conformational change resulting in protection of both cleavage sites. Solely the electron transfer reaction yielding reduced $FADH_2$ in the substrate-reduced state (SR-state) leads to exposure of the Δ23 restriction site coupled to release of the membrane anchor and thus to the formation of activated *Ec*POX Δ23.

Although the previously created minimal model describes fairly the three different *Ec*POX conformations it lacks one aspect. One can assumed, that the substrate-bound enzyme (Δ101 and Δ23 protected) is not directly converted to the substrate-reduced state (Δ101 protected and Δ23 accessible) due to flavin reduction. It seems more likely that electrons are transferred to FAD but the conformational change proceeds afterwards. Thus, a new enzyme conformation needs to be introduced: a substrate-reduced enzyme in which the Δ23 and Δ101 cleavage sites are still protected, while FAD is already reduced (figure 24). This conformation is now called SR II. Accordingly, SR III resembles the state where the Δ23 cleavage site is exposed and membrane anchor is released due to the second structural rearrangement. In this regard equilibrium of SR II and SR III is established if no stabilizers like lipids or proteases are present which fix species SR III. The position of the equilibrium is of central importance for *Ec*POX functionality since SR III is the only conformation capable for efficient membrane binding *in vivo* or proteolytic activation *in vitro* (figure 24).

In the following section alteration of the SR II:SR III equilibrium due to amino acid substitution in the different variants will be detailed discussed and compared to the wt enzyme. One can assume that equilibrium is shifted towards species SR III in enzyme variants showing decreased membrane anchor stabilization and partial release. Analysis if the SR II:SR III position was performed by limited proteolysis and monitored with two methods: SDS-PAGE and Q_0 activity assay.

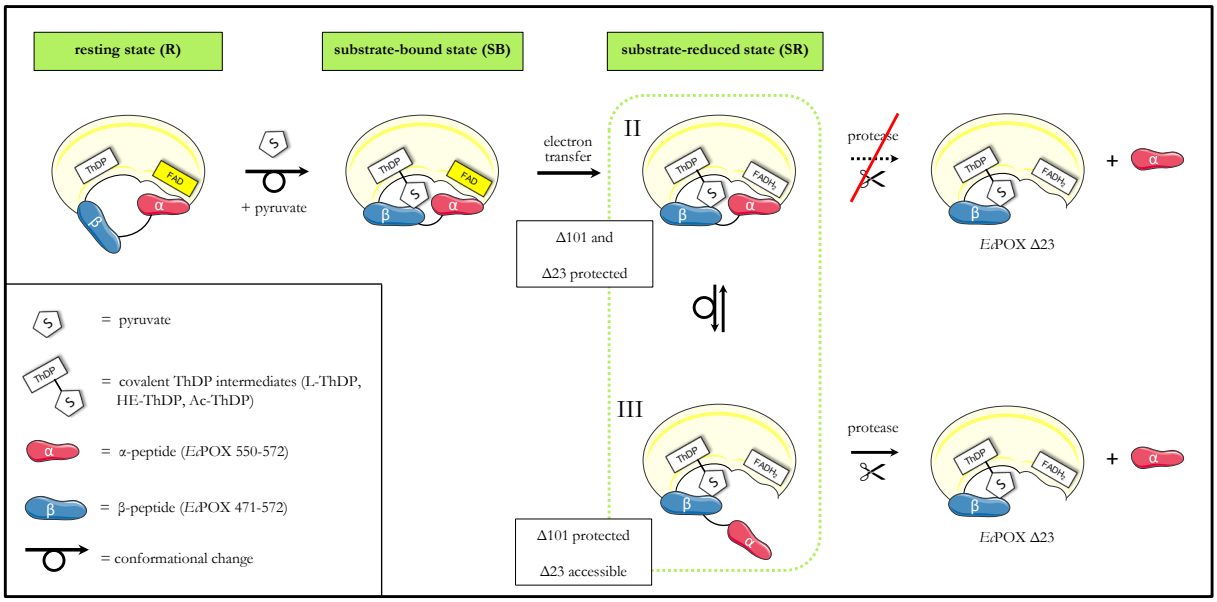

figure 24: Supposed model of proteolytic *Ec*POX activation. In the **resting state (R)** the Δ101 cleavage site is accessible whereas the Δ23 restriction site is protected. The **substrate-bound state (SB)** is induced by formation of covalent ThDP-intermediates, while FAD remains unaffected. Both protease cleavage sites are protected. The **substrate-reduced state (SR)** is formed due to pyruvate-induced reduction of FAD. Equilibrium of two forms is established: **SR II** represents an enzyme species where the flavin cofactor is already reduced, but the Δ23 cleavage site is still protected. **SR III** resembles the enzyme after the second conformational change with an exposed Δ23 cleavage site and a released membrane anchor. Only state III is competent to produce activated *Ec*POX Δ23 upon proteolytic digestion. The functional tetramer of *Ec*POX is simplified illustrated as monomer for better visualization. Note that the alpha-peptide is displayed separately from the beta-peptide, although the alpha-peptide resembles the C-terminal part of the beta-peptide.

Determination of the position of the SR II:SR III equilibrium by SDS-PAGE

Limited proteolysis was used to investigate the activation process and to locate the position of the SR II:SR III equilibrium. While enzyme state SR II should remain uncleaved during the proteolysis reaction, SR III can be digested to activated *Ec*POX Δ23 (figure 24). Thus, the position of SR II:SR III equilibrium was determined indirectly via Δ23 formation exclusively generated from SR III. Since SR III is continuously removed from equilibrium due to digestion, the full-length enzyme is completely converted over time to *Ec*POX Δ23.

SDS-PAGE can be applied to detect the formation of *Ec*POX Δ23 [35]. Here, the enzyme was reduced with pyruvate followed by addition of alpha-chymotrypsin to initiate the digestion reaction. Gel samples were taken after distinct time points and analyzed by SDS-PAGE. The position of the SR II:SR III equilibrium of different variants with respect to the wt enzyme was compared using the half-life ($t_{1/2}$) of the digestion reaction. The half-life, which corresponds to the time where 50 % of the full-length protein is cleaved to Δ23, was used to calculate the rate constant k_{act} of the activation process assuming single-exponential formation of Δ23 (equation 4). In this regard, a higher k_{act} (derived from a smaller $t_{1/2}$) resembles an increased amount of SR III in equilibrium with respect to the wt enzyme.

To investigate whether amino acid substitutions in the variant also alter other conformational changes than the SR II→SR III transition the digestion reactions was also performed with the resting-state enzyme (R-state). In an additional digestion approach MAP was added instead of pyruvate to generate the

phosphonolactyl-ThDP intermediate. Generation of this pre-decarboxylation mimic induces the first conformational change from the R-state to the SB-state.

As example proteolysis reactions of *Ec*POX wt and variant I554G, which is supposed to be involved in membrane anchor stabilization, are shown exemplary in figure 25 and table 11. Digestion patterns of other variants are presented in the appendix (chapter 8.6) and all rate constants of proteolytic activation are summarized in table 11.

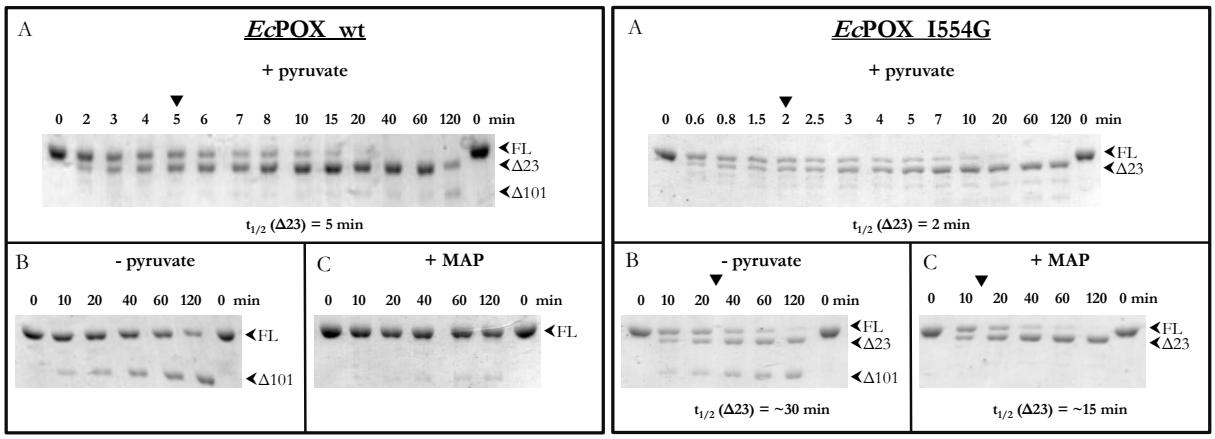

figure 25: Proteolytic digestion of *Ec*POX wt and I554G monitored by SDS-PAGE. A: + pyruvate. 48.4 µM of *Ec*POX was reduced with 200 mM pyruvate for 10 min at room temperature and 0.4 µM alpha-chymotrypsin was added to initiate digestion reaction. Gel samples were prepared after distinct time points and 0.6 µg of proteolyzed *Ec*POX were analyzed by SDS-PAGE. **B: - pyruvate.** *Ec*POX was treated similar to A, but pyruvate was omitted. **C: + MAP.** *Ec*POX was treated similar to A, but 20 mM MAP was added as substitute for pyruvate. The different protein bands are indicated as followed: FL = full-length protein, Δ23 = *Ec*POX Δ550-572, Δ101 = *Ec*POX Δ471-572. Half-life of the digestion reaction ($t_{1/2}$), where half of the full-length protein is cleaved to Δ23, is highlighted (▼).

*Ec*POX wt shows an activation rate of 0.14 min^{-1} ($t_{1/2}$ = 5 min) in the presence of pyruvate. As already stated above, without any substrate the wt enzyme is cleaved into Δ101, whereas the addition of MAP prevents the proteolysis reaction. Remarkably, variant I554G shows a 2.5fold increased k_{act} = 0.35 min^{-1} ($t_{1/2}$ = 2 min) if the enzyme is reduced with pyruvate. Surprisingly, also in the presence of MAP or without substrate Δ23 generation is detected.

Determination of the SR II:SR III equilibrium by activity assay

As second method the Q_0 activity assay was applied to determine the amount of SR III in equilibrium. Here, increase in activity due to formation of Δ23 from SR III was used. Since Δ23 exhibits a 30-fold accelerated activity compared to the full-length form of the wt enzyme (full-length wt: k_{cat} = 6.6 ± 0.2 s^{-1}, Δ23: k_{cat} = 185.8 ± 2.7 s^{-1}, chapter 4.1.1) the increase in activity can be directly correlated to the amount of generated Δ23. Due to the fact that incubation of enzyme state SR II with protease would not lead to truncation of *Ec*POX it was assumed that catalytic activity of SR II is similar to the resting-state protein (R-state).

The proteolysis reaction is performed identical to proteolysis visualized by SDS-PAGE but progress of digestion is monitored by Q_0 steady-state assay. Increase in catalytic activity is displayed in dependence of

incubation time with alpha-chymotrypsin (figure 26). The rate constant k_{act} of this assay is determined by a single-exponential equation (equation 5) and should correspond to k_{act} derived from SDS-PAGE analysis. Again activation of *Ec*POX wt in comparison to variant I554G is shown exemplary (figure 26). Activation of other variants is displayed in the appendix (chapter 8.6) and summarized in table 11.

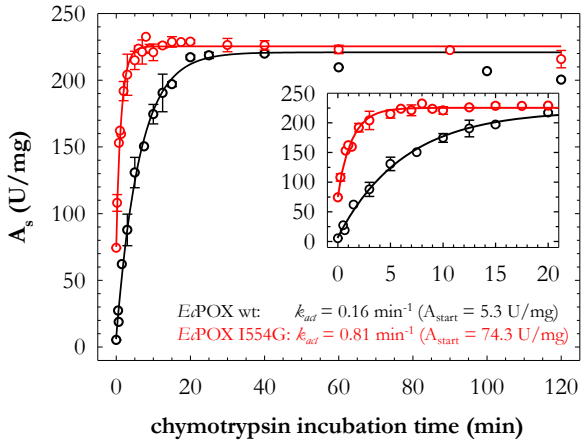

figure 26: Proteolytic activation of *Ec*POX wt and I554G monitored by Q_0 steady-state assay. Proteolytic digestion was performed similar to the SDS-PAGE experiment and activated enzyme was examined by Q_0 steady-state assay after distinct time points. Increase in activity (dots) due to Δ23 formation was analyzed by a single exponential equation (lines). Inset: Enlargement of the first 20 minutes.

The rate constants of activation obtained by Q_0 steady-state assay are in good agreement to k_{act} determined by SDS-PAGE (table 11). I554G is converted 5fold faster to the corresponding Δ23 variant than wt. As already observed in steady-state kinetics, the resting-state activity (in this regard the activity prior to alpha-chymotrypsin addition) was higher than in the wt enzyme.

Proteolytic activation of *Ec*POX variants

Putative signal transfer variants F465A, Y278F, Y549A and F260A:

*Ec*POX F465A is not activated by addition of alpha-chymotrypsin. Only traces of Δ23 are detected by SDS-PAGE if F465A is digested in the presence of pyruvate. The majority of the protein is rapidly cleaved to inactivate *Ec*POX Δ101. This result is not astonishing, since no complete flavin reduction is observed (chapter 4.1.2) which is a prerequisite for the structural transition SR II→SR III. Additionally, in the presence of MAP also Δ101 is formed which implies that the conformational transition R→SB (leading to protection of the Δ101 cleavage site due to substrate binding) is altered. This finding is further supported by the observation that formation of Δ101 from the resting state protein is enhanced. Thus, a central role of Phe465 in the structural reorganization induced by covalent substrate binding and in the electron transfer process from HE-ThDP to FAD is feasible.

Wt-like behavior is observed for variant *Ec*POX F260A with similar activation rates derived from both assays. Also proteolysis of the resting state and substrate-bound state shows no deviations to *Ec*POX wt. Thus, residue Phe260 seems to neither participate in the signal transfer nor in release of membrane anchor prior to membrane binding.

Contrary results are observed for *Ec*POX Y278F. The half-life of pyruvate-reduced enzyme is 4fold increased with respect to the wt enzyme (*Ec*POX wt: $t_{1/2}$ = 5 min, Y278F: $t_{1/2}$ = 20 min). Since all steps

leading to reduced flavin are not affected (chapter 4.1.2), the SR II:SR III equilibrium seems to be shifted towards the SR II form with a shielded Δ23 cleavage site. However, Tyr278 is an active site residue and is not involved in membrane anchor stabilization at the protein surface. Thus, information transfer from the active site to the membrane anchor seems disturbed in the variant Y278F. This residue could act as initial sensor for perception of the reduced flavin.

Limited proteolytic digestion of variant Y549A was also performed although the primary cleavage site of Δ23 (*Ec*POX Y549-M550) is altered in this mutant. However, it was reported that other proteases like trypsin (preferred cleavage C-terminal to Lys or Arg) and even proteases with broader specificity like subtilisin or proteinase K exclusively process the full-length enzyme of *Ec*POX to Δ23 after pyruvate addition [18]. Therefore, the presence of Tyr549 at the primary cleavage site seems to be of less importance. Proteolysis of Y549A in the presence of pyruvate shows no significant deviations to the wt enzyme. Pyruvate-reduced enzyme is completely digested to Δ23 with a $t_{1/2}$ of 5 minutes. Remarkably, a slight amount of Δ23 is formed in the absence of pyruvate or in the presence of MAP. This is also observed for several variants potentially involved in membrane anchor stabilization by hydrophobic interactions and is detailed described later. In summary, this observation is explained by an already released membrane anchor in the resting state or substrate-bound state.

table 11: H**alf-lives and k_{act} of proteolytic activation derived from SDS-PAGE and Q_0 activity assay for *Ec*POX variants.** The half-life $t_{1/2}$ corresponds to formation of Δ23 from pyruvate-reduced enzyme monitored by SDS-PAGE. $t_{1/2}$ was used to calculate k_{act} from SDS-PAGE (equation 4). k_{act} determined by Q_0 activity assay was calculated using a single-exponential equation 5. $t_{1/2}$ determined by SDS-PAGE – pyruvate corresponds to the half-life of Δ23 formation where pyruvate was omitted from the digestion approach. (- = no Δ23 formation was detected)

***Ec*POX variant**	**$t_{1/2}$ determined by SDS-PAGE (min)**	**k_{act} calculated from SDS-PAGE (min^{-1})**	**k_{act} determined by Q_0 assay (min^{-1})**	**$t_{1/2}$ determined by SDS-PAGE - pyruvate (min)**
wt	5	0.14	0.16 (± 0.01)	-
F465A	-	-	-	-
Y278F	20	0.04	0.06 (± 0.002)	-
Y549A	5	0.14	0.16 (± 0.04)	>>120
F260A	5	0.14	0.19 (± 0.02)	-
D328A, D348A, Q537A (*Ec*POX 3x)	5	0.14	n. d.	-
L565A	2.5	0.28	0.51 (± 0.04)	~120
L565G	2	0.35	0.42 (± 0.04)	10
I554A	3	0.23	0.52 (± 0.03)	>120
I554G	2	0.35	0.81 (± 0.06)	~30
L565G, I554G (*Ec*POX 2G)	~0.75	0.92	0.69 (± 0.13)	<<10
W570G	~1.75	0.40	0.29 (± 0.02)	>120

Potential alpha-peptide binding variants 3x, I554A/G, L565A/G, 2G, W570G:

Wt-like behavior is observed for variant *Ec*POX 3x lacking electrostatic interactions for stabilization of the membrane anchor. Thus, it is suggested that the SRII:SR III equilibrium is similar positioned as in *Ec*POX wt and that the conformational transition SR II→SR III is not altered. Therefore, participation of residues Asp328, Asp348 and Gln537 in stabilization or membrane anchor release from the protein seems unlikely.

Similar results as previously shown for variant I554G are also observed for the other variants (L565A/G, I554A/G, 2G, W570G) that are supposed to be involved in hydrophobic membrane anchor binding. Those variants show an increased activation rate of pyruvate-reduced enzyme compared to *Ec*POX wt. One can speculate that due to removal of hydrophobic contacts in those variants the SR II:SR III equilibrium is shifted towards the SR III-state which resembles membrane anchor release from the protein surface. Further, an indirect proportionality of the resting-state k_{cat} and the half-life of digestion is observed (figure 27). As seen in steady-state kinetics, Gly substitutions with a minimal hydrophobic character show a higher activity than the corresponding Ala variants.

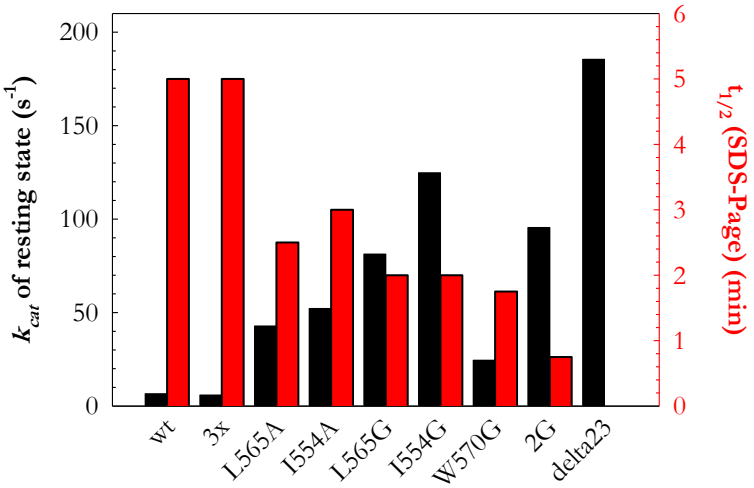

figure 27: Correlation of resting-state activity with observed half-life of Δ23 generation determined by SDS-PAGE. k_{cat} of the resting-state enzyme was calculated from Q_0 steady-state assay using Michaelis-Menten equation (table 8). $t_{1/2}$ of proteolytic digestion with pyruvate-reduced enzyme was determined by SDS-PAGE (table 11).

Remarkably, variants L565A/G, I554A/G, 2G and W570G are also truncated to activated Δ23 in the absence of pyruvate as seen by SDS-PAGE (table 11). In those variants already in the resting state a conformation is present in which the Δ23 cleavage site and accordingly the membrane anchor is exposed. Therefore, the minimal model of different *Ec*POX conformation needs to be further extended.

Second extension of the minimal model

The R-state was hitherto described by a conformation showing an exposed Δ101 cleavage site, while the Δ23 restriction site is protected (later termed R I). The new conformation R III represents now an *Ec*POX structure with hidden Δ101 cleavage site and accessible Δ23 restriction locus. As described above for conformations SR II and SR III (figure 24) the structural conversion between R I and R III might proceed with the help of a third conformation where both cleavage sites are protected (R II). One can assume that due to reversibility of the structural transitions equilibrium of these three conformations is established.

Since no formation of Δ23 is observed for the resting state of the wt enzyme, the position of the R-state equilibrium is strongly shifted towards R I and R II. The thermodynamic barrier for the structural transition R II→R III seems to be too high leading to an absence of R III in equilibrium. However, variants potentially involved in hydrophobic membrane anchor binding (I554A/G, L565A/G, 2G, W570G) show an increased amount of R III in equilibrium. This leads to quantitative formation of activated Δ23 also in the absence of pyruvate in the digestion approach. Thus, a decreased stabilization of the membrane anchor at the protein surface seems to lower the barrier of the R II→R III transition and the membrane anchor is partially released.

Similar observations can be made if variants which are potentially involved in hydrophobic membrane anchor binding are incubated with MAP during proteolysis. Under this condition these variants are converted to activated Δ23, while the wt enzyme remains uncleaved. Thus, also enzyme state SB must be described as equilibrium of three conformations. The position of this equilibrium is shifted towards state SB II in the wt enzyme, while in those variants also state SB III accumulates.

4.1.5 *Ec*POX activation by the membrane mimic SDS

Limited proteolysis was used in chapter 4.1.4 to investigate the activation process of *Ec*POX. Both applied assays required an established equilibrium of conformations SR II and SR III of the enzyme to generate activated *Ec*POX Δ23. Given that the proteolysis assay is an artificial system, the results previously observed were validated by stimulations of *Ec*POX with SDS. This activation system is probably more native-like since SDS mimics the cell membrane.

The activation model of SDS

It was reported that *Ec*POX shows an increased activity if detergents or lipids are present in *in vitro* assays [34]. The molecular mechanism of interaction of the enzyme with such amphiphiles is still uncertain due to the fact that no structures of *Ec*POX in complex with detergents or lipids are available. However, interactions of those amphiphilic molecules with the enzyme are supposed to be restricted to the membrane anchor, since activity of the proteolytically activated Δ23 variant failed to be further accelerated by addition of amphiphiles [18]. One could speculate that lipids or detergents stabilize the exposed membrane anchor of pyruvate-reduced *Ec*POX similar to the native membrane by induction of a helical structure.

A similar mode of activation was proposed for SDS-stimulation and proteolysis for *Ec*POX (figure 28). The enzyme is reduced with pyruvate leading to equilibrium of enzyme forms SR II and SR III. While the membrane anchor is still attached to the protein surface in SR II, possible interactions with SDS are supposed to maintain resting-state activity. Remarkably, only conformation SR III resembles a released membrane anchor which could be stabilized by SDS contacts leading to accelerated activity. The increase in activity can be directly correlated to the amount of SR III in equilibrium.

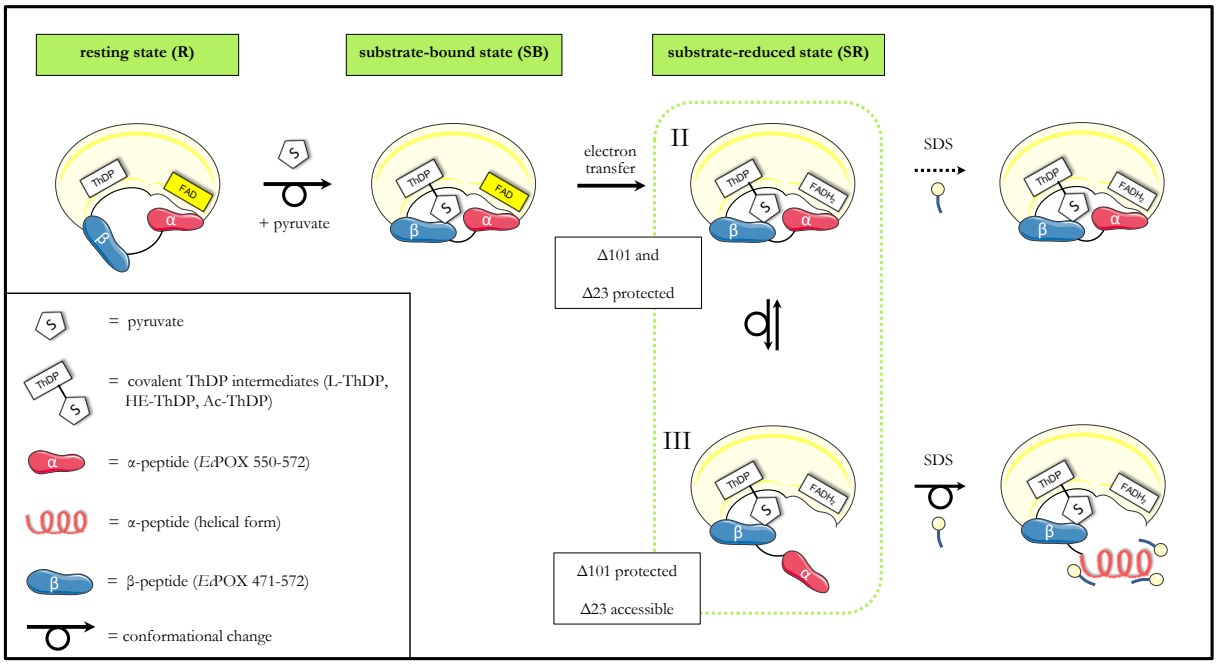

figure 28: Supposed model of SDS-mediated *Ec*POX activation. In the **resting state (R)** the Δ101 cleavage site is accessible whereas the Δ23 restriction site is protected. The **substrate-bound state (SB)** is induced by formation of covalent ThDP-intermediates, while FAD remains unaffected. Both protease cleavage sites are shielded. The **substrate-reduced state (SR)** is formed due to pyruvate-induced reduction of FAD. Equilibrium of two forms is established: **SR II** represents an enzyme species where the flavin cofactor is already reduced, but the Δ23 cleavage site is still protected. **SR III** resembles the enzyme after the second conformational change with an exposed Δ23 cleavage site and a released membrane anchor. Only state III is competent to be activated by SDS leading to helix formation of the membrane anchor. The functional tetramer of *Ec*POX is simplified illustrated as monomer for better visualization. Note that the alpha-peptide is displayed separately from the beta-peptide, although the alpha-peptide resembles the C-terminal part of the beta-peptide. Different conformations of the R- and SB-state as previously determined by proteolysis experiments (chapter 4.1.4) were omitted for reasons of clarity.

However, activation of *Ec*POX with SDS illustrates not only the transition SR II→SR III but also the property of the membrane anchor to form an amphipathic helix. One can assumes that only a properly folded helix can be stabilized by SDS resulting in the desired activity acceleration. Therefore, this method additionally allows analysis of the intrinsic helix propensity of the membrane anchor which might be altered due to amino acid substitutions in variants I554A/G, L565A/G, 2G and W570G.

SDS-mediated activation assay

To study the influence of different amino acid residues on the activation in a native-like system *Ec*POX is stimulated with SDS in an assay constructed similar to the proteolysis experiments. The enzyme is pre-incubated with pyruvate to establish SR II:SR III equilibrium. Addition of SDS leads preferentially to stabilization of the SR III-state which is therefore gradually removed from equilibrium.

After initiation of the activation process by addition of different amounts of SDS, the increase in activity is determined after distinct time points using the Q_0 steady-state assay (figure 29 A and B). Afterwards, obtained activities are displayed in dependence of the SDS concentration (figure 29 C). Although this figure is not time-resolved, for one specific SDS concentration the lowest activity corresponds to an SDS incubation time of approximately one minute and the final activity to enzyme stimulated for 30 min with SDS. To compare the different variants the final activity is converted to relative activity by adjusting the

maximum activity to 100 %. Activation studied with different amounts of SDS allows determination of $SDS_{0.5}$, the SDS concentration where 50 % of the protein is activated after half of the measuring time (figure 29 D). $SDS_{0.5}$ describes the affinity of *Ec*POX for SDS molecules and was used as a measure to compare the different variants. Thus, an increase of $SDS_{0.5}$ with respect to the wt enzyme can indicate a smaller amount of SR III in equilibrium or a disturbed helix formation.

SDS-mediated activation of *Ec*POX variants

EcPOX wt:

Kinetics of SDS-mediated activation of *Ec*POX wt and variant L565A are exemplary shown in figure 29 A and B. Data of other variants are illustrated in the appendix (chapter 8.4) and summarized in figure 29 D. The wt enzyme is completely activated in the presence of 100 µM SDS. At this concentration the activation process is already finished within the dead time of the assay (approximately one minute). Intermediary activation is observed if 20-70 µM SDS are added. In those cases the activity is increased with longer SDS incubation time. $SDS_{0.5}$ was determined to be 50 µM.

Putative signal transfer variants F465A, Y278F, Y549A and F260A:

Variant F465A is not activated by SDS which resembles results observed in the proteolysis reactions. Since both assays rely on exposition of the membrane anchor in state SR III based on functional FAD reduction, the observed effects can be correlated to an impaired electron transfer to the flavin cofactor due to the substitution of Ala for Phe.

*Ec*POX Y278F shows nearly no activation if assayed with 30 µM SDS and complete activation only at 150 µM detergent. In comparison to the wt enzyme Y278F needs an approximately 1.5fold higher SDS amount to reach a similar activation level (*Ec*POX wt: $SDS_{0.5}$ = 50 µM, Y278F: $SDS_{0.5}$ = 70 µM). Since the amino acid sequence of the membrane-anchor is not altered in this variant, the observed results only correspond to a shift of the SR II:SR III equilibrium towards the SR II-state. The same effect was observed for proteolytic activation (chapter 4.1.4). Both experiments imply an important role of Tyr278 on the activation process starting from the reduced flavin cofactor.

A approximately 1.7fold decreased $SDS_{0.5}$ is detected for Y549A. Although the exchanged residue of this variant is located at the N-terminal end of the membrane anchor an influence on helix formation cannot be excluded. However, it seems more likely that the lowered $SDS_{0.5}$ is caused by a shift of the SR II:SR III equilibrium towards the membrane binding competent species SR III in the variant.

Wt-like activation is observed for *Ec*POX F260A with a $SDS_{0.5}$ of 50 µM. As already indicated in proteolysis reaction Phe260 does not seem to play a central role in release of the membrane anchor and helix formation and is therefore not involved in the activation process.

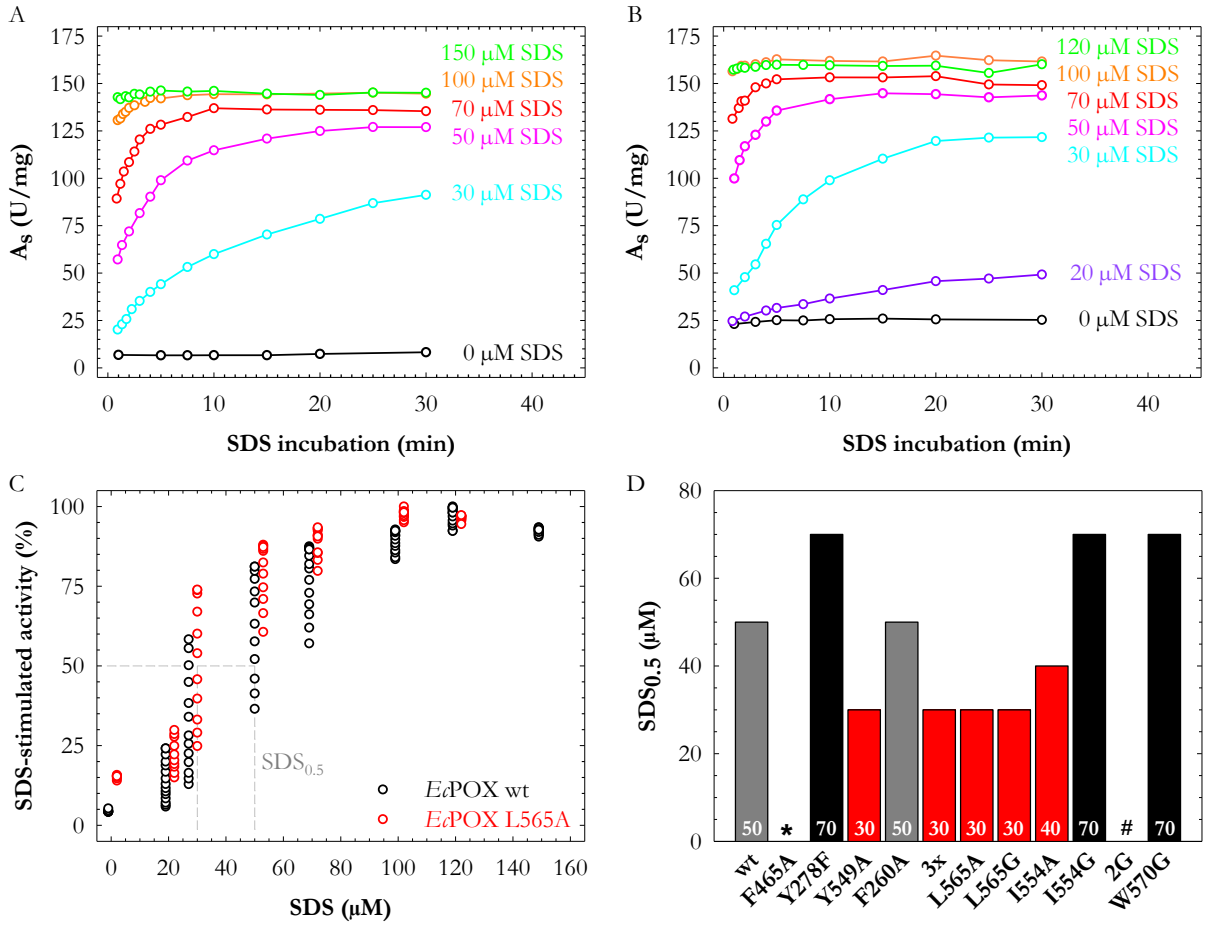

figure 29: SDS-mediated activation of *Ec*POX variants. 160 nM *Ec*POX were pre-incubated with 200 mM pyruvate. The activation process was initiated by addition of different SDS amounts and activity was monitored by Q_0 steady-state assay. A: Kinetics of *Ec*POX wt activation. B: Kinetics of *Ec*POX L565A activation. C: Comparison of SDS-mediated activation of *Ec*POX wt and L565A in dependence of the desired SDS concentration. Each ensemble of data points at a given SDS concentration resembles one curve of A and B. The gray dashed line highlights $SDS_{0.5}$. D: Comparison of $SDS_{0.5}$ values of *Ec*POX variants. $SDS_{0.5}$ values are displayed as bar plot and by white numbers. Red color indicates a $SDS_{0.5}$ smaller than wt whereas black color illustrates a $SDS_{0.5}$ higher than wt. (* F465 was not activated with SDS. # *Ec*POX 2G was already completely activated without SDS)

Potential alpha-peptide binding variants 3x, I554A/G, L565A/G, 2G, W570G:

Variants supposed to be involved in hydrophobic stabilization of the membrane anchor (I554A, L565A/G, 2G) show a decreased $SDS_{0.5}$ value compared with the wt enzyme. The most pronounced effect is observed for *Ec*POX 2G which is already completely activated in the resting state. Thus, one can suggest that the equilibrium between SR II and SR III is shifted towards the SDS-binding competent SR III-state in those variants. These findings are in line with proteolysis experiments and foster the idea that the membrane anchor is stabilized at the protein surface by hydrophobic interactions.

A similar observation can be made for variant *Ec*POX 3x which lacks the prominent electrostatic interactions and hydrogen bonds of the membrane anchor to the protein core. Compared to *Ec*POX wt the determined $SDS_{0.5}$ value is 1.7fold decreased which reveals accumulation of state SR III in equilibrium. However, this result is in contrast to proteolytic digestion approaches which show a wt-like equilibrium position. One could speculate that due to its amphiphilic nature SDS is able to provide electrostatic

interactions contrary to the protein surface. Thus, SDS could increase the amount of the exposed form of the membrane anchor which leads to accelerated activity compared to the wt enzyme.

An opposite effect is observed for *Ec*POX I554G and W570G. For both variants a $SDS_{0.5}$ of 70 µM is determined. These findings are in contrast to proteolysis experiments where the equilibrium of SR II and SR III is shifted towards the SR III-state and a partially released membrane in the resting state is detected. Therefore, the decreased $SDS_{0.5}$ value is most likely caused by a disturbed helix formation due to the amino acid exchanges in both variants which leads to a decreased affinity for SDS molecules. One could propose that the $SDS_{0.5}$ would be even lower but that the accumulation of SDS-binding competent SR III in equilibrium counteracts disturbed generation of the helix.

4.1.6 Temperature-induced unfolding of *Ec*POX

It was previously reported that the full-length enzyme of *Ec*POX is significantly stable, since it resists a heat precipitation step during purification [15]. Contrary, pyruvate-reduced enzyme tends to aggregate [18]. Thus, it was suggested that the reduced enzyme resembles the membrane-bound *Ec*POX protein, while oxidized *Ec*POX corresponds to a typical cytosolic enzyme [111]. Temperature-labile behavior is also observed for the proteolytically activated *Ec*POX Δ23, which aggregates at conditions where the full-length enzyme is particular stable.

Analysis of the resting-state conformations by thermal unfolding

Stability of full-length *Ec*POX, proteolytically activated Δ23 and several variants was investigated by temperature-induced inactivation. Unfolding was monitored by far-UV CD spectroscopy at 208 nm. At this area mainly alpha-helical parts of the protein produce a negative signal, which disappears due to unfolding at higher temperatures (figure 30).

Temperature-dependent unfolding of the *Ec*POX protein is an irreversible process since refolding trials of the unfolded protein by stepwise decrease in temperature did not generate a functional enzyme (data not shown). Nevertheless, an apparent melting temperature was determined with the equation of Pace [87] which is typically used to examine melting temperatures of reversible unfolding processes. Thus, only an apparent T_m was obtained with this method. Since the experiments were performed under identical conditions the determined T_m could be used for qualitative comparison of different variants.

The different *Ec*POX variants were only examined in the absence of substrate which exclusively allows statements concerning the resting state of the enzyme. The obtained results should therefore correlated to proteolysis experiments of resting-state *Ec*POX in the absence of pyruvate and MAP. In this regard, a decreased melting temperature indicates a partly released membrane anchor from the protein surface.

Thermal unfolding of *Ec*POX variants

EcPOX wt and activated ⊿23:

Compared to full-lenght *Ec*POX wt activated Δ23 shows a by 15 °C decreased apparent T_m (figure 30 B and table 12). However, it is astonishing that such an enormous difference is caused by deletion of 23 amino acids which resemble only a surface-attached membrane anchor of the protein. Thus, a stabilizing effect of this membrane anchor to the entire protein structure besides membrane binding is suggested.

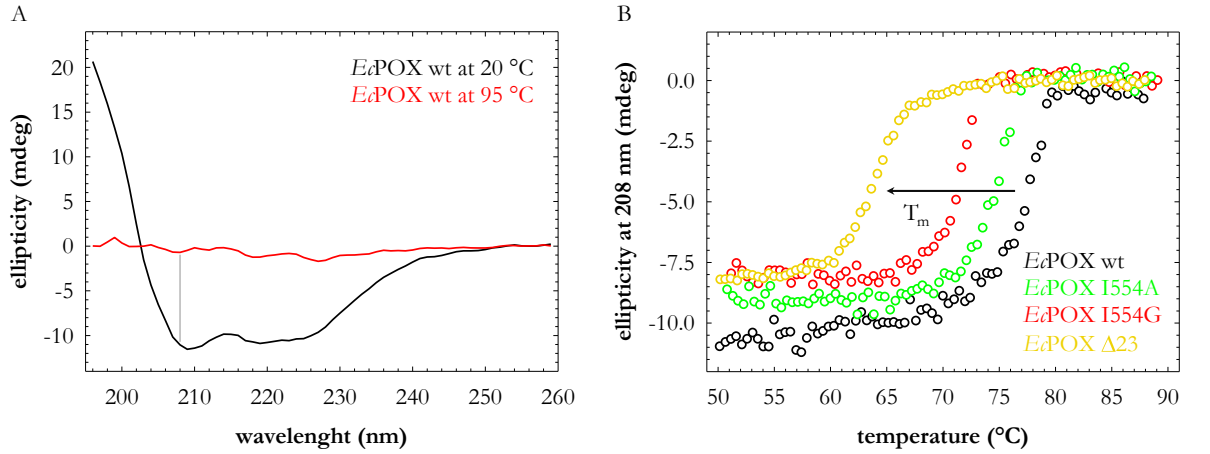

figure 30: Thermal unfolding of *Ec*POX wt and selected variants. A: CD spectra of native (20 °C) and unfolded (95 °C) *Ec*POX wt (0.1 mg/mL, path lenght 1 mm). The signal at 208 nm (grey line) was used for temperature-dependent denaturation. B: Temperature-dependent unfolding of *Ec*POX wt and selected variants at 208 nm. Progress curves were used to calculate the apparent melting temperature T_m by equation 6. The shift of the observed melting temperature T_m for the variants is indicated by an arrow. Unfolding curves of other variants are displayed in the appendix (chapter 8.3) and calculated T_m are presented in table 12.

Putative signal transfer variants Y549A and F260A:

The observed T_m of *Ec*POX F260A is only slightly decreased compared to the wt enzyme. Thus, the membrane anchor is still attached to the protein in the variant which is in good agreement to proteolytic digestion experiments of the resting-state enzyme.

Contrary, variant Y549A shows a significantly by 5 °C decreased T_m. As already indicated by proteolysis reactions the membrane anchor of *Ec*POX Y549A seems to be destabilized leading to a partial release and thus to an enhanced thermal unfolding similar to *Ec*POX Δ23.

Potential alpha-peptide binding variants 3x, I554A/G, L565A/G, 2G, W570G:

Variant *Ec*POX 3x lacking three prominent electrostatic interactions and hydrogen bonds to the membrane anchor shows similar unfolding like the wt protein. One can conclude that this mutant reflects the wt enzyme with a membrane anchor clamped to the protein. This finding is in line with previous analysis of limited proteolysis in the absence of substrate.

table 12: Apparent melting temperatures of *Ec*POX variants. Apparent T_m was calculated from unfolding curves (figure **30** B) using equation 6. (n. d. = not determined)

***Ec*POX variant**	**app. T_m (°C)**
wt	78.4
wt Δ23	63.8
F465A	n. d.
Y278F	n. d.
Y549A	73.0
F260A	76.7
D328A, D348A, Q537A (*Ec*POX 3x)	78.4
L565A	73.5
L565G	71.0
I554A	74.8
I554G	71.6
L565G, I554G (*Ec*POX 2G)	67.8
W570G	76.1

Almost all variants supposed to be involved in hydrophobic membrane anchor binding show a decreased T_m value compared with *Ec*POX wt. Gly variants with a minimal hydrophobic character compared to the native Leu or Ile unfold at lower temperatures similar to activated *Ec*POX Δ23. This finding also correlates with an increased k_{cat} of the resting state analyzed by Q_0 steady-state assay (figure 31). However, in both assays substitutions of Ala for Ile and Leu lead to results less pronounced. Therefore, Ala mutants show still wt-like properties, while the Gly variants are more similar to Δ23.

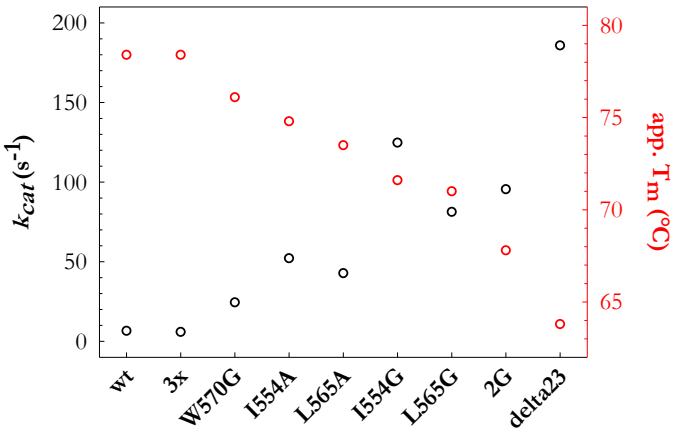

figure 31: Correlation of resting-state activity with the apparent melting temperature of *Ec*POX variants. k_{cat} of the resting-state enzyme was determined by Q_0 steady-state assay (table 8). Apparent T_m was obtained from thermal unfolding curves (table 12).

4.1.7 *Ec*POX structure determination by X-ray crystallography

The crystal structures of full-length and proteolytically activated *Ec*POX revealed only minor structural changes [35]. A prominent difference within the active site was repositioning of Phe465 between both cofactors upon activation, which was interpreted to facilitate electron transfer between the thiamine and flavin cofactors. Due to truncation of the membrane anchor, a reorganization of the residual membrane binding domain was also observed in Δ23 which results in improved accessibility of the active site.

Crystal structures of *Ec*POX variants in the resting state were generated and analyzed focusing both on differences within the active site and on the polypeptide chain conformation of the membrane anchor and its relative orientation to the remaining part of the molecule. The determined resting-state structures were compared to the structure of the full-length protein or activated Δ23, respectively (pdb: 3EY9 and 3EYA, [35]). Results should be related to proteolysis and thermal unfolding experiments of the resting state of each variant.

Crystal structures of *Ec*POX variants

Crystallization of several variants was performed similar to the wt enzyme [82] and bright yellow crystals grew typically within one week. After cryo-protection, the crystals were measured at different synchrotrons resulting in datasets within 3.24 to 2.8 Å resolution range (table 7 and table 13).

All *Ec*POX variant crystals are isomorphous with wt enzyme which crystallized in tetragonal space group $P4_32_12$ with two molecules of *Ec*POX per asymmetric unit. The final structures were solved by using the full-length structure of *Ec*POX wt as initial model and further refinements (chapter 3.25). Data collection and final refinement statistics are summarized in the appendix (chapter 8.7) and root-mean-square deviations (r.m.s.d.) compared to the wt structure are displayed table 13. Due the low resolution of the crystal structures one should be aware that minor but important changes of central amino acids were potentially not resolved in the calculated electron density maps.

Putative signal transfer variants Y278F, Y549A and F260A:

Variant Y278F is investigated with special focus on the interaction of the substituted amino acid with the flavin cofactor and on the architecture of the active site. Comparison of the obtained Y278F structure with the wt enzyme reveals neither deviations of the overall structural organization of the protein nor rearrangements within the active site (figure 32 A and table 13). Additionally, the position and conformation of Phe278 side chain in the variant was not changed significantly to Tyr278 in the wt enzyme. Noteworthy, for the six ring atoms of Phe278 the occupancy was refined to 70 %. This implicates an important role of the proposed hydrogen bond to the N5-atom of the flavin in stabilizing the conformation of Tyr278. If this interaction is disrupted by deletion of the hydroxyl function in the variant, the side chain seems to be more flexible and the position shows an increased uncertainty in the crystal. Nevertheless, this minor change could not explain the significant differences of Y278F compared to the wt observed in proteolysis and flavin reduction experiments.

table 13: R.m.s.d. values of variant structures of *Ec*POX and *Lp*POX. R.m.s.d. values were calculated based on the position of the Cα-atoms with the program lsqman [112] using the *Ec*POX wt structure (pdb: 3EY9), *Ec*POX Δ23 (pdb: 3EYA) and *Lp*POX wt structure (unpublished high-resolution at 1.09 Å structure of *Lp*POX wt was friendly provided by Dr. Danilo Meyer, Department of Bioanalytics, Göttingen). All amino acids were included in the model. Amino acid residues which deviate more than 3 Å from the models were excluded from r.m.s.d. calculations and are listed in the table. All excluded residues were mainly located in highly flexible loop regions. A, B and I-J in the table indicate different chains in the structures. (n. c. = no crystals were obtained, n. d. = not determined, [a]= only the tetramer composed of subunits I-L was used for r.m.s.d. calculations)

variants	final resolution (Å)	r. m. s. d. (Å)	excluded amino acid residues
F465A	n. c.	n. c.	-
Y278F	2.96	0.195	B: Lys2, Leu476
Y549A	2.79	0.120	B: Lys2
F260A	3.08	0.125	B: Lys2
D328A, D348A, Q537A (*Ec*POX 3x)	3.20	0.162	B: Lys2
L565A	3.24	0.204	A: Gly474, B: Lys2
L565G	n. c.	n. c.	-
I554A	3.02	0.183	A: Gly474, B: Lys2
I554G	2.90	0.190	A: Leu476, B: Trp475, Leu476
L565G, I554G (*Ec*POX 2G)	n. d.	n. d.	-
W570G	n. d.	n. d.	-
***Ec*POX Δ23:Q_0**	3.20	0.140[a]	I/J/K/L: Met1, Gly479[a]
***Lp*POX F289Y**	1.43	0.061	B: Thr9

Variants Y549A and F260A were also analyzed concerning rearrangements within the active site and potential release of the membrane anchor from the monomer surface. Both variants show no significant structural deviations to the wt enzyme (table 13). Active site residue Phe465 reveals identical conformation as observed in the non-activated *Ec*POX structure and points away from both cofactors (figure 32 B). Further, the membrane anchor is still bound at the protein and reveals no elevated flexibility. For variant F260A these findings are in agreement to previous results obtained from proteolysis and thermal unfolding experiments which predict Phe260 to play no central role in membrane anchor stabilization or in the signal transfer from $FADH_2$ to the membrane anchor. Contrary, analysis of variant Y549A clearly indicated a partially released membrane anchor already in the resting state which cannot be observed in the crystal. This phenomenon is also observed for variants supposed to be involved in hydrophobic membrane anchor binding.

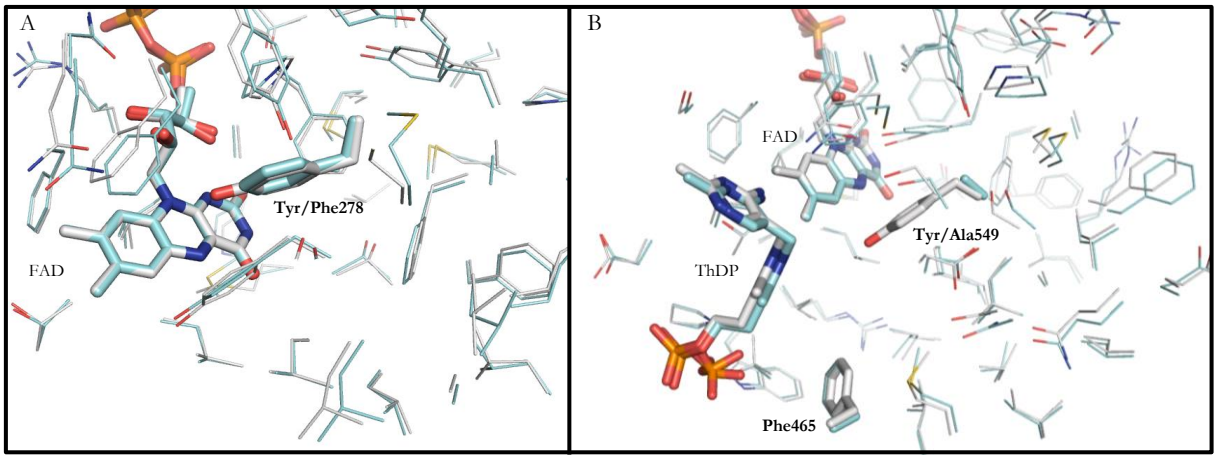

figure 32: Comparison of the crystal structures of *Ec*POX variants Y278F and Y549A with *Ec*POX wt. A: Comparison of *Ec*POX Y278F (blue) with the full-length enzyme (wt) of *Ec*POX (white). No significant structural changes are detected within the active site in the variant. B: Comparison of *Ec*POX Y549A (blue) with the full-length enzyme (wt) of *Ec*POX (white). Phe465 and Ala549 occupy an identical position in the variant as in the wt enzyme.

Although crystals of F465A were measured, structure determination of this variant failed. All crystals constituted of multiple layers and were not usable to determine the structure. Several attempts to improve the crystal properties, including screening of buffer conditions, were applied but failed.

Potential alpha-peptide binding variants 3x, I554A/G, L565A:

*Ec*POX 3x which lacks electrostatic interactions and hydrogen bonds to the membrane anchor shows a wt-like structure (table 13). This is in agreement with other experiments like proteolysis and temperature-induced unfolding.

No significant structural changes compared to the wt enzyme can be detected for variants I554A/G and L565A presumably involved in hydrophobic membrane anchor binding (table 13 and chapter 8.9). Although proteolytic digestion and thermal unfolding experiments reveal a partially released membrane anchor already in the resting state, this part is found attached to the protein surface in all three crystal structures (chapter 8.9). Thus, the obtained structures reflect species R I where the Δ23 cleavage site is protected, while the Δ101 restriction site is accessible.

To exclude that the obtained crystal structures suffered from model bias since the full-length structure was used as initial model a simulated annealing omit map as calculated with CNS was generated for variant *Ec*POX I554G. The obtained electron density mFo-DFc omit map shows that the protein backbone and amino acid side chains of the membrane anchor are defined up to residue 572, which argues against a model biased structure (figure 33 A).

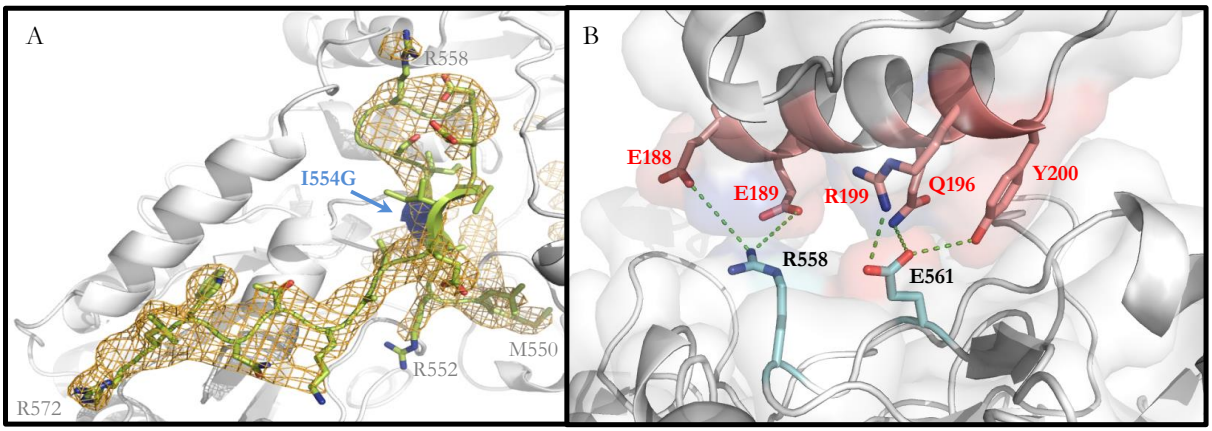

figure 33: Crystal structure of variant *Ec*POX I554G. A: Simulated annealing omit map for *Ec*POX I554G. The protein-attached membrane anchor (residues M550-R572) is presented in green whereas the protein core is shown as white cartoon. The obtained mFo-DFc omit map for the membrane anchor (simulated annealing omit map was calculated with CNS) is shown as orange mesh countered at +4 σ. The position of the exchanged residue I554G is indicated by a blue arrow. B: Crystal contacts of two subunits of *Ec*POX I554G. Potential interactions of two subunits within the crystal are shown as green dashed lines. Residues of the membrane anchor are presented as blue sticks whereas interacting side chains of the other subunit are depicted in red.

However, it seems reasonable that the obtained crystal structures of variants I554A/G and L565A do not reflect the solution state of the enzyme. Due to contacts of the subunits within the crystal the membrane anchor could be forced into this fixed conformation although it is more relaxed in solution (figure 33 B). Additionally, although equilibrium of three different R-states is supposed to be established it seems possible that only conformation R I with a protein-bound membrane anchor tends to crystallize under the given conditions.

4.2 Structural analysis of the membrane-associated membrane anchor

Analysis of the *Ec*POX-bound membrane anchor (alpha-peptide) indicates formation of two beta-strands and unstructured loops [35]. However, secondary structure predictions of the amino acid sequence of the isolated alpha-peptide reveal formation of a helix [29]. Indeed, it could be shown that the isolated peptide adopts a helical structure in the presence of the surface-active agent SDS, while in the absence of lipids or detergents the structure of the alpha-peptide is characterized by an increased amount of random-coil parts [35].

The influence of alpha-peptide sequence on stabilization to the protein surface of *Ec*POX was earlier described in chapter 4.1. This part focusses on the impact of membranes and mimics thereof on helix formation of the alpha-peptide and subsequent membrane binding. Similar to membrane anchor stabilization at the protein surface also the primary sequence of the alpha-peptide can affect intrinsic helix propensity. Further, properties of the membrane like surface charge and tension or lipid composition might improve or inhibit helix formation and concomitant bilayer association. For analysis of these different conditions only the isolated membrane anchor instead of the entire protein was used as simplified system. Far-UV CD spectroscopy allow initial insights on the global alpha-peptide

conformation, while liquid-state NMR studies reveal information about the three-dimensional structure on the atomic level. Therefore, labeling of the alpha-peptide with the heavy atoms ^{15}N and ^{13}C was necessary.

4.2.1 Preparation of the alpha-peptide

Heavy-atom labeling of the peptide is possible in two different ways. On the one hand the peptide can be chemically synthesized from labeled amino acids. However, not all labeled amino acids are commercially available and some amino acids are composed of labeled and non-labeled N- and C-atoms. Synthesized peptide samples derived from those amino acids would consist of several incompletely labeled species. On the other hand recombinant expression of the alpha-peptide in ^{15}N- and ^{13}C-containing media can be applied. Thereby, heavy atoms are introduced in the peptide during expression in the bacterial cell. This method was chosen for alpha-peptide labeling within this thesis. Since the final amount of pure peptide after expression was typically low due to numerous purification steps, optimization of the expression and purification procedures had to be performed.

Expression and purification of non-labeled alpha-peptide

The non-labeled alpha-peptide was recombinantly expressed as SUMO-alpha fusion construct in *E. coli* in rich media (figure 34 A). The SUMO-protein, which is N-terminal fused to the alpha-peptide (23 amino acids), exhibits a polyhistidine-tag which allowed purification by Ni affinity columns. The SUMO-protein was cleaved off by specific digestion with SUMO-protease which selectively recognizes the three-dimensional fold of SUMO [113]. Finally, both the protease and the SUMO-protein were removed from the peptide by a second Ni-affinity column since the peptide was untagged after cleavage.

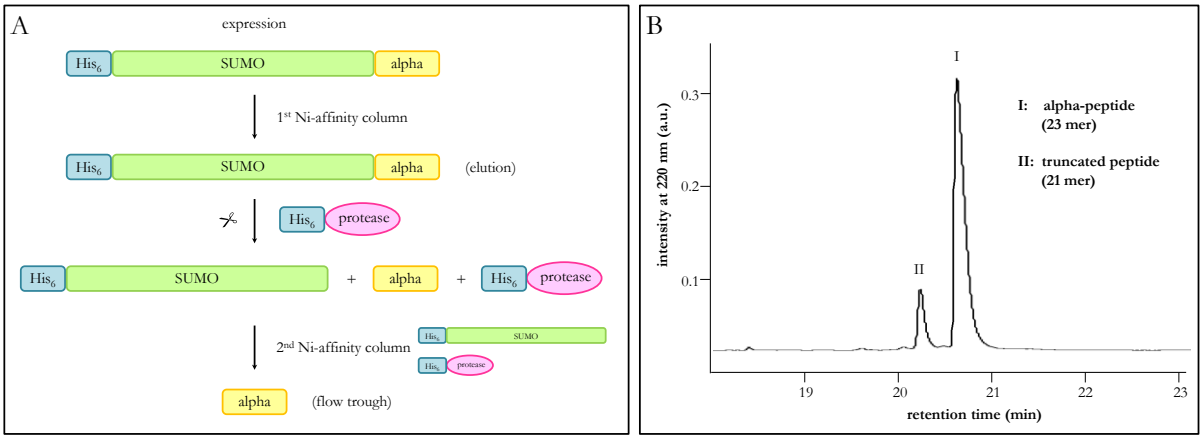

figure 34: A: Purification scheme of the SUMO-alpha fusion construct. The alpha-peptide is expressed as SUMO-fusion construct with an N-terminal polyhistidine-tag (His_6) and purified by Ni-affinity column. The SUMO-protein is cleaved by the SUMO-protease which also contains a polyhistidine-tag. Protease and SUMO-protein are removed from the alpha-peptide by a second Ni-affinity column and the alpha-peptide is found in the flow through. **B: Reversed-phase HPLC analysis of the obtained alpha-peptide fraction.** The alpha-peptide fraction from a standard purification was loaded on a C18 column and eluted with the analytical gradient (chapter 3.17). Fractions of peak I and II were collected and analyzed by mass spectrometry. Peak I was identified to be the desired alpha-peptide (23 mer) whereas peak II contained truncated peptide species like a 21 mer.

Reversed-phase HPLC analysis of the obtained peptide revealed that beside the full-length alpha-peptide also shorter fragments are generated (figure 34 B). Those species were identified by mass spectrometry as C-terminal truncated fragments of the entire alpha-peptide. To avoid these impurities in the peptide fraction expression and purification procedure were optimized (data not shown). While temperature changes did not lead to accumulation of the entire alpha-peptide, decreased expression time after induction showed a higher amount of the alpha-peptide compared to the unfavored fragments. Further, protease inhibitors were added during purification. However, no effect compared to untreated SUMO-alpha purification was detected. Thus, it is reasonable to conclude that degradation of the alpha-peptide already occurs during expression in *E. coli* cells and cannot be prevented. To remove truncated peptide fragments the obtained peptide solution was purified by reversed-phase HPLC.

Expression and purification of heavy-atom labeled alpha-peptide

Expression of labeled alpha-peptide was performed in M9 minimal media relying on the method of Marley and co-workers [84]. According to their procedure high cell mass is generated in rich media followed by exchange to media containing the labeled nutrients. During this step cells are dissolved in a smaller volume to generate a high cell density, which provides higher yields with respect to the applied cultivation volume. Finally, a short recovery period allows clearance of unlabeled substances followed by induction of protein expression. Purification of the alpha-peptide was similar to non-labeled peptide samples.

Prior to labeling several optimization trials were either performed in unlabeled media or with cells derived from expression in unlabeled media. With regard to the highest yield the following expression and purification parameters were optimized:

- cell density after media exchange
- expression time and temperature
- cell amount used for purification
- desalting step for imidazole removal prior to digestion
- removal of SUMO-protein and -protease after digestion

The final expression and purification procedure is detailed described in chapters 3.14 and 3.15. With this procedure 1.3 mg pure labeled alpha-peptide were obtained from 250 mL labeled media.

Determination of ^{13}C- and ^{15}N-incorporation rate

To investigate the amount of incorporated ^{15}N- and ^{13}C-atoms into the labeled alpha-peptide the HPLC-purified peptide was subjected to mass spectrometry analysis. A molecular weight difference of 151 g/mol calculated from non-labeled (2639 g/mol) and labeled (2790 g/mol) alpha-peptide corresponds to complete incorporation of ^{13}C and ^{15}N. Mass spectrometry analysis of the non-labeled peptide revealed the expected molecular weight of 2640.45 g/mol (figure 35 A). For samples of the labeled peptide a mass shift to 2766.68 - 2791.74 g/mol is detected (figure 35 B) which correspond to 84 – 100 % enrichment of

^{15}N and ^{13}C. Remarkably, the peak with the highest intensity (2789.74 g/mol) indicates 99 % successful heavy-atom incorporation

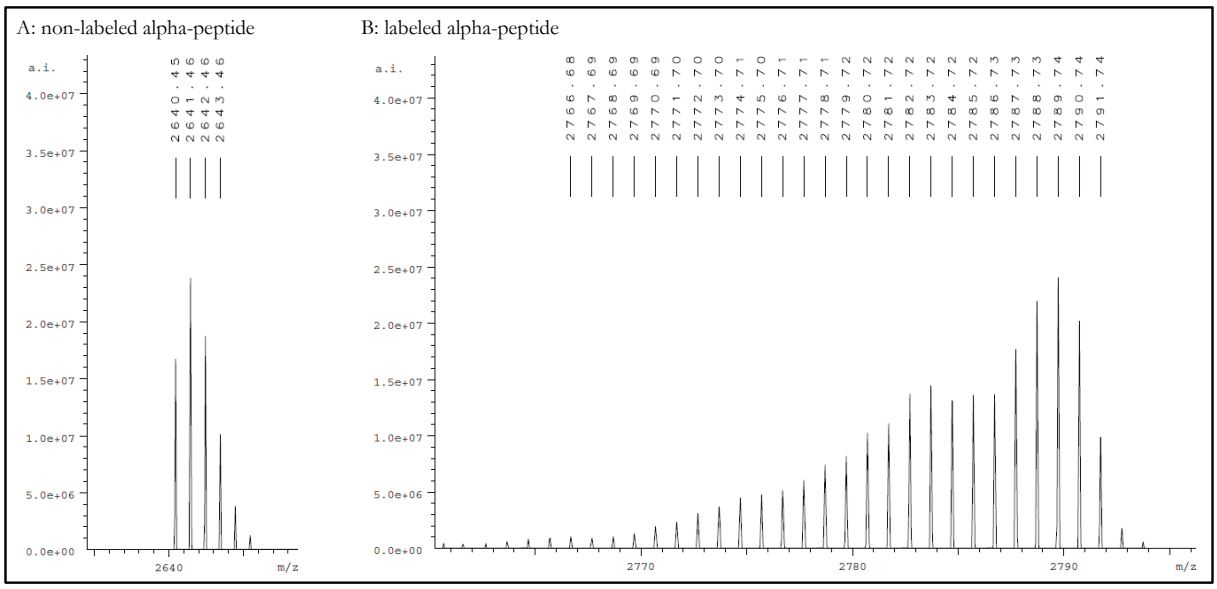

figure 35: Mass spectrometry analysis of non-labeled (A) and labeled (B) alpha-peptide. HPLC purified peptide samples were analyzed by electro spray ionization mass spectrometry performed by Dr. Holm Frauendorf (Department Zentrale Analytik und Massenspektrometrie, Göttingen). Spectra were deconvoluted prior to use. Molecular weight of the non-labeled peptide was determined to be 2640.45 g/mol and molecular weights of the labeled peptide were determined between 2766.68-2793.74 g/mol.

The enrichment of more than 84 % heavy atoms and the amount of labeled alpha-peptide were sufficient for structural studies by liquid-state NMR. Since a successful heavy-atom incorporation method is the base to examine the alpha-peptide structure in the presence of diverse lipids, extensive analysis with various membrane-like systems and varying lipid compositions are now possible.

4.2.2 Analysis of the alpha-peptide structure by far-UV CD spectroscopy

Analysis of the secondary structure of peptides and proteins by far-UV CD spectroscopy reveals insights into the overall fold [114] [115]. Deconvolution of obtained spectra can further examine the contribution of secondary structure elements to the global conformation. Here, CD spectroscopy was used to analyze the influence of detergent micelles (applied as membrane mimics) on helix formation of the alpha-peptide. Therefore, the peptide was reconstituted with 50 mM SDS or 50 mM DPC in buffer (figure 36). Both detergent concentrations were set at 20 x the CMC to ensure formation of micelles. Prior to the measurement the CMC was determined in the corresponding buffer system by ITC (chapter 8.1). Besides detergents also trifluoroethanol was added to the peptide to induce a distinct helical structure [95]. Afterwards, all spectra were deconvoluted with the implemented chirascan software CDNN [96].

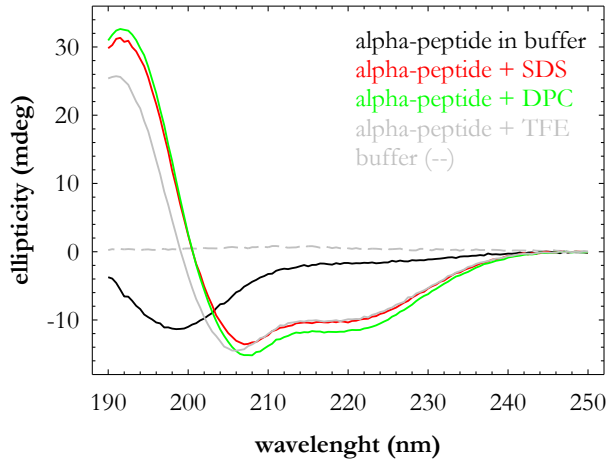

figure 36: Far-UV CD spectra of the alpha-peptide in detergents. 0.1 mg/mL alpha-peptide was examined by far-UV CD spectroscopy in a 1 mm cuvette at 20 °C. Measurements were performed in buffer (50 mM NaH_2PO_4 pH 6.0) supplemented with SDS (50 mM), DPC (50 mM) or trifluoroethanol (50 % (v/v)).

The alpha peptide adopts a random-coiled structure in the absence of detergents (figure 36 and table 14). Remarkably, the addition of SDS or DPC micelles leads to induction of a structure containing 41 % and 46 % helical motifs. Similar observations can be made for the alpha-peptide in the presence of trifuoroethanol (33 % helix). These results are in good agreement to the work of Weidner who reported 47 % helix amount due to SDS addition [45].

table 14: Secondary structure content of the alpha-peptide in the presence of detergent micelles. Percentage of secondary structure elements was calculated with the program CDNN [96] from spectra of figure 36.

	alpha-helix (%)	beta-sheet (%)	turn (%)	coil (%)
alpha-peptide in buffer	5	25	26	44
alpha-peptide + 50 mM SDS	41	16	18	25
alpha-peptide + 50 mM DPC	46	13	17	24
alpha-peptide + 50 % (v/v) trifluoroethanol	33	16	21	30

Noteworthy, the zwitterionic detergent DPC leads to a slightly increased helix amount compared to the anionic SDS, which raises the question if the peptide conformation is different in both detergents. Since solution-state NMR studies of the SDS-bound peptide revealed an extended helix [45], it seems reasonable that the DPC-attached alpha-peptide forms a more compressed helical motif. Comparison of the structure of both detergents indicates that especially the head group of DPC is more related to the native phospholipids phosphatidylglycerol and phosphatidylethanolamine found in the *E. coli* membranes (figure 37). Thus, one can assume that the conformation induced by DPC reflects more likely the native membrane-bound alpha-peptide. In this regard, NMR-studies of the peptide:DPC complex could reveal further insights.

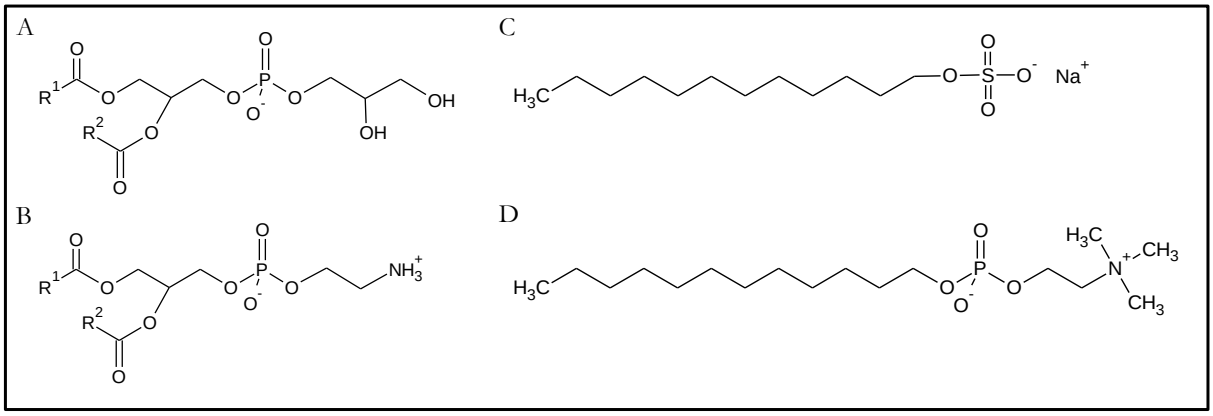

figure 37: Structural comparison of *E. coli* phospholipids and detergents. A: phosphatidylglycerol B: phosphatidylethanolamine, C: SDS, D: DPC. (R^1 and R^2 represent fatty acid tails)

Although it is demonstrated that the amphiphiles SDS and DPC mediate formation of a helical structure of the hitherto unstructured alpha-peptide it remains unclear how strong curvature and surface tension enhance this conformation. Since detergents are known to induce helices in peptides and proteins [116] it seems questionable if the observed alpha-peptide conformation is only related to properties of the used membrane mimic. It needs to be proven if membrane-like systems like bicelles and vesicles also lead to formation of an amphipathic helix of the alpha-peptide. In contrast to micelles lipid vesicles or bicelles better resemble the lipid bilayer due to the flat surface which severely reduced surface curvature and tension [46] (figure 38).

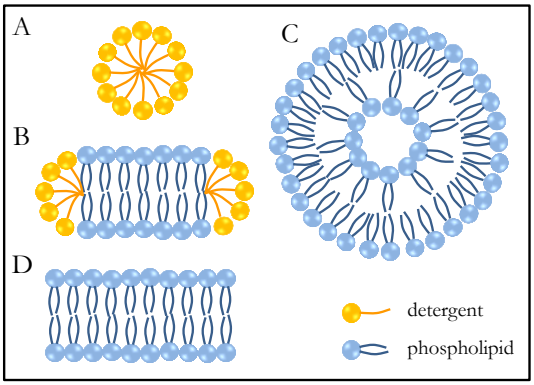

figure 38: Schematic representation of membrane mimics. A: Micelles formed from detergent molecules exhibit high curvature and surface tension. **B: Bicelles** are binary assemblies of long-chain lipids and detergents or short-chain lipids. Due to their planar bilayer formed of long-chain lipids surface tension and curvature are severely reduced. **C. Liposomes** resemble the native cell with a bilayer entrapped volume. Depending on their size curvature and surface tension may vary. **D: Membranes** are composed of lipid bilayers with almost no surface tension and curvature.

4.2.3 NMR structure determination in the presence of DPC micelles

Secondary structure analysis of the alpha-peptide in the presence of DPC micelles revealed a slight increase of the helical amount compared to incubation with SDS. It is suggested that the increased percentage of the helix motif is reflected in a partly altered structure of the peptide. Since the alpha-peptide helix determined in complex with SDS indicates an extended conformation it can be assumed that the DPC-induced helix is more compressed.

To investigate this hypothesis in a preliminary experiment the heavy atom-labeled alpha-peptide was subjected to liquid-state NMR studies in the presence of DPC micelles. Analyses were performed by Dr.

Piotr Wysoczanski and Prof. Dr. Markus Zweckstetter at the Department of Structure Determination of Proteins Using NMR (Max Planck Institute for Biophysical Chemistry, Göttingen).

Unfortunately, until the end of this thesis only a preliminary structure was available which revealed alpha-helix formation of the alpha-peptide in the presence of DPC micelles. Further, it was indicated that Arg of the peptide are involved in the interaction with the polar head groups of DPC. Few indications were obtained which opens speculation that hydrophobic Val13, Ile14 and Leu17 might be embedded into the core of micelles. Further analysis need to be performed to assign solve the structure of the entire peptide and positions of amino acid side chains.

The preliminary results are consistent with the previous structure of the alpha-peptide determined in the presence of SDS micelles (figure 10). Similar to the DPC-reconstituted peptide structure also the presence of SDS induces formation of an alpha-helix with Val13, Ile14 and Leu17 constituting the core of this helical motif [45]. Also the electrostatic interactions between positively charged Arg with the phosphate moieties of DPC are expected. It was shown for membrane binding of other amphipathic helices that these interactions are necessary to attract the peptide from the bulk solvent to the membrane surface [56] [58] [59]. However, an interesting point that needs to be studied is release of the membrane anchor from the membrane to ensure reversibility of binding. Therefore, variants of the alpha-peptide should be generated where several positively or negatively charged and hydrophobic amino acids are exchanged to Ala to study the impact of the desired amino acid on membrane binding and release of the alpha-peptide.

4.3 Investigations of the electron transfer from *Ec*POX to Q_8

A fundamental step in *Ec*POX catalysis is the electron transfer from the reduced flavin cofactor to the membrane-bound Q_8 leading to the regenerated enzyme and reduced Q_8 [17]. This energy-conserving step depends on translocation of *Ec*POX from the cytosol to the cell membrane to get access to the membrane-dissolved substrate Q_8. However, how the electrons are shuffled from the active site into the membrane remains open. One could speculate that the head group of ubiquinone can partly leave the membrane and penetrates the active site. This mechanism could allow electron tunneling between cofactor and substrate within a short distance of 14 Å [67]. On the other hand it can be proposed that electrons hop with the help of the protein backbone and side chains to Q_8. In this case, ubiquinone could remain located at the membrane interface. Both electron transfer mechanism and substrate interaction modes seem possible and need to be further investigated.

The reaction of reduced *Ec*POX with the substrate Q_8 can be simply described as followed:

$$Ec\text{POX-FADH}_2 + Q_8 \rightarrow Ec\text{POX-FAD} + Q_8H_2$$

Reduced pyruvate oxidase transfers two electrons to Q_8, which is subsequently reduced yielding Q_8H_2 and the regenerated enzyme. However, mandatory translocation of *Ec*POX to the membrane, which harbors Q_8, is missing in this scheme. In order to analyze the interaction of the enzyme with its substrate in more

detail a reconstitution of Q_8 into membranes or vesicles would be essential. To simplify analysis, the water-soluble analog Q_0, which lacks the isoprenoid tails, was used as Q_8 substitute. Importantly, it was assumed that binding and electron transfer of Q_0 and Q_8 proceed similar.

4.3.1 Proteolysis under steady-state conditions

Limited proteolysis was already applied to investigate conformational changes during the catalytic cycle. It was shown that formation of covalent ThDP intermediates reveals a non-cleaved enzyme, while truncation of *Ec*POX by 23 amino acids is only observed if the flavin cofactor is reduced [35]. Thus, formation of *Ec*POX Δ23 can be directly correlated to the flavin cofactor redox state.

This finding was used to analyze the flavin redox state under steady-state conditions where both pyruvate and Q_0 are present in saturating amounts to allow continuous turnover. A modified proteolysis assay was established as described earlier for analysis of *Ec*POX activation (chapter 4.1.4). Here, the enzyme was pre-reduced with pyruvate (which typically reveals formation of *Ec*POX Δ23 after proteolytic cleavage) but turnover was initiated by addition of Q_0. After 30 seconds steady state was established and alpha-chymotrypsin was added. On the one hand Q_0 conversion was monitored by UV-Vis spectroscopy. Additionally, samples were prepared after distinct time points to study *Ec*POX digestion to Δ23 by SDS-Page. Since higher protein concentrations were required for SDS-Page analysis compared to steady-state activity assays (chapter 3.19), Q_0 concentration was also increased to 10.4 mM (typical steady-state assay: 500 µM Q_0). Thus, absorbance had to be measured apart from the maximum Q_0 at 500 nm. As reference experiments *Ec*POX was subjected to digestion both in the absence of pyruvate or Q_0. Additionally, Q_0 conversion was also monitored by UV-Vis spectroscopy without proteolytic cleavage. The combination of proteolytic patterns and Q_0 conversion curves are displayed in figure 39.

Analysis of Q_0 conversion in the absence of alpha-chymotrypsin shows complete depletion within 10 minutes (figure 39 A top). However, if the protease is added after steady state is established, the reaction is only slightly enhanced with a total reaction time of 7 minutes. This minor difference indicates that only a small amount of Δ23 is generated during proteolysis. In fact, this conclusion is supported SDS-PAGE analysis (figure 39 A bottom). Only traces of Δ23 are formed if pyruvate and Q_0 are present in the digestion approach and the major amount of *Ec*POX remains uncleaved. Once Q_0 is completely depleted (after 7 minutes) and the excess of pyruvate results in complete reduction of *Ec*POX, the proteolysis reaction proceeds rapidly leading to quantitative Δ23 formation within two minutes. The reference experiments show that in the absence of Q_0 Δ23 is formed with a half-life of two minutes (figure 39 B). If pyruvate is omitted, 50 % of the full-length enzyme is cleaved to Δ101 after 20 minutes (figure 39 C).

These experiments illustrate that under turnover conditions *Ec*POX remains intact and the Δ101 and Δ23 cleavage sites are protected. Shielding of both restriction sites is caused by formation of covalent ThDP intermediates from pyruvate. Therefore, the flavin cofactor needs to be mainly oxidized in steady state. The only way this can be ensured is that flavin reoxidation by Q_0 is faster than all steps leading to FAD

reduction. In other words, once $FADH_2$ is present electrons are rapidly shuffled to Q_0 which ensures a mainly oxidized flavin.

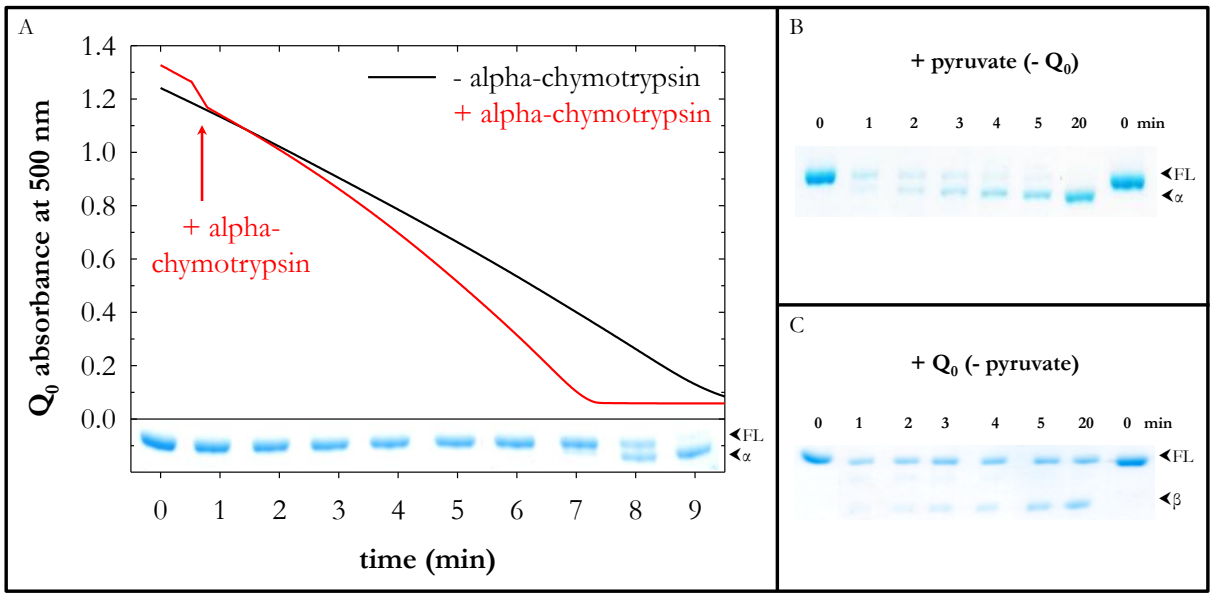

figure 39: Limited proteolysis of *Ec*POX under steady-state conditions. A: top: Q_0 conversion by *Ec*POX in the absence and presence of alpha-chymotrypsin (top) and the corresponding SDS-PAGE analysis of *Ec*POX digestion in under steady-state conditions (bottom). 0.186 mg/mL *Ec*POX were pre-reduced with 200 mM pyruvate and turnover was initiated by addition of 10.4 mM Q_0. After 30 seconds 20 µg/mL alpha-chymotrypsin were added to start proteolysis. Q_0 conversion was monitored at 500 nm and 20°C. Simultaneously, gel samples were prepared after distinct time points. B. Proteolytic digestion of *Ec*POX in the absence of Q_0. Digestion was performed similar to A but 10.4 mM Q_0 were omitted. C. Proteolytic digestion of *Ec*POX in the absence of pyruvate. Digestion was performed similar to A but pyruvate was omitted.

These observations are in line with previous investigations of microscopic kinetic events in *Ec*POX catalysis. Kinetic analysis of single catalytic steps revealed that covalent binding of pyruvate to the thiamine cofactor is the rate limiting step [45]. In combination with data from proteolysis under turnover conditions one can suggest that this is also the case during steady state.

4.3.2 Crystal structure of an *Ec*POX:Q complex

To analyze whether the active site of *Ec*POX can directly interact with Q_8 X-ray crystallography was applied. Therefore, crystal structures of proteolytically activated *Ec*POX Δ23 in complex with Q_0, the water-soluble analog of Q_8, should be generated. If Q_0 could be detected in the active site of *Ec*POX, direct electron tunneling between the flavin and Q_8 can be suggested.

*Ec*POX Δ23 was co-crystallized with varying concentrations of Q_0 at 20 °C similar to *Ec*POX Δ23. Crystals appeared within a few weeks in the presence of 10 molar equivalents Q_0 and were directly flash-cooled in a liquid nitrogen without further cryo-protections. Data collection was performed at the in-house source of the Department of Molecular Structural Biology and a final resolution of 3.2 Å was obtained for the best crystal. *Ec*POX Δ23:Q_0 complex crystallized in space group $P2_12_12_1$ with three tetramers per asymmetric unit. The structure was solved by using activated *Ec*POX as initial model and

performing further refinements. Data collection and preliminary refinement statistics are summarized in the appendix (chapter 8.7).

After initial rigid body refinement additional electron density and positive difference density is detected in all 12 subunits between both cofactors in the active site. It seems unlikely that side chain residues of the protein matrix are positioned in this area. Thus, in preliminary trials the substrate Q_0 was fitted into this density and one additional refinement cycle was performed. The obtained model and densities indicate that Q_0 could occupy this position in the active site (figure 40). Hydrogen bonding between amino acid side chains and the peptide backbone could stabilize Q_0. Additionally, the orientation of refined Q_0 could imply that native Q_8 potentially binds in the same manner with the isoprenoid anchor sticking out of the active site towards the membrane (figure 40). However, it was observed that occupancy and the position of Q_0 seem to vary between the subunits. Therefore, crystal quality and resolution should be improved to obtain a more detailed interaction model.

It was tried to obtain crystals of better quality by soaking of existing *Ec*POX Δ23 crystals in soaking solutions supplemented with different concentrations of Q_0 and for varying periods of time. Unfortunately, in most cases crystals cracked in the given soaking solution or the final resolution was even worse than observed for unsoaked crystals or crystals obtained using co-crystallization. Further optimizations should be performed by screening of buffer conditions and Q_0 concentrations for both co-crystallization and soaking approaches. Additionally, the Q_8-analogs Q_1 and Q_2 could be applied. It seems possible that a more fixed orientation of the benzoquinone ring can be observed due to one or two isoprenoid units attached in Q_1 and Q_2 which might interact with the protein surface near the active site and thus stabilize the position of 6-membered ring.

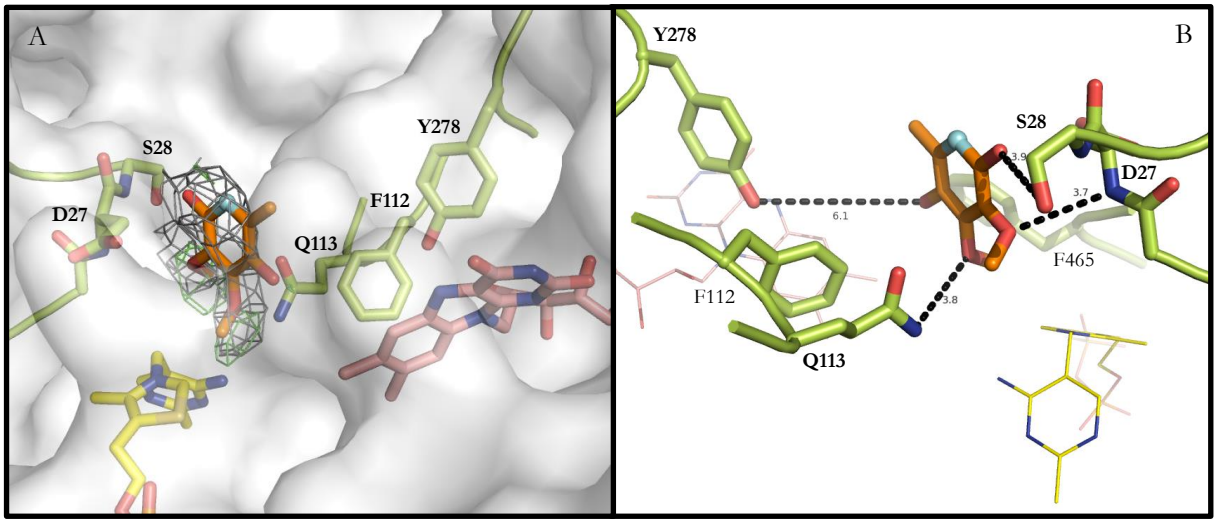

figure 40: Structure of an *Ec*POX Δ23:Q_0 complex. Q_0 is presented as orange stick model and the blue sphere indicates postion of a potential isoprenoid tail. The protein core is presented as white surface and selected amino acids are highlighted as green sticks. The cofactors ThDP (yellow) and FAD (rose) are depicted as sticks or lines. A: Electron density representation of bound Q_0 in the active site of *Ec*POX. Gray 2mFo-Fc density is countered at 1.2 σ and green mFo-DFc density is countered at +3 σ. B: Q_0 is bound at the active site of *Ec*POX by hydrogen bonds (black dashed lines) to side chains and the protein backbone. For representation monomer J of *Ec*POX Δ23 was used.

Due to poor resolution of the best crystal no final conclusion should be drawn from this preliminary structure. However, it could be speculated that Q_0 can bind in the active site with an orientation also suitable for native Q_8. Thus, it seems possible that Q_8 could partially leave the lipid bilayer to enter the active site and receive electrons from reduced flavin. In this case, no further participation of amino acid side chains or the protein would be necessary which would argue for electron tunneling rather that hopping.

4.4 Analysis of oxygen reactivity of *Ec*POX and *Lp*POX

Analysis of the artificial oxidative half-reaction revealed that Tyr278 is involved in suppression of unfavored oxygen reactivity in *Ec*POX. Due to its interactions with the N5-flavin atom as well as with the neighboring C4a-atom (figure 14) one can suggested that the hydroxyl moiety of Tyr278 represses binding of oxygen and thus determines *Ec*POX to act as dehydrogenase rather than as oxidase. This hypothesis was proved by mutational analysis of pyruvate oxidase from *Lactobacullis plantarum* which harbors Phe289 at the same position. The *Ec*POX-related enzyme *Lp*POX is known to be a real oxidase which converts molecular oxygen as native substrate [75]. It is supposed that Phe289 promotes increased reactivity towards oxygen in *Lp*POX whereas Tyr278 in *Ec*POX inhibits this reaction. Therefore, *vice versa* substitutions of *Lp*POX and *Ec*POX were performed leading to the variants *Lp*POX F289Y, which shall resemble *Ec*POX wt, and *Ec*POX Y278F, which may mimic *Lp*POX wt.

4.4.1 The catalytic cycle of *Lp*POX

Although both flavoenzymes are classified into different groups according to their oxygen reactivity, the catalytic cycle of *Lp*POX is similar to that of *Ec*POX [74] (figure 41). As observed in *Ec*POX pyruvate conversion yields HE-ThDP after decarboxylation. Subsequently, a single electron transfer step leads to formation of a flavin radical species. The second electron transfer to the flavin is coupled to phosphorolytic cleavage yielding acetyl phosphate. Finally, flavin regeneration is mediated by reoxidation with molecular oxygen.

As described for *Ec*POX, the redox state of the flavin cofactor is used to assign reductive and oxidative half-reaction for *Lp*POX [24]. Thus, the derived rate constants k_{red} and k_{reoxi} are not related to microscopic rates of individual reactions of the catalytic cycle but are mixed constants including several catalytic processes. Although k_{red} and k_{reoxi} resemble different steps of the enzymatic pathway they were used to examine the influence of Tyr or Phe near the flavin N5- and C4a-locus on oxygen reactivity of the desired enzyme.

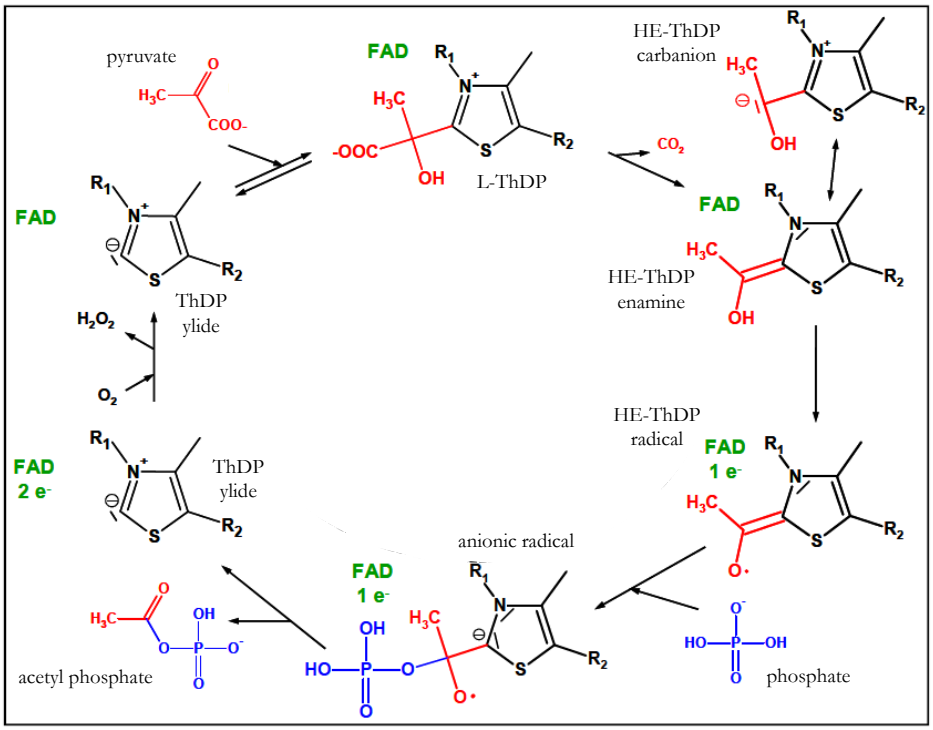

figure 41: Catalytic cycle of *Lp*POX. After activation of ThDP (not shown) pyruvate is bound yielding L-ThDP. Subsequently, decarboxylation leads to formation of HE-ThDP intermediate. Single electron transfer to FAD results in HE-ThDP radical intermediate. Phosphorolytic cleavage is coupled to the second electron transfer step. $FADH_2$ is regenerated with molecular oxygen yielding hydrogen peroxide. Figure was taken from Meyer [80] and slightly modified. (R^1 = aminopyrimidine moiety, R^2 = diphosphate anchor).

4.4.2 Flavin reduction at aerobic and anaerobic conditions

To determine the rate constants k_{red} and k_{reoxi} a similar experimental setup as described for *Ec*POX (chapters 4.1.2 and 4.1.3). Pre-steady-state kinetics with single turnover conditions for FAD were applied to analyze pyruvate-induced flavin reduction in the absence of electron acceptors. Additionally, steady-state conditions allowed calculation of the rate constant of the flavin reoxidation by molecular oxygen. Results of *Ec*POX Y278F were detailed described in chapters 4.1.2 and 4.1.3.

Upon pyruvate-induced flavin reduction in the absence of oxygen a lag-phase is observed, which resembles initial catalytic steps like pyruvate binding and decarboxylation (figure 42 A). Although this phase reflects only a small part of the overall amplitude (<10 %), kinetic traces were fitted with a double-exponential equation including the lag-phase and FAD reduction. In contrast to *Ec*POX Y278F the reductive half-reaction is significantly altered in *Lp*POX F289Y (figure 42 and table 15). k_{red} is 6.7fold decreased in the variants (16 ± 0.029 s^{-1}) relative to the wt enzyme (107 ± 0.689 s^{-1}) indicating that FAD reduction or previous catalytic steps are severely impaired.

Remarkably, no oxidized FAD is observed in the steady state for variant *Lp*POX F289Y at aerobic conditions, while 56 % of the flavin cofactor is oxidized in the wt (figure 42 B and table 15). The rate constants of the reoxidation were calculated for the wt enzyme (k_{reoxi} = 136 ± 0.877 s^{-1}) and for the F289Y variant (k_{reoxi} = 0.84 ± 0.002 s^{-1}) according to equation 10. Therefore, 5 % of oxidized FAD was estimated in the steady state, which corresponds to the threshold of the applied method. However, the rate constant of the variant is overvalued since the amount of oxidized flavin is only estimated to 5 % and seems to be lower.

As detailed described earlier, flavin reduction is not affected in *Ec*POX variant Y278F but a 2fold increased reoxidation rate is observed compared to *Ec*POX wt enzyme (table 15).

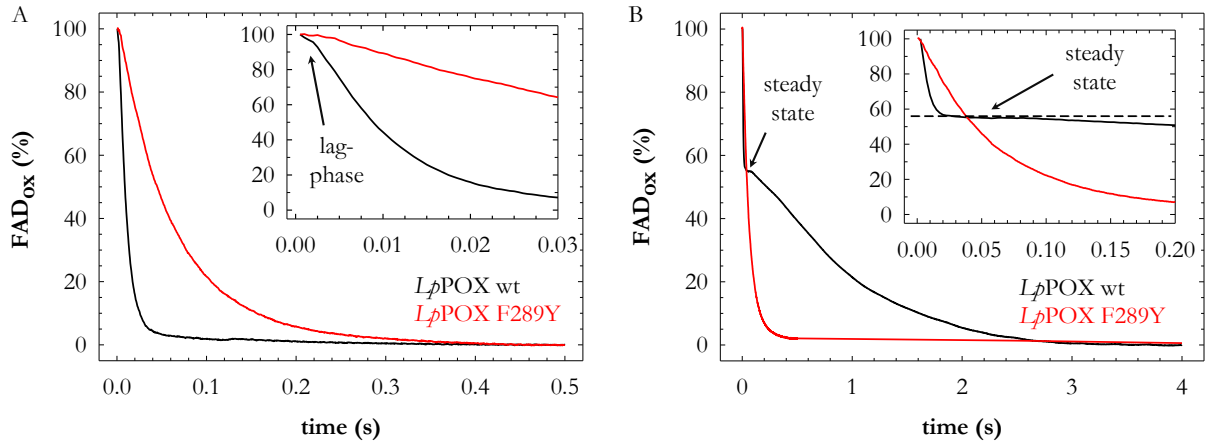

figure 42: Anaerobic (A) and aerobic (B) flavin reduction of *Lp*POX wt and F289Y. 2 mg/mL of *Lp*POX were rapidly mixed with 100 mM pyruvate. Flavin reduction was monitored at 457 nm and 25 °C. Progress curves were converted to relative amount of oxidized flavin. A: Anaerobic flavin reduction. The rate constants of the lag-phase and the main phase were determined by a double-exponential equation (fit not shown). Inset: FAD reduction within the first 30 milliseconds. The lag-phase (apparently 2-4 milliseconds) is highlighted by an arrow. B: Aerobic flavin reduction. The position of the steady state is indicated by an arrow. Inset: FAD reduction within the first 200 milliseconds. The dashed line highlights the amount of oxidized FAD in the steady state for *Lp*POX wt (56 %). For F289Y variant a maximum amount of 5 % oxidized FAD was estimated.

The obtained results implicate that flavin reoxidation is dramatically decreased in *Lp*POX F289Y due to the substitution of Phe by Tyr. In combination with the observed effects of *Ec*POX Y278F this finding fosters the idea that solely Tyr can efficiently prevent oxygen attack to the reduced state of the flavin at positions N5 and C4a. However, it is yet unclear, how Tyr ensures this function, since the only difference to Phe is a single hydroxyl moiety. One could speculate that the Tyr-OH suppresses oxygen attack by a steric hindrance or by disturbing correct positioning of oxygen to FAD.

table 15: Overview of rate constants of reductive and oxidative half-reaction for *Lp*POX wt, *Ec*POX wt and selected variants. For *Ec*POX k_{red} was determined using a single-exponential equation from progress curves of the reductive half-reaction (table 9). For *Lp*POX k_{red} was determined using a double-exponential equation including a lag-phase from progress curves of the reductive half-reaction (figure 42 A). k_{reoxi} was calculated from progress curves of flavin reduction at steady-state conditions (figure 42 B and figure 21) using equation 10. ([a] = a maximal amount of oxidized flavin was estimated to be 5 % in the steady state)

enzyme	k_{red} (s^{-1})	k_{reoxi} (s^{-1})	FAD : $FADH_2$ (%)
***Lp*POX wt**	107 (± 0.689)	136 (± 0.877)	56 : 44
***Lp*POX F289Y**	16 (± 0.029)	(<) 0.84 (± 0.002)	(<) 5 : 95 [a]
***Ec*POX wt**	1.94 (± 0.001)	0.58 (± 0.0003)	22 : 78
***Ec*POX Y278F**	2.1 (± 0.002)	1.11 (± 0.001)	35 : 65

To exclude that active site rearrangements caused the observed effects of the *Ec*POX and *Lp*POX variant the structure of both variants was solved by X-ray crystallography. Results of *Ec*POX Y278F are described in chapter 4.1.7.

4.4.3 Crystal structure of *Lp*POX F289Y

The variant *Lp*POX F289Y crystallized like wt in space group $C222_1$ with half of the tetramer per asymmetric unit and a final resolution of 1.43 Å was obtained. To solve the structure of the variant a structure of the wt in the ground state (unpublished high-resolution structure at 1.09 Å of *Lp*POX wt was friendly provided by Dr. Danilo Meyer, Department of Bioanalytics, Göttingen) was used as initial model and further refined. Data collection and final refinement statistics are summarized in the appendix (chapter 8.7) and r.m.s.d. values compared to the wt structure are presented in table 13.

The crystal structure of *Lp*POX F289Y was analyzed with particular attention to deviations near the flavin cofactor due to the substitution of Tyr for Phe289. No significant differences of the overall structure or within the active site can be detected (figure 43) which is also reflected in the low r.m.s.d. value (table 13). Thus, it can be concluded that the decreased reduction and reoxidation rate of the flavin cofactor (chapter 4.4.2) are not caused by detectable structural reorganizations within the enzyme due to the exchange of Phe289 to Tyr.

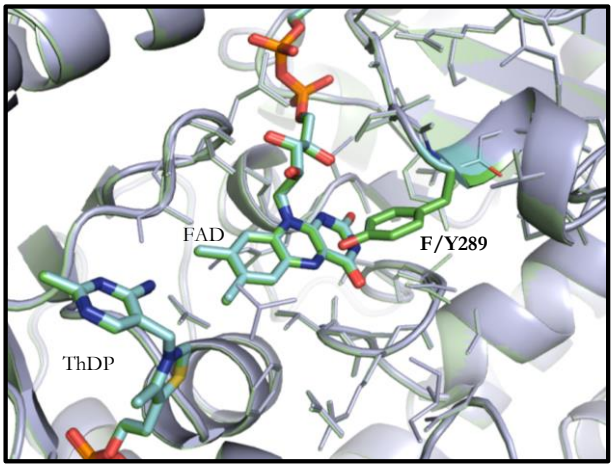

figure 43: Comparison of the crystal structures of *Lp*POX variant F289Y with *Lp*POX wt. The wt enzyme is depicted in blue whereas the variant is shown in green. The thiamine and flavin cofactors and the exchanged amino acid F/Y289 are highlighted by stick. Surrounding amino acids of the active site are indicated by lines. No significant changes of the exchanged side chain or other amino acids within the active site can be detected.

5. Discussions

5.1 Signal perception and information transfer from the active site to the protein surface

The activation process of *Ec*POX is initiated by reduction of the flavin cofactor with pyruvate [35]. This change of the flavin redox state triggers membrane anchor release from the protein, which subsequently leads to membrane association [12] and manifold enhancement of the catalytic activity of *Ec*POX [13]. This thesis shows how the protein matrix senses the FAD redox state and how the information is transferred from the active site to the membrane anchor clamped to the protein surface.

5.1.1 Tyr278 senses the flavin redox state

The OH-moiety of Tyr278 is located in 3.2 Å proximity to FAD and forms a hydrogen bond to the redox active flavin-N5-atom (figure 44). It is supposed that Tyr278 utilizes this interaction to sense the redox state of the flavin and thus plays a central role in initiating membrane anchor release. This hypothesis was investigated by the substitution of Phe for Tyr278 where hydrophobicity and space are similar but hydrogen bonding is impaired.

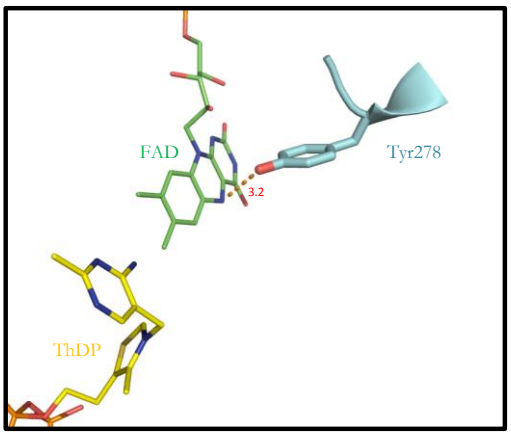

figure 44: Orientation of Tyr278 to the flavin and thiamine cofactors. In full-length *Ec*POX Tyr278 (blue) is located within the active site in close proximity to both cofactors and interacts with the flavin-N5 by a hydrogen bond.

Both, the steady-state activity of non-activated enzyme and reduction of the flavin cofactor were only slightly affected in variant *Ec*POX Y278F. However, analysis by limited proteolysis and SDS-mediated activation revealed that the activation process was significantly altered in Y278F. Since both assays are based on the amount of species SR III (showing a released membrane anchor) in equilibrium it is suggested that this equilibrium is shifted in Y278F towards the membrane anchor-attached conformation SR II compared to the wt enzyme. This can be explained by a defective sensing and communicating mechanism from the active site to the membrane anchor in the variant.

A significant role of the hydrogen bond between Tyr278 and the flavin-N5 was deciphered by X-ray crystallography. The orientation of Phe in the crystal was similar to Tyr278 in the wt enzyme structure. However, the position of Phe was more flexible in Y278F. Thus, the interaction of FAD with Tyr278

seems to be important for correct positioning of the sensor which might be relevant for efficient signal transfer.

Concluding, Tyr278 is the initial actor of a cascade which senses the flavin redox state and transfers this information to mediate membrane anchor release. However, further amino acid residues seem to be involved in this cascade since exchange of Tyr278 does not lead to a complete loss of activation.

A similar redox switch mechanism as observed for *Ec*POX is also described for the peripheral membrane protein proline utilization A (PutA) from *E. coli* [117]. It was shown that due to proline-induced reduction of the flavin cofactor conformational changes occur which lead to exposure of a membrane anchor and subsequently to membrane attachment [118]. Although little is known about the membrane binding domain of PutA it was speculated that the C-terminus of PutA might be involved in membrane association [117]. Additionally, it was demonstrated that Arg431 plays an important role in reductive activation of this enzyme. Arg431 is located near the flavin cofactor and forms a hydrogen bond to the flavin-N5 (figure 45) similar to Tyr278 in *Ec*POX. Although the exchange of Arg431 to Met does not affect proline-triggered reduction the PutA variant is not able to bind lipids anymore [118]. Therefore, the authors speculated that the hydrogen bond between Arg431 and the N5-locus of the flavin has a profound impact on the redox switching mechanism of PutA. However, the question remained open how the signal is further transmitted from Arg431 to the protein surface.

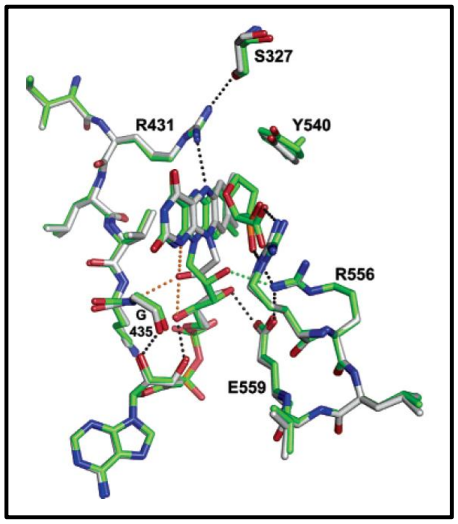

figure 45: Position of Arg431 to the flavin cofactor in PutA from *E. coli*. Green sticks represent oxidized PutA whereas white sticks highlight dithionite-reduced PutA. Figure was taken from [118].

5.1.2 Phe465 and Tyr549 do not cooperate during activation

Comparison of the crystal structure of full-length *Ec*POX with the proteolytically activated Δ23 structure indicated that Phe465 and Tyr549 are involved in the information transfer from the active site to the membrane anchor. In the activated enzyme Phe465 swings between both cofactors upon proteolytic activation and might clash with Tyr549 which is located at the N-terminal edge of the membrane anchor (figure 46). Accordingly, Tyr549 is displaced from the catalytic center due to repulsion which subsequently leads to destabilization of the protein-bound membrane anchor. In this regard, a cooperating action of both amino acids would be suggested. However, it seems possible that also a more competitive action of

Tyr549 and Phe465 initiates *Ec*POX activation. Tyr549 might occupy the position of Phe465 in the resting state and could inhibit rearrangement of Phe465. Thus, activation and repositioning of Phe465 would only occur after Tyr549 removal. To decipher which mode promotes membrane anchor release of *Ec*POX both residues were exchanged by Ala.

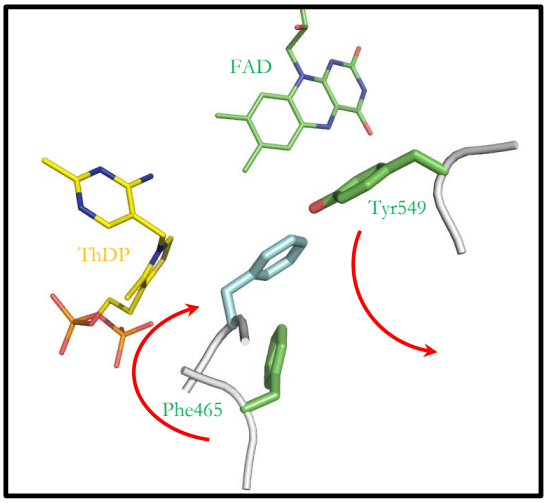

figure 46: Interaction of Phe465 and Tyr549 upon activation. Phe465 swings between ThDP (yellow) and FAD (green) upon activation and Tyr549 is displaced from the active site. Side chains of full-length *Ec*POX are shown in green, while amino acid residues of activated enzyme are represented as blue sticks *Ec*POX Δ23. Structural rearrangements upon proteolytic activation are highlighted by red arrows.

Phe465 is involved in flavin reduction and the first conformational change

The substitution of Ala for Phe465 led to 70fold decreased steady-state activity compared with the wt enzyme. Additionally, variant F465A was not activated by proteolysis or with SDS. However, these effects could be related to an impaired electron transfer from the thiamine to the flavin cofactor due to the exchange of Ala for Phe465. In fact, analysis of flavin reduction showed a 100fold decreased k_{red}. These results confirm previous investigations of *Ec*POX F465A which deciphered Phe465 to facilitate the electron transfer reaction from ThDP to FAD [45]. Exchange of the corresponding Phe479 to Trp or Tyr in *Ec*POX-related *Lp*POX shows also a significantly impaired flavin reduction rate [119]. Unfortunately, no suitable crystals of *Ec*POX F465A could be generated to elucidate how the substitution of Phe465 influences the active site architecture.

Limited proteolysis of F465A revealed that independently of the addition of pyruvate or MAP in all cases quantitative formation of non-active *Ec*POX Δ101 was observed. Therefore, the first conformational transition R→SB, which leads to protection of the Δ101 cleavage site and is typically induced by pyruvate binding to ThDP, is disturbed in F465A. Also the second structural change SR II→SR III is impaired in the variant. However, this is expected as in F465 reduction of the flavin cofactor, which is the mandatory signal for this second transition, is dramatically disturbed.

In summary, vital roles of Phe465 on reduction of the flavin cofactor and on the first structural transition leading to the protection of the Δ101 cleavage site are observed. However, no conclusions concerning the interaction with Tyr549 can be drawn.

Phe465 and Tyr549 do not interact during activation

Analysis of variant Y549A showed a partially activated enzyme already in the resting state. Also investigations of the activation process by proteolysis and SDS-stimulated activity measurements revealed rather improved than disturbed activation due to the substitution of Ala. These results argue against a steric clash of Phe465 and Tyr549 which promotes membrane anchor release. Beside cooperating action of Phe465 and Tyr549 also a competitive action of Tyr549 was possible. However, the crystal structure of Y549A showed that Phe465 is still located in the non-activated position which argues against an inhibiting role of Tyr549.

The obtained results reveal no obvious interaction of Phe465 and Tyr549 during activation. Instead, data indicate that Tyr549 stabilizes the membrane anchor in the protein-bound form. This function is discussed later (chapter 5.2.4).

5.1.3 Phe260 is not involved in the signal transfer process

Phe260 is located on the protein surface near membrane anchor residues Ile554 and Leu565 (figure 47). Crystal structure analysis of the full-length protein (where the membrane anchor is protein-bound) and *Ec*POX Δ23 (where the membrane anchor is removed) indicate alternative conformations of Phe260. Interconversion between both orientations would lead to a steric clash with Ile554 and Leu565 which might trigger membrane anchor exposure. This assumption was examined by substitution of Ala for Phe260.

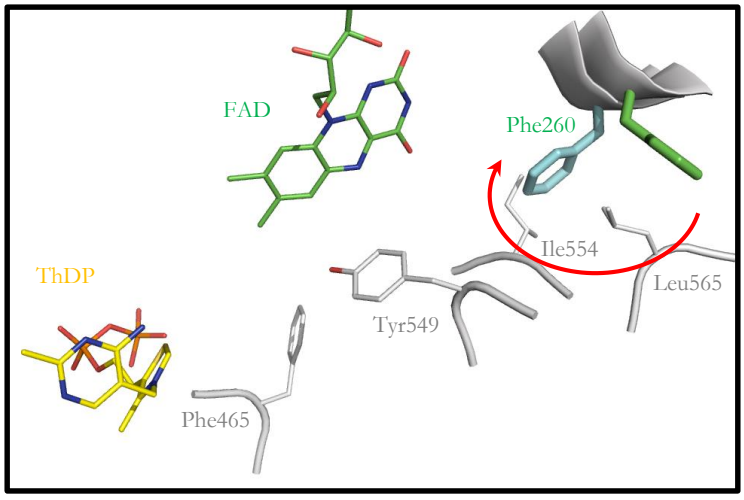

figure 47: Clash of Phe260 with Ile554 and Leu565 upon activation. Interconversion of Phe260 between the non-activated (green) and activated (blue) conformation upon activation leads to a clash with Ile554 and Leu565 (gray lines). The cofactors ThDP (yellow) and FAD (green) indicate the position of the catalytic center. Structural rearrangements upon proteolytic activation are highlighted by red arrows.

Results of different experiments revealed no specific role of Phe260 on the signal transfer from the active site to the membrane anchor of *Ec*POX. Wt-like activity was observed in the steady-state activity assay or if *Ec*POX F260A was activated by limited proteolysis and with SDS. These results disprove the hypothesis that Phe260 functions as conformational switch in combination with Ile554 and Leu565 and promotes *Ec*POX activation.

5.2 Stabilization of the membrane anchor at the protein surface

The membrane anchor of *Ec*POX is bound at the protein surface by a four-stranded half-barrel motif and several electrostatic, polar and non-polar interactions [35]. However, it was shown that the same polypeptide sequence forms an amphipathic helix in the presence of SDS micelles which were applied as membrane mimic [45]. The question arises how these two conformations of the membrane anchor are stabilized in the particular environment.

5.2.1 Electrostatic interactions and hydrogen bonds play a minor role in membrane anchor binding to *Ec*POX

Analysis of the crystal structure of full-length *Ec*POX reveals two prominent electrostatic contacts (D328-R572 and D348-R558) and one hydrogen bond (Q537-E564) between the membrane anchor and the protein surface (figure 48) [35]. Since these interactions bind both ends of the anchor as well as the center they may facilitate association of the membrane anchor to the protein. To investigate the impact of these contacts the triple mutant *Ec*POX 3x (D328A, D348A, Q537A) was generated where the amino acids of the protein part were exchanged to Ala. Note that the primary sequence of the membrane anchor was not affected in this variant.

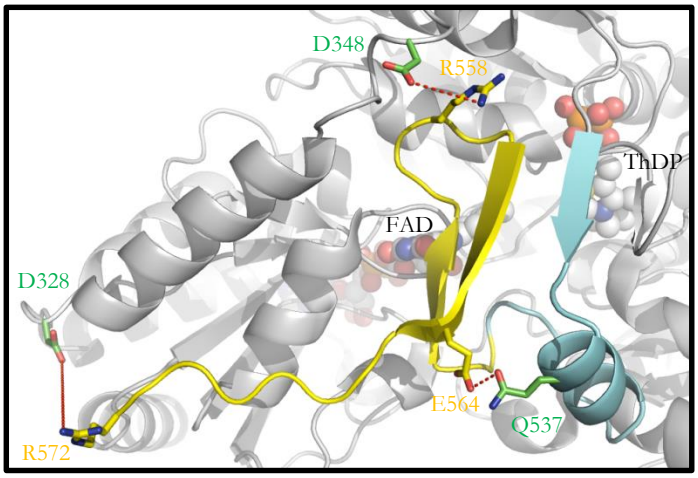

figure 48: Membrane anchor stabilization of resting-state *Ec*POX by electrostatic interactions and hydrogen bonds. Prominent electrostatic interactions and hydrogen bonds of the membrane anchor (yellow sticks) to the protein surface (green sticks) are shown as red dashed lines. The protein core is shown as white cartoon and cofactors ThDP and FAD are depicted as spheres and highlight the position of the active site. The membrane anchor is displayed in yellow cartoon, while the linker region is indicated in blue cartoon format. In the triple mutant amino acids shown as green sticks were exchanged to Ala within this thesis.

Steady-state activity, thermal unfolding and limited proteolysis in the absence of pyruvate revealed that the membrane anchor is still clamped to the protein in the resting state of *Ec*POX 3x. This finding was further supported by the crystal structure which showed a protein-bound lipid binding domain. Also proteolytic digestion of the pyruvate-reduced enzyme confirmed that the conformational transition SR II→SR III is not affected in the triple variant. This implies a similar activation process as in the wt enzyme. Only experiments with SDS demonstrated that a smaller amount of the detergent was necessary to activate the variant to a similar level like *Ec*POX wt.

Summarizing the obtained results, an influence of electrostatic interactions and hydrogen bonds on membrane anchor association to the protein seems unlikely. Consequently, the major forces which suppress membrane anchor release are most likely of hydrophobic nature.

5.2.2 Hydrophobic interactions of Ile554, Leu565 and W570 mainly contribute to membrane anchor association to *Ec*POX

Besides electrostatic contacts and hydrogen bonds the protein-bound membrane anchor interacts with the protein core via hydrophobic areas. A prominent hydrophobic patch is formed between Phe260 (which was also predicted to act as conformational switch), Ile554 and Leu565 (figure 49 A). Additionally, Trp570 sticks into a pocket composed of different amino acids of the protein surface at the protein surface. While Phe260, Ile554 and Leu565 seem to stabilize the center of the membrane anchor, Trp570 binds the C-terminal edge to the protein core. However, analysis of the binding cavity of Trp570 reveals no obvious hydrophobic contacts but rather two counterparts perfectly fitting to each other (figure 49 B).

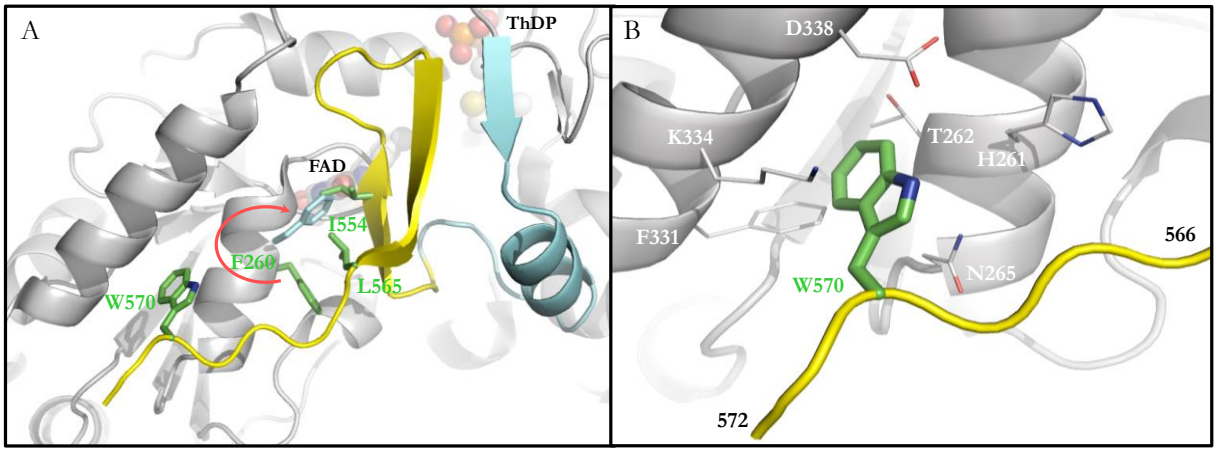

figure 49: Hydrophobic interactions of the membrane anchor with the protein surface. A: The membrane anchor (yellow) is attached to the protein core (white) by hydrophobic interactions. Central amino acids exchanged within this thesis are shown as green (resting-state *Ec*POX) and blue (Δ23) sticks. The cofactors ThDP and FAD are depicted as white spheres and highlight the position of the active site. The red arrow indicates conformational changes upon proteolytic activation. The linker region is shown in blue. B: The pocket which stabilizes W570 (green sticks) at the protein surface is composed of charged, polar and hydrophobic residues (gray lines).

The impact of these hydrophobic interactions was investigated by variants I554A/G, L565A/G, W570A/G and the double variant 2G (I554G, L565G). Hydrophobic amino acids were replaced by Ala and Gly which are still nonpolar but show decreased hydrophobicity. Note that all amino acid exchanges alter the primary sequence of the membrane anchor.

Hydrophobic interactions stabilize the attached membrane anchor

Analyses of the steady-state activity and thermal unfolding already implied a partial released membrane anchor in the resting state of all variants. Remarkably, the double variant 2G was completely activated in the resting state and showed similar catalytic efficiency as observed for *Ec*POX Δ23. These findings were further supported by proteolytic digestion experiments revealing that activated Δ23 was generated quantitatively in the absence of pyruvate. Thus, the resting-state equilibrium in the variants is significantly shifted towards species R III which is characterized by exposure of the membrane anchor and removal of the autoinhibitory, active-site covering helix. Also studies of the flavin reduction and artificial reoxidation

are in line with the previous findings since improved accessibility to the active sites is observed for the variants which argues for a partly exposed membrane anchor.

However, in all determined crystal structures of the variants the membrane anchor was found attached to the protein core resembling state R I. It can be speculated that although in solution equilibrium of several *Ec*POX conformers exists only one particular species crystallizes under the given conditions. Therefore, X-ray crystallography cannot be used to decipher the conformational equilibrium and cannot determine the activation process on a molecular level.

Additionally, also the SR II:SR III equilibrium is shifted significantly towards state SR III in all variants which was demonstrated by a decreased half-life for proteolytic digestion with pyruvate-reduced enzymes. These results were supported by decreased $SDS_{0.5}$ values for variants I554A, L565A/G and 2G.

Also the beta-half-barrel motif is involved in membrane anchor binding

The obtained results foster the idea that hydrophobic interactions mainly stabilize the membrane anchor at the protein and thus play a central role in the activation process. However, also the structural organization of the membrane anchor seems to contribute to protein association. Both Leu565 and Ile554 are located in two beta-strands which are involved in formation of the four-stranded half-barrel that stabilizes main parts of the membrane anchor at the protein.

Exchanges of Leu565 and Ile554 seem to disturb formation of this structural element leading to membrane anchor release already in the absence of reduced flavin. This assumption is supported by differentiated results for Ala and Gly mutants. While activation in the resting state is less pronounced if Ala is substituted for Ile554 and Leu565, exchanges to Gly lead to *Ec*POX Δ23-like activities. According to Chou an Fasman [120] it can be speculated that Ala is still able to form the beta-strand whereas Gly acts as breaker and causes severe disorder of the membrane anchor structure.

A central role of half-barrel structure on membrane anchor stabilization was also observed by Bertagnolli and Hager [121] who analyzed C-terminal deletion variants of *Ec*POX. They elucidated by proteolysis studies that a deletion of 7 residues (*Ec*POX Δ566-572) produces an enzyme with wt-like activity. Surprisingly, if 8 or 11 C-terminal amino acids are cleaved off (*Ec*POX Δ565-572/Δ562-572) constitutively activated *Ec*POX is generated. Similar to exchanges of Ile554 and Leu565 truncation of the C-terminal edge of the membrane anchor leads to removal of one strand of the half-barrel motif (residues 560-565) which seems to destabilize the entire lipid binding domain resulting in *Ec*POX Δ23-like activity.

5.2.3 Phe260 does not participate in membrane anchor stabilization

In chapter 5.1.3 it was shown that Phe260 plays no central role in the information transfer from the active site to the protein surface. However, Phe260 is supposed to form a hydrophobic patch in combination with Ile554 and Leu565 and thus might fix the membrane anchor to the protein core. To analyze this hypothesis also variant F260A was examined.

Contrary to I554A/G and L565A/G for variant F260A no improved membrane anchor release was detected. Similar to the wt enzyme digestion of F260A in the absence of pyruvate did not lead to formation of *Ec*POX Δ23. Also no significant decrease in the apparent melting temperature was observed. These findings were supported by the crystal structure of F260A where the membrane binding domain is found bound to the protein surface. These results argue against increased accessibility of the active site and indicate a completely attached membrane anchor in the resting state. Only an increased flavin reduction and slightly enhanced reoxidation rate might imply that the membrane anchor is exposed to some extent. In summary, similar to studies of the signal transfer process Phe260 has no central function in membrane anchor stabilization.

5.2.4 Tyr549 stabilizes the membrane anchor at the protein by interactions with the active site

Tyr549, which is located at the N-terminal end of the membrane anchor, was supposed to interact with Phe465 leading to displacement of the lipid binding domain upon activation. However, analysis of Y549A could not confirm this hypothesis. The obtained results rather revealed that Tyr549 might stabilize the membrane anchor at the protein surface.

The exchange Tyr549 to Ala generated an activated enzyme with a released membrane anchor already in the resting state. This was demonstrated by steady-state activity, thermal unfolding and limited proteolysis in the absence of pyruvate. Analysis of flavin reduction and artificial reoxidation revealed increased accessibility of the active site when compared to the wt enzyme and thus support the idea of improved membrane anchor release. These findings are in line with activation by SDS which implied a shift of the SR II:SR III equilibrium towards SR III in the variant. However, the crystal structure argued against an exposed membrane anchor.

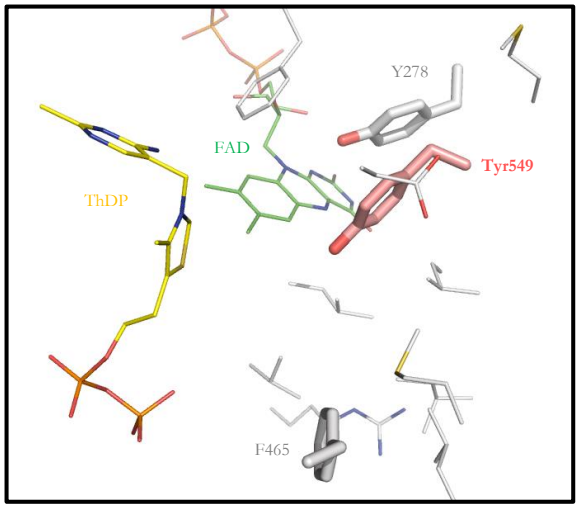

figure 50: Active site interactions of Tyr549 in full-length *Ec*POX. Tyr549 is represented in rose sticks whereas surrounding amino acids of the active site are shown as gray sticks and lines. The cofactors ThDP (yellow) and FAD (green) are shown as lines. No obvious interaction partners of Tyr549 can be detected.

In summary, most results support the hypothesis that Tyr549 stabilizes the membrane anchor at the protein by interactions with the active site of full-length *Ec*POX. It can be assumed that either a hydrogen bond of the hydroxyl moiety fixes the position of Tyr549 or that hydrophobic contacts provided by the

phenyl ring might be responsible for Tyr549 association to the active site. However, analysis of the crystal structure revealed no obvious interaction partners for Tyr549 (figure 50).

Concluding, it can be speculated that Tyr549 might be the final amino acid of the signal transfer cascade initiated from the flavin cofactor. Induced by formation of $FADH_2$ Tyr549 could be released from the active site leading to exposure of the entire membrane anchor.

5.3 Stabilization of the membrane anchor at the membrane

Besides the half-barrel structure composed of the protein-attached membrane a helical structure of the membrane anchor was predicted from the primary amino acid sequence [29]. In fact, Neumann and Weidner *et al.* could show that the isolated membrane anchor forms an amphipathic helix in the presence of artificial SDS micelles which were applied as membrane mimics [45] [35]. To investigate which factors influence membrane binding properties of the peptide anchor modulations of the membrane anchor sequence were exploited.

5.3.1 Helix formation of the membrane anchor is disturbed in *Ec*POX I554G and W570G

The previously discussed variants Ile554G/A, Leu565G/A, 2G and W570G were investigated concerning their properties of membrane anchor attachment to the protein core. Notably, in those variants also the primary sequence of the membrane anchor is altered which might influence the intrinsic helix propensity and concomitant bilayer association. This hypothesis was analyzed by activity measurements stimulated by SDS which served as model of the *Ec*POX membrane.

Ile554 and W570 influence the intrinsic helix propensity of the membrane anchor

Improved SDS-mediated activation compared to the wt enzyme was observed for variants Ile554A, Leu565G/A and 2G. Remarkably, the Gly variants of Ile554 and W570 showed impaired activation by the detergent demonstrated by an increased $SDS_{0.5}$ value. A disturbed SR II→SR III transition could be excluded since proteolytic activation was substantially increased for I554G and W570G. Consequently, affinity to the amphiphile was decreased in both variants indicating disturbed helix formation. These observations are consistent with secondary structure analysis by Chou and Fasman [120] who predicted that Ala is a strong alpha-helix former whereas Gly acts as helix breaker. Remarkably, the exchange of Leu565 to Gly did not alter the intrinsic helix propensity of the membrane anchor. Since Leu565 is located in the center of the putative helix it seems likely that neighboring residues stabilize the entire helical fold. On contrast, no stabilization is possible for Ile554 and W570 since they are positioned at the N- and C-terminal edges of the helix revealing a central role of both residues on helix formation and *Ec*POX membrane binding. Nevertheless, the behavior observed for the entire protein should be additionally verified with similar variants of the isolated membrane anchor and analyzed by liquid-state NMR.

Other amino acids affect helix formation and membrane binding

In former studies also other amino acids of the membrane anchor were shown to be crucial for membrane binding of *Ec*POX. Significant alterations of the lipid-binding ability were observed when the acidic Glu564 and hydrophobic Leu 565 are replaced by Pro [122]. However, exchanges to Pro severely interfere with both, the protein- and membrane-bound conformation of the anchor peptide, and results are hard to interpret. Minor effects were detected for variants A553V and R572G [122] which are located at the helix edges similar to Ile554 and Trp570. While Ile554 and Trp570 were shown in this thesis to be crucial for helix formation, Ala553 and Arg572 seem to be of less importance.

Besides the influence of single amino acids also the length of the peptide, that is mandatory for efficient membrane binding, was examined before. The deletion of three residues from the C-terminal part (*Ec*POX Δ570-572) results in defective lipid association [122]. An additional mutant lacking 9 C-terminal residues shows even more pronounced effects. Therefore, a membrane anchor of at least 21 amino acids seems to be essential to efficiently form the helical structure and bind to lipids or detergents.

5.4 Electron transfer to Q_8

Electron transfer from $FADH_2$ to Q_8 confronts *Ec*POX with a challenging task since substrate and enzyme are localized in two different compartments. To solve this problem *Ec*POX binds peripherally to the lipid bilayer [18]. However, the molecular mechanism of electron transfer remains unclear. One can speculate that electrons hop with the help of the protein matrix to Q_8 or that the ubiquinone partly leaves the membrane and enters the active site to accept the reducing equivalents directly from the flavin via tunneling.

5.4.1 The crystal structure of an *Ec*POX Δ23:Q_0 complex indicates Q_0 interactions within the active site

To investigate whether ubiquinone sticks into the active site to regenerate the flavin cofactor a crystal structure of activated *Ec*POX Δ23 with an accessible active site in complex with Q_0 was solved. After initial refinements additional electron density and positive difference density were observed in the active sites of the 12 subunits in the asymmetric unit. Preliminary trials to fit Q_0 into this density succeeded and potential hydrogen bonds with Tyr278, Ser28, Gln113 and Asp27 were detected. Also the orientation of Q_0 suggests that the native substrate Q_8 might bind similar with the isoprenoid tail sticking out of the active site towards the membrane. Although an out-of-the membrane binding of Q_8 was indicated by these results final conclusions should be drawn from an interaction model received from crystals of better quality and higher resolution.

Out-of-the-membrane binding of ubiquinones

The mechanism of Q_8 desorption out of the membrane into the active site of *Ec*POX was first described by Schloss *et al.* in 1988 [123]. The authors analyzed inhibitors of the thiamine diphosphate-dependent

flavoenzyme acetohydroxyacid synthase. They found that Q_0 and Q_1 inhibit this enzyme although both molecules obviously share no similarities to the substrate pyruvate or to the allosteric effectors Val, Leu and Ile. In combination with the high sequence similarity of acetohydroxyacid synthase with *Ec*POX [123] the authors concluded that both enzymes have the same ancestor and that a ubiquinone binding site exists in both enzymes. However, until now no structural evidence were available which support this proposal.

Remarkably, only recently it turned out that desorption of a ubiquinone out-of the-membrane into a cytosol-localized active site is not a unique feature of *Ec*POX catalysis. Several crystal structures of subunits or the entire respiratory chain complex I were solved and an ubiquinone binding site was identified [124] [125] [126]. Complex I catalyzes the electron transfer from NADH to ubiquinone which is coupled to translocation of four protons across the membrane [127]. In all structures of complex I the ubiquinone binding site is located in the cytosolic part of the complex (figure 51 A) revealing a distance of 15-60 Å from the benzoquinone head group to the membrane surface [128] [129] [125] [124]. Although the distances determined from different crystal structures vary it is obvious that ubiquinone has to move out of the membrane to accept the electrons. Therefore, the entire complex provides a narrow channel to stabilize the isoprenoid tail [124].

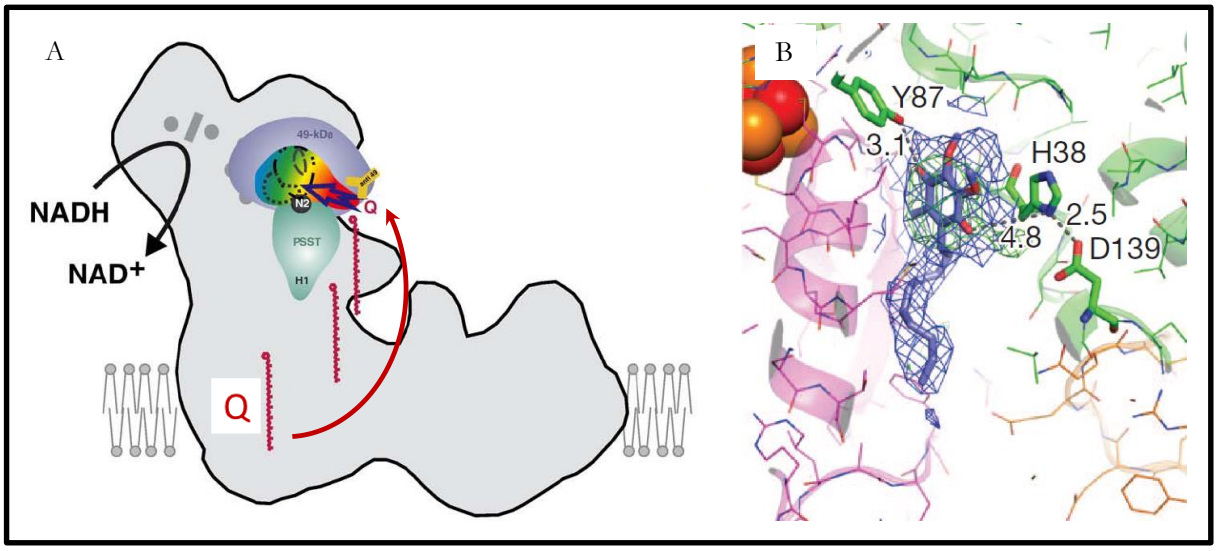

figure 51: Ubiquinone binding in respiratory chain complex I. A: Schematic drawing of the out-of-the-membrane binding mechanism of ubiquinone. Ubiquinone (dark red) has to enter the Q-binding site in the 49 kDa-domain of mitochondrial complex I localized 35 Å away from the membrane surface in the peripheral arm to accept electrons. Movement of ubiquinone out of the membrane is indicated by a red arrow. Figure was taken from Zickermann *et al.* [129] and slightly modified. B: Ubiquinone interactions within Q-site found at the interface of three subunits (colored orange, green and pink) of complex I from *Thermus thermophilus*. Blue 2mFo–DFc density (countered at 1 σ) assigns the position of decylubiquinone (ubiquinone analog, blue sticks). The keto groups of the ubiquinone head group interact with Tyr87 and His38 (green sticks) of the protein. Both residues are essential for reductase activity of complex I and are predicted to protonate electron-reduced Q^{2-}. Here, ubiquinone presumably has to move 15 Å away from the membrane to get reduced. Figure was taken from Baradaran *et al.* [124].

<u>The ubiquinone binding site of *Ec*POX is similar to other enzymes</u>

Comparison of the interaction mode of Q_0 in *Ec*POX with other ubiquinone-reducing enzymes reveals several similarities. The FAD-Q_0 distance in the *Ec*POX Δ23: Q_0 complex is approximately 8 Å which is consistent with spaces of 7-12 Å between electron donor and ubiquinone observed in other enzymes [124] [130] [131]. Additionally, coordination of ubiquinone by active site residues is similar in ubiquinone-

reducing enzymes. In *Ec*POX Q_0 is presumably bound via hydrogen bonds to Tyr278, Ser28, Gln113 and the N-backbone atom of Asp27 (figure 40 B). Also Zhang *et al.* reported that hydrogen bonding to the backbone nitrogen and carbonyl group of Gly272 and Gly273 with the keto functions of ubiquinone is observed in the electron transfer flavoprotein-ubiquinone oxidoreductase [130]. Further, in multiple enzymes interactions of the keto moiety with Tyr is detected (figure 51 B) [130] [124] [126]. It was reported that these Tyr residues are pivotal for enzymatic activity [132] [128] and are proposed to protonate electron-reduced Q^{2-}. Baradaran and coworkers even suggested that either formation of anionic Q^{2-} or deprotonation of Tyr87 might initiate a conformational transition of the enzyme [124] inducing the proton translocation across the membrane in complex I.

A similar mechanism can be proposed for *Ec*POX. Reduction of Q_8 should consequently lead to removal of the enzyme from the membrane to enable access to cytosolic pyruvate which initiates the next cycle of substrate conversion and membrane binding. So far it is unclear how release of membrane-bound *Ec*POX is promoted. Analysis of available crystal structures of *Ec*POX reveals that Ser28 and Tyr278 could participate in this process (figure 40 B). However, the exchange of Tyr278 to Phe, which is defective in proton donation, does not lead to a complete loss of activity (chapter 4.1.1) which argues against an essential role of Tyr278 as proton donor. Whether Ser28 is involved in protonation of Q_8 and potential membrane release of *Ec*POX needs to be explored.

Ubiquinone binds to the active site of *Ec*POX and allows direct tunneling of electrons

Since the crystal structure of an *Ec*POX Δ23:Q_0 complex reveals an interaction of Q_0 with the active site it can be proposed that electrons are directly transferred from reduced flavin to Q_8 via tunneling rather than hopping. The determined distance of approximately 8 Å between Q_0 and the flavin is consistent with typical tunneling distances of 14 Å in biological systems [67]. Additionally, entering of Q_8 seems reasonable with regard to the physiological function of *Ec*POX. Direct tunneling of electrons ensures that energy in form of reducing equivalents is conserved. Contrary, hopping of electrons could lead to unfavored reduction of other electron acceptors within the bilayer. In that case, pyruvate-derived energy could be lost and the catalytic reaction of *Ec*POX would be wasteful.

5.5 Inhibition of the artificial reoxidation reaction in *Ec*POX

The final step in *Ec*POX catalysis is regeneration of the flavin by electron transfer to membrane-bound Q_8 [17]. Interestingly, the *Ec*POX-related enzyme *Lp*POX, which also catalyzes oxidative decarboxylation of pyruvate, utilizes molecular oxygen for flavin reoxidation [73]. However, such a reaction needs to be inhibited in *Ec*POX by the protein matrix to conserve the pyruvate-derived energy. Inspired by the crystal structure Tyr278 was predicted to prevent *Ec*POX from unfavored oxygen reactivity since it is located in 3.2 Å vicinity to the reactive N5- and C4a-locus of the flavin. Noteworthy, *Lp*POX contains Phe289 at this position which might promote oxidase activity. This hypothesis was studied by reciprocal amino acid substitutions in both enzymes.

5.5.1 Tyr278 inhibits unpreferred oxidase activity in *Ec*POX

Analysis of pyruvate-induced flavin reduction and reoxidation by molecular oxygen revealed that the substitution of Phe for Tyr278 in *Ec*POX leads to an increased reactivity towards oxygen whereas the exchange of Phe289 by Tyr in *Lp*POX prevents oxygen-mediated reoxidation. These results confirm the assumption that Tyr near the flavin cofactor suppresses unpreferred oxidase activity, while Phe supports it. It can be speculated that the hydroxyl function of Tyr inhibits the reaction of $FADH_2$ with oxygen due to decreased accessibility of the flavin-N5 and -C4a.

Could other factors cause the altered oxygen reactivity?

To elucidate whether active site rearrangements caused the observed kinetic differences, crystal structures of both variants were determined in the absence of substrates. Since no structural differences could be detected upon comparison with the corresponding wt enzymes the observed alterations can be directly related to the mutations.

Another explanation for the kinetic differences upon amino acid exchange close to the flavin could be the modulation of the flavin cofactor redox potential. Analysis of the protein-bound flavin redox potential by titration with redox active dyes could prove this suggestion [133]. However, it was shown for L-galactono-γ-lactone dehydrogenase that an exchange of the N5-flavin-interacting Ala for Gly yields a catalytically competent oxidase [134]. In this regard only a slight modulation of the flavin redox potential was observed for the variant compared to the wt enzyme. Thus, the significant oxidase activity could not be explained by this minor effect.

Do oxygen channels within the enzyme determine oxygen reactivity?

Although the reoxidation rate was 2fold increased for variant *Ec*POX Y278F the enzyme was not converted into a real oxidase. Its reoxidation rate is still far away from typical oxidases with rate constants up to 1.5×10^6 $M^{-1}s^{-1}$ as reported for glucose oxidase [135]. One can suggest that other factors like oxygen channels and cavities, which facilitate oxygen binding and migration to the active site rather than catalysis, might be suboptimal designed in *Ec*POX. It was shown for other monooxygenases and oxidases that these tunnels and niches provided by the protein mainly harbor hydrophobic residues, which comprise an ideal environment to store gaseous oxygen and guide it from the solvent into the reactive centers [136].

Since oxygen travelling through an enzyme is hard to investigate, the PyMol plugin MOLE [137] was used to simulate oxygen channels within the protein structure of *Ec*POX and *Lp*POX wt and variants by a search algorithm. The resulting oxygen pathways are displayed in figure 52. Surprisingly the oxygen molecule seems to attack the flavin cofactor from the *si* site opposite to the Phe/Tyr residue in both enzymes. This would argue against a steric interference of the Tyr-OH moiety. Noteworthy, in *Lp*POX oxygen seems to migrate from two directions into the active site to the flavin, while in *Ec*POX only tunnels leading to the *si* site of the flavin were found. A disturbed oxygen migration in *Ec*POX could explain the observation that the substitution of Phe for Tyr278 did not convert *Ec*POX into a real oxidase.

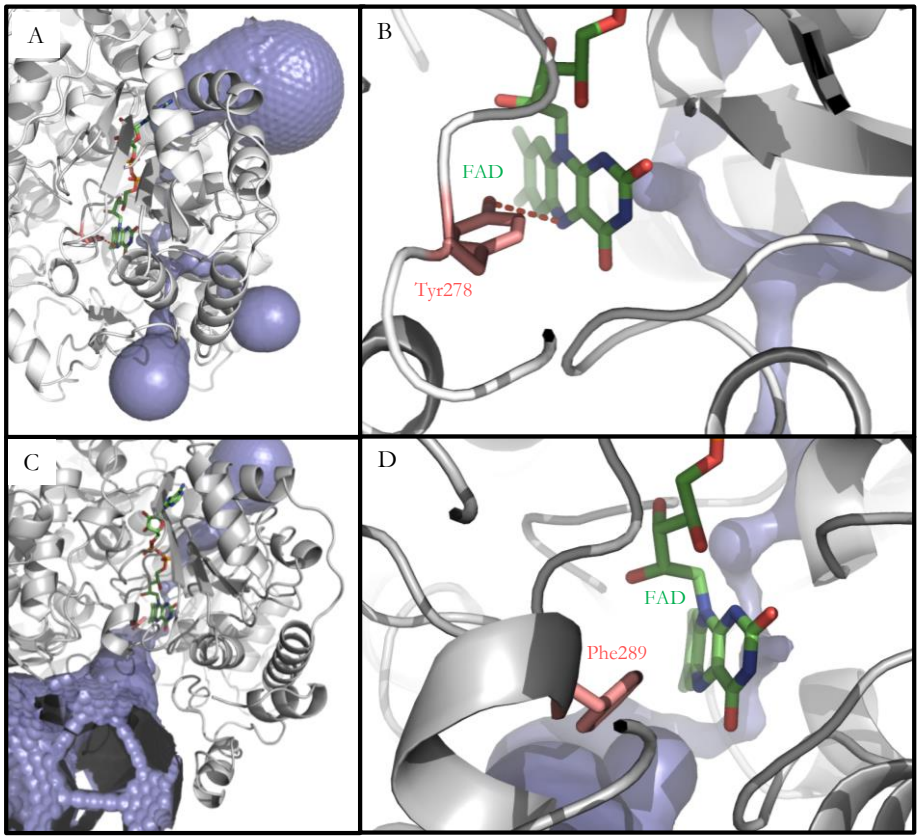

figure 52: Potential oxygen channels in *Ec*POX and *Lp*POX. Oxygen channels (blue) were simulated in structures of full-length *Ec*POX wt (A and B) and *Lp*POX wt (C and D) (unpublished high-resolution structure of *Lp*POX wt was friendly provided by Dr. Danilo Meyer, Department of Bioanalytics, Göttingen) by a search algorithm of the program MOLE [137]. Similar results were obtained when the corresponding variant structures of *Ec*POX and *Lp*POX were used for calculation of oxygen channels.

However, the static structures determined by X-ray crystallography lack protein movements during catalysis which could expose alternative oxygen channels. For example, it was reported for toluene/o-xylene monooxygenase hydroxylase that slight protein motions are mandatory for oxygen passing the di-iron active site [138]. Similar scenarios seem possible for *Lp*POX and *Ec*POX, since both proteins are supposed to undergo conformational changes due to pyruvate binding [45] which could provide further oxygen tunnels (unpublished data of Dr. Danilo Meyer, Department of Bioanalytics, Göttingen). Notably, the active site of activated EcPOX Δ23 is completely accessible to oxygen. To prove whether the simulated channels have a functional role in solution amino acid substitutions of small side chains to bulkier residues should decrease oxidase activity in both enzymes.

Tyr and Phe also determine oxygen reactivity in other pyruvate-converting oxidases and dehydrogenases

To examine whether regulation of oxygen reactivity by Tyr and Phe is a general principle, alignments of the protein sequences of *Ec*POX and *Lp*POX with selected pyruvate-converting oxidases and dehydrogenases from several organisms were performed with the program ClustalW2 [139]. Remarkably, all proteins classified as pyruvate dehydrogenases contain a Tyr at this particular position, while categorized oxidases harbor Phe (table 16). This is an unexpected observation since in most cases the proteins share only a sequence identity of 30-50 % to *Ec*POX or *Lp*POX. Thus, pyruvate-depending oxidases seem to require Phe near the flavin, whereas dehydrogenases suppress oxygen reactivity by a Tyr. Very likely the hydroxyl moiety of Tyr occupies the oxygen binding site in those enzymes. However, no

extensive generalizations should be made since this finding only corresponds to pyruvate-converting oxidases and dehydrogenases.

table 16: Sequence alignment of selected pyruvate-converting oxidases and dehydrogenases from different organisms. Enzymes classified as dehydrogenases were aligned with the *Ec*POX sequence, while assigned oxidases were compared to *Lp*POX. ClustalW2 was used for alignments [139]. Only a segment of the amino acid sequence is depicted.

pyruvate-dependent enzyme	organism	accession	amino acid sequence segment	identity to ***Ec*POX**	number of residues
p. oxidase	*E. coli* K-12	P07003	MMNADTLVLLGTQFPYRAFYPTDAKII-289	100 %	572
p. dehydrogenase	*Y. pestis*	Q7CHH9	MLNADTLILLGTQFPYRAFYPTHANII-289	78 %	573
p. dehydrogenase	*M. abscessus* 5S-0422	ZP_15350632	LEETEVLLMLGTDFPYRQFYPPKATVI-277	53 %	567
p. dehydrogenase	*S. coelicolor* A3(2)	NP_630260	THECDLLLLIGTDFPYNAFLPDDVKIA-290	52 %	580
p. dehydrogenase	*C. glutamicum*	Q8NMG5	SNEADLLILLGTDFPYSDFLPKD-NVA-288	45 %	579
p. dehydrogenase	*F. acidarmanus* fer1	ZP_05569937	IEKSDLIIFLGTIFPYTQFLKNVDNIQ-284	30 %	549
				identity to ***Lp*POX	
p.oxidase	*L. plantarum* WCFS1	P37063	LAQADVVLFVGNNYPFAEVSKAFKNTR-300	100 %	603
p.oxidase	*S. pneumoniae* TIGR4	Q54970	VFEADTVLFLGSNFPFAEVYEAFKNTE-294	48 %	591
p.oxidase	*C. sp.* AT7	ZP_02184772	VKEADTVLFVGSNFPFAEVENTFANVE-296	45 %	593
p.oxidase	*L.mes. subsp. Mes.* J18	YP_005174351	VLEADTVLFVGTNFPFSEVEGTFRNVD-300	45 %	606
p.oxidase	*M. bourgensis* MS2	YP_006545209	VLESDLVIACG--ASFSDLTGIPE-DK-294	31 %	539

The local environment of flavin-N5 and -C4a plays an important role in oxygen reactivity of flavoenzymes

Oxidase activity controlled by the environment near the reactive flavin atoms is not a unique principle only observed for pyruvate oxidases and dehydrogenases but is also detected in other flavoenzymes. However, in these cases other amino acids than Tyr and Phe are involved. It was shown that lactate monooxygenase is converted into an oxidase by exchanging Gly99 for Ala, which is located near the N5-C4a locus of FAD [77]. This result is further supported by the finding that glycolate oxidase, which has an analogous active site to lactate monooxygenase, also contains an Ala at the desired position [78]. Thus, it can be speculated that an increased space near the reactive centers of the flavin cofactor ensures higher oxygen reactivity. Contrary to this in aryl-alcohol oxidase the exchange of a Phe near the N5-atom for a bulkier Trp results in a 2fold increased oxidation rate [140]. Here the results are interpreted in a way that a more hydrophobic environment due to Trp replacement facilitates the electron transfer reaction and that Trp is involved in correct positioning of oxygen prior to reduction.

Although no general conclusion concerning the different oxygen reactivities of flavoenzymes should be drawn, results of this thesis highlight the important role of an interaction of the flavin cofactor with the protein matrix on the catalytic mechanism.

6. Summary

6.1 The molecular mechanism of activation and membrane binding of *Ec*POX

The peripheral membrane protein pyruvate oxidase from *E. coli* is activated at elevated concentrations of pyruvate. This leads to reduction of protein-bound flavin which is the initial signal for cytosolic exposure of the hitherto protein-associated membrane anchor and subsequently triggers membrane binding. Association to the lipid bilayer promotes accessibility to Q_8 and enhances the catalytic activity of *Ec*POX by several orders of magnitude. Aim of this thesis was to elucidate the molecular mechanism which controls activation and membrane binding in *Ec*POX. Therefore, variants of Tyr278, Phe465, Y549, Phe260, Ile554, Leu565, Trp570, Asp328, Asp348 and Gln537 were investigated.

Taken together the results obtained in this thesis, a molecular activation and membrane binding model of *Ec*POX can be proposed (figure 53). This scheme is an extension of the minimal model presented in the introduction (figure 5) but comprises additional *Ec*POX conformations found in various variants of *Ec*POX.

In the cytosolic resting state (R) an equilibrium of two *Ec*POX conformations is established. While state R I represents a conformation where the beta-peptide segment is partly released from the protein, species R II resembles a compact enzyme structure with both alpha- and beta-peptide parts clamped to the protein core. Since R I is characterized by a more accessible active site compared to R II it is suggested that this protein conformation is competent to bind the substrate pyruvate.

Binding of pyruvate to state R I and concomitant formation of covalent ThDP intermediates initiates formation of the substrate-bound species (SB) of *Ec*POX. Immediately after pyruvate binding a first conformational transition from SB I to the compact SB II-state is induced leading to quantitative formation of SB II. Interconversion between SB I and SB II is promoted by Phe465 which swings between the thiamine and flavin cofactor in SB II and thus mediates protein association of the beta-peptide segment.

Formation of SB II also enables the electron transfer between the thiamine and flavin cofactor, which is facilitated by Phe465, yielding the reduced flavin in the substrate-reduced state (SR). Reduced flavin initiates the second conformational change from SR II to SR III. The latter species resembles the *Ec*POX conformation with a released membrane anchor (alpha-peptide) competent for membrane binding. Several amino acids are involved in this structural rearrangement. Tyr278 senses the flavin redox state and might initiate the signal transfer cascade from the flavin to the membrane anchor. Tyr549 could be the final receptor for this signal and seems to play an important role in membrane anchor stabilization at the protein surface. Similar functions are attributed to Ile554, Leu565 and Trp570 which fix the membrane binding domain at the protein via hydrophobic interactions. Electrostatic contacts (Asp328-Arg572 and Asp348-Arg558) and hydrogen bonds (Glu564-Gln537) play only a minor role. Additionally, no involvement of Phe260 is observed.

Once the membrane anchor is exposed the presence of membranes induces the third conformational change. This change seems to be restricted to the membrane anchor which folds into an amphipathic helical structure at the lipid bilayer and mediates membrane association of *Ec*POX. Crucial amino acid residues that control helix formation and membrane binding are Ile554 and Trp570 which are positioned at the N- and C-terminal helix edge, respectively. Additionally, bilayer association of the membrane anchor removes an autoinhibitory part of the membrane binding domain from the protein core which enhances the enzymatic activity by several orders of magnitude.

Attached to the membrane *Ec*POX catalysis is completed by electron shuffling to Q_8. Therefore, the ubiquinone moves out of the membrane into the active site of *Ec*POX to accept the electrons. In this regard Try278 and/or Ser28 might protonate the anionic reduced Q_8^{2-} and hypothetically initiate another conformational switch which promotes subsequent membrane dissociation of the enzyme. Besides this potential function Tyr278 was also deciphered to prevent the flavin cofactor from wasteful reoxidation by molecular oxygen.

6.2 Conclusions

In this thesis the activation and membrane binding mechanism of pyruvate oxidase from *E.coli* was investigated. *Ec*POX is a peripheral membrane protein and was used as well-suited model system to analyze the impact of multiple amino acids on an enzymes activation mechanism and eventual bilayer association. Intensive kinetic and thermodynamic studies were performed in combination with X-ray crystallography. The results allowed the creation of a molecular activation model and give insights into a close coupling mechanism of catalysis and compartmentalization of an occasionally active enzyme.

It was shown that amino acids within the active site mediate pyruvate-induced reduction of the protein-bound flavin cofactor. The flavin redox state is also sensed by specific amino acids. Thus, the flavin acts as redox switch and a signal transfer cascade starting from the reduced flavin leads to exposure of the hitherto protein-bound membrane anchor. This membrane anchor is attached to the protein surface by hydrophobic interactions with the protein core. Upon activation these contacts are disturbed by conformational changes of the protein and the lipid binding domain to ensure membrane anchor exposure. Concomitant to release of the membrane anchor also an autoinhibitory helix is removed from the protein which leads to a great enhancement of the catalytic activity of *Ec*POX. Finally, the membrane anchor undergoes a last conformational transition in the presence of membranes. Bilayer association of the enzyme is thereby promoted by the formation of an amphipathic helix from the membrane anchor. Similar to the stabilization at the protein the membrane anchor is also bound to the membrane by hydrophobic contacts. Attached to the bilayer *Ec*POX has then access to its substrate Q_8 and can complete its catalytic cycle. Initial results suggest that Q_8 leaves the membrane and penetrates the active site of *Ec*POX according to an out-of-the membrane mechanism.

Knowing the impact of particular amino acids on specific steps of *Ec*POX activation allowed to track the pathway of activation. It remains to be studied whether the observations made for *Ec*POX can be assigned to other peripheral membrane binding enzymes. However, since the mechanisms of *Ec*POX activation are based on general principles (like protein association of the membrane anchor being of hydrophobic nature) it can be suggested that similar processes also govern the behavior of other enzymes and proteins.

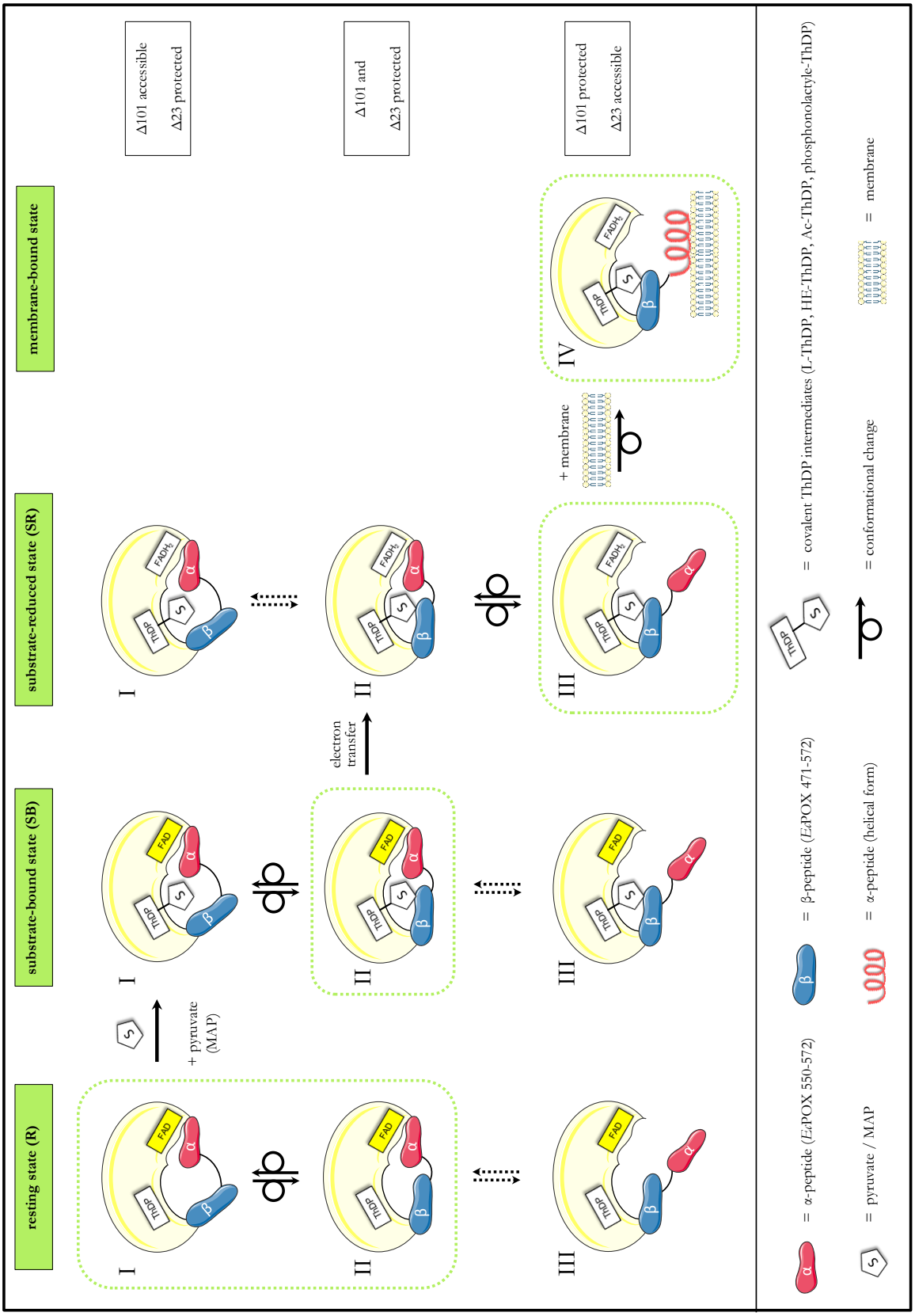

figure 53: Molecular mechanism of activation and membrane binding of *Ec*POX. Green boxes highlight the prominent species of *Ec*POX in equilibrium and indicate the suggested activation pathway. Final electron transfer of membrane-attached *Ec*POX to Q_8 is omitted for reasons of clarity. The functional tetramer of *Ec*POX is simplified illustrated as monomer for better visualization. Note that the alpha-peptide is presented separately from the beta-peptide, although the alpha-peptide resembles the C-terminal part of the beta-peptide. Detailed explanations are given in the text.

7. References

1. Maston, G.A., S.K. Evans, and M.R. Green, Transcriptional Regulatory Elements in the Human Genome. *Annual Review of Genomics and Human Genetics*, **2006**. **7**(1): p. 29-59.
2. McNurlan, M.A., New perspectives in the control of body protein metabolism. *British Journal of Nutrition*, **2012**. **108**(SupplementS2): p. S94-S104.
3. Hershko, A. and A. Ciechanover, The Ubiquitin System for Protein Degradation. *Annu Rev Biochem*, **1992**. **61**(1): p. 761-807.
4. Vandamme, J., D. Castermans, and J.M. Thevelein, Molecular mechanisms of feedback inhibition of protein kinase A on intracellular cAMP accumulation. *Cellular Signalling*, **2012**. **24**(8): p. 1610-1618.
5. Farazi, T.A., G. Waksman, and J.I. Gordon, The Biology and Enzymology of ProteinN-Myristoylation. *Journal of Biological Chemistry*, **2001**. **276**(43): p. 39501-39504.
6. Macfarlane, R.G., An Enzyme Cascade in the Blood Clotting Mechanism, and its Function as a Biochemical Amplifier. *Nature*, **1964**. **202**(4931): p. 498-499.
7. Mendel, S., *et al.*, The N-terminal domain of the regulatory subunit is sufficient for complete activation of acetohydroxyacid synthase III from Escherichia coli. *J Mol Biol*, **2003**. **325**(2): p. 275-84.
8. Schlessinger, J., Cell Signaling by Receptor Tyrosine Kinases. *Cell*, **2000**. **103**(2): p. 211-225.
9. Carr, C.M. and P.S. Kim, A spring-loaded mechanism for the conformational change of influenza hemagglutinin. *Cell*, **1993**. **73**(4): p. 823-832.
10. Strecker, T., *et al.*, The role of myristoylation in the membrane association of the Lassa virus matrix protein Z. *Virology Journal*, **2006**. **3**(1): p. 93.
11. Franco, M., *et al.*, Myristoylation-facilitated Binding of the G Protein ARF1 to Membrane Phospholipids Is Required for Its Activation by a Soluble Nucleotide Exchange Factor. *Journal of Biological Chemistry*, **1996**. **271**(3): p. 1573-1578.
12. Mather, M., *et al.*, Escherichia coli pyruvate oxidase: interaction of a peripheral membrane protein with lipids. *Biophys J*, **1982**. **37**(1): p. 87-8.
13. Russell, P., H.L. Schrock, and R.B. Gennis, Lipid activation and protease activation of pyruvate oxidase. Evidence suggesting a common site of interaction on the protein. *J Biol Chem*, **1977**. **252**(21): p. 7883-7.
14. Hager, L.P., Trypsin activation of a ferricyanide-linked pyruvic acid oxidation. *J Biol Chem*, **1957**. **229**(1): p. 251-63.
15. Williams, F.R. and L.P. Hager, A crystalline flavin pyruvate oxidase. *J Biol Chem*, **1961**. **236**: p. PC36-7.
16. Williams, F.R. and L.P. Hager, Crystalline flavin pyruvate oxidase from Escherichia coli. I. Isolation and properties of the flavoprotein. *Arch Biochem Biophys*, **1966**. **116**(1): p. 168-76.
17. Cunningham, C.C. and L.P. Hager, Reactivation of the lipid-depleted pyruvate oxidase system from Escherichia coli with cell envelope neutral lipids. *J Biol Chem*, **1975**. **250**(18): p. 7139-46.
18. Russell, P., L.P. Hager, and R.B. Gennis, Characterization of the proteolytic activation of pyruvate oxidase. Control by specific ligands and by the flavin oxidation-reduction state. *J Biol Chem*, **1977**. **252**(21): p. 7877-82.
19. Breslow, R., On the Mechanism of Thiamine Action. IV.1 Evidence from Studies on Model Systems. *J Am Chem Soc*, **1958**. **80**(14): p. 3719-3726.
20. Schellenberger, A. and G. Hubner, [On the theory of thiamine pyrophosphate action. IV. Mechanism and kinetics of recombination, and binding conditions deduced therefrom at the

active center of yeast pyruvate decarboxylase]. *Hoppe Seylers Z Physiol Chem*, **1967**. **348**(5): p. 491-500.

21. Muller, Y.A., *et al.*, A thiamin diphosphate binding fold revealed by comparison of the crystal structures of transketolase, pyruvate oxidase and pyruvate decarboxylase. *Structure*, **1993**. **1**(2): p. 95-103.

22. Kern, D., *et al.*, How thiamine diphosphate is activated in enzymes. *Science*, **1997**. **275**(5296): p. 67-70.

23. Mather, M.W. and R.B. Gennis, Kinetic studies of the lipid-activated pyruvate oxidase flavoprotein of Escherichia coli. *Journal of Biological Chemistry*, **1985**. **260**(30): p. 16148-55.

24. Ghisla, S. and V. Massey, Mechanisms of flavoprotein-catalyzed reactions. *Eur J Biochem*, **1989**. **181**(1): p. 1-17.

25. Patel, M.S. and T.E. Roche, Molecular biology and biochemistry of pyruvate dehydrogenase complexes. *FASEB J*, **1990**. **4**(14): p. 3224-33.

26. Brown, T.D., M.C. Jones-Mortimer, and H.L. Kornberg, The enzymic interconversion of acetate and acetyl-coenzyme A in Escherichia coli. *J Gen Microbiol*, **1977**. **102**(2): p. 327-36.

27. Chang, Y.Y., A.Y. Wang, and J.E. Cronan, Jr., Expression of Escherichia coli pyruvate oxidase (PoxB) depends on the sigma factor encoded by the rpoS(katF) gene. *Mol Microbiol*, **1994**. **11**(6): p. 1019-28.

28. Abdel-Hamid, A.M., M.M. Attwood, and J.R. Guest, Pyruvate oxidase contributes to the aerobic growth efficiency of Escherichia coli. *Microbiology*, **2001**. **147**(Pt 6): p. 1483-98.

29. Recny, M.A., *et al.*, Characterization of the alpha-peptide released upon protease activation of pyruvate oxidase. *J Biol Chem*, **1985**. **260**(26): p. 14287-91.

30. Chang, Y.Y. and J.E. Cronan, Jr., Detection by site-specific disulfide cross-linking of a conformational change in binding of Escherichia coli pyruvate oxidase to lipid bilayers. *J Biol Chem*, **1995**. **270**(14): p. 7896-901.

31. Wang, A.Y., Y.Y. Chang, and J.E. Cronan, Jr., Role of the tetrameric structure of Escherichia coli pyruvate oxidase in enzyme activation and lipid binding. *J Biol Chem*, **1991**. **266**(17): p. 10959-66.

32. Grabau, C. and J.E. Cronan, Jr., In vivo function of Escherichia coli pyruvate oxidase specifically requires a functional lipid binding site. *Biochemistry*, **1986**. **25**(13): p. 3748-51.

33. Chang, Y.Y. and J.E. Cronan, An Escherichia coli mutant deficient in pyruvate oxidase activity due to altered phospholipid activation of the enzyme. *Proc Natl Acad Sci U S A*, **1984**. **81**(14): p. 4348-52.

34. Blake, R. and L.P. Hager, Activation of pyruvate oxidase by monomeric and micellar amphiphiles. *J Biol Chem*, **1978**. **253**(6): p. 1963-71.

35. Neumann, P., *et al.*, Structural basis for membrane binding and catalytic activation of the peripheral membrane enzyme pyruvate oxidase from Escherichia coli. *Proc Natl Acad Sci U S A*, **2008**. **105**(45): p. 17390-5.

36. Schrock, H.L. and R.B. Gennis, High affinity lipid binding sites on the peripheral membrane enzyme pyruvate oxidase. Specific ligand effects on detergent binding. *J Biol Chem*, **1977**. **252**(17): p. 5990-5.

37. Hamilton, S.E., M. Recny, and L.P. Hager, Identification of the high-affinity lipid binding site in Escherichia coli pyruvate oxidase. *Biochemistry*, **1986**. **25**(25): p. 8178-83.

38. Widmann, M., R. Radloff, and J. Pleiss, The Thiamine diphosphate dependent Enzyme Engineering Database: A tool for the systematic analysis of sequence and structure relations. *BMC Biochemistry*, **2010**. **11**(1): p. 9.

39. Muller, Y.A., *et al.*, The refined structures of a stabilized mutant and of wild-type pyruvate oxidase from Lactobacillus plantarum. *J Mol Biol*, **1994**. **237**(3): p. 315-35.

40. Hecht, H.J., *et al.*, Crystal structure of glucose oxidase from Aspergillus niger refined at 2.3 A resolution. *J Mol Biol*, **1993**. **229**(1): p. 153-72.

41. Crosby, J. and G.E. Lienhard, Mechanisms of thiamine-catalyzed reactions. A kinetic analysis of the decarboxylation of pyruvate by 3,4-dimethylthiazolium ion in water and ethanol. *J Am Chem Soc*, **1970**. **92**(19): p. 5707-16.

42. Bertagnolli, B.L. and L.P. Hager, Activation of Escherichia coli pyruvate oxidase enhances the oxidation of hydroxyethylthiamin pyrophosphate. *J Biol Chem*, **1991**. **266**(16): p. 10168-73.

43. Pang, S.S., R.G. Duggleby, and L.W. Guddat, Crystal structure of yeast acetohydroxyacid synthase: a target for herbicidal inhibitors. *J Mol Biol*, **2002**. **317**(2): p. 249-62.

44. Tittmann, K., *et al.*, Electron transfer in acetohydroxy acid synthase as a side reaction of catalysis. Implications for the reactivity and partitioning of the carbanion/enamine form of (alpha-hydroxyethyl)thiamin diphosphate in a "nonredox" flavoenzyme. *Biochemistry*, **2004**. **43**(27): p. 8652-61.

45. Weidner, A., Studien zur Struktur, Funktion und Aktivierung der membran-assoziierten Pyruvatoxidase aus *Escherichia coli*. . *Phd thesis*, **2010**.

46. Wang, G., NMR of membrane-associated peptides and proteins. *Curr Protein Pept Sci*, **2008**. **9**(1): p. 50-69.

47. Gao, X. and T.C. Wong, Studies of the binding and structure of adrenocorticotropin peptides in membrane mimics by NMR spectroscopy and pulsed-field gradient diffusion. *Biophys J*, **1998**. **74**(4): p. 1871-88.

48. Chou, J.J., *et al.*, Micelle-induced curvature in a water-insoluble HIV-1 Env peptide revealed by NMR dipolar coupling measurement in stretched polyacrylamide gel. *J Am Chem Soc*, **2002**. **124**(11): p. 2450-1.

49. Burn, P., Talking point Amphitropic proteins: a new class of membrane proteins. *Trends Biochem Sci*, **1988**. **13**(3): p. 79-83.

50. Johnson, J.E. and R.B. Cornell, Amphitropic proteins: regulation by reversible membrane interactions (review). *Mol Membr Biol*, **1999**. **16**(3): p. 217-35.

51. Consonni, S.V., *et al.*, cAMP regulates DEP domain-mediated binding of the guanine nucleotide exchange factor Epac1 to phosphatidic acid at the plasma membrane. *Proceedings of the National Academy of Sciences*, **2012**. **109**(10): p. 3814-3819.

52. Jackson, L.P., *et al.*, A Large-Scale Conformational Change Couples Membrane Recruitment to Cargo Binding in the AP2 Clathrin Adaptor Complex. *Cell*, **2010**. **141**(7): p. 1220-1229.

53. Friesen, J.A., H.A. Campbell, and C. Kent, Enzymatic and cellular characterization of a catalytic fragment of CTP:phosphocholine cytidylyltransferase alpha. *J Biol Chem*, **1999**. **274**(19): p. 13384-9.

54. Kimura, N. and N. Shimada, Evidence for complex formation between GTP binding protein(Gs) and membrane-associated nucleoside diphosphate kinase. *Biochem Biophys Res Commun*, **1990**. **168**(1): p. 99-106.

55. Anderson, K.E., *et al.*, Translocation of PDK-1 to the plasma membrane is important in allowing PDK-1 to activate protein kinase B. *Curr Biol*, **1998**. **8**(12): p. 684-91.

56. Cornell, R.B. and S.G. Taneva, Amphipathic helices as mediators of the membrane interaction of amphitropic proteins, and as modulators of bilayer physical properties. *Curr Protein Pept Sci*, **2006**. **7**(6): p. 539-52.

57. Johnson, J.E. and R.B. Cornell, Membrane-binding amphipathic alpha-helical peptide derived from CTP:phosphocholine cytidylyltransferase. *Biochemistry*, **1994**. **33**(14): p. 4327-35.

58. Johnson, J.E., *et al.*, Both acidic and basic amino acids in an amphitropic enzyme, CTP:phosphocholine cytidylyltransferase, dictate its selectivity for anionic membranes. *J Biol Chem*, **2003**. **278**(1): p. 514-22.

59. Bernstein, L.S., *et al.*, RGS4 binds to membranes through an amphipathic alpha -helix. *J Biol Chem*, **2000**. **275**(24): p. 18520-6.

60. Zhou, H. and J. Lutkenhaus, Membrane binding by MinD involves insertion of hydrophobic residues within the C-terminal amphipathic helix into the bilayer. *J Bacteriol*, **2003**. **185**(15): p. 4326-35.

61. Arnold, R.S. and R.B. Cornell, Lipid regulation of CTP: phosphocholine cytidylyltransferase: electrostatic, hydrophobic, and synergistic interactions of anionic phospholipids and diacylglycerol. *Biochemistry*, **1996**. **35**(30): p. 9917-24.

62. Vogel, H., Incorporation of melittin into phosphatidylcholine bilayers. Study of binding and conformational changes. *FEBS Lett*, **1981**. **134**(1): p. 37-42.

63. Johnson, J.E., *et al.*, Conformation and lipid binding properties of four peptides derived from the membrane-binding domain of CTP:phosphocholine cytidylyltransferase. *Biochemistry*, **1998**. **37**(26): p. 9509-19.

64. Forneris, F. and A. Mattevi, Enzymes without borders: mobilizing substrates, delivering products. *Science*, **2008**. **321**(5886): p. 213-6.

65. Voityuk, A.A., Long-range electron transfer in biomolecules. Tunneling or hopping? *J Phys Chem B*, **2011**. **115**(42): p. 12202-7.

66. Onuchic, J.N., *et al.*, Pathway analysis of protein electron-transfer reactions. *Annu Rev Biophys Biomol Struct*, **1992**. **21**: p. 349-77.

67. Page, C.C., *et al.*, Natural engineering principles of electron tunnelling in biological oxidation-reduction. *Nature*, **1999**. **402**(6757): p. 47-52.

68. Mattevi, A., To be or not to be an oxidase: challenging the oxygen reactivity of flavoenzymes. *Trends Biochem Sci*, **2006**. **31**(5): p. 276-83.

69. Juárez, O., J.E. Morgan, and B. Barquera, The Electron Transfer Pathway of the Na+-pumping NADH:Quinone Oxidoreductase from Vibrio cholerae. *Journal of Biological Chemistry*, **2009**. **284**(13): p. 8963-8972.

70. Umhau, S., *et al.*, The x-ray structure of D-amino acid oxidase at very high resolution identifies the chemical mechanism of flavin-dependent substrate dehydrogenation. *Proc Natl Acad Sci U S A*, **2000**. **97**(23): p. 12463-8.

71. van Pée, K.-H. and S. Unversucht, Biological dehalogenation and halogenation reactions. *Chemosphere*, **2003**. **52**(2): p. 299-312.

72. Gross, E., *et al.*, Structure of Ero1p, source of disulfide bonds for oxidative protein folding in the cell. *Cell*, **2004**. **117**(5): p. 601-10.

73. Tittmann, K., *et al.*, Radical phosphate transfer mechanism for the thiamin diphosphate- and FAD-dependent pyruvate oxidase from Lactobacillus plantarum. Kinetic coupling of intercofactor electron transfer with phosphate transfer to acetyl-thiamin diphosphate via a transient FAD semiquinone/hydroxyethyl-ThDP radical pair. *Biochemistry*, **2005**. **44**(40): p. 13291-303.

74. Tittmann, K., *et al.*, Mechanism of elementary catalytic steps of pyruvate oxidase from Lactobacillus plantarum. *Biochemistry*, **2000**. **39**(35): p. 10747-54.

75. Sedewitz, B., K.H. Schleifer, and F. Gotz, Purification and biochemical characterization of pyruvate oxidase from Lactobacillus plantarum. *J Bacteriol*, **1984**. **160**(1): p. 273-8.

76. Madigan, M., *et al.*, Brock - Biology of Microorgansms. , **2009**. **12**.

77. Sun, W., C.H. Williams, Jr., and V. Massey, The role of glycine 99 in L-lactate monooxygenase from Mycobacterium smegmatis. *J Biol Chem*, **1997**. **272**(43): p. 27065-76.

78. Stenberg, K. and Y. Lindqvist, Three-dimensional structures of glycolate oxidase with bound active-site inhibitors. *Protein Sci*, **1997**. **6**(5): p. 1009-15.

79. Wille, G., Infrarotspektroskopische, strukturelle und kinetische Untersuchung der Pyruvatoxidase aus *Lactobacillus plantarum*. *Phd thesis*, **2005**.

80. Meyer, D., Kinetische und strukturelle Untersuchung der Katalysemechanismen ausgewählter Kofaktor-abhängiger Enzyme - Implikationen für die Decarboxylierung von α-Ketosäuren durch Thiamindiphosphat-abhängige Enzyme. *PhD thesis*, **2009**.

81. Dower, W.J., J.F. Miller, and C.W. Ragsdale, High efficiency transformation of E. coli by high voltage electroporation. *Nucleic Acids Res*, **1988**. **16**(13): p. 6127-45.

82. Weidner, A., *et al.*, Crystallization and preliminary X-ray diffraction analysis of full-length and proteolytically activated pyruvate oxidase from Escherichia coli. *Acta Crystallogr Sect F Struct Biol Cryst Commun*, **2008**. **64**(Pt 3): p. 179-81.

83. Wille, G., *et al.*, Redox-triggered FTIR difference spectra of FAD in aqueous solution and bound to flavoproteins. *Biochemistry*, **2003**. **42**(50): p. 14814-21.

84. Marley, J., M. Lu, and C. Bracken, A method for efficient isotopic labeling of recombinant proteins. *J Biomol NMR*, **2001**. **20**(1): p. 71-5.

85. Bradford, M.M., A rapid and sensitive method for the quantitation of microgram quantities of protein utilizing the principle of protein-dye binding. *Anal Biochem*, **1976**. **72**: p. 248-54.

86. Pace, C.N., *et al.*, How to measure and predict the molar absorption coefficient of a protein. *Protein Sci*, **1995**. **4**(11): p. 2411-23.

87. Pace, C.N., *et al.*, Conformational stability and thermodynamics of folding of ribonucleases Sa, Sa2 and Sa3. *J Mol Biol*, **1998**. **279**(1): p. 271-86.

88. Wille, G., *et al.*, The catalytic cycle of a thiamin diphosphate enzyme examined by cryocrystallography. *Nat Chem Biol*, **2006**. **2**(6): p. 324-8.

89. Kabsch, W., Automatic processing of rotation diffraction data from crystals of initially unknown symmetry and cell constants. *Journal of Applied Crystallography*, **1993**. **26**(6): p. 795-800.

90. Meyer, D., *et al.*, Unexpected tautomeric equilibria of the carbanion-enamine intermediate in pyruvate oxidase highlight unrecognized chemical versatility of thiamin. *Proc Natl Acad Sci U S A*, **2012**. **109**(27): p. 10867-72.

91. Emsley, P. and K. Cowtan, Coot: model-building tools for molecular graphics. *Acta Crystallogr D Biol Crystallogr*, **2004**. **60**(Pt 12 Pt 1): p. 2126-32.

92. Murshudov, G.N., A.A. Vagin, and E.J. Dodson, Refinement of macromolecular structures by the maximum-likelihood method. *Acta Crystallogr D Biol Crystallogr*, **1997**. **53**(Pt 3): p. 240-55.

93. Adams, P.D., *et al.*, PHENIX: building new software for automated crystallographic structure determination. *Acta Crystallogr D Biol Crystallogr*, **2002**. **58**(Pt 11): p. 1948-54.

94. Brunger, A.T., *et al.*, Crystallography & NMR system: A new software suite for macromolecular structure determination. *Acta Crystallogr D Biol Crystallogr*, **1998**. **54**(Pt 5): p. 905-21.

95. Buck, M., Trifluoroethanol and colleagues: cosolvents come of age. Recent studies with peptides and proteins. *Q Rev Biophys*, **1998**. **31**(3): p. 297-355.

96. Böhm, G., **1997**.

97. Delaglio, F., *et al.*, NMRPipe: a multidimensional spectral processing system based on UNIX pipes. *J Biomol NMR*, **1995**. **6**(3): p. 277-93.

98. Vranken, W.F., *et al.*, The CCPN data model for NMR spectroscopy: development of a software pipeline. *Proteins*, **2005**. **59**(4): p. 687-96.

99. Schwarzinger, S., *et al.*, Sequence-dependent correction of random coil NMR chemical shifts. *J Am Chem Soc*, **2001**. **123**(13): p. 2970-8.

100. Vuister, G.W. and A. Bax, Quantitative J correlation: a new approach for measuring homonuclear three-bond J(HNH.alpha.) coupling constants in 15N-enriched proteins. *J Am Chem Soc*, **1993**. **115**(17): p. 7772-7777.

101. Shen, Y., *et al.*, TALOS+: a hybrid method for predicting protein backbone torsion angles from NMR chemical shifts. *J Biomol NMR*, **2009**. **44**(4): p. 213-23.

102. Marsh, J.A., *et al.*, Sensitivity of secondary structure propensities to sequence differences between alpha- and gamma-synuclein: implications for fibrillation. *Protein Sci*, **2006**. **15**(12): p. 2795-804.

103. Berjanskii, M.V. and D.S. Wishart, A simple method to predict protein flexibility using secondary chemical shifts. *J Am Chem Soc*, **2005**. **127**(43): p. 14970-1.

104. Taheri-Kafrani, A. and A.-K. Bordbar, Energitics of micellizaion of sodium n-dodecyl sulfate at physiological conditions using isothermal titration calorimetry. *Journal of Thermal Analysis and Calorimetry*, **2009**. **98**(2): p. 567-575.

105. Tong, W., *et al.*, Critical Micellar Concentrations of Quaternary Ammonium Surfactants with Hydroxyethyl Substituents on Headgroups Determined by Isothermal Titration Calorimetry. *Journal of Chemical & Engineering Data*, **2010**. **55**(9): p. 3766-3771.

106. Paula, S., *et al.*, Thermodynamics of Micelle Formation as a Function of Temperature: A High Sensitivity Titration Calorimetry Study. *The Journal of Physical Chemistry*, **1995**. **99**(30): p. 11742-11751.

107. Tittmann, K., *et al.*, Activation of thiamin diphosphate and FAD in the phosphatedependent pyruvate oxidase from Lactobacillus plantarum. *J Biol Chem*, **1998**. **273**(21): p. 12929-34.

108. Cunningham, C.C. and L.P. Hager, Crystalline pyruvate oxidase from Escherichia coli. II. Activation by phospholipids. *J Biol Chem*, **1971**. **246**(6): p. 1575-82.

109. Mather, M., *et al.*, Studies of the flavin adenine dinucleotide binding region in Escherichia coli pyruvate oxidase. *J Biol Chem*, **1982**. **257**(21): p. 12887-92.

110. Enroth, C., *et al.*, Crystal structures of bovine milk xanthine dehydrogenase and xanthine oxidase: structure-based mechanism of conversion. *Proc Natl Acad Sci U S A*, **2000**. **97**(20): p. 10723-8.

111. O'Brien, T.A., *et al.*, Conformational studies of Escherichia coli pyruvate oxidase. *Biochim Biophys Acta*, **1982**. **705**(3): p. 321-9.

112. Sierk, M.L. and G.J. Kleywegt, Deja vu all over again: finding and analyzing protein structure similarities. *Structure*, **2004**. **12**(12): p. 2103-11.

113. Malakhov, M.P., *et al.*, SUMO fusions and SUMO-specific protease for efficient expression and purification of proteins. *J Struct Funct Genomics*, **2004**. **5**(1-2): p. 75-86.

114. Greenfield, N.J. and G.D. Fasman, Computed circular dichroism spectra for the evaluation of protein conformation. *Biochemistry*, **1969**. **8**(10): p. 4108-4116.

115. Reed, J. and T.A. Reed, A set of constructed type spectra for the practical estimation of peptide secondary structure from circular dichroism. *Anal Biochem*, **1997**. **254**(1): p. 36-40.

116. Parker, W. and P.S. Song, Protein structures in SDS micelle-protein complexes. *Biophys J*, **1992**. **61**(5): p. 1435-9.

117. Menzel, R. and J. Roth, Enzymatic properties of the purified putA protein from Salmonella typhimurium. *J Biol Chem*, **1981**. **256**(18): p. 9762-6.

118. Zhang, W., *et al.*, Redox-induced changes in flavin structure and roles of flavin N(5) and the ribityl 2'-OH group in regulating PutA--membrane binding. *Biochemistry*, **2007**. **46**(2): p. 483-91.

119. Meyer, D., Mechanistische Analyse der Elektronentransferreaktion in Pyruvatoxidase aus *Lactobacillus plantarum*. *Diploma thesis*, **2004**.

120. Chou, P.Y. and G.D. Fasman, Prediction of the secondary structure of proteins from their amino acid sequence. *Adv Enzymol Relat Areas Mol Biol*, **1978**. **47**: p. 45-148.

121. Bertagnolli, B.L. and L.P. Hager, Minimum requirements for protease activation of flavin pyruvate oxidase. *Biochemistry*, **1991**. **30**(33): p. 8131-8137.

122. Grabau, C., Y.Y. Chang, and J.E. Cronan, Jr., Lipid binding by Escherichia coli pyruvate oxidase is disrupted by small alterations of the carboxyl-terminal region. *J Biol Chem*, **1989**. **264**(21): p. 12510-9.

123. Schloss, J.V., L.M. Ciskanik, and D.E.V. Dyk, Origin of the herbicide binding site of acetolactate synthase. *Nature*, **1988**. **331**(6154): p. 360-362.

124. Baradaran, R., *et al.*, Crystal structure of the entire respiratory complex I. *Nature*, **2013**. **494**(7438): p. 443-8.

125. Efremov, R.G., R. Baradaran, and L.A. Sazanov, The architecture of respiratory complex I. *Nature*, **2010**. **465**(7297): p. 441-5.

126. Berrisford, J.M. and L.A. Sazanov, Structural basis for the mechanism of respiratory complex I. *J Biol Chem*, **2009**. **284**(43): p. 29773-83.

127. Galkin, A., S. Drose, and U. Brandt, The proton pumping stoichiometry of purified mitochondrial complex I reconstituted into proteoliposomes. *Biochim Biophys Acta*, **2006**. **1757**(12): p. 1575-81.

128. Tocilescu, M.A., *et al.*, Exploring the ubiquinone binding cavity of respiratory complex I. *J Biol Chem*, **2007**. **282**(40): p. 29514-20.

129. Zickermann, V., *et al.*, Architecture of complex I and its implications for electron transfer and proton pumping. *Biochim Biophys Acta*, **2009**. **1787**(6): p. 574-83.

130. Zhang, J., F.E. Frerman, and J.J. Kim, Structure of electron transfer flavoprotein-ubiquinone oxidoreductase and electron transfer to the mitochondrial ubiquinone pool. *Proc Natl Acad Sci U S A*, **2006**. **103**(44): p. 16212-7.

131. Feng, Y., *et al.*, Structural insight into the type-II mitochondrial NADH dehydrogenases. *Nature*, **2012**. **491**(7424): p. 478-482.

132. Kashani-Poor, N., *et al.*, A central functional role for the 49-kDa subunit within the catalytic core of mitochondrial complex I. *J Biol Chem*, **2001**. **276**(26): p. 24082-7.

133. Koder, R.L., *et al.*, Flavin thermodynamics explain the oxygen insensitivity of enteric nitroreductases. *Biochemistry*, **2002**. **41**(48): p. 14197-205.

134. Leferink, N.G., *et al.*, Identification of a gatekeeper residue that prevents dehydrogenases from acting as oxidases. *J Biol Chem*, **2009**. **284**(7): p. 4392-7.

135. Roth, J.P. and J.P. Klinman, Catalysis of electron transfer during activation of O2 by the flavoprotein glucose oxidase. *Proc Natl Acad Sci U S A*, **2003**. **100**(1): p. 62-7.

136. Baron, R., *et al.*, Multiple pathways guide oxygen diffusion into flavoenzyme active sites. *Proc Natl Acad Sci U S A*, **2009**. **106**(26): p. 10603-8.

137. PetYek, M., *et al.*, MOLE: A Voronoi Diagram-Based Explorer of Molecular Channels, Pores, and Tunnels. *Structure (London, England : 1993)*, **2007**. **15**(11): p. 1357-1363.

138. Song, W.J., *et al.*, Tracking a defined route for O(2) migration in a dioxygen-activating diiron enzyme. *Proc Natl Acad Sci U S A*, **2011**. **108**(36): p. 14795-800.

139. Larkin, M.A., *et al.*, Clustal W and Clustal X version 2.0. *Bioinformatics*, **2007**. **23**(21): p. 2947-2948.

140. Hernández-Ortega, A., *et al.*, Modulating O2 Reactivity in a Fungal Flavoenzyme: INVOLVEMENT OF ARYL-ALCOHOL OXIDASE PHE-501 CONTIGUOUS TO CATALYTIC HISTIDINE. *Journal of Biological Chemistry*, **2011**. **286**(47): p. 41105-41114.

141. Olofsson, G. and W. Loh, On the use of titration calorimetry to study the association of surfactants in aqueous solutions. *Journal of the Brazilian Chemical Society*, **2009**. **20**: p. 577-593.

8. Appendix

8.1 Determination of the critical micelle concentration of SDS and DPC by ITC

ITC was used to determine the CMC of the detergents SDS and DPC in water and 50 mM NaH_2PO_4 pH 6.0 (buffer) according to [104]. As example a thermogram of the CMC determination of SDS in water is shown. Negative peaks at the beginning of the titration correspond to demicellization events whereas positive peaks at the end of the measurement indicate micelles dilution [141]. The point of inflection in the lower figure corresponds to the CMC which was calculated according to [106]. The determined CMCs are listed in table 17.

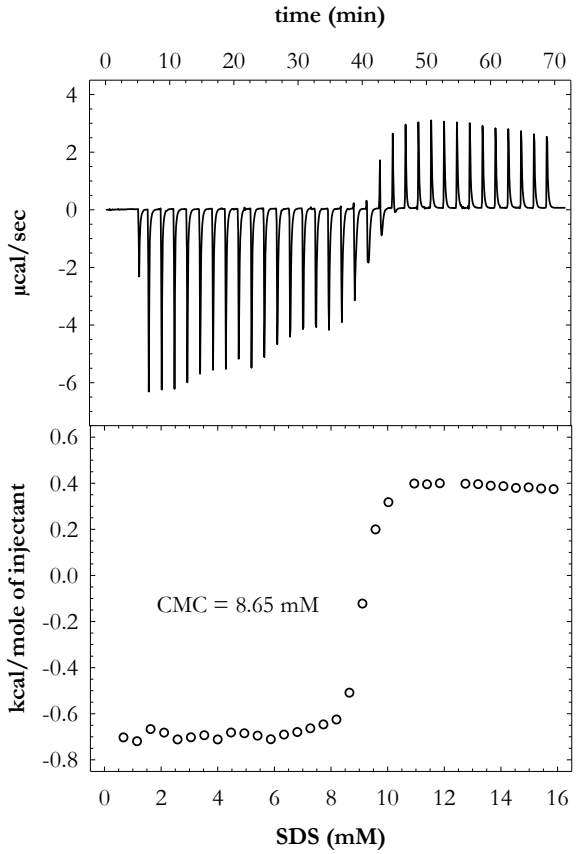

table 17: CMC of SDS and DPC.

detergent in water/buffer	CMC (mM)
SDS in water	8.6 (± 0.4)
SDS in buffer	1.9 (± 0.1)
DPC in water	1.6 (± 0.1)
DPC in buffer	1.3 (± 0.1)

8.2 Steady-state activity of *Ec*POX variants

Steady-state activity of *Ec*POX variants in dependence of the pyruvate concentration. Data (dots) were fitted according to Michaelis-Menten equation (lines).

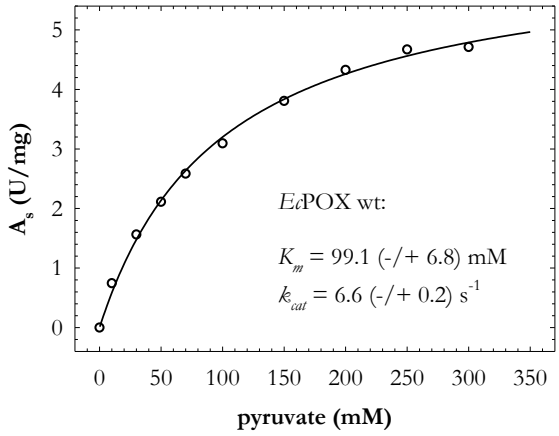

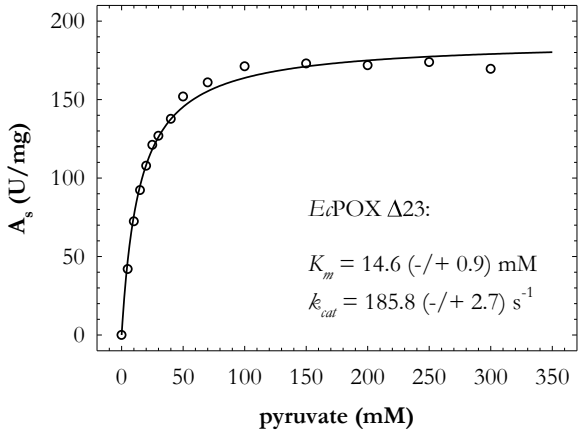

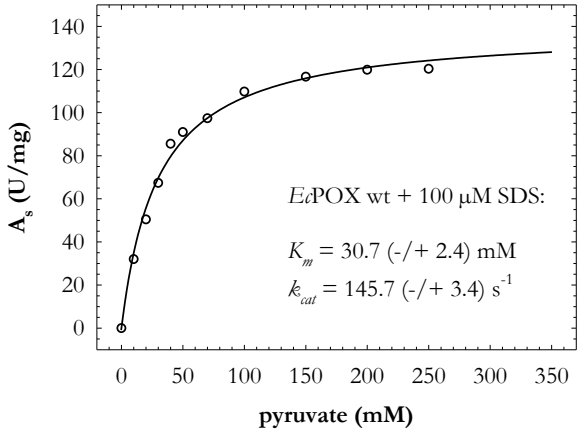

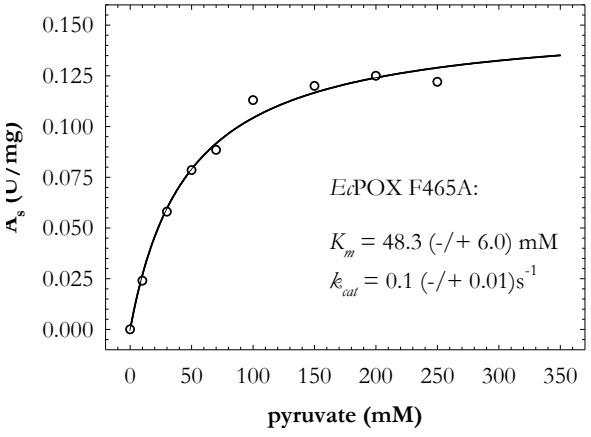

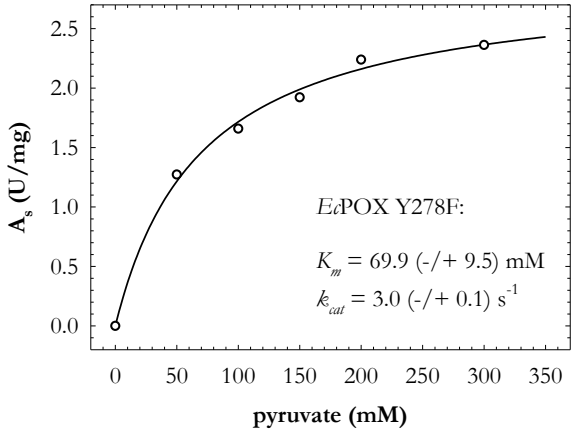

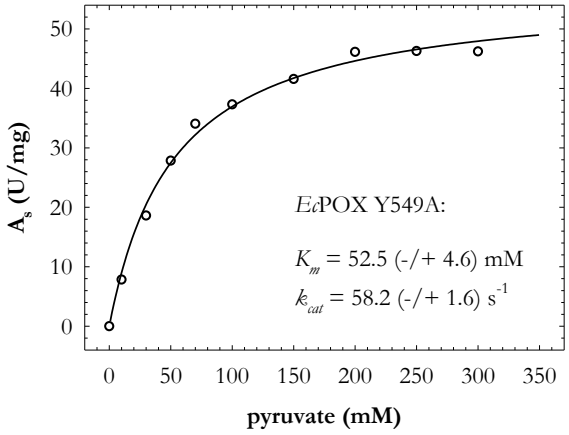

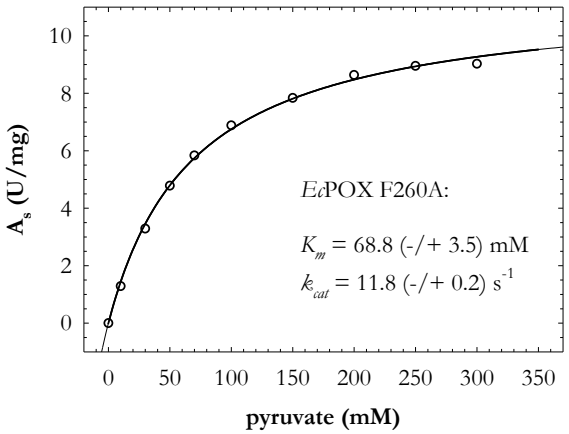
*Ec*POX F260A:
K_m = 68.8 (-/+ 3.5) mM
k_{cat} = 11.8 (-/+ 0.2) s^{-1}
A_s (U/mg)
pyruvate (mM)

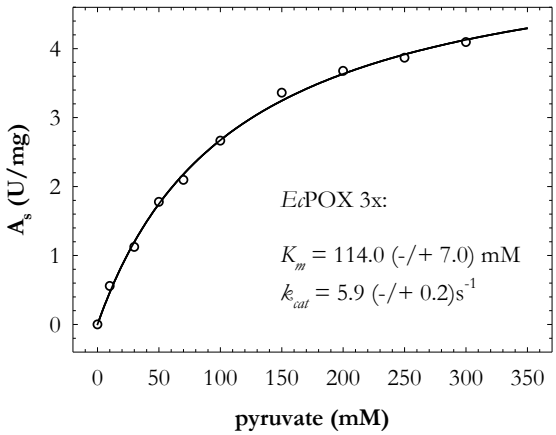
*Ec*POX 3x:
K_m = 114.0 (-/+ 7.0) mM
k_{cat} = 5.9 (-/+ 0.2)s^{-1}
A_s (U/mg)
pyruvate (mM)

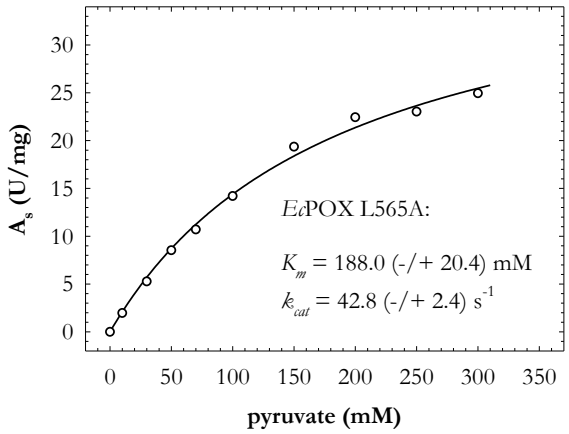
*Ec*POX L565A:
K_m = 188.0 (-/+ 20.4) mM
k_{cat} = 42.8 (-/+ 2.4) s^{-1}
A_s (U/mg)
pyruvate (mM)

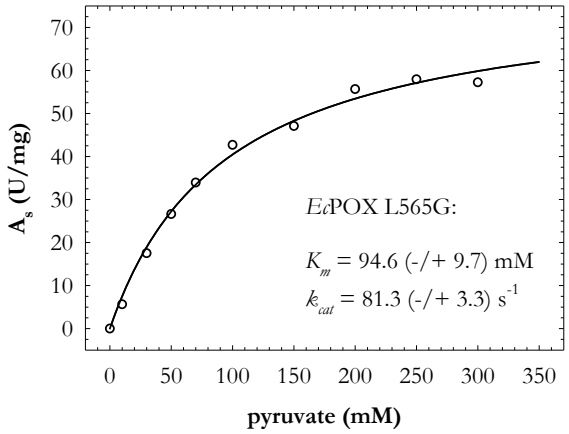
*Ec*POX L565G:
K_m = 94.6 (-/+ 9.7) mM
k_{cat} = 81.3 (-/+ 3.3) s^{-1}
A_s (U/mg)
pyruvate (mM)

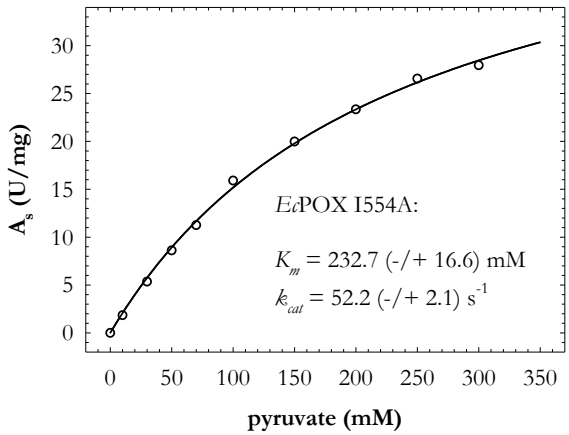
*Ec*POX I554A:
K_m = 232.7 (-/+ 16.6) mM
k_{cat} = 52.2 (-/+ 2.1) s^{-1}
A_s (U/mg)
pyruvate (mM)

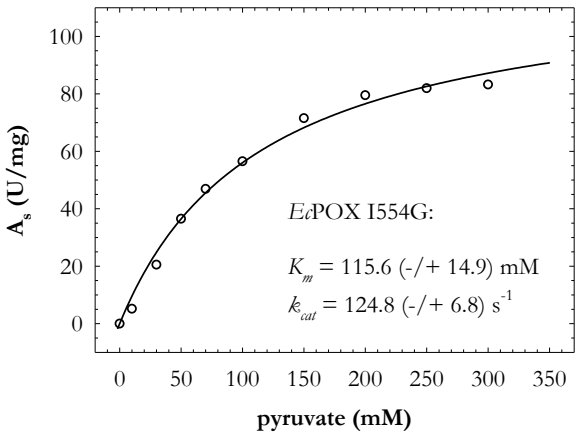
*Ec*POX I554G:
K_m = 115.6 (-/+ 14.9) mM
k_{cat} = 124.8 (-/+ 6.8) s^{-1}
A_s (U/mg)
pyruvate (mM)

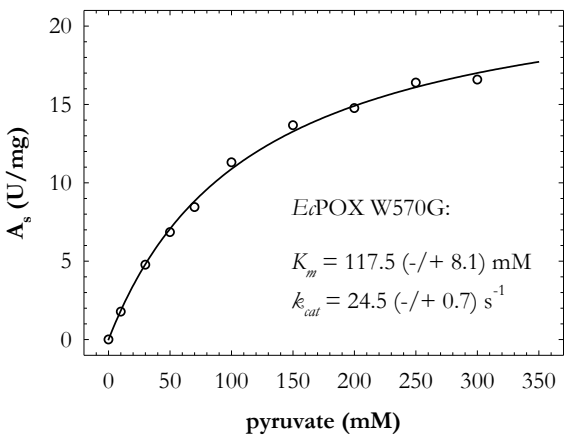
*Ec*POX W570G:
K_m = 117.5 (-/+ 8.1) mM
k_{cat} = 24.5 (-/+ 0.7) s^{-1}
A_s (U/mg)
pyruvate (mM)

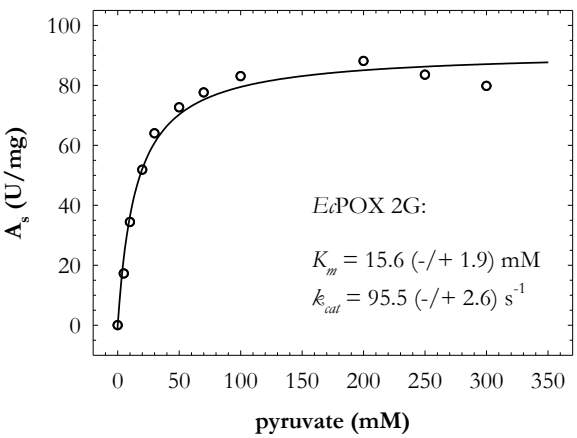
*Ec*POX 2G:
K_m = 15.6 (-/+ 1.9) mM
k_{cat} = 95.5 (-/+ 2.6) s^{-1}
A_s (U/mg)
pyruvate (mM)

8.3 Temperature-induced unfolding of *Ec*POX variants

Temperature-dependent unfolding of *Ec*POX wt and selected variants (0.1 mg/mL) was observed at 208 nm by CD spectroscopy. Progress curves were used to calculate the apparent melting temperature T_m by equation 6.

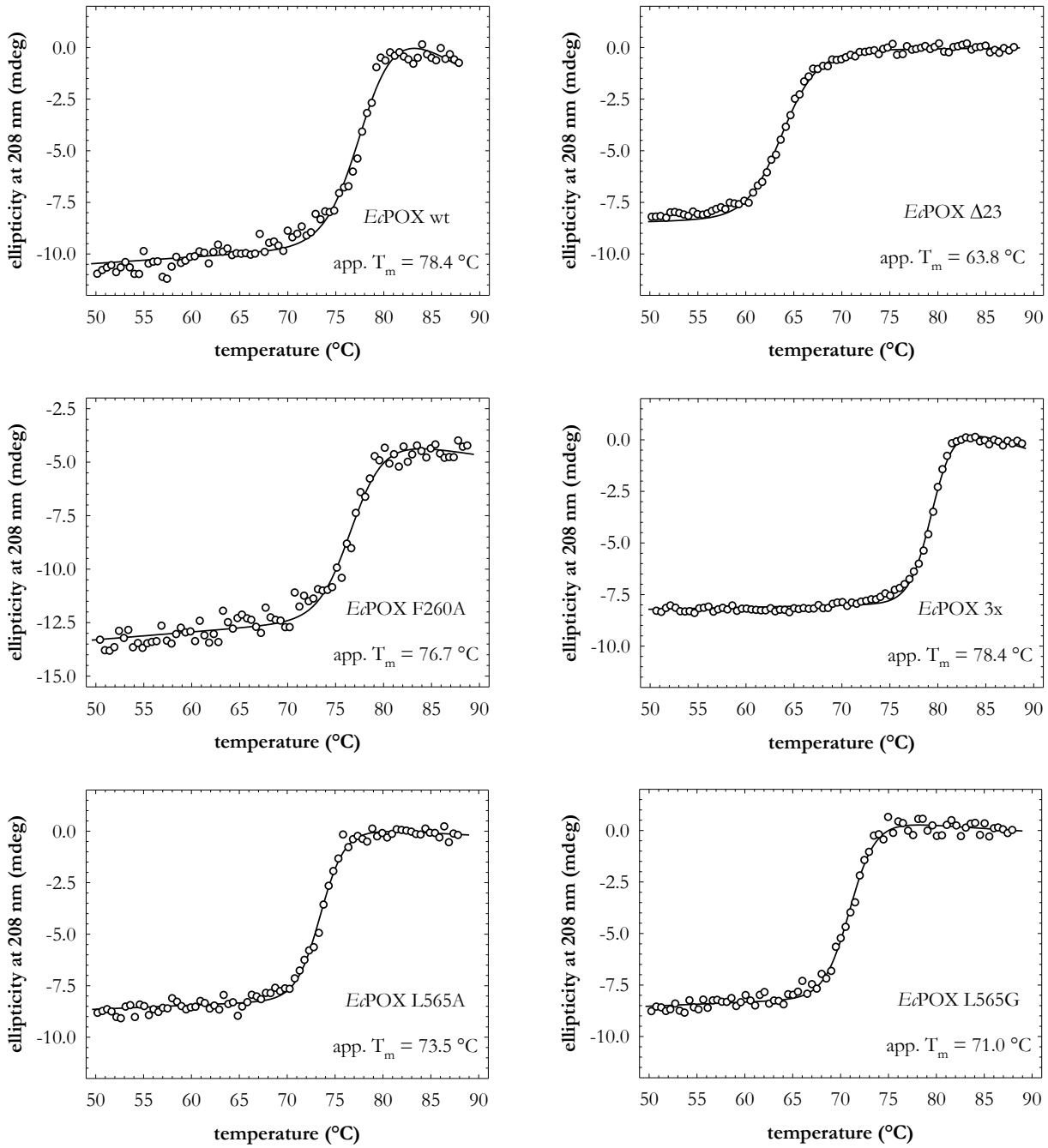

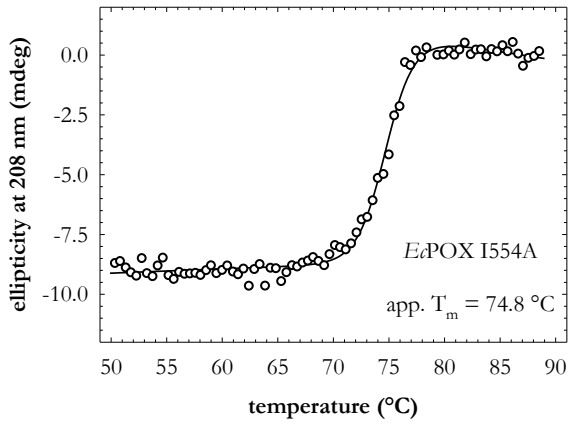
ellipticity at 208 nm (mdeg)
0.0
-2.5
-5.0
-7.5
-10.0
50 55 60 65 70 75 80 85 90
temperature (°C)
EcPOX I554A
app. Tm = 74.8 °C

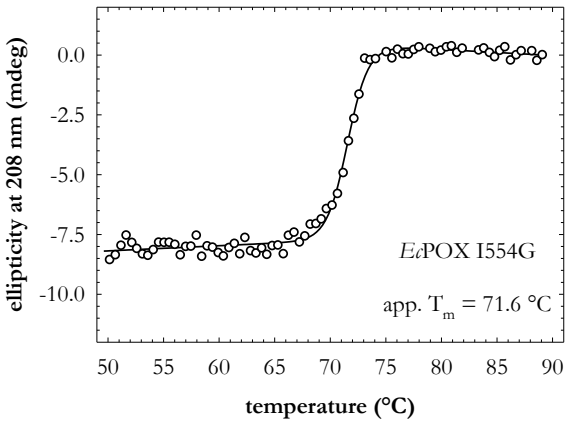
ellipticity at 208 nm (mdeg)
0.0
-2.5
-5.0
-7.5
-10.0
50 55 60 65 70 75 80 85 90
temperature (°C)
EcPOX I554G
app. Tm = 71.6 °C

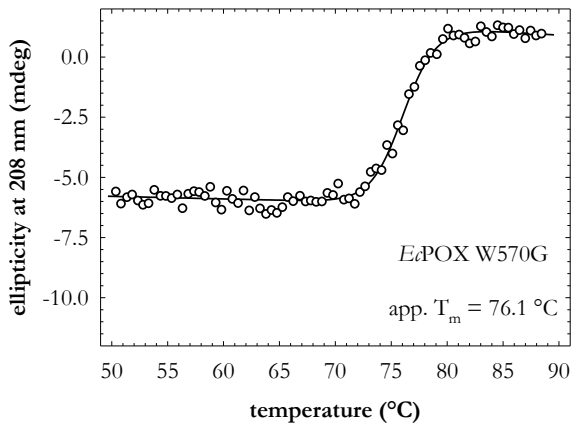
ellipticity at 208 nm (mdeg)
0.0
-2.5
-5.0
-7.5
-10.0
50 55 60 65 70 75 80 85 90
temperature (°C)
EcPOX W570G
app. Tm = 76.1 °C

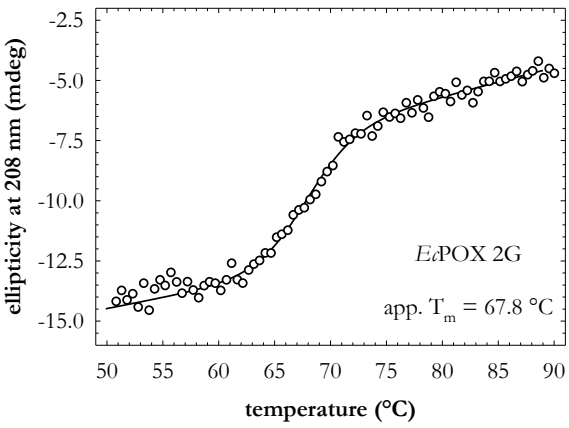
ellipticity at 208 nm (mdeg)
-2.5
-5.0
-7.5
-10.0
-12.5
-15.0
50 55 60 65 70 75 80 85 90
temperature (°C)
EcPOX 2G
app. Tm = 67.8 °C

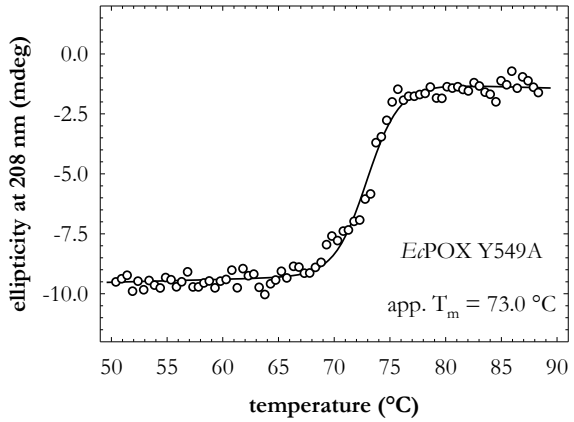
ellipticity at 208 nm (mdeg)
0.0
-2.5
-5.0
-7.5
-10.0
50 55 60 65 70 75 80 85 90
temperature (°C)
EcPOX Y549A
app. Tm = 73.0 °C

8.4 SDS-mediated activation of *Ec*POX variants

*Ec*POX activity stimulated by different amounts of SDS was analyzed by Q_0 steady-state assay. Therefore, 160 nM *Ec*POX were pre-incubated with 200 mM pyruvate. Activation was initiated by addition of SDS and activity was monitored by Q_0 steady-state assay. A: Kinetics of *Ec*POX activation. B: Comparison of SDS-mediated activation of *Ec*POX wt and the examined variant in dependence of the desired SDS concentration. Each ensemble of data points at a given SDS concentration resembles one curve of A. $SDS_{0.5}$ (highlighted by gray dashed lines) resembles the SDS concentration at which approximately 50 % of the protein is activated after half of the measuring time (30 min).

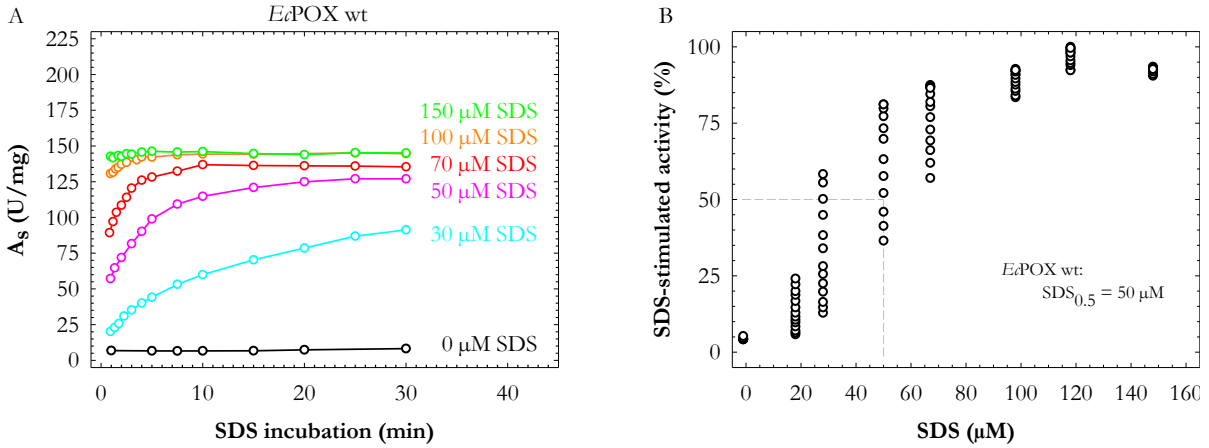

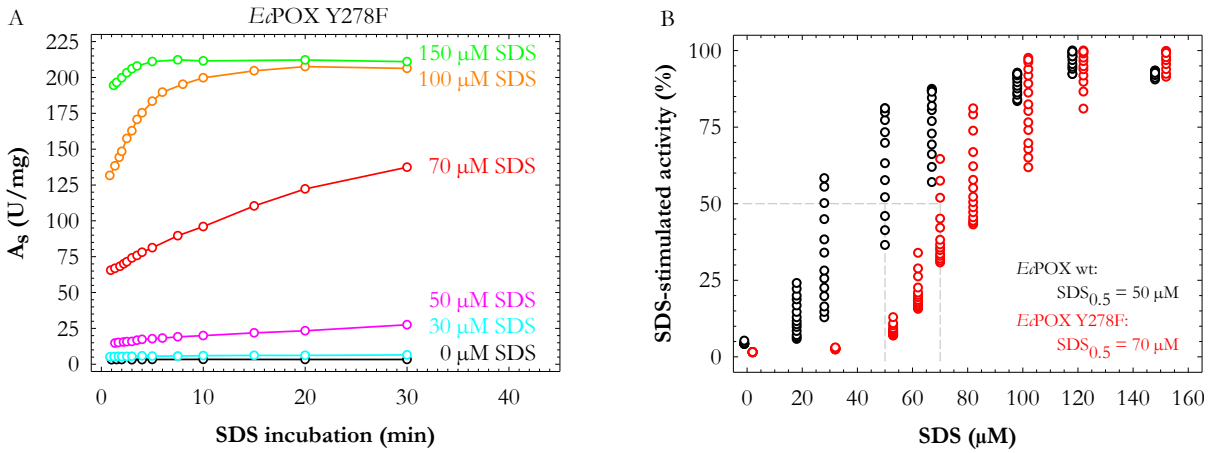

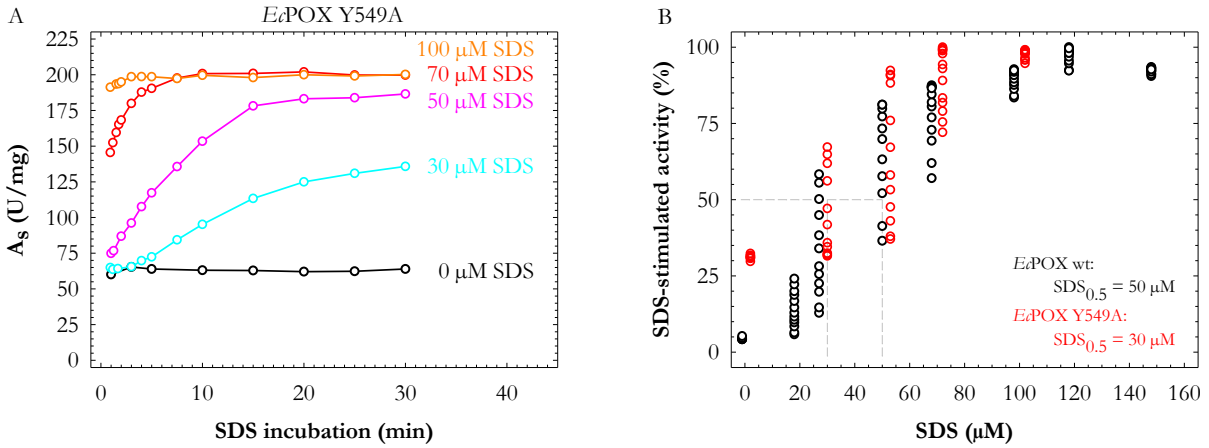

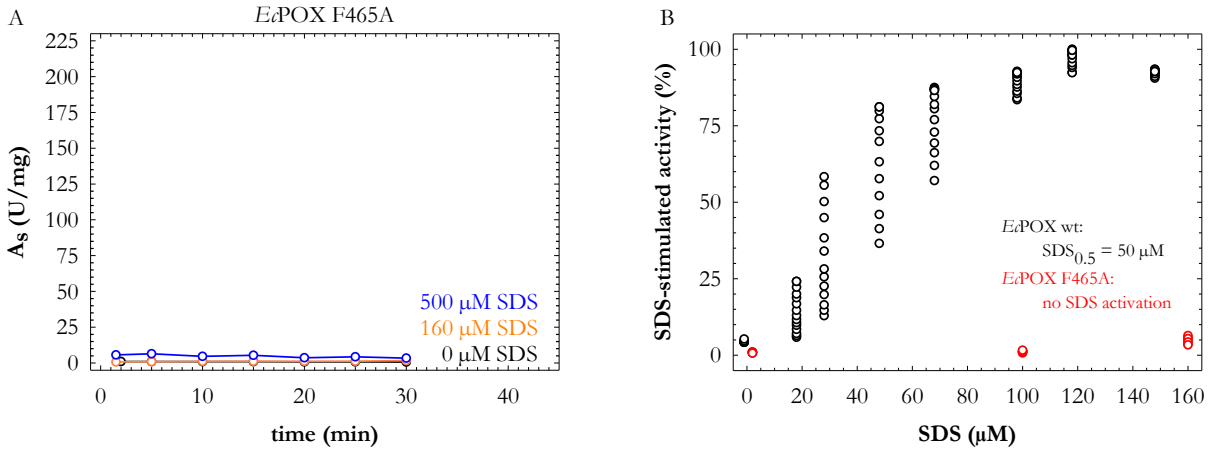
A
EdPOX F465A
As (U/mg)
time (min)
500 µM SDS
160 µM SDS
0 µM SDS
B
SDS-stimulated activity (%)
SDS (µM)
EdPOX wt:
SDS0.5 = 50 µM
EdPOX F465A:
no SDS activation

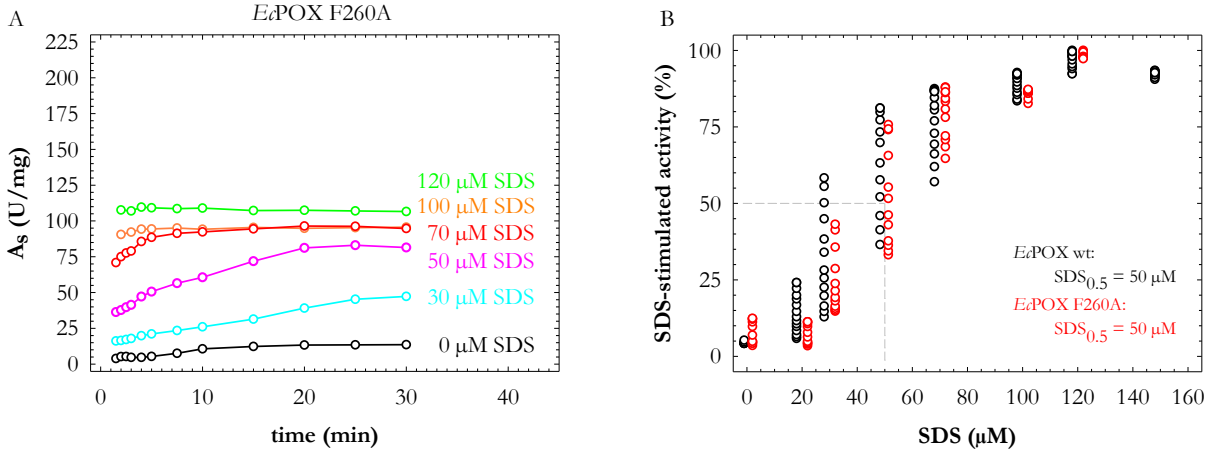
A
EdPOX F260A
As (U/mg)
time (min)
120 µM SDS
100 µM SDS
70 µM SDS
50 µM SDS
30 µM SDS
0 µM SDS
B
SDS-stimulated activity (%)
SDS (µM)
EdPOX wt:
SDS0.5 = 50 µM
EdPOX F260A:
SDS0.5 = 50 µM

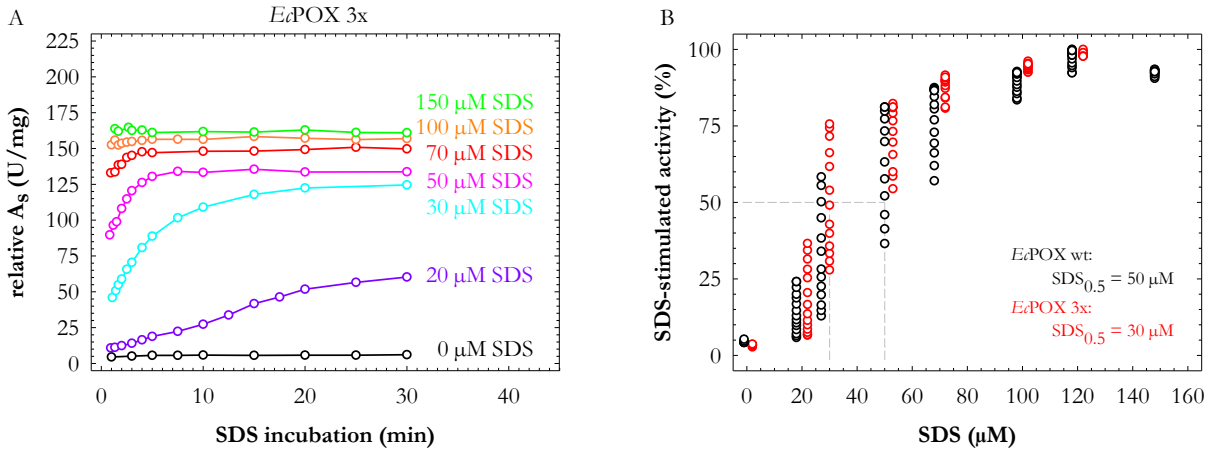
A
EdPOX 3x
relative As (U/mg)
SDS incubation (min)
150 µM SDS
100 µM SDS
70 µM SDS
50 µM SDS
30 µM SDS
20 µM SDS
0 µM SDS
B
SDS-stimulated activity (%)
SDS (µM)
EdPOX wt:
SDS0.5 = 50 µM
EdPOX 3x:
SDS0.5 = 30 µM

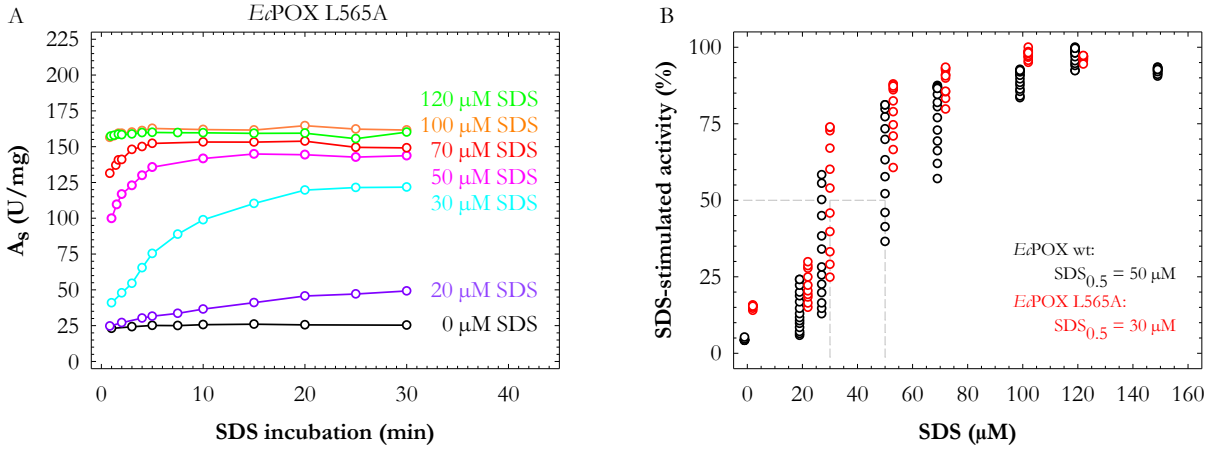
A
EdPOX L565A
As (U/mg)
SDS incubation (min)
120 µM SDS
100 µM SDS
70 µM SDS
50 µM SDS
30 µM SDS
20 µM SDS
0 µM SDS
B
SDS-stimulated activity (%)
SDS (µM)
EdPOX wt:
SDS0.5 = 50 µM
EdPOX L565A:
SDS0.5 = 30 µM

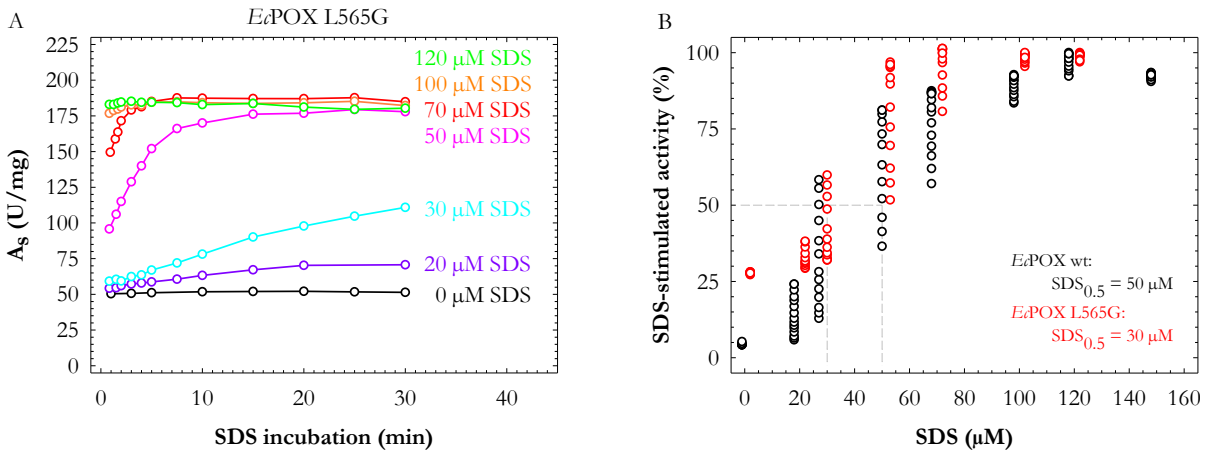
A
EdPOX L565G
120 µM SDS
100 µM SDS
70 µM SDS
50 µM SDS
30 µM SDS
20 µM SDS
0 µM SDS
As (U/mg)
SDS incubation (min)
B
SDS-stimulated activity (%)
EdPOX wt:
SDS0.5 = 50 µM
EdPOX L565G:
SDS0.5 = 30 µM
SDS (µM)

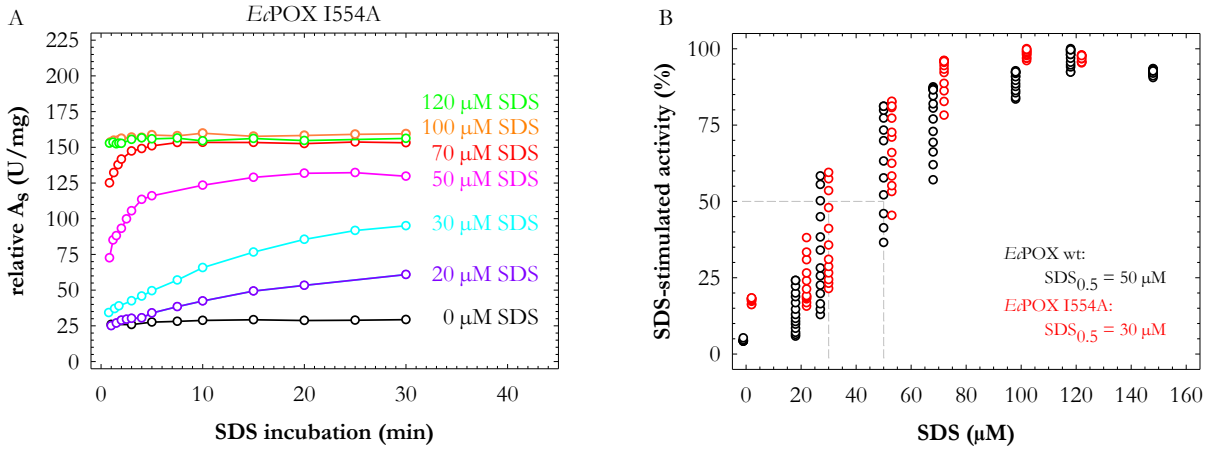
A
EdPOX I554A
120 µM SDS
100 µM SDS
70 µM SDS
50 µM SDS
30 µM SDS
20 µM SDS
0 µM SDS
relative As (U/mg)
SDS incubation (min)
B
SDS-stimulated activity (%)
EdPOX wt:
SDS0.5 = 50 µM
EdPOX I554A:
SDS0.5 = 30 µM
SDS (µM)

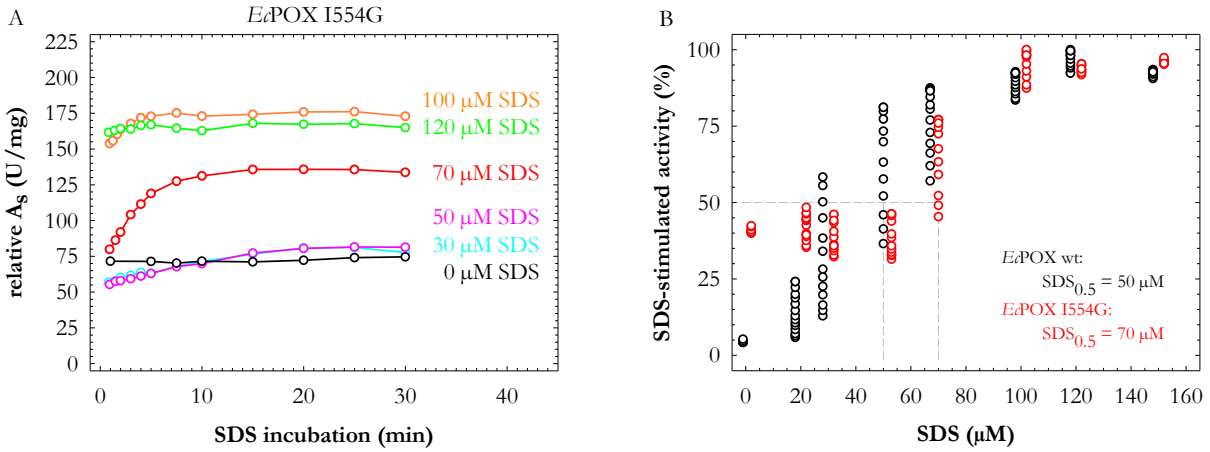
A
EdPOX I554G
100 µM SDS
120 µM SDS
70 µM SDS
50 µM SDS
30 µM SDS
0 µM SDS
relative As (U/mg)
SDS incubation (min)
B
SDS-stimulated activity (%)
EdPOX wt:
SDS0.5 = 50 µM
EdPOX I554G:
SDS0.5 = 70 µM
SDS (µM)

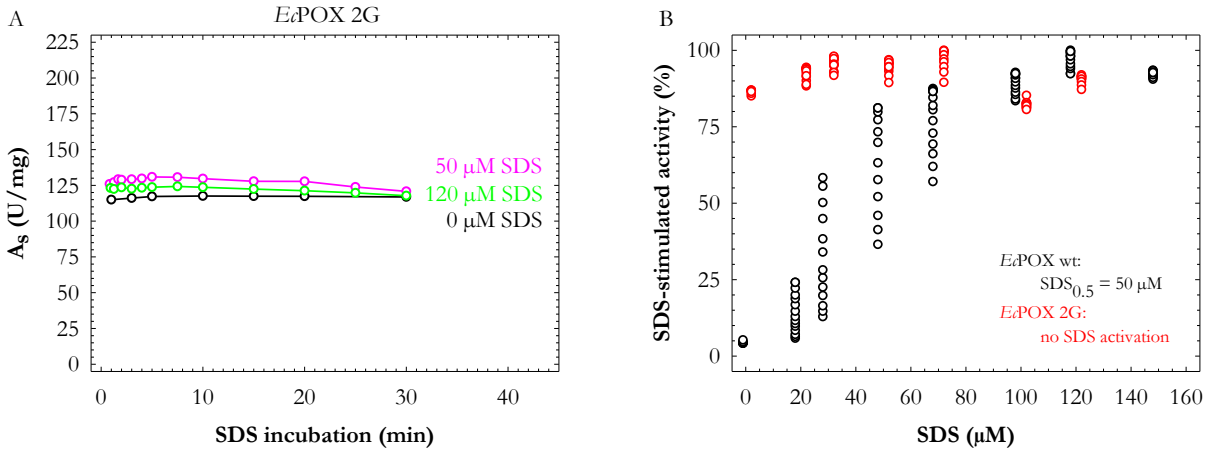
A
EdPOX 2G
50 µM SDS
120 µM SDS
0 µM SDS
As (U/mg)
SDS incubation (min)
B
SDS-stimulated activity (%)
EdPOX wt:
SDS0.5 = 50 µM
EdPOX 2G:
no SDS activation
SDS (µM)

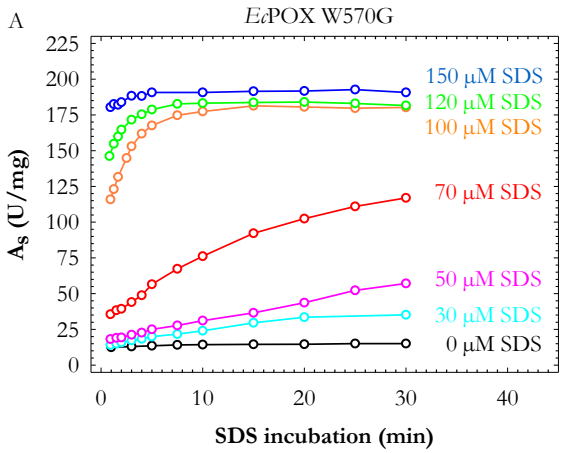
A
EdPOX W570G
225
200
175
150
125
100
75
50
25
0
As (U/mg)
150 µM SDS
120 µM SDS
100 µM SDS
70 µM SDS
50 µM SDS
30 µM SDS
0 µM SDS
0
10
20
30
40
SDS incubation (min)

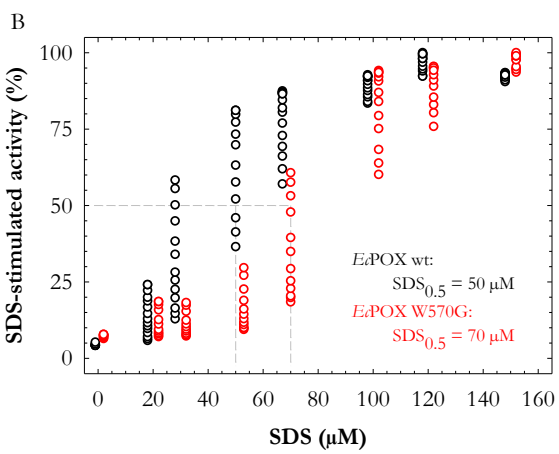
B
100
75
50
25
0
SDS-stimulated activity (%)
EdPOX wt:
SDS0.5 = 50 µM
EdPOX W570G:
SDS0.5 = 70 µM
0
20
40
60
80
100
120
140
160
SDS (µM)

8.5 Aerobic and anaerobic flavin reduction of *Ec*POX variants

Anaerobic (A) and aerobic (B) flavin reduction of *Ec*POX variants was determined at 438 nm with a path length of 1 cm and at 20 °C. 2 mg/mL of *Ec*POX were rapidly mixed with 200 mM pyruvate in the absence or presence of oxygen. Progress curves were converted to relative amount of oxidized flavin prior to use. A: Anaerobic flavin reduction. The rate constant of flavin reduction was determined by a single-exponential equation (fit not shown). B: Aerobic flavin reduction. Position of the steady state, at which flavin reduction and reoxidation are in equilibrium, is indicated by an arrow.

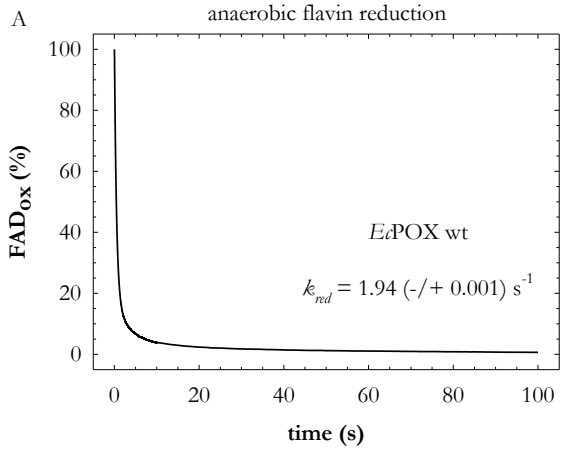

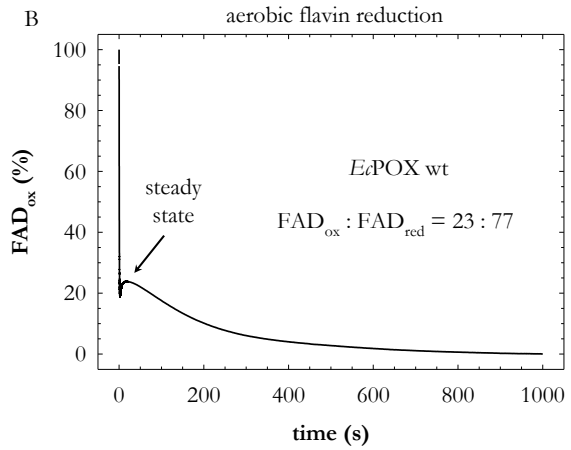

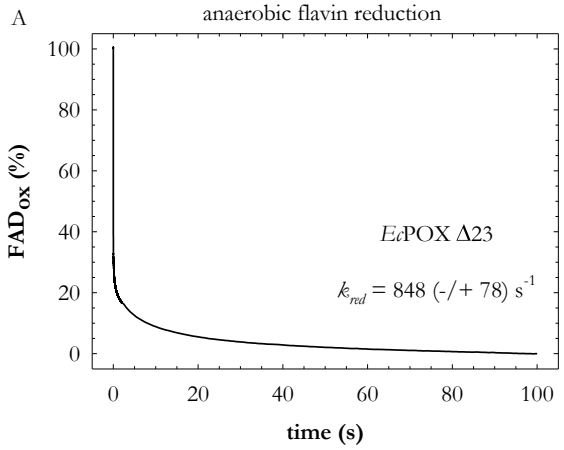

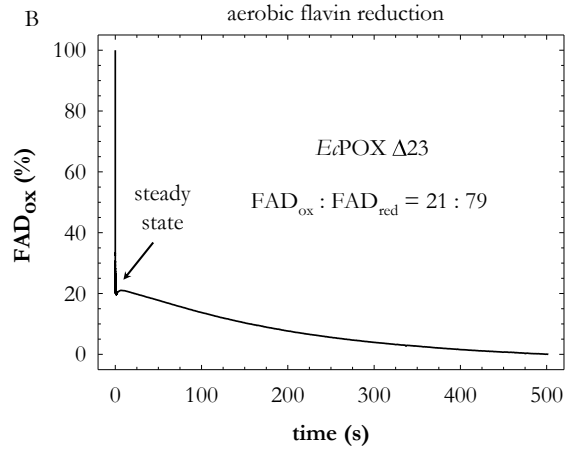

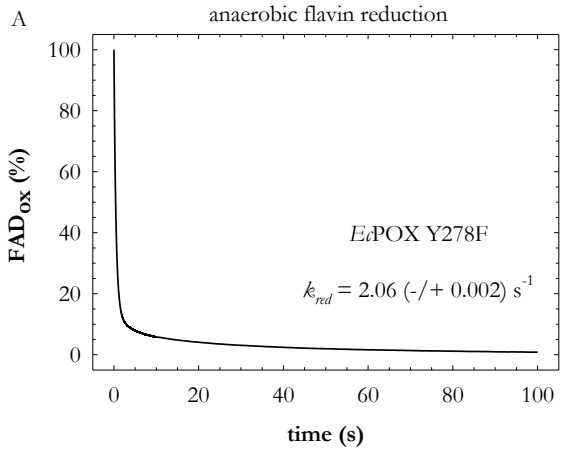

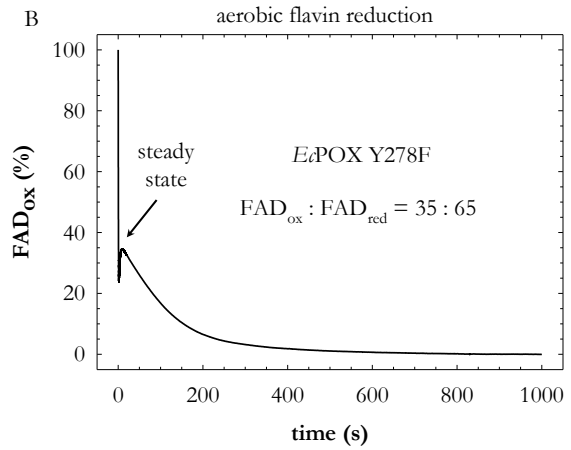

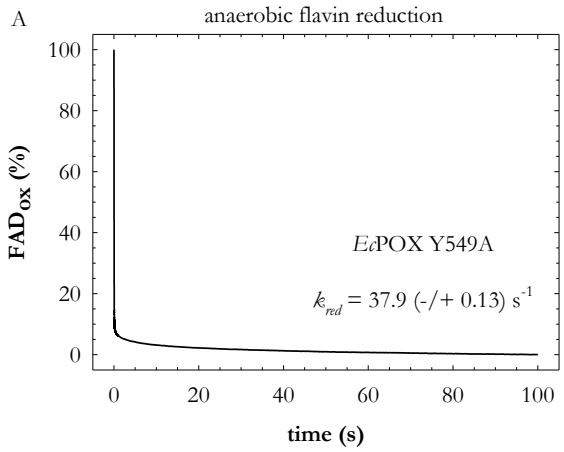
A
anaerobic flavin reduction
FAD$_{ox}$ (%)
time (s)
*Ec*POX Y549A
k_{red} = 37.9 (-/+ 0.13) s^{-1}

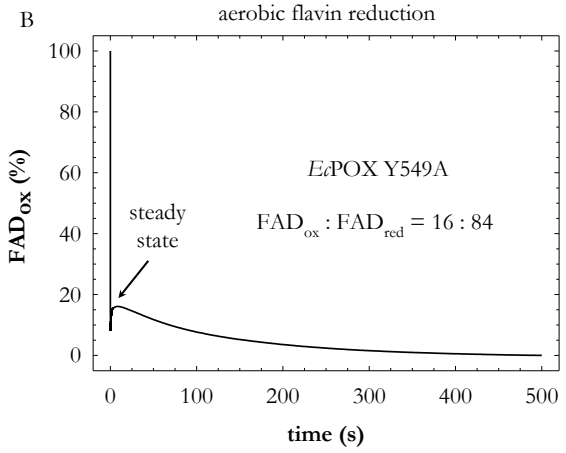
B
aerobic flavin reduction
FAD$_{ox}$ (%)
time (s)
*Ec*POX Y549A
steady state
FAD$_{ox}$: FAD$_{red}$ = 16 : 84

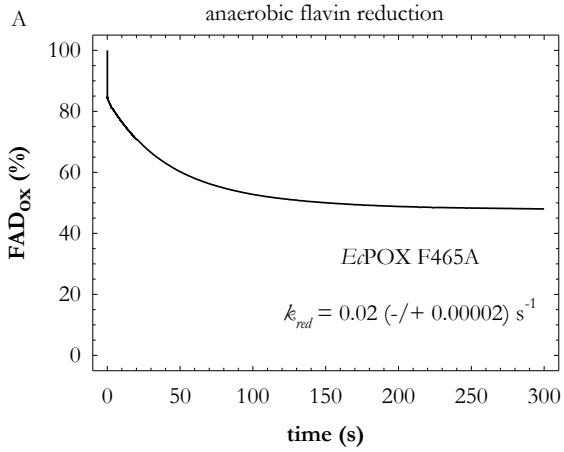
A
anaerobic flavin reduction
FAD$_{ox}$ (%)
time (s)
*Ec*POX F465A
k_{red} = 0.02 (-/+ 0.00002) s^{-1}

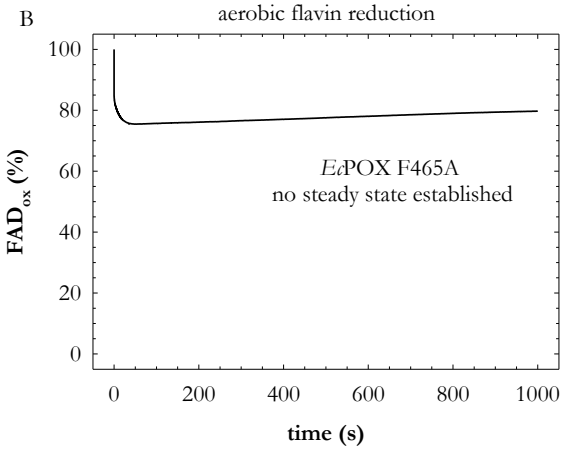
B
aerobic flavin reduction
FAD$_{ox}$ (%)
time (s)
*Ec*POX F465A
no steady state established

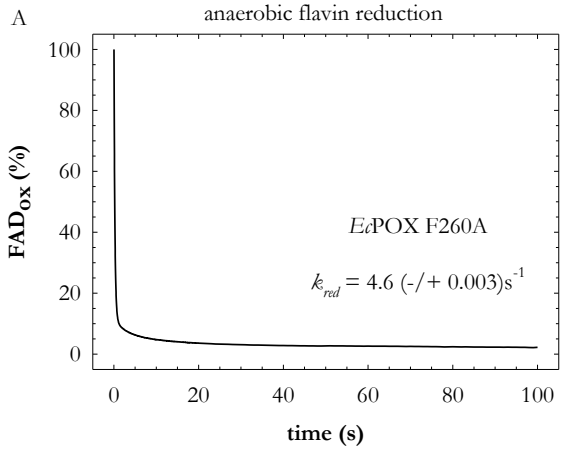
A
anaerobic flavin reduction
FAD$_{ox}$ (%)
time (s)
*Ec*POX F260A
k_{red} = 4.6 (-/+ 0.003)s^{-1}

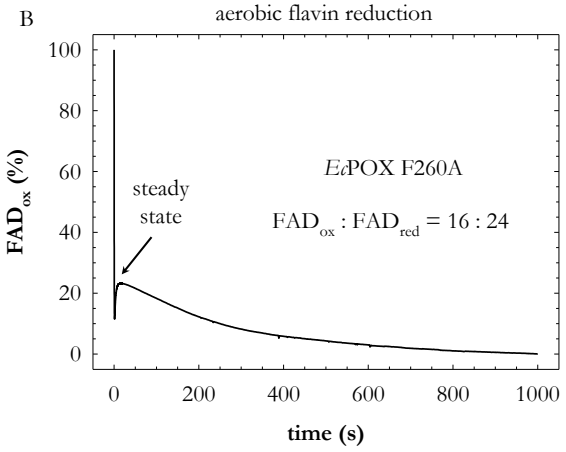
B
aerobic flavin reduction
FAD$_{ox}$ (%)
time (s)
*Ec*POX F260A
steady state
FAD$_{ox}$: FAD$_{red}$ = 16 : 24

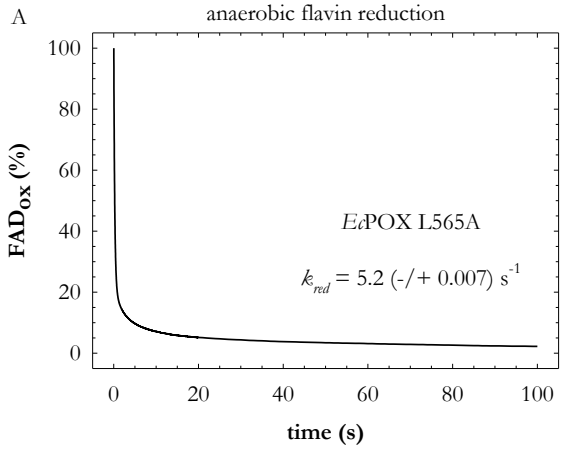
A
anaerobic flavin reduction
FAD$_{ox}$ (%)
time (s)
*Ec*POX L565A
k_{red} = 5.2 (-/+ 0.007) s^{-1}

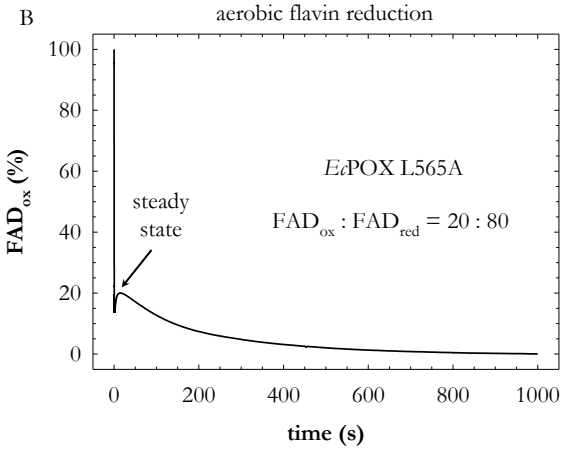
B
aerobic flavin reduction
FAD$_{ox}$ (%)
time (s)
*Ec*POX L565A
steady state
FAD$_{ox}$: FAD$_{red}$ = 20 : 80

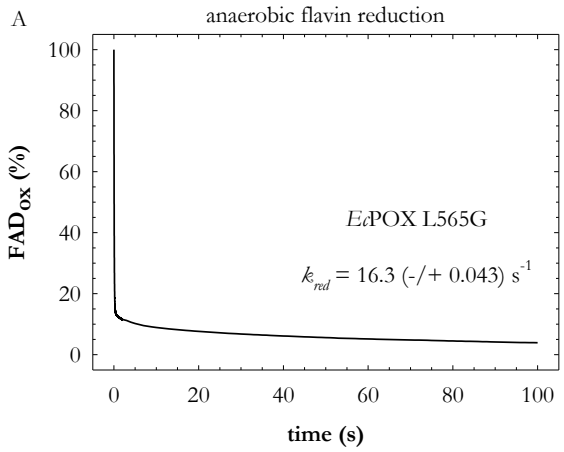
A
anaerobic flavin reduction
FAD$_{ox}$ (%)
time (s)
*Ec*POX L565G
k_{red} = 16.3 (-/+ 0.043) s^{-1}

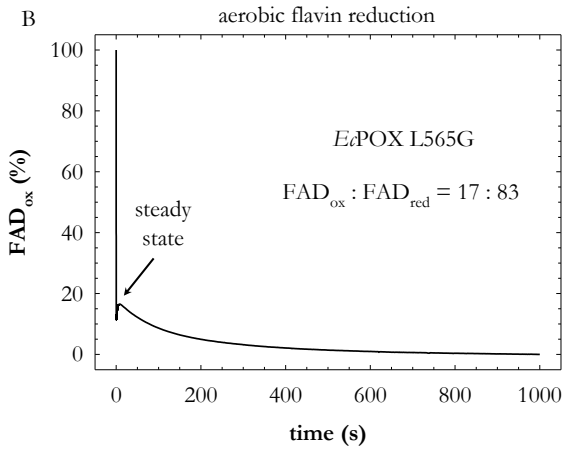
B
aerobic flavin reduction
FAD$_{ox}$ (%)
time (s)
*Ec*POX L565G
FAD$_{ox}$: FAD$_{red}$ = 17 : 83
steady state

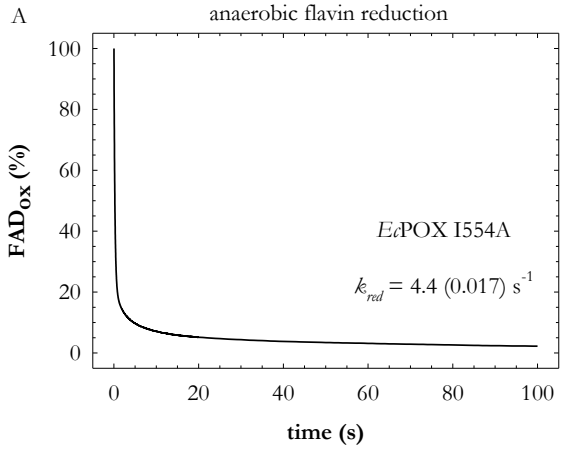
A
anaerobic flavin reduction
FAD$_{ox}$ (%)
time (s)
*Ec*POX I554A
k_{red} = 4.4 (0.017) s^{-1}

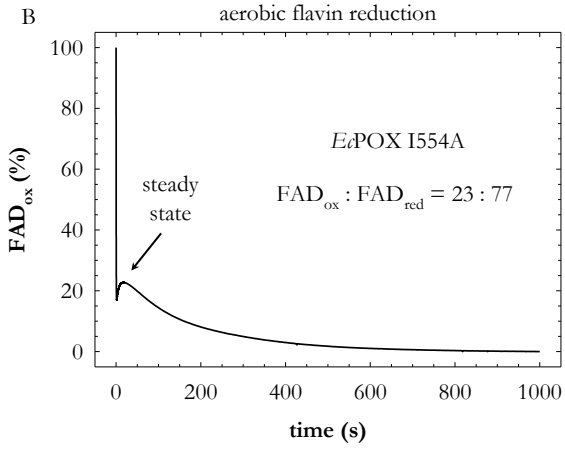
B
aerobic flavin reduction
FAD$_{ox}$ (%)
time (s)
*Ec*POX I554A
FAD$_{ox}$: FAD$_{red}$ = 23 : 77
steady state

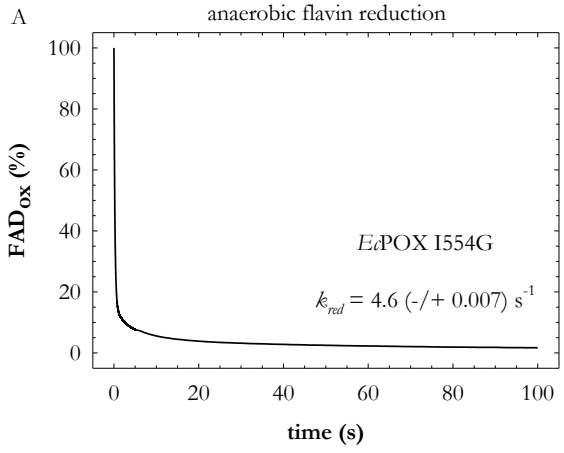
A
anaerobic flavin reduction
FAD$_{ox}$ (%)
time (s)
*Ec*POX I554G
k_{red} = 4.6 (-/+ 0.007) s^{-1}

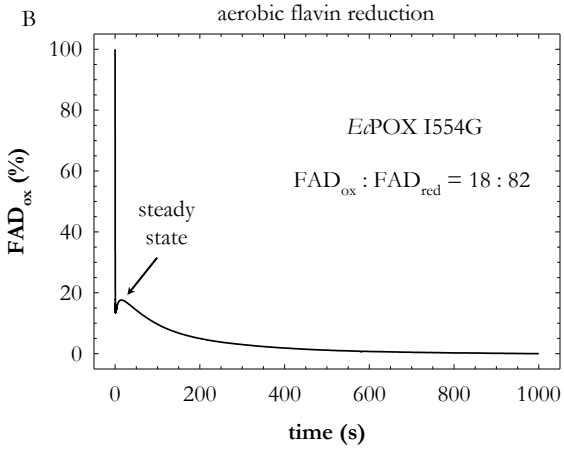
B
aerobic flavin reduction
FAD$_{ox}$ (%)
time (s)
*Ec*POX I554G
FAD$_{ox}$: FAD$_{red}$ = 18 : 82
steady state

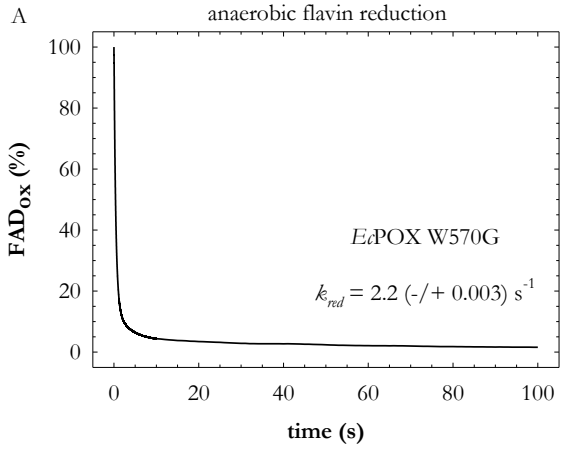
A
anaerobic flavin reduction
FAD$_{ox}$ (%)
time (s)
*Ec*POX W570G
k_{red} = 2.2 (-/+ 0.003) s^{-1}

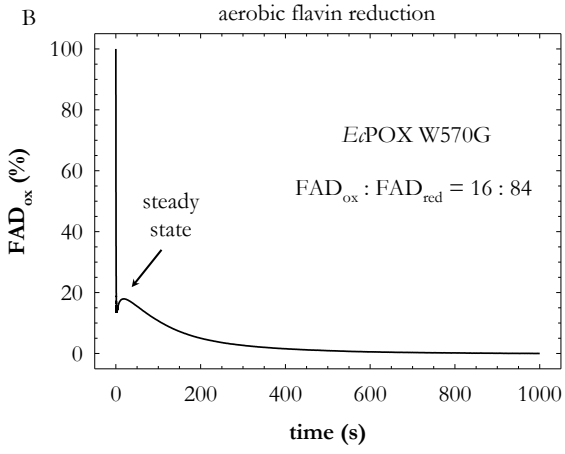
B
aerobic flavin reduction
FAD$_{ox}$ (%)
time (s)
*Ec*POX W570G
FAD$_{ox}$: FAD$_{red}$ = 16 : 84
steady state

8.6 Limited proteolysis of *Ec*POX variants

Proteolytic activation of *Ec*POX variants was monitored by SDS-PAGE (A-C) and Q_0 steady-state assay (D). 48.4 μM of *Ec*POX was digested at room temperature by 0.4 μm alpha-chymotrypsin. A-C: Gel samples were prepared after distinct time points and 0.6 μg of proteolyzed *Ec*POX were analyzed by SDS-PAGE. A: *Ec*POX was pre-reduced with 200 mM pyruvate for 10 min prior to protease addition. B: *Ec*POX was digested in the absence of substrate. C: *Ec*POX was incubated with 20 mM MAP for 10 min prior to protease addition. The different protein bands are indicated as followed: FL = full-length protein, Δ23 = *Ec*POX Δ550-572, Δ101 = *Ec*POX Δ471-572. Half-life of the digestion reaction ($t_{1/2}$), where half of the full-length protein is cleaved to Δ23, is highlighted (▼). D: Proteolytic digestion was performed similar to the SDS-PAGE experiments but activated enzyme was examined by Q_0 steady-state assay after distinct time points. Increase in activity (dots) due to Δ23 formation was analyzed by a single exponential equation (lines). Inset: Enlargement of the first minutes of digestion.

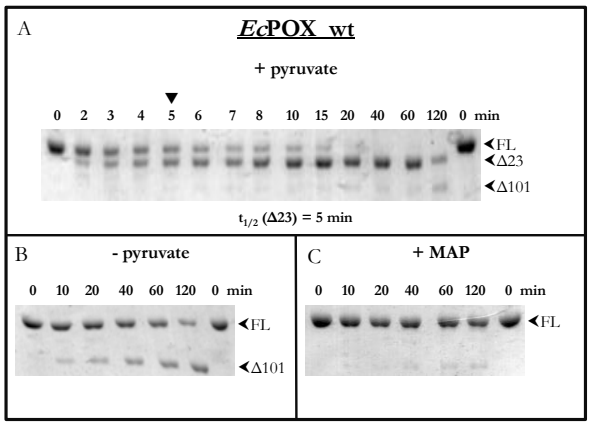

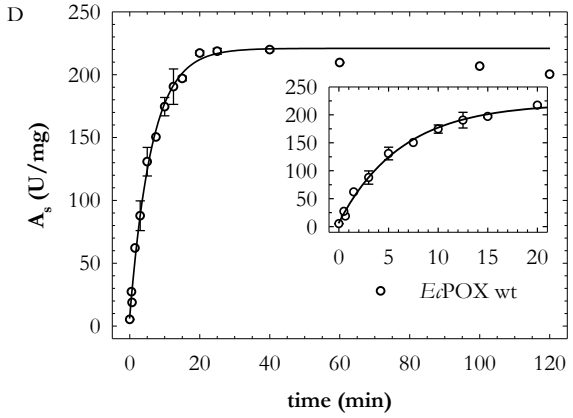

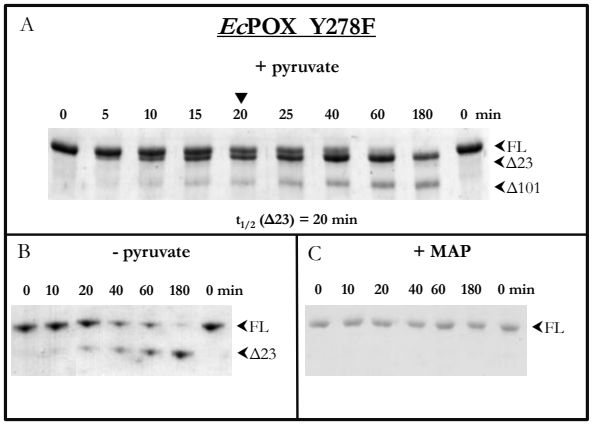

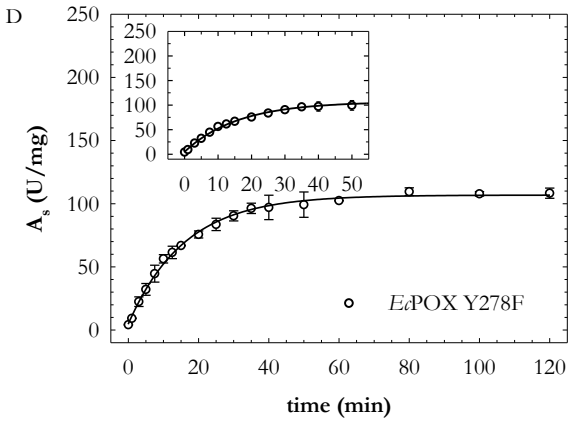

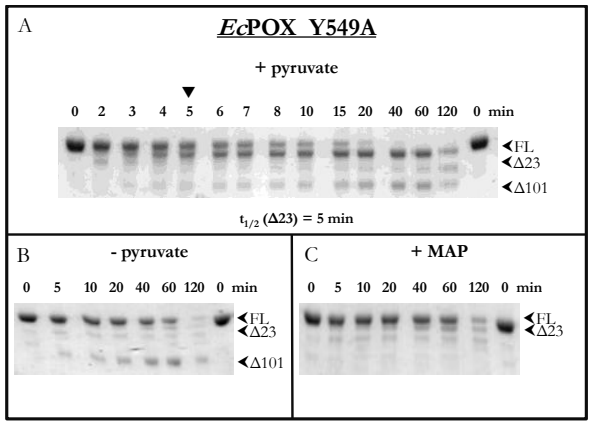
A
*Ec*POX Y549A
+ pyruvate
0 2 3 4 5 6 7 8 10 15 20 40 60 120 0 min
FL
Δ23
Δ101
$t_{1/2}$ (Δ23) = 5 min
B
- pyruvate
0 5 10 20 40 60 120 0 min
C
+ MAP
0 5 10 20 40 60 120 0 min

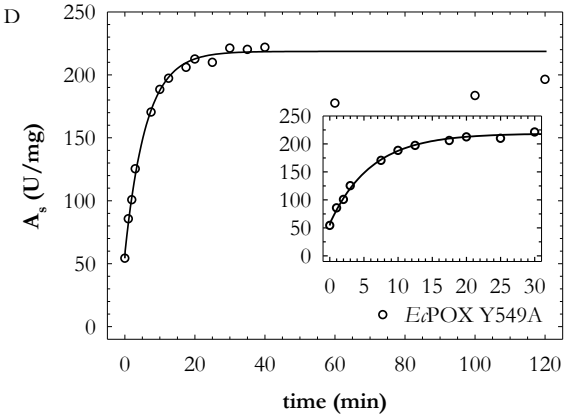
D
A_s (U/mg)
time (min)
*Ec*POX Y549A

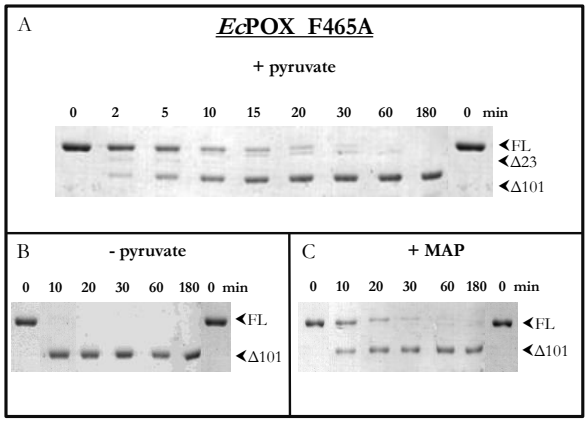
A
*Ec*POX F465A
+ pyruvate
0 2 5 10 15 20 30 60 180 0 min
FL
Δ23
Δ101
B
- pyruvate
0 10 20 30 60 180 0 min
C
+ MAP
0 10 20 30 60 180 0 min

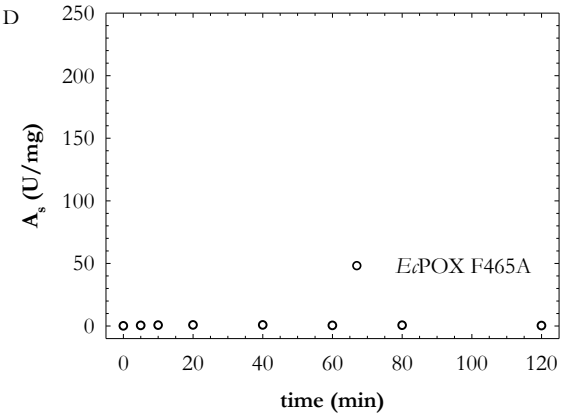
D
A_s (U/mg)
time (min)
*Ec*POX F465A

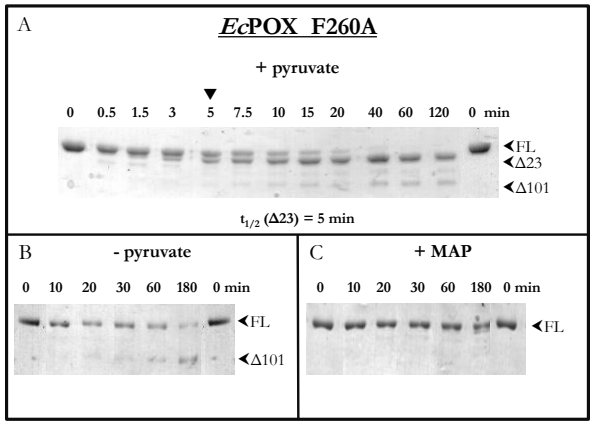
A
*Ec*POX F260A
+ pyruvate
0 0.5 1.5 3 5 7.5 10 15 20 40 60 120 0 min
FL
Δ23
Δ101
$t_{1/2}$ (Δ23) = 5 min
B
- pyruvate
0 10 20 30 60 180 0 min
C
+ MAP
0 10 20 30 60 180 0 min

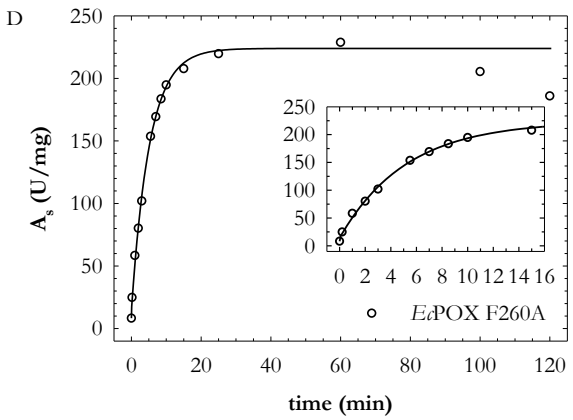
D
A_s (U/mg)
time (min)
*Ec*POX F260A

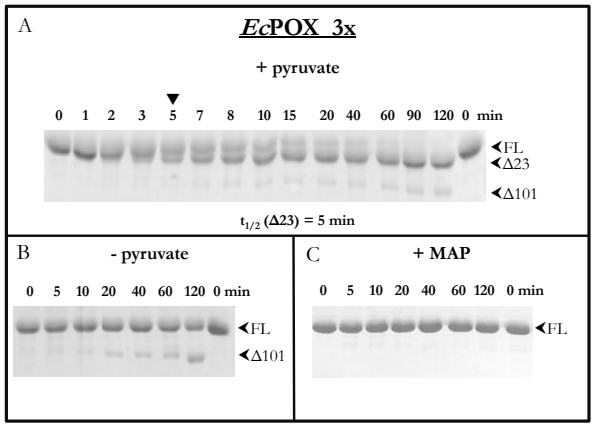
A
*Ec*POX 3x
+ pyruvate
0 1 2 3 5 7 8 10 15 20 40 60 90 120 0 min
FL
Δ23
Δ101
$t_{1/2}$ (Δ23) = 5 min
B
- pyruvate
0 5 10 20 40 60 120 0 min
C
+ MAP
0 5 10 20 40 60 120 0 min

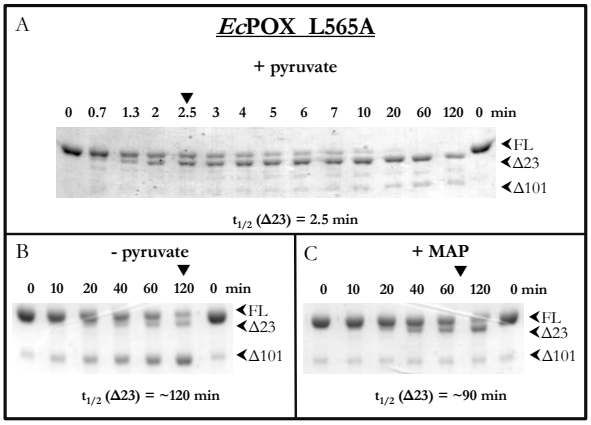
A
*Ec*POX L565A
+ pyruvate
0 0.7 1.3 2 2.5 3 4 5 6 7 10 20 60 120 0 min
FL
Δ23
Δ101
$t_{1/2}$ (Δ23) = 2.5 min
B
- pyruvate
0 10 20 40 60 120 0 min
$t_{1/2}$ (Δ23) = ~120 min
C
+ MAP
0 10 20 40 60 120 0 min
$t_{1/2}$ (Δ23) = ~90 min

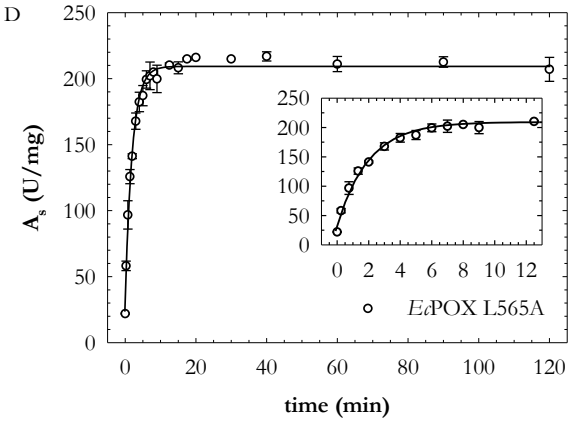
D
A_s (U/mg)
time (min)
*Ec*POX L565A

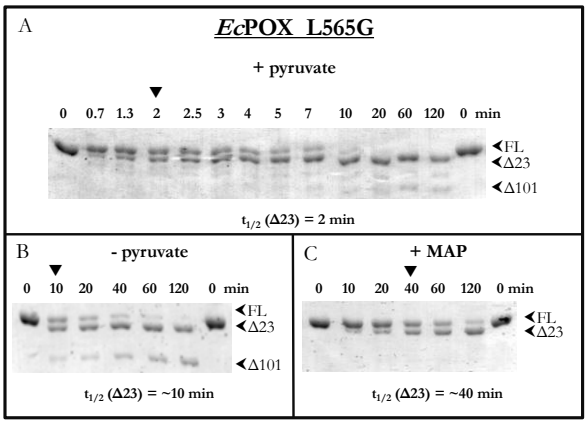
A
*Ec*POX L565G
+ pyruvate
0 0.7 1.3 2 2.5 3 4 5 7 10 20 60 120 0 min
FL
Δ23
Δ101
$t_{1/2}$ (Δ23) = 2 min
B
- pyruvate
0 10 20 40 60 120 0 min
$t_{1/2}$ (Δ23) = ~10 min
C
+ MAP
0 10 20 40 60 120 0 min
$t_{1/2}$ (Δ23) = ~40 min

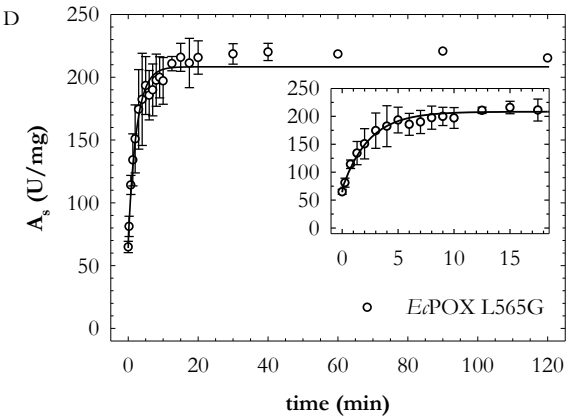
D
A_s (U/mg)
time (min)
*Ec*POX L565G

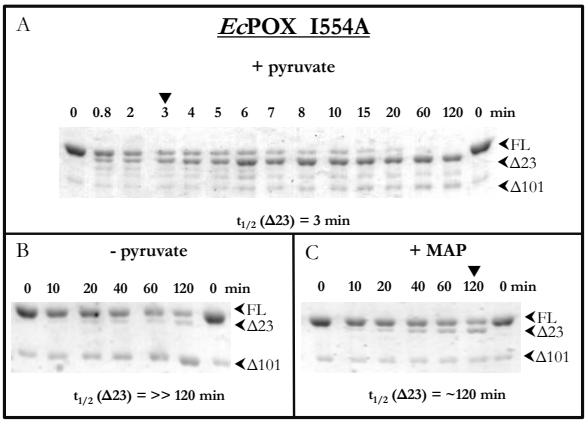
A
*Ec*POX I554A
+ pyruvate
0 0.8 2 3 4 5 6 7 8 10 15 20 60 120 0 min
FL
Δ23
Δ101
$t_{1/2}$ (Δ23) = 3 min
B
- pyruvate
0 10 20 40 60 120 0 min
$t_{1/2}$ (Δ23) = >> 120 min
C
+ MAP
0 10 20 40 60 120 0 min
$t_{1/2}$ (Δ23) = ~120 min

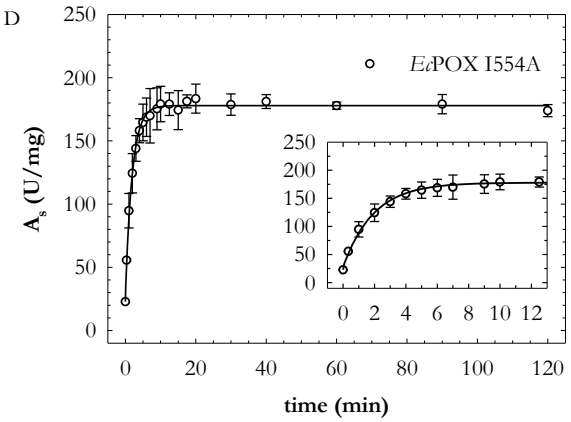
D
A_s (U/mg)
time (min)
*Ec*POX I554A

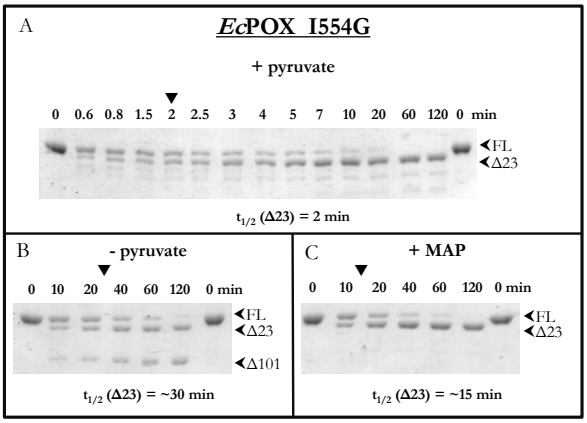
A
*Ec*POX I554G
+ pyruvate
0 0.6 0.8 1.5 2 2.5 3 4 5 7 10 20 60 120 0 min
FL
Δ23
$t_{1/2}$ (Δ23) = 2 min
B
- pyruvate
0 10 20 40 60 120 0 min
Δ101
$t_{1/2}$ (Δ23) = ~30 min
C
+ MAP
0 10 20 40 60 120 0 min
$t_{1/2}$ (Δ23) = ~15 min

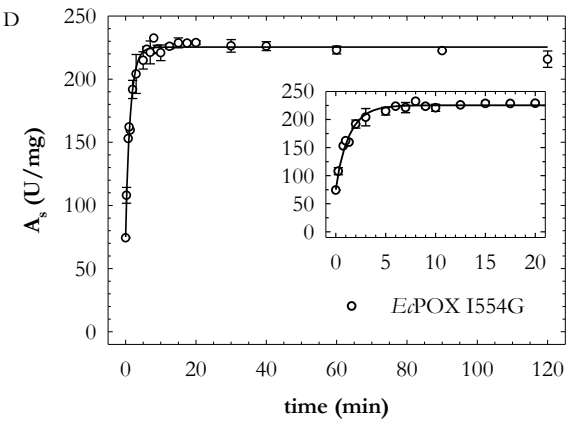
D
A_s (U/mg)
time (min)
*Ec*POX I554G

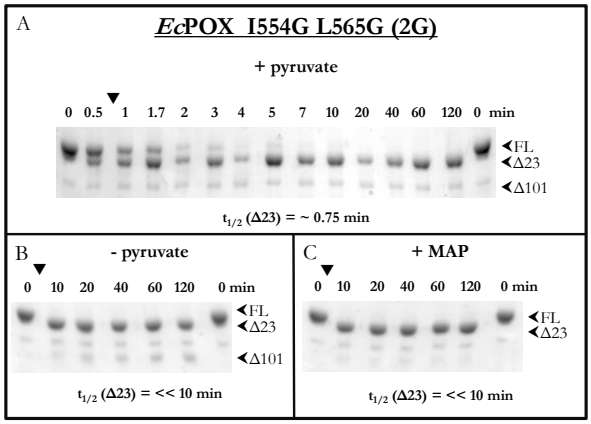
A
*Ec*POX I554G L565G (2G)
+ pyruvate
0 0.5 1 1.7 2 3 4 5 7 10 20 40 60 120 0 min
FL
Δ23
Δ101
$t_{1/2}$ (Δ23) = ~ 0.75 min
B
- pyruvate
0 10 20 40 60 120 0 min
FL
Δ23
Δ101
$t_{1/2}$ (Δ23) = << 10 min
C
+ MAP
0 10 20 40 60 120 0 min
FL
Δ23
$t_{1/2}$ (Δ23) = << 10 min

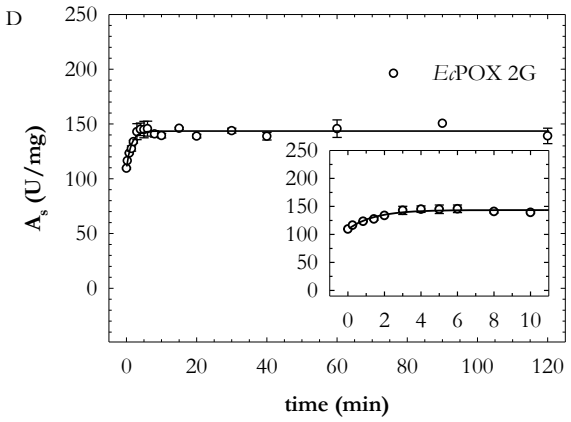
D
*Ec*POX 2G
A_s (U/mg)
time (min)

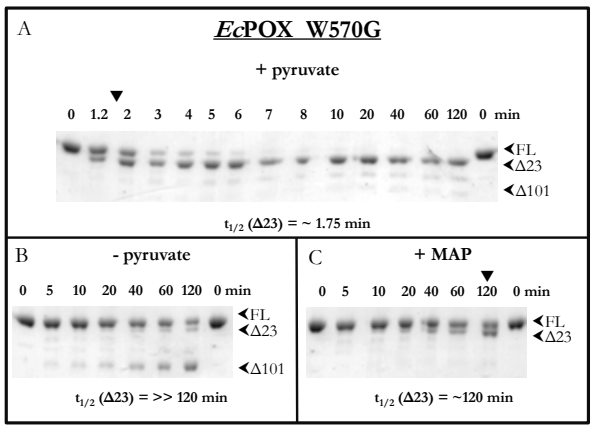
A
*Ec*POX W570G
+ pyruvate
0 1.2 2 3 4 5 6 7 8 10 20 40 60 120 0 min
FL
Δ23
Δ101
$t_{1/2}$ (Δ23) = ~ 1.75 min
B
- pyruvate
0 5 10 20 40 60 120 0 min
FL
Δ23
Δ101
$t_{1/2}$ (Δ23) = >> 120 min
C
+ MAP
0 5 10 20 40 60 120 0 min
FL
Δ23
$t_{1/2}$ (Δ23) = ~120 min

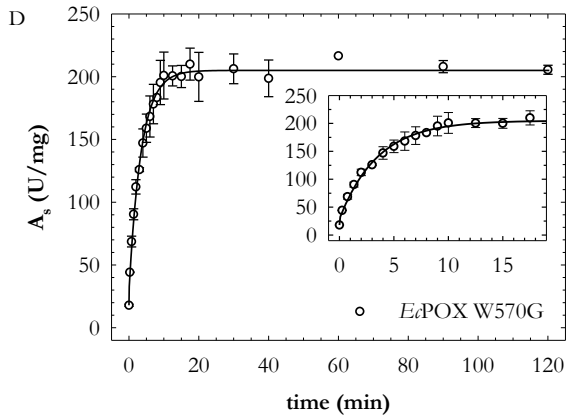
D
*Ec*POX W570G
A_s (U/mg)
time (min)

8.7 Data collection and refinements statistics of crystal structures

table 18: Statistics of crystal structures of *Ec*POX and *Lp*POX variants and the *Ec*POX Δ23:Q_0 complex. Values in parentheses refer to the highest resolution shell.

	***Ec*POX Δ23:Q_0**	***Lp*POX F289Y**	***Ec*POX F260A**	***Ec*POX Y549A**	***Ec*POX Y278F**
data collection					
wavelength, Å	1.541790	0.918410	0.918410	0.918410	0.918410
space group	$P2_12_12_1$	$C222_1$	$P4_32_12$	$P4_32_12$	$P4_32_12$
cell parameters: a, Å	204.051	119.480	152.014	152.496	150.290
b, Å	205.915	154.330	152.014	152.496	150.290
c, Å	214.627	165.440	153.789	154.206	152.970
α, β, γ, °	90, 90, 90	90, 90, 90	90, 90, 90	90, 90, 90	90, 90, 90
monomers per asymmetric unit	12	2	2	2	2
resolution range, Å	47.49-3.2	48.431-1.434	48.58-3.084	48.71-2.793	45.972-2.96
	(3.3-3.2)	(1.53-1.43)	(3.18-3.08)	(2.89-2.79)	(3.06-2.96)
R_{merge}, %	12.1	7.7	7	7	5.7
	(57.6)	(56.5)	(57.6)	(61.4)	(54.1)
completeness, %	98.8	99.8	99.9	98.9	99.2
	(99.9)	(99.8)	(100)	(88.9)	(99.2)
no. of reflections	481184	1036381	247638	396594	297100
	(42472)	(186634)	(22825)	(23164)	(28702)
redundancy	3.3	3.8	7.3	8.8	8.1
	(3.3)	(3.7)0.114	(7.5)	(5.8)	(8.3)
I/σ	8.30	15.04	24.69	23.98	24.36
	(2.16)	(2.52)	(4.12)	(2.85)	(4.12)
refinement					
resolution range, Å	47.49-3.2	48.431-1.434	48.58-3.084	48.71-2.793	2.96- 45.972
	(3.3-3.2)	(1.53-1.43)	(3.18-3.08)	(2.89-2.79)	(2.96-3.06)
Wilson B, $Å^2$	70.83	9.27	81.07	81.07	80.08
R_{cryst}, %	18.69	15.34	18.61	19.66	19.31
	(27.59)	(30.13)	(26.69)	(33.98)	(34.55)
R_{free}, %	24.53	17.17	22.79	22.84	22.03
	(31.86)	(33.96)	(32.86)	(36.79)	(39.21)
no. of nonhydrogen atoms					
protein	49007	11307	8841	8841	8735
water	0	1612	0	0	0
sulfate, phosphate, glycerol, Q_0	144	54	0	0	0
FAD, ThDP, Mg^{2+}	936	160	158	158	158
r.m.s.d. from ideality					
bond lengths, Å	0.003	0.013	0.014	0.017	0.006
bond angles, °	0.798	1.541	1.628	1.834	1.102
average B-factors, $Å^2$					
protein atoms	72.44	82.14	80.99	80.99	87.67
water	-	85.79	-	-	-
sulfate, phosphate, glycerol, Q_0	60.28	74.36	-	-	-
FAD, ThDP, Mg^{2+}	65.34	71.90	70.26	75.12	69.98

Extension of table 18.

	***Ec*POX I554G**	***Ec*POX I554A**	***Ec*POX L565A**	***Ec*POX 3x**
data collection				
wavelength, Å	1.239530	1.239530	0.918410	0.8
space group	$P4_32_12$	$P4_32_12$	$P4_32_12$	$P4_32_12$
cell parameters: a, Å	151.692	150.730	149.966	151.710
b, Å	151.692	150.730	149.966	151.710
c, Å	156.369	151.880	151.436	151.650
α, β, γ, °	90, 90, 90	90, 90, 90	90, 90, 90	90, 90, 90
monomers per asymmetric unit	2	2	2	2
resolution range, Å	48.11-2.90 (3-2.9)	47.67-3.02 (3.13-3.02)	47.84-3.24 (3.34-3.24)	47.97-3.2 (3.3-3.2)
R_{merge}, %	3.1 (64.2)	3.5 (60.9)	6.8 (67.3)	7.5 61.1
completeness, %	98.8 (99.8)	93.4 (96.5)	98.1 (98.3)	97.3 (98.5)
no. of reflections	2024560. (19670)	270344 (25843)	198172 (17550)	209758 (17569)
redundancy	5.0 (5.1)	8.3 (8.4)	7.2 (7.4)	6.8 (7.2)
I/σ	28.54 (3.10)	33.99 (3.83)	23.96 (3.27)	21.62 (3.78)
refinement				
resolution range, Å	48.11-2.90 (3-2.9)	47.67-3.02 (3.13-3.02)	47.84-3.24 (3.34-3.24)	47.97-3.2 (3.3-3.2)
Wilson B, $Å^2$	81.07	81.06	81.06	80.91
R_{cryst}, %	19.96 (35.93)	16.27 (27.24)	18.93 (26.49)	16.86 (23.15)
R_{free}, %	24.16 (37.06)	22.70 (38.03)	26.33 (38.34)	23.03 (31.95)
no. of nonhydrogen atoms				
protein	8834	8836	8836	8821
water	0	0	0	0
sulfate, phosphate, glycerol, Q_0	0	0	0	0
FAD, ThDP, Mg^{2+}	158	158	158	158
r.m.s.d. from ideality				
bond lengths, Å	0.017	0.015	0.014	0.014
bond angles, °	1.863	1.748	1.618	1.656
average B-factors, $Å^2$				
protein atoms	81.00	82.14	87.67	82.76
water	-	-	-	-
sulfate, phosphate, glycerol, Q_0	-	-	-	-
FAD, ThDP, Mg^{2+}	73.35	71.89	69.98	72.00

8.8 Amino acid sequence alignments

The primary amino acid sequence of *Ec*POX, *Lp*POX and the catalytic subunit of acetohydroxyacid synthase (AHAS) from *yeast* were aligned with ClustalW2 [139].

```
EcPOX           ---------------------------MKQT------VAAYIAKTLESAGVKRIWGVTGDS 28
LpPOX           ------------------------MVMKQTKQTNILAGAAVIKVLEAWGVDHLYGIPGGS 36
AHAS            APSFNVDPLEQPAEPSKLAKKLRAEPDMDTSFVGLTGGQIFNEMMSRQNVDTVFGYPGGA 60
                                       :*       .  . : :.  .*. ::* .*.:

EcPOX           LNGLSDSLNRMG-TIEWMSTRHEEVAAFAAGAEAQLSGELAVCAGSCGPGNLHLINGLFD 87
LpPOX           INSIMDALSAERDRIHYIQVRHEEVGAMAAAADAKLTGKIGVCFGSAGPGGTHLMNGLYD 96
AHAS            ILPVYDAIHNSD-KFNFVLPKHEQGAGHMAEGYARASGKPGVVLVTSGPGATNVVTPMAD 119
                :  : *::      :.::  :**: ..  * . *: :*: .*   :.***  :::. : *

EcPOX           CHRNHVPVLAIAAHIPSSEIGSGYFQETHPQELFRECSHYCELVSSPEQIPQVLAIAMRK 147
LpPOX           AREDHVPVLALIGQFGTTGMNMDTFQEMNENPIYADVADYNVTAVNAATLPHVIDEAIRR 156
AHAS            AFADGIPMVVFTGQVPTSAIGTDAFQEADVVGISRSCTKWNVMVKSVEELPLRINEAFEI 179
                .  : :*::.: .:. :: :. . *** .   :  . :.:   . .   :*  :  *:.

EcPOX           AVLNR-GVSVVVLPGDVA----LKPAPEGATMHW--YHAPQPVVTPEE--EELRKLAQLL 198
LpPOX           AYAHQ-GVAVVQIPVDLP----WQQIPAEDWYAS--ANSYQTPLLPEPDVQAVTRLTQTL 209
AHAS            ATSGRPGPVLVDLPKDVTAAILRNPIPTKTTLPSNALNQLTSRAQDEFVMQSINKAADLI 239
                *   : *  :* :* *:.     :  *          :   .    *   : : : :: :

EcPOX           RYSSNIALMCGSGCAGAH---KELVEFAGKIKAPIVHALRGKEHVEYDNPYDVGMTGLIG 255
LpPOX           LAAERPLIYYGIGARKAG---KELEQLSKTLKIPLMSTYPAKGIVADRYPAYLGSANRVA 266
AHAS            NLAKKPVLYVGAGILNHADGPRLLKELSDRAQIPVTTTLQGLGSFDQEDPKSLDMLGMHG 299
                  :..  :  * *        : * :::   : *:  :  .   .    *  :.  .  .

EcPOX           FSSGFHTMMNADTLVLLGTQFPYRAF--------------YPTDAKIIQIDINPASIGAH 301
LpPOX           QKPANEALAQADVVLFVGNNYPFAEVS-----------KAFKNTRYFLQIDIDPAKLGKR 315
AHAS            CATANLAVQNADLIIAVGARFDDRVTGNISKFAPEARRAAAEGRGGIIHFEVSPKNINKV 359
                  ..  :: :** :: :* .:                         :::::::* .:.

EcPOX           SKVDMALVGDIKSTLRALLPLVEEKADRKFLDKALEDYRDARKGLDDLAKPSEKAIHPQY 361
LpPOX           HKTDIAVLADAQKTLAAILAQVSERESTPWWQANLANVKNWRAYLASLEDKQEGPLQAYQ 375
AHAS            VQTQIAVEGDATTNLGKMMSKIFPVKERSEWFAQINKWKKEYP-YAYMEETPGSKIKPQT 418
                 :.::*: .*  ..*  ::. :    .       : . :.       : .     ::.

EcPOX           LAHEISHFAADD---AIFTCDVGTPTVWAARYLKMNGKRRLLGSFNHGSMANAMPHGVGA 418
LpPOX           VLRAVNKIAEPD---AIYSIDVGDINLNANRHLKLTPSNRHITSNLFATMGVGIPGAIAA 432
AHAS            VIKKLSKVANDTGRHVIVTTGVGQHQMWAAQHWTWRNPHTFITSGGLGTMGYGLPAAIGA 478
                : : :.:.*      .* : .**   : * :: .    .  : *   .:*. .:* .:.*

EcPOX           QATEPERQVVAMCGDGGFSMLMGDFLSVVQMKLPVKIVVFNNSVLGFVAMEMKAGG-YLT 477
LpPOX           KLNYPERQVFNLAGDGGASMTMQDLATQVQYHLPVINVVFTNCQYGFIKDEQEDTNQNDF 492
AHAS            QVAKPESLVIDIDGDASFNMTLTELSSAVQAGTPVKILILNNEEQGMVTQWQSLFYEHRY 538
                :   **  *. : **.. .* : :: : **   **  :::.*   *::    .

EcPOX           DGTELHDTNFARIAEACGITGIRVEKASEVDEALQRAFSIDG--PVLVDVVVAKEELAIP 535
LpPOX           IGVEFNDIDFSKIADGVHMQAFRVNKIEQLPDVFEQAKAIAQHEPVLIDAVITGDRPLPA 552
AHAS            SHTHQLNPDFIKLAEAMGLKGLRVKKQEELDAKLKEFVSTKG--PVLLEVEVDKKVPVLP 596
                  ..  : :* ::*:.  : .:**:* .::   ::.  :     ***::. :  .    .

EcPOX           PQIKLEQAKGFSLYMLRAIISGRGDEVIELAKTNWLR-------------- 572
LpPOX           EKLRLDSATSSAADIEAFKQRYEAQDLQPLSTYLKQFGLDDLQHQIGQGGF 603
AHAS            ---MVAGGSGLDEFINFDPEVERQQTELRHKRTGGKH-------------- 630
                    :  ...    :       . :
```

Sequence identity to *Ec*POX: *Lp*POX = 28 %

AHAS = 23 %

8.9 Comparison of the crystal structures of *Ec*POX I554G with full-length *Ec*POX wt

The crystal structure of *Ec*POX I554G is shown as example since it is identical to structures of variants F260A, I554A, L565A and *Ec*POX 3x. The full-length enzyme is depicted in orange whereas the variant I554G is shown in green. The position of the exchanged amino acid (Ile/Gly554) in the variant is highlighted by a blue sphere. The membrane anchor is detected completely attached to the protein core (A) an all variants and no significant structural changes of the overall structure or within the active site (B) are observed.